



European Commission
Research Programme of the Research Fund for Coal and Steel

INNOSEIS

Valorization of innovative anti-seismic devices

WORK PACKAGE 4 – DELIVERABLE 4.2

Volume on case studies for mid/high-rise buildings

Coordinator:

National Technical University of Athens - NTUA, Greece

Beneficiaries:

Universitatea Politehnica Timisoara - UPT, Romania

Politecnico di Milano - POLIMI, Italy

Universita Degli Studi di Napoli Federico II - UNINA, Italy

Universita di Pisa - UNIPI, Italy

Rheinisch-Westfaelische Technische Hochschule Aachen - RWTH, Germany

Instituto Superior Tecnico - IST, Portugal

Universitet po Arhitektura Stroitelstvo i Geodezija - UACEG, Bulgaria

Universiteit Hasselt - UHasselt, Belgium

Maurer Sohne Engineering GmbH & CO KG - MSE, Germany

Convention Europeenne de la Construction Metallique ASBL - ECCS, Belgium

Grant Agreement Number: 709434

04/12/2017

AUTHORS:

POLITECNICO DI MILANO (POLIMI)

Department of Architecture, Built Environment and Construction Engineering
Piazza Leonardo da Vinci, 32, 20133 Milan, Italy

Chapters 2, 6

Authors: Carlo Andrea Castiglioni, Amin Alavi

HASSELT UNIVERSITY

Construction Engineering Research Group

Campus Diepenbeek, Agoralaan building H, BE3590 Diepenbeek, Belgium

Chapter 3

Authors: Jose Henriques, Herve Degee

RHEINISCH-WESTFAELISCHE TECHNISCHE HOCHSCHULE AACHEN (RWTH)

Institute of Steel Construction

52074 Aachen, Germany

Chapter 4

Authors: Benno Hoffmeister, Marius Pinkawa

NATIONAL TECHNICAL UNIVERSITY OF ATHENS (NTUA)

Institute of Steel Structures

15780 Athens, Greece

Chapter 5

Authors: Ioannis Vayas, Pavlos Thanopoulos, Panagiotis Tsarpalis

INSTITUTO SUPERIOR TÉCNICO (IST)

Department of Civil Engineering, Architecture and Georesources

Av. Rovisco Pais, 1049-001 Lisbon, Portugal

Chapter 7

Authors: Luís Calado, Jorge M. Proença, João Sio

POLITEHNICA UNIVERSITY OF TIMISOARA (UPT)

Department of Steel Structures and Structural Mechanics

Ioan Curea Street, no.1, Timisoara, Romania

Chapters 8, 9

Authors of Chapter 8: Adriana Chesoi, Aurel Stratan, Dan Dubina

Authors of Chapter 9: Calin Neagu, Florea Dinu, Dan Dubina

UNIVERSITET PO ARCHITEKTURA STROITELSTVO I GEODEZIJA (UACEG)

Department of Steel and Timber Structures

1 Hr. Smirnenski blvd. 1046 Sofia, Bulgaria

Chapter 10

Authors: Tzvetan Georgiev, Dimo Zhelev, Lora Raycheva, Nikolaj Rangelov

UNIVERSITY OF PISA (UNIP)

Department of Civil and Industrial Engineering

56122 Pisa, Italy

Chapter 11

Authors: Walter Salvatore, Francesco Morelli, Andrea Piscini

MAURER SOHNE ENGINEERING GMBH & CO. KG (MSE)

Frankfurter Ring 193

80807 Munich, Germany

Chapters 12, 13

Authors of Chapter 12: Emanuele Gandelli, Christiane Butz

Authors of Chapter 13: Emanuele Gandelli, Valentina Renzi, Christiane Butz

CONTENTS

CONTENTS	V
1 INTRODUCTION	1
2 INERD PIN CONNECTIONS	3
2.1 General information.....	3
2.1.1 Introduction	3
2.2 Description of the building.....	3
2.2.1 Geometry and general assumptions	3
2.2.2 Material	3
2.3 Seismic analysis.....	6
2.3.1 Simulation	6
2.3.2 Seismic design situation.....	6
2.3.3 Response Spectrum Analysis	7
2.4 Design Summary.....	8
2.4.1 Design of building without dissipative elements	8
2.4.2 Design of buildings with FUSEIS bolted beam splices	11
2.4.3 Design of building with INERD pin connection	13
2.5 Verification of codified limits for the entire building.....	17
2.5.1 Damage limitation – limitation of inter-story drift	17
2.5.2 Second order effects	17
2.5.3 Soft Storey Constraint.....	18
2.6 Structural detailing	19
2.6.1 FUSEIS Bolted Beam Splices	19
2.6.2 INERD Pin Connections.....	21
2.7 References.....	22
3 CBF- U-PLATE INERD CONNECTION	25
3.1 General	25
3.1.1 Introduction	25
3.1.2 Description of building.....	25
3.2 Basic and non-seismic design.....	28
3.2.1 Selection of the U-PLATE INERD CONNECTION	28
3.2.2 Simulation of the U-PLATE INERD CONNECTION	29
3.2.3 Design for static combinations	31
3.3 Seismic analysis.....	32

3.3.1	Seismic design situation.....	32
3.3.2	Response Spectrum Analysis	32
3.4	Detailed design	35
3.4.1	Design properties of the U-PLATE INERD CONNECTION.....	35
3.4.2	Damage limitation – limitation of interstorey drift.....	36
3.4.3	Second order effects	37
3.4.4	Final verification of dissipative U-PLATE INERD CONNECTION	37
3.4.5	Capacity design of non-dissipative members.....	38
3.5	Structural detailing	39
3.6	References.....	40
4	FUSEIS BEAM LINKS	43
4.1	General	43
4.1.1	Introduction	43
4.1.2	Description of building.....	43
4.2	Analysis and dimensioning.....	46
4.2.1	Simulation	46
4.2.2	Design for static and seismic combinations	47
4.3	Detailed design	52
4.3.1	Limitation of interstorey drift – Damage limitation	52
4.3.2	Limitation of interstorey drift – P-delta effects (ULS).....	53
4.3.3	Design of dissipative devices	54
4.3.4	Capacity design of non-dissipative members.....	55
4.3.5	Lateral torsional buckling	55
4.3.6	FUSEIS columns.....	56
4.3.7	FUSEIS beam links	57
4.3.8	Shear panel verification.....	58
4.3.9	Seismic link classification.....	59
4.4	Structural detailing	59
4.5	Conclusions.....	61
4.6	References.....	61
5	FUSEIS PIN-LINK SYSTEM	63
5.1	General	63
5.1.1	Introduction	63
5.1.2	Description of the FUSEIS pin link system.....	63
5.1.3	Geometry and general assumptions	65
5.2	Basic and non-seismic design.....	67

5.2.1	Simulation	67
5.2.2	Analysis and design	67
5.3	Seismic analysis.....	71
5.3.1	Seismic design	71
5.3.2	Limitation of inter-storey drift.....	71
5.3.3	Magnitude of 2 nd order effects.....	72
5.3.4	Dissipative elements verifications	72
5.3.5	Non-dissipative elements verifications	74
5.4	Structural detailing	76
5.5	References.....	79
6	BOLTED FUSEIS BEAM SPLICE	81
7	WELDED FUSEIS BEAM SPLICE.....	83
7.1	General	83
7.1.1	Introduction	83
7.1.2	Description of the building.....	83
7.2	Basic and non-seismic design.....	88
7.2.1	Preliminary design of the welded FUSEIS beam splices and reinforcing zones	88
7.2.2	Simulation	90
7.2.3	Design for static combinations	91
7.2.4	Seismic analysis	92
7.3	Detailed design	94
7.3.1	Damage limitation – limitation of inter-story drift	94
7.3.2	Second order effects	95
7.3.3	Final verification of the welded FUSEIS beam splices	97
7.3.4	Final verification of the conventional bracings.....	98
7.3.5	Capacity design of non-dissipative elements and members	99
7.4	Structural detailing	100
7.5	References.....	103
8	REPLACEABLE BOLTED LINKS	105
8.1	Introduction	105
8.2	Description of building	105
8.2.1	Geometry and general assumptions	105
8.2.2	Modelling for linear elastic analysis.....	107
8.3	Persistent design situation	108
8.3.1	Ultimate Limit State	108

8.3.2	Serviceability Limit State	108
8.4	Response spectrum analysis	108
8.5	Global imperfections and 2 nd order effects	108
8.6	Seismic design	108
8.6.1	Ultimate Limit State - Dissipative elements design	109
8.6.2	Ultimate Limit State – Non - dissipative elements design.....	109
8.6.3	Limitation of inter-story drift.....	110
8.6.4	Dual configurations	110
8.6.5	Weak beam-strong column	111
8.6.6	Re-centring verification	112
8.6.7	Links removal and frame re-centring.....	114
8.7	Structural detailing	115
8.8	References.....	118
9	REPLACEABLE SHEAR PANELS.....	120
9.1	General	120
9.1.1	Introduction	120
9.1.2	Description of building.....	120
9.1.3	Persistent design situation	123
9.1.4	Response spectrum analysis	125
9.1.5	Global imperfections and 2 nd order effects	126
9.1.6	Seismic design	126
9.1.7	Re-centring verification	130
9.2	Structural detailing	130
9.3	References.....	133
10	CBF-MB	134
10.1	General	134
10.1.1	Introduction	134
10.1.2	Description of building.....	134
10.2	Basic and non-seismic design.....	137
10.2.1	Preliminary selection of modified braces	137
10.2.2	Preliminary check of brace slenderness.....	139
10.2.3	Simulation	140
10.2.4	Design for static combinations	141
10.3	Seismic analysis.....	142
10.3.1	Seismic design situation.....	142
10.3.2	Response Spectrum Analysis	143

10.4 Detailed design	145
10.4.1 Damage limitation – limitation of interstorey drift.....	145
10.4.2 Second order effects	145
10.4.3 Final verification of dissipative members.....	146
10.4.4 Transition stage	147
10.4.5 Capacity design of non-dissipative members.....	148
10.5 Structural detailing	149
10.6 References.....	153
11 SSCD	154
11.1 General	154
11.1.1 Introduction	154
11.1.2 Description of the building.....	154
11.2 Preliminary design.....	156
11.2.1 Determination of actions	156
11.2.2 Pre-sizing of structural elements – Pinned steel frames	157
11.2.3 Pre-sizing of structural elements – SSCD	158
11.2.4 Pre-sizing of structural elements – r.c. shear walls	159
11.2.5 Modelling and structural analysis of the case study	160
11.2.6 Optimization of proposed solution	168
11.3 Conclusions.....	175
11.4 References.....	176
12 TRSH.....	178
12.1 General	178
12.2 Design rules	178
12.2.1 General	178
12.2.2 Preliminary design.....	179
12.2.3 Design for linear elastic analysis.....	180
12.3 High-rise case-study building	183
12.3.1 Description of the building frame.....	183
12.3.2 Preliminary design.....	185
12.3.3 Linear elastic analysis	188
12.4 Conclusions.....	194
12.5 References.....	195
12.6 Annex A: “FEMA 695” q-factor estimation	195
13 MSSH.....	198
13.1 General	198

13.2 Design rules	198
13.2.1 General	198
13.2.2 Preliminary design.....	199
13.2.3 Design for linear elastic analysis	200
13.3 High-rise case-study building	203
13.3.1 Description of the building frame.....	203
13.3.2 Preliminary design.....	205
13.3.3 Linear elastic analysis	207
13.4 Conclusions.....	214
13.5 References.....	214
13.6 Annex A: “FEMA 695” q-factor estimation	215

1 INTRODUCTION

This Volume presents twelve elaborated case studies demonstrating implementation of innovative seismic systems and devices in earthquake-resistant structural design. They have been developed within the activities of the European disseminating project INNOSEIS by eight academic and one industrial partners. The Volume illustrates conceptual planning, analysis based on code adopted methods, design and detailing for practical applications of specific joints and connections.

The case studies are based on the specific recommendations presented in “Volume with pre-normative design guidelines for innovative devices” where supplementary clauses of EN 1998-1 are formulated and are in compliance with the design philosophy and methodology of EN 1998-1, 2004.

Almost all working examples have been developed on a provisory design project for new four or eight-storey office building that will be built in high seismicity area.

The case study in chapter 2 combines two systems (INERD PIN CONNECTIONS and BOLTED FUSEIS BEAM SPLICE) so it is a proper example for implementation of more novelties in one design project.

2 INERD PIN CONNECTIONS

2.1 General information

2.1.1 Introduction

In the frame of the European Research Programs “Dissipative devices for seismic resistant steel frames” RFSR-CT-2008-00032 (Acronym: FUSEIS) and “Two Innovations for Earthquake Resistant Design” (Acronym: INERD) under contract number 7210-PR-316, two innovative dissipative systems, named FUSEIS2 and INERD™ pin connections were introduced and relevant design guides developed. Current report presents the high-mid-rise case study (4-storey) equipped with both FUSEIS bolted beam splices and INERD pin connections, as well as it introduces the design procedures for steel and composite buildings in which the systems are used as seismic resistant systems.

The case study elaborated comprises the conceptual design, modelling and analysis by linear response spectrum analysis methods (RSA), detailed design of main dissipative and non-dissipative members and basic structural detailing of some connections.

2.2 Description of the building

2.2.1 Geometry and general assumptions

An archetype configurations which are vertically regular and square-plan, have been selected. The building considered as a general office (class-B) and it is designed according to EN1993-1 [1] /EN1998-1 [2] and to the specific design guideline of the dissipative system [3].

A common plan view has been selected for the building. The number of bays in both direction is 3 with a span length of equal to 8m. The height of each story is set to be 4m. The building consists of a steel-concrete composite moment resisting frame in the Y direction and concentrically braced steel frame in X direction. Bolted beam splices are included in the structure at the end of the all beams in Y direction, (FUSEIS bolted beam splice) [4], while the INERD™ [5] pin connections are equipped at the end of all steel bracing elements in X direction. The concentric bracing system is located to accommodate the columns around their weak axis bending and the FUSEIS bolted beam splices are located in the direction along which the column are placed with strong axes bending. Diaphragms are assumed rigid, thus neglecting membrane (in-plane) deformations.

2.2.2 Material

2.2.2.1 Non-dissipative zones

The materials used in the three buildings are given below:

- Structural steel: S355
- Concrete: C25/30

- Steel sheeting: Fe320
- Reinforcing steel: B500C

2.2.2.2 Dissipative zones

During the earthquake, it is expected that the dissipative zones yield before other zones i.e., non-dissipative zones, hence, according to EC 1998-1, the yield strength $f_{y,max}$ of the dissipative zones must be satisfied by Eq. (2.1).

$$f_{y,max} \leq 1,1 \gamma_{ov} f_y \quad \text{Eq. (2.1)}$$

where

γ_{ov} is the overstrength factor, the recommended value is 1.25

f_y is the nominal yield strength of the steel

2.2.2.3 Loads and load combinations

A summary of the applied loads is given in the following; and Table 2.1 represents the coefficients for the various load combinations.

- Dead Loads:
2.75 kN/m² composite slab + steel sheeting
- Superimposed Loads:
Services, ceiling, raised floor: 0.70 kN/m² for intermediate floors
1.00 kN/m² for top floor
Perimeter walls 4.00 kN/m
- Live Loads:
Offices (Class B): 3.00 kN/m²
Movable partitions 0.80 kN/m²
Total live load: 3.80 kN/m²
Snow load to be ignored
- Seismic Load:
Importance factor: $\gamma_I = 1.0$
Peak ground acceleration: $\alpha_{gR} = 0.20 \cdot g$
Ground Type C – Type 1 spectrum:
 $S = 1.15$ $T_B = 0.20 \text{ sec}$ $T_C = 0.60 \text{ sec}$ $T_D = 2.00 \text{ sec}$
Lower bound factor: $\beta = 0.2$
Vertical ground acceleration to be ignored.
Behaviour factor $q=4$

Table 2.1: Coefficients for the various load combinations

Coefficient	Value
γ_G	1.35
γ_Q	1.50
Ψ_2 Office (Class B)	0.30
Ψ_2 Roof	0.00
φ Correlated floors	0.80
φ Roof	1.00

The seismic masses are calculated according to Eq. (2.2) and presented in Table 2.2.

$$\sum_{j>1} G_{k,j} + \sum_{i>1} \Psi_{2,i} \cdot \varphi_i \cdot Q_{k,i} \quad \text{Eq. (2.2)}$$

Table 2.2: Quantification of seismic masses

Seismic mass for typical floors		317.52 t
Concrete and metal deck self-weight + Composite IPE and HEA + IPE450 (Gk1,1)	$(2.75 \cdot 24.0 \cdot 24.0 + 73.01 + 59.63 + 85.717) / 9.81$	183.73 t
Utilities, ceiling, floor finishing (Gk2,1)	$0.70 \cdot 24.0 \cdot 24.0 / 9.81$	41.10 t
Perimeter walls (Gk3,1)	$4 \cdot 4 \cdot 24 / 9.81$	39.14 t
Partitions (Qk1,1)	$0.8 \cdot 0.3 \cdot 0.8 \cdot 24 \cdot 24 / 9.81$	11.27 t
Imposed loads (Qk2,1)	$0.8 \cdot 0.3 \cdot 3.0 \cdot 24 \cdot 24 / 9.81$	42.28 t
Seismic mass for roof		242.44 t
Concrete and metal deck self-weight + Composite IPE and HEA + IPE450 (Gk1,2)	$(2.75 \cdot 24.0 \cdot 24.0 + 73.01 + 59.63 + 85.717) / 9.81$	183.73 t
Utilities, ceiling, floor finishing (Gk2,2)	$1.00 \cdot 24.0 \cdot 24.0 / 9.81$	58.72 t
Imposed loads (Qk,1)	$0 \cdot 1 \cdot 24.0 \cdot 24.0 \cdot 3 / 9.81$	0.00 t
Columns and CBF mass		27.22 t
Total		587.18 t

2.3 Seismic analysis

2.3.1 Simulation

A building with both FUSEIS bolted beam splice and INERD pin connections may be simulated with a linear-elastic model by appropriate beam elements. The simulation has done based on the design rules which are intended to ensure that yielding, will take place in the fuse prior to any yielding or failure elsewhere. Therefore, the design of buildings with FUSEIS bolted beam splice and INERD pin connections is based on the assumption that the fuses are able to dissipate energy by the formation of plastic bending mechanisms.

The modelling of the buildings were performed by means of the finite element program SAP2000. All beams and columns were simulated as beam elements, while no-section shell elements were used for the distribution of the load's area. Figure 2.1 shows the schematic view of the building under the consideration.

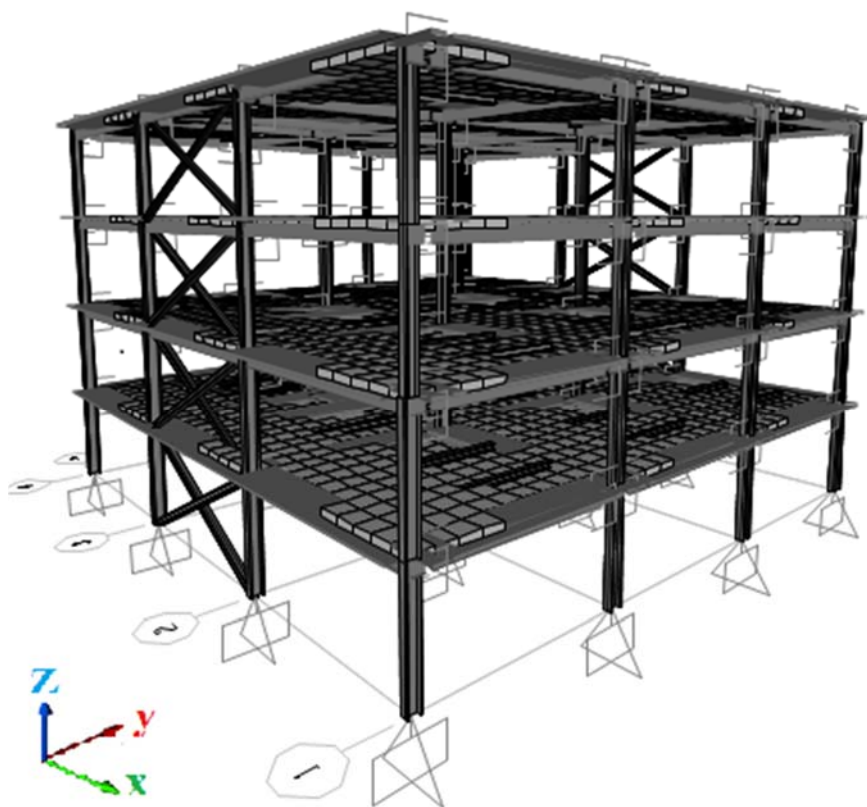


Figure 2.1: Schematic View of the 4-Storey Building

2.3.2 Seismic design situation

Since, the building is recognized as regular in plan and in height. Hence, theoretically the center of masses and the center of rigidity are coincide. according to EC 1998-1:2004 [2], to account for uncertainties in the location of masses and thus for the rotational component of the seismic motion, additional accidental mass eccentricity of 5% in both directions are considered. To account for the torsional

effects, the story seismic forces in both main directions were calculated based on the lateral force method of EC 1998-1: 2004 [2]. The final seismic design situation accounting for accidental torsional effects was derived by Eq. (2.3) and Eq. (2.4).

$$E = E_x + 0.3E_y \pm T \quad \text{Eq. (2.3)}$$

$$E = 0.3E_x + E_y \pm T \quad \text{Eq. (2.4)}$$

Where:

T is considered as $T_x + T_y$;

T_x and T_y are accidental torsional effects of applied story seismic force with eccentricity of 5% in X and Y direction, respectively;

E_x and E_y are results of analysis without accidental torsion by applying RSA in X and Y direction, respectively.

The seismic combination is calculated according to Eq. (2.5).

$$\sum_{j>1} G_{k,j} + \sum_{i>1} \psi_2 \times Q_{k,i} + E \quad \text{Eq. (2.5)}$$

where:

$G_{k,j}$ is the gravity load effects in seismic design situation;

$Q_{k,i}$ is the movable load effects in seismic design situation;

ψ_2 is given in Table 2.1;

E is the effect of the seismic action including accidental torsional effects.

2.3.3 Response Spectrum Analysis

The response spectrum analysis which permits the multiple modes of response of a building to be taken into account in the frequency domain is considered in design scenario. In this kind of analysis, the response of a structure defined as a combination of many modes that in a vibrating string correspond to the harmonics. For each mode, a response is read from the design spectrum, based on the modal frequency and the modal mass then, they are combined to provide an estimate of the total response of the structure by calculating the magnitude of forces in all directions. The combination method used in this research is square root of the sum of the squares (SRSS).

The first, second and third natural modes of vibrations are presented Figure 2.2. They correspond to the X and Y translational and the torsional mode, in that order. The results from the analysis are summarized in Table 2.3. The table indicates that 2 more translational modes were needed to activate the modal mass participation more than 90% of the total mass in Y-direction.

Table 2.3: Modal mass participating ratio and periods of vibration

Mode no.	Translation	Period [s]	Mass participating in X-direction (%)	Mass participating in Y-direction (%)
1	Y	1.17	0.00	72
2	X	1.12	81	0.00
3	TORSION	0.82	0.00	0.00
4	Y	0.41	0.00	13
5	X	0.36	12	0.00
6	TORSION	0.27	0.00	0.00
7	Y	0.26	0.00	10
8	X	0.2	4	0.00
Sum of mass participating			97	95

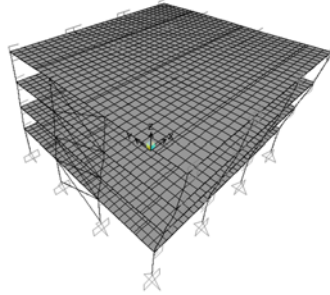
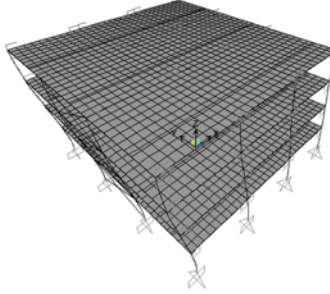
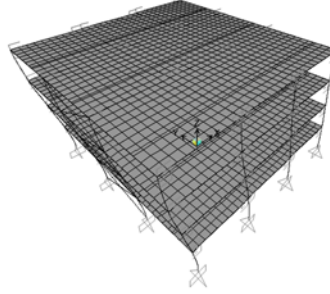
Mode I	Mode II	Mode III
		
Translation in Y	Translation in X	Torsional

Figure 2.2: Natural fundamental vibration

2.4 Design Summary

2.4.1 Design of building without dissipative elements

2.4.1.1 Design Process

In the building design process, the cross-sections of the relevant structural elements should be first pre-designed for the same building but without any dissipative elements i.e. Bolted Beam Splice and INERD pin connection, considering the relevant limit states. The bolted beam splices then should be included at the all beam ends that belong to the MRF system. While INERD pin connection should be included at the ends of all bracing in the CBF system.

2.4.1.2 Simulation

The analysis and design of the building, was performed by means of the finite element program SAP2000. The composite slabs were designed by the program SymDeck Designer, which takes into account construction phases both for the ultimate and serviceability limit states. Columns are designed as steel members, with their section varying depending on the floor.

For all floors IPE450 has been chosen for primary composite beams. Secondary beams are composite and simply supported with steel profile HEA200. Construction phases were critical for the design of these beams, so temporary supports need to be placed in order to reduce both bending deformation and section size. Slabs are composite for all floors. They have been designed and checked according to the requirements of EuroCode 4 [6] for all possible situations and no temporary supports are needed during construction phases.

Figure 2.3 shows the plan view of the case study. Figure 2.4 and Figure 2.5 represent the archetype structure and elevation view of the examined case study in Y-direction and X-direction, respectively. Finally, Figure 2.6 represents the schematic representation of the composite slab. The thickness of the steel sheet is 0.80mm and the longitudinal reinforcement is Ø8/100. The steel beam is assumed to be connected to the concrete slab with the full shear transfer.

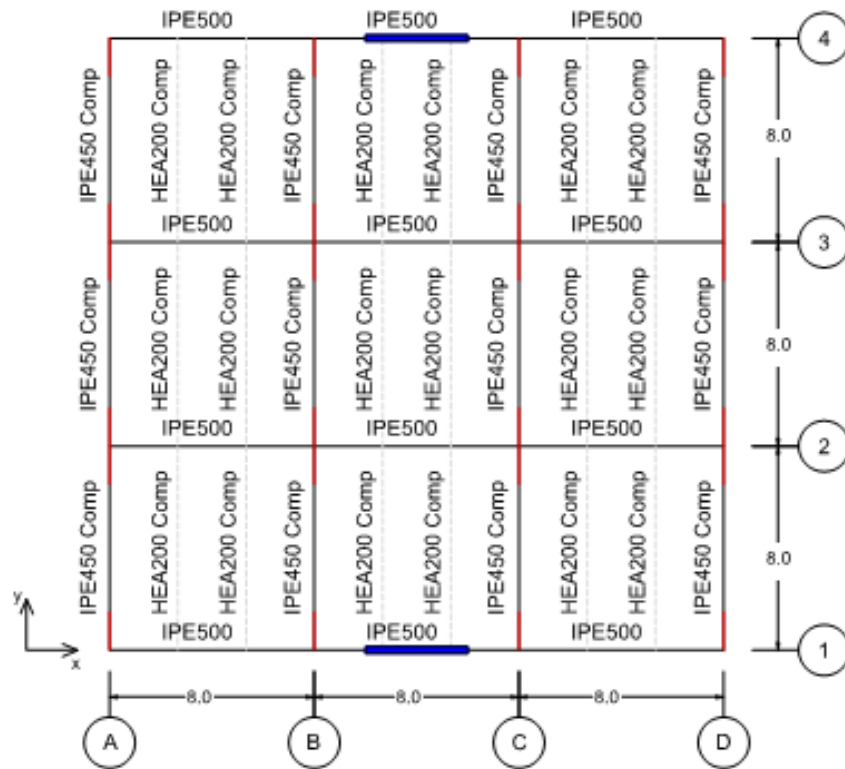


Figure 2.3: Plan view of the case study building

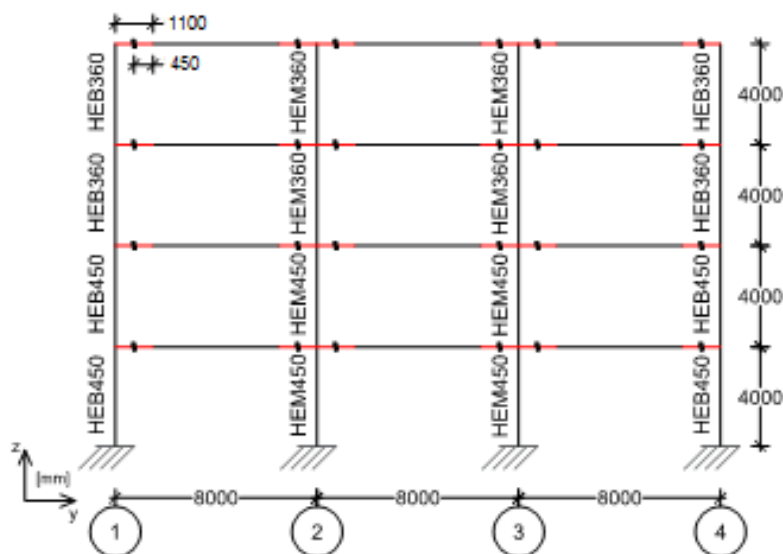


Figure 2.4: Side view of the case study building in Y-direction

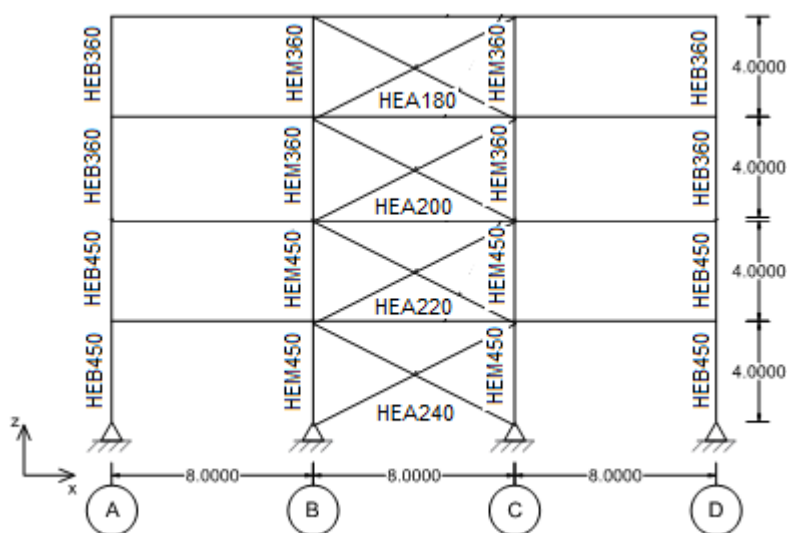


Figure 2.5: Side view of the case study building in X-direction

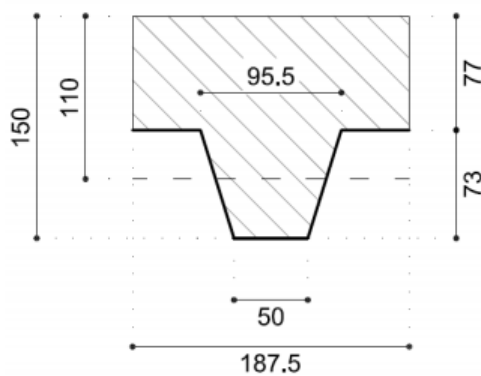


Figure 2.6: Schematic representation of the composite slab

2.4.2 Design of buildings with FUSEIS bolted beam splices

To design a building equipped with FUSEIS bolted beam splices, different steps should be carried out.

After designing the conventional building without dissipative elements and verification of all codified requirements according to EC 1993-1-1: 2005 [7] and EC 1998-1: 2004 [2]. At the end of this step, the cross sections of the steel columns and the composite steel-concrete beams are selected. Using a response spectrum reduced to the elastic one by behaviour factor assumed (in first iteration) according to EC8, seismic response spectrum analysis (RSA) on the building is performed and the bending moment M_{Ed} at the ends of the beams are identified. These values are taken as reference for the performance required to the dissipative beam splices in terms of moment resistance ($M_{Ed} \approx M_{y, fuse}$). In fact, in the building subjected to the design seismic actions (ULS), the exploitation of the post-elastic resources of the dissipative and reparable joints is to be guaranteed. It is worth noting that the distribution of the bending moment associated to seismic actions is not uniform along the different floors, resulting that the beams of lower stories are more stressed than the ones of the upper levels. This observation leads to assume several reference resistance thresholds of beam splices for multi-storey buildings. Therefore, the final layout of the structure should be characterized by increasing beam splice dimensions for lower beam levels in order to activate a global collapse mechanism and avoid the onset of brittle soft-storey mechanisms.

2.4.2.1 Design of Bolted Beam Splices

Generally, two main parameters of the joints govern the verification results: the bending moment resistance and the initial elastic stiffness of the FUSEIS beam splices.

Once it is clear the moment resistance and the stiffness level required to verify the structure, the geometrical properties of beam splices have been finalized.

The area of flange plate for storey 3 and 4 is calculated referring to the hogging moment resistance required (230 kNm).

The level arm z is calculated from the center of rotation in the middle of the rebars and the flange plate.

$$z = h_a + h_p + \frac{h_c}{2} = 450mm + 73mm + \frac{77}{2}mm = 561.5 mm \quad \text{Eq. (2.6)}$$

$$A_{f, fuse} = \frac{M_{Rd, fuse}^-}{f_{yd} z} = \frac{150 \times 10^6 Nmm}{\frac{235}{1.15} \frac{N}{mm^2} \times 561.5 mm} = 1307 mm^2 \quad \text{Eq. (2.7)}$$

Fixing the width of the flange plate equal to 170 mm, slightly lower than the flange width of the steel beam IPE450 (190 mm); the thickness of the plate is obtained.

$$t_{f,fuse} = \frac{1307 \text{ mm}^2}{170 \text{ mm}} = 7.7 \text{ mm} \quad \text{Eq. (2.8)}$$

Therefore, a thickness of 8 mm is selected. The web plates of the bolted beam splice are designed to resist shear forces only. According to the capacity design principles, the maximum shear forces that could possibly be developed on the beam ends depend on the resistant capacities of the beams. Table 2.4 shows the dimension of the flange and web plates.

Table 2.4: Dimension of the flange plates

Storey	Flange Plate (mm)	Web Plate (mm)
1-2	170x8	170x6
3-4	170x10	170x6

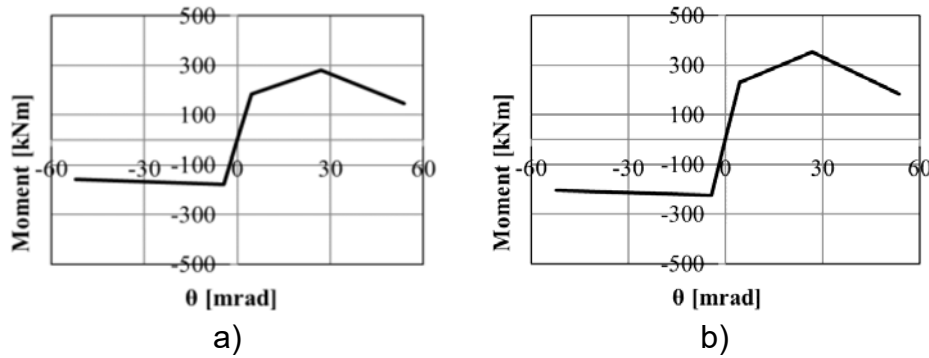


Figure 2.7: Beam Splices Hysteresis Rule in Terms of Moment-Rotation a)170x8mm b)170x10mm

The free buckling length is calculated for the beam splices.

$$L_0 = \frac{2 \sqrt{2} M_p}{A f_y \sqrt{\varepsilon}} = \frac{2 \sqrt{2} \times \left(\frac{1}{4}\right) \times 170 \text{ mm} \times 8 \text{ mm}^2 \times 235 \text{ N/mm}^2}{8 \text{ mm} \times 170 \text{ mm} \times 235 \text{ N/mm}^2 \times \sqrt{0.002}} = 126 \text{ mm} \quad \text{Eq. (2.9)}$$

Therefore, a free buckling length equal to 130 mm is applied for all beam splice joints.

In order to design the rebars, to optimize the solution, an iterative procedure should be conducted, aiming at obtaining a lower amount of rebar quantity. The following values were estimated. One should notice that only the rebars positioned within the effective width of the slab will account for the bending resistance.

Table 2.5: Area of longitudinal rebars in the beam splices

	A, upper rebar (mm ²)	A, lower rebar (mm ²)
Beam Splice	6000	3000

The bolts are designed with grade 8.8 M16 having 90mm long so that the shear stresses are transferred through the unthreaded portion of the bolt's body. 2 washers can be employed on the bolts body.

2.4.3 Design of building with INERD pin connection

Braced frames with pin INERD-connections may be designed according to the general rules of EC 1998-1:2004 [2] and EC1993-1-1:2005 [7], duly modified in order to consider that energy dissipation is taking place in the pin connections and not in the tension braces.

The INERD pin connections designed according to Table 2.9 to ensure the more efficient response of the connections, all the geometric requirements given in Table 2.9 are satisfied.

The pin dimensions are 50 x 60 mm, S 235. The clear distance between external and internal eye-bars is equal to $a = 70$ mm.

2.4.3.1 Verification of the brace dimensions

$$N_{Ed} \leq N_{b,Rd} \quad \text{Eq. (2.10)}$$

Table 2.6: Verification of the brace dimensions

Storey	N_{Ed} (kN)	$N_{b,Rd}$ (kN)	Verification Check
1	538	540	OK
2	279	394	OK
3	188	280	OK
4	104	200	OK

$N_{b,Rd}$ buckling resistance of the diagonal

2.4.3.2 Verification of the pin dimensions

Verification of design yield strength of the pin connection ($P_{y,Rd}$)

$$P_{y,Rd} = \frac{P_{y,Rk}}{\gamma_{Mser}} \geq N_{E,ser} \quad \text{Eq. (2.11)}$$

Where $P_{y,Rk}$ is the yield strength of the connection can be calculated by the following formula;

$$P_{y,Rk} = \frac{2 \cdot M_p}{(a/1.1)} \quad \text{Eq. (2.12)}$$

$$M_p = W_{pl} \cdot f_y \quad \text{Eq. (2.13)}$$

$$W_p = bh^2/12 \quad \text{Eq. (2.14)}$$

Where

f_y is the yield stress of pin

M_p is the plastic moment of pin cross section

W_{pl} is the plastic modulus of pin cross section

h is the pin height

b is the pin width

γ_{Mser} is the partial safety factor of resistance (=1.0)

$N_{E,ser}$ is the design force of the diagonal at the damage limitation state can be evaluated by the following criteria

$$N_{E,ser} = \frac{N_{ed}}{\nu} \quad \text{Eq. (2.15)}$$

N_{Ed} is the design force of the diagonal

ν is the reduction factor which takes into account the lower return period of the seismic action associated with the damage limitation requirement equal to 2.5.

Table 2.7: Verification of the pin dimensions

Storey	$P_{y,Rd}$ (kN)	$N_{E,ser}$ (kN)	Verification Check
1	276	269	OK
2	276	166	OK
3	276	117	OK
4	276	83.5	OK

Verification of deformation capacity of the pin connection (δ_{lim})

$$\delta_{lim} = 0.8a \geq \frac{D.H.\cos\varphi}{2} \quad \text{Eq. (2.16)}$$

a is the clear distance between internal and external eye-bars

D is the lateral drift ratio

H is the storey height

φ is the angle of inclination of the diagonal

$$a \geq \frac{D.H.\cos\varphi}{2 * 0.8} = 53.6mm \quad \text{Eq. (2.17)}$$

Verification of design ultimate strength of the pin connection ($P_{u,Rd}$)

$$P_{u,Rd} = \frac{P_{u,Rk}}{\gamma_{M0}} \geq N_{Ed} \quad \text{Eq. (2.18)}$$

Where

$P_{u,Rk}$ ultimate strength of the connection

$$P_{u,Rk} = \frac{4 \cdot M_p}{(a/1.1)} \quad \text{Eq. (2.19)}$$

γ_{M0} partial safety factor of resistance (=1.0)

Table 2.8: Verification of design ultimate strength of the pin connection

Storey	$P_{y,Rk}$ (kN)	N_{Ed} (kN)	Verification Check
1	554	538	OK
2	554	279	OK
3	554	188	OK
4	554	104	OK

2.4.3.3 Verification of eye-bars dimensions

The thicknesses of the eye bars shall additionally verify the following requirements:

Table 2.9: Geometric requirements for INERD pin connections

Shape of the pin cross section	$h \leq b \leq 2 \cdot h$
Minimum distance between plates	$a \geq h$
Thickness of external plates:	$t_{ext} \geq 0.75 \cdot h$
Thickness of internal plates:	$t_{int} \geq 0.5 \cdot t_{ext}$ for two plates $t_{int} \geq t_{ext}$ for one plate
Basic dimensions of an INERD pin connection: b the width of the pin h the height of the pin t_{ext} the thickness of the external plate t_{int} the thickness of the internal plate a the clear distance between the internal and external plates	

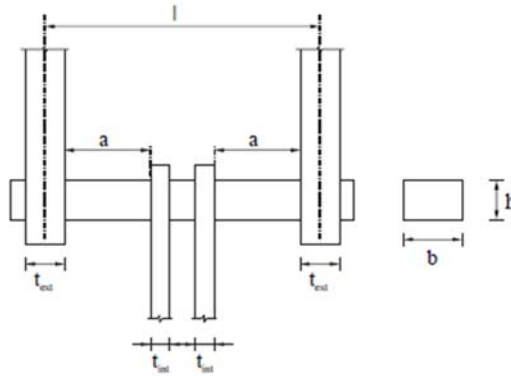


Figure 2.8: INERD pin connection geometry

According to the above mention requirements the dimension of eye bars are chosen as follows:

$$T_{\text{ext}} = 36\text{mm}$$

$$T_{\text{int}} = 18\text{mm}$$

Steel quality of the eye-bars designed to be equal than that of the pin = S235.

Verification of gross sectional failure

The connection element verified for the capacity design as follows:

$$P_{Ed} \leq N_{t,Rd} \quad \text{Eq. (2.20)}$$

Where

P_{Ed} is the capacity design force calculated by the following equation

$$P_{Ed} = 1.3 * P_{Rd} \quad \text{Eq. (2.21)}$$

$$N_{t,Rd} = A \cdot f_y / \gamma_{M1} \quad \text{Eq. (2.22)}$$

Table 2.10: Verification of gross sectional failure

Storey	P_{Ed} (kN)	$N_{t,Rd}$ (kN)	Verification Check
1	699	2478.5	OK
2	362.7	2075.1	OK
3	244.4	1736.3	OK
4	135.2	1462	OK

2.5 Verification of codified limits for the entire building

2.5.1 Damage limitation – limitation of inter-story drift

Assuming that the building has ductile non-structural elements, the verifications is:

$$d_r \cdot v \leq 0.0075h = 0.0075 \cdot 4 = 30 \text{ mm} \quad \text{Eq. (2.23)}$$

where $v = 0.5$ is the reduction factor according to EC 1998-1:2004 §4.4.3.2 (1) [2], h is the story height and d_r is the design inter-story drift. Table 2.11 includes the results from the analysis of each story.

Table 2.11: Check of the lower bound for the horizontal design spectrum

X-Direction				
Story	1	2	3	4
$d_{r,max}$ [m]	0.015	0.016	0.012	0.006
$d_{r,max} \cdot v$ [m]	0.0075	0.008	0.006	0.003
≤ 0.030 [m]	OK	OK	OK	OK
Y-Direction				
Story	1	2	3	4
$d_{r,max}$ [m]	0.026	0.028	0.021	0.012
$d_{r,max} \cdot v$ [m]	0.013	0.014	0.0105	0.006
≤ 0.030 [m]	OK	OK	OK	OK

where $d_{r,max}$ is the maximum design inter-story drift value within each directional earthquake combination, obtained by the production of the elastic inter-story drift and the behavior factor.

2.5.2 Second order effects

The sensitivity to second order effects is estimated by the inter-story drift sensitivity coefficient θ given by Eq. (2.24), where P_{tot} and V_{tot} are the total gravity load at and above the story considered in the seismic design situation and the total seismic story shear at the story under consideration, respectively. Second-order effects (P- Δ effects) need not be taken into account if the following condition is fulfilled in all storeys:

$$\theta = \frac{P_{tot} \cdot d_r}{V_{tot} \cdot h} \leq 0.1 \quad \text{Eq. (2.24)}$$

Table 2.12 gives the calculated values of θ for directional earthquake combination X and Y, respectively.

Table 2.12: 2nd order effects

X-Direction				
Story	1	2	3	4
d_r / h [m]	0.0037	0.004	0.0029	0.0015
P_{tot} [kN]	3841	2874	1876	879
V [kN]	579	466	379	224
Θ [rad]	$0.025 < 0.1$	$0.025 < 0.1$	$0.015 < 0.1$	$0.006 < 0.1$
Y-Direction				
Story	1	2	3	4
d_r / h [m]	0.0065	0.0071	0.0053	0.0029
P_{tot} [kN]	3841	2874	1876	879
V [kN]	579	466	379	224
Θ [rad]	$0.043 < 0.1$	$0.044 < 0.1$	$0.026 < 0.1$	$0.011 < 0.1$

2.5.3 Soft Storey Constraint

Since, in multi-storey buildings formation of a soft storey plastic mechanism shall be prevented, as such a mechanism might entail excessive local ductility demands in the columns of the soft storey. Hence, the following condition should be satisfied at all joints of primary or secondary beams with primary columns:

$$\sum M_{RC} \geq 1.3 \sum M_{Rb} \quad \text{Eq. (2.25)}$$

Where

$\sum M_{RC}$ is the sum of the design values of the moments of resistance of the columns framing the joint.

$\sum M_{Rb}$ is the sum of the design values of the moments of resistance of the beams framing the joint.

Table 2.13: Soft Storey Checking

Storey	$\sum M_{RC}$		$\sum M_{Rb}$		Condition
	Interior	Exterior	Interior	Exterior	
1	2x2453 kN.m	2x1296 kN.m	2x117 kN.m	1117 kN.m	OK
2	2x2453 kN.m	2x1296 kN.m	2x117 kN.m	1117 kN.m	OK
3	2x2453 kN.m	2x1296 kN.m	2x117 kN.m	1117 kN.m	OK
4	2x2453 kN.m	2x1296 kN.m	2x117 kN.m	1117 kN.m	OK

Note that, 2 denotes the number of columns or beams in the relevant direction.

2.6 Structural detailing

The following Figures describe the structural detailing for FUSEIS Bolted Beam Splices of the flange plate equal to 170x8mm and INERD Pin Connections as an example for the third storey.

2.6.1 FUSEIS Bolted Beam Splices

Figure 2.9 shows the overall detailing of the FUSEIS system followed by section A-A and section B-B.

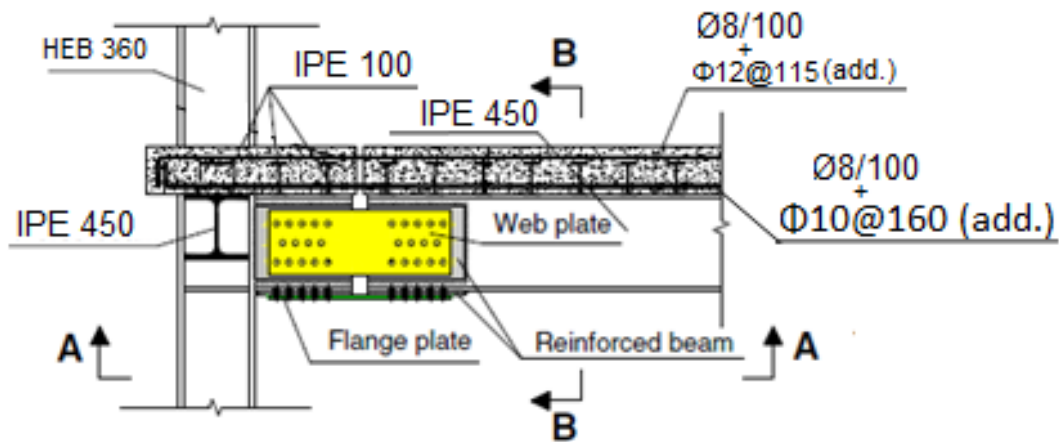


Figure 2.9: Overall Detailing of the FUSEIS System

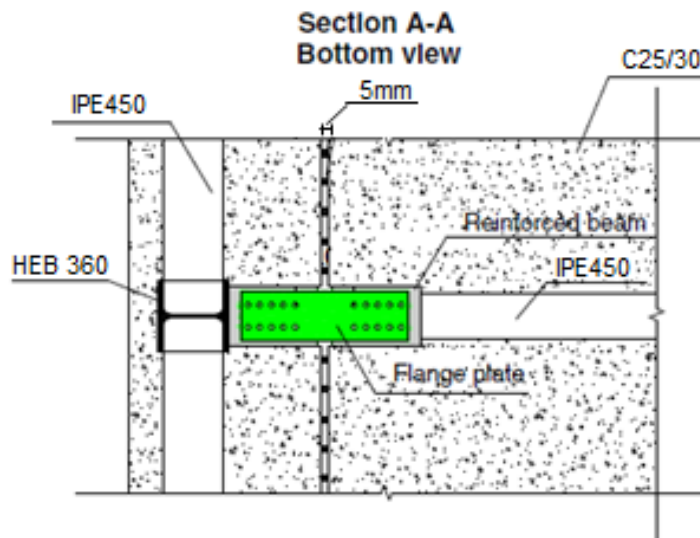


Figure 2.10: Section A-A, Bottom View

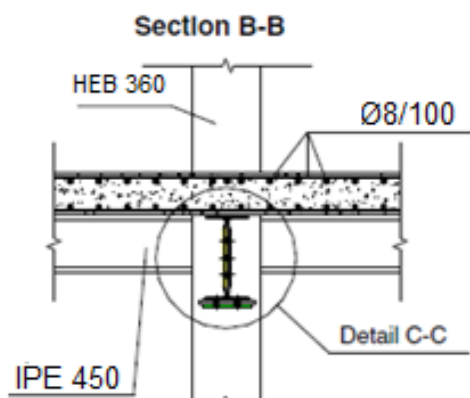


Figure 2.11: Section B-B, Front View

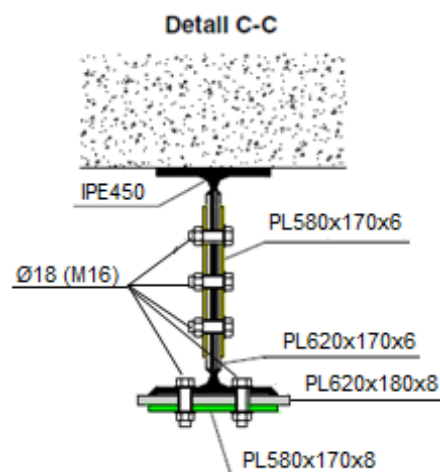


Figure 2.12: Detail C-C, FUSEIS and Additional Plates

Figure 2.13 and Figure 2.14 display the typical web and flange plate, respectively.

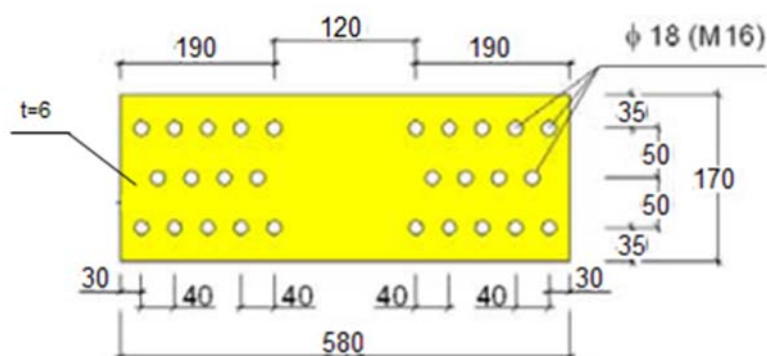


Figure 2.13: Typical Web Plate

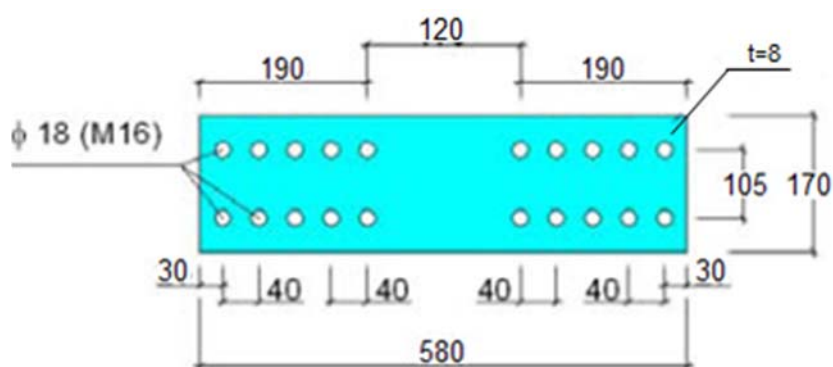


Figure 2.14: Typical Flange Plate

2.6.2 INERD Pin Connections

Figure 2.15 represents the overall view of INERD pin connections followed by detail A-A, Figure 2.16, and detail B-B, Figure 2.17.

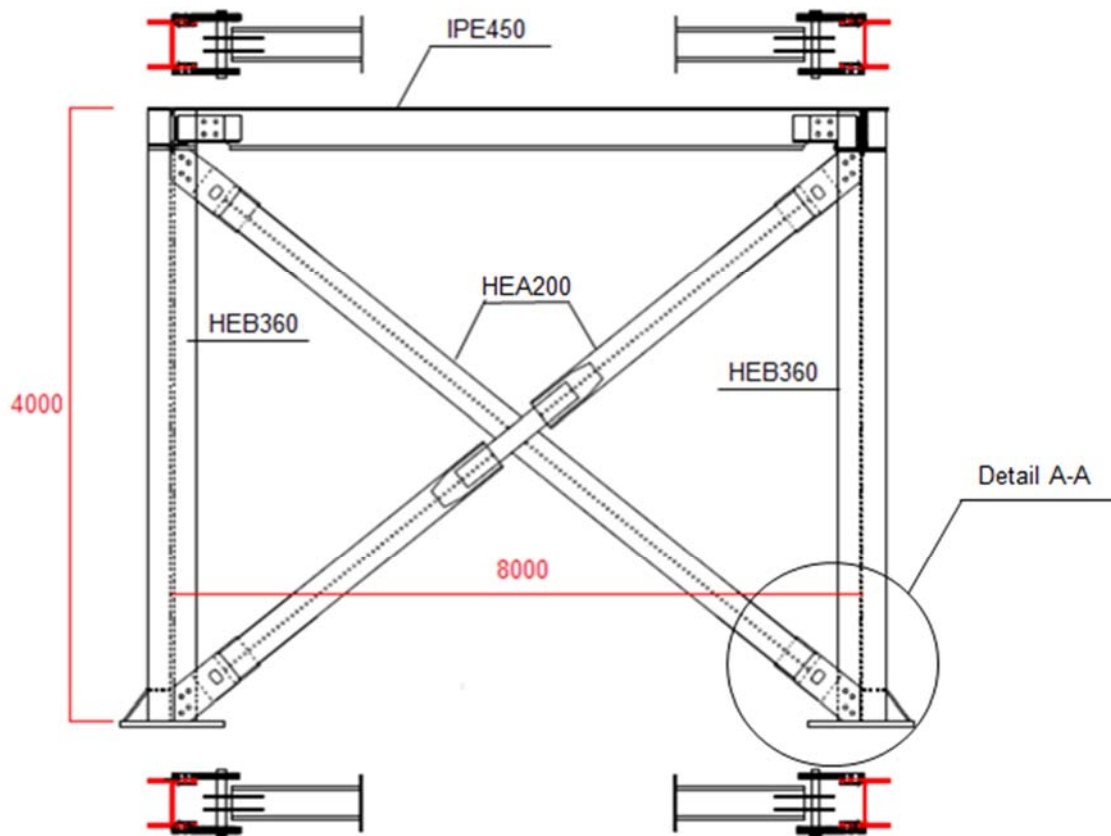


Figure 2.15: Overall View of INERD Pin Connections

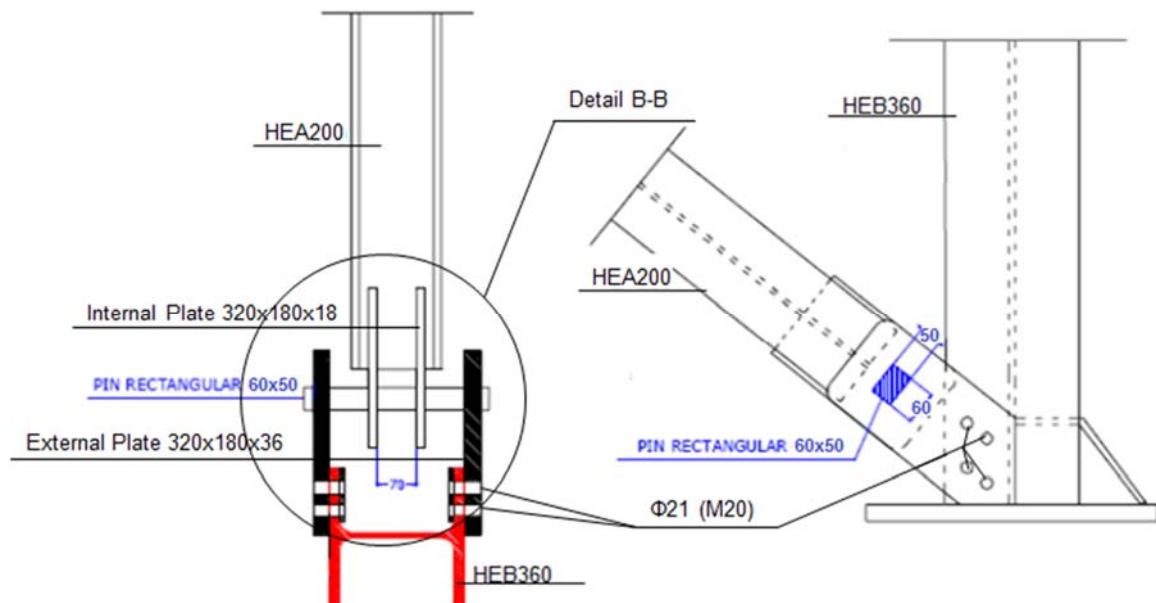


Figure 2.16: Detail A-A

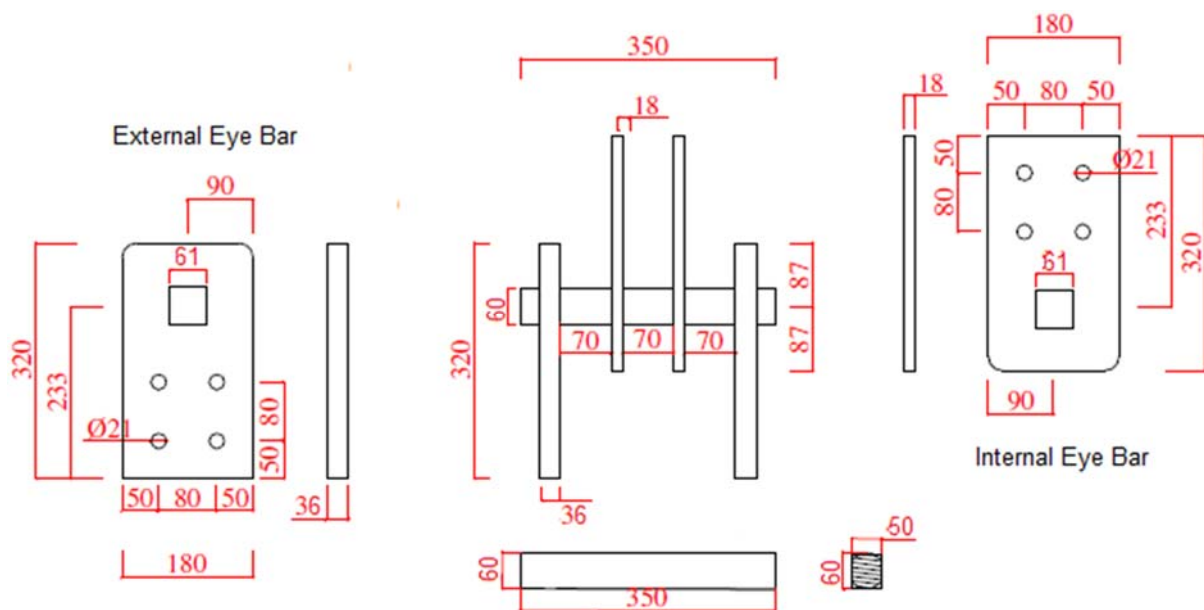


Figure 2.17: Detail B-B

2.7 References

- [1] "EN 1993-1-1: Eurocode 3: Design of Steel Structures. Part 1-1: General Rules and Rules for Buildings," 2005.
- [2] *EC 1998-1: 2004 Design of Structures for Earthquake Resistance-part 1: General rules, seismic actions and rules for buildings.* British Standards, 2004.
- [3] *INNOSIS Project RFCS-02-2015, Valorization of Innovative Anti-Seismic Devices, DESIGN GUIDELINES, Deliverable 3.2.* ECCS, 2017.
- [4] C. Castiglioni, A. Drei, A. Kanyilmaz, L. Calado, and I. Vayas, "Numerical and Experimental Results of Project FUSEIS (Seismic Resistant Composite Steel Frames)," 2012.

- [5] A. Plumier, C. Doneux, C. Castiglioni, and J. Brescianini, *Two INnovations for Earthquake Resistant Design: The INERD Project*. 2006.
- [6] “EC 1994-1-1:2004; Eurocode 4: Design of Composite Steel and Concrete Structures-Part 1-1: General rules and rules for buildings,” *Eur. Stand.*, 2004.
- [7] *EC 1993-1-1: 2005; Design of steel structures —Part 1-1: General rules and rules for buildings*. 2005.

3 CBF- U-PLATE INERD CONNECTION

3.1 General

3.1.1 Introduction

This case study refers to the seismic design of a new four-storey steel office building. It aims at demonstration of implementation of the Concentrically Braced Frames with U-Device developed within the INERD research project (U-PLATE INERD CONNECTION). The case study elaborated refers to conceptual design, modelling and analysis by linear response spectrum analysis methods (RSA), detailed design of main dissipative and non-dissipative members and basic structural detailing of U-PLATE INERD CONNECTION. The design of members and connections is performed according to [1, 2]. Given flexibility that the U-PLATE INERD CONNECTION introduces in the structural response, the structure becomes too sensible to 2nd order effects and therefore it is not recommended to be implemented in high-rise buildings. Thus, no example is presented for buildings with more than 4 storey.

3.1.2 Description of building

3.1.2.1 Geometry and general assumptions

The case study deals with a four-storey frame building with three 8m bays in both directions. The gravity frames are composed of beams and columns, located at each structural axis. Nominally pinned beam-to-column joints and pinned column bases are assumed. The horizontal resisting systems consist of concentric braces. The U-PLATE INERD CONNECTION is used to perform the connection between braces and columns. Due to the limited resistance and stiffness of these connections, in the present case study 4 braces for each orthogonal direction are considered, as illustrated in Figure 3.1. However, the number of braces in each direction is case dependent and the designer should choose accordingly.

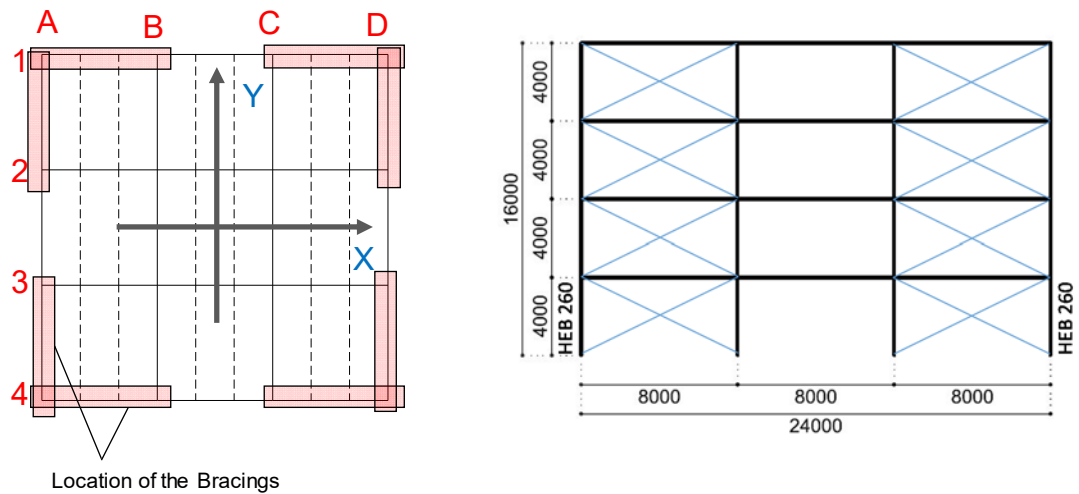


Figure 3.1: Storey plan and elevation

Hot rolled HEB profiles for columns and IPE profiles [3] for storey beams are used for all gravity frames. Both storey slabs (storeys and roof) are designed with steel beams and concrete deck. Composite action with the concrete slab is not considered. However, dowels connecting main and secondary beams to the concrete deck are used to provide structural integration and storey diaphragm action. Diaphragms are assumed rigid, thus neglecting membrane (in-plane) deformations.

The braces consist in hot rolled profiles HEA connected to the columns by means of U-PLATE INERD CONNECTION. The latter consist of one bent U-shaped thick plates (Figure 3.2) and are the dissipative elements of the structure.



Figure 3.2: U-PLATE INERD CONNECTION

3.1.2.2 Materials

At this stage, no model is available for the design of U-PLATE INERD CONNECTION; therefore, the design is based on the results of the experimental tests performed within the research project INERD [3]. In these experimental tests, steel grade S355 was used for the U-PLATE INERD CONNECTIONS.

Both, braces and gravity frame, are designed assuming S355 steel grade. Storey slabs are designed as composite slabs combining steel deck 1mm thickness, concrete C25/30 and reinforcing steel B500B are assumed. The composite slab design is not part of the present report.

3.1.2.3 Loads and load combinations

Table 3.1 summarizes the adopted gravity loads and seismic action parameters. Top storey loads are adopted as accessible roof. It is assumed that snow load intensity is less than the imposed roof load and the altitude of construction site is below 1000 meters. Consequently, the snow load is excluded from the seismic design situation.

Table 3.1: Loads and actions

Vertical loads	
Concrete and metal deck self-weight	2.75 kN/m ²
Utilities, ceiling, storey or roof finishing: – First storeys – Roof	0.70 kN/m ² 1.00 kN/m ²
Facades: Perimeter wall (not considered in the roof).	4.00 kN/m
Partitions, only at first storey	0.80 kN/m ²
Imposed loads 1 st storey (category B): Imposed loads roof (category I → B):	3.00 kN/m ² 3.00 kN/m ²
Seismic action	
Design response spectrum for elastic analysis Reference peak ground acceleration Importance class II (Ordinary building) Ground type Behaviour factor q Damping ratio Factors for storey occupancy Factors for roof occupancy Seismic combination coefficient First storey Roof	Type 1 $a_{g,R} = 0.24g$ $\gamma_I = 1.0$ B ($T_B = 0.15$ s, $T_C = 0.50$ s) 3.0 5% $\varphi = 0.80$ $\varphi = 1.00$ $\psi_2 = 0.30$, $\psi_E = 0.24$ $\psi_2 = 0.30$, $\psi_E = 0.30$

The seismic masses are calculated according to Eq. (3.1) and presented in Table 3.2.

$$\sum_{j>1} G_{k,j} + \sum_{i>1} \psi_{E,i} \cdot Q_{k,i} \quad \text{Eq. (3.1)}$$

Table 3.2: Seismic masses

Seismic mass storey 1, 2 and 3 = 295.3 t	
Concrete and metal deck self-weight – (G _{k1,1})	2.75x24.0x24.0/9.81 = 161.5 t
Utilities, ceiling, storey finishing – (G _{k2,1})	0.70x24.0x24.0/9.81 = 41.1 t
Facades – (G _{k3,1})	4.0x4.0x24.0/9.81 = 39.1 t
Imposed loads – (Q _{k,1}). Ψ_E	3.0x24.0x24.0x0.24/9.81= 42.3 t
Partitions – (Q _{k,2})	0.8x24.0x24.0*0.24/9.81 = 11.3 t
Seismic mass roof = 273 t	
Concrete and metal deck self-weight – (G _{k1,2})	2.75x24.0x24.0/9.81 = 161.5 t
Utilities, ceiling, storey finishing – (G _{k2,2})	1.00x24.0x24.0/9.81 = 58.7 t
Imposed loads – (Q _{k,2}). Ψ_E	3x24.0x24.0x0.3/9.81= 52.8 t
Steel skeleton seismic mass = 113.4 t	

Seismic masses for the building are summarized in Table 3.3.

Table 3.3: Seismic masses per storey

Storey mass = 295.3 t	Roof mass = 273 t	Skeleton mass = 113.4 t
Total seismic mass = 1272.3 t		

3.2 Basic and non-seismic design

3.2.1 Selection of the U-PLATE INERD CONNECTION

As mentioned before, up to this stage no model exists for the design of the U-PLATE INERD CONNECTION and therefore, the selection of the device geometric and material properties has to be based on the experimental tests of the INERD project [3]. Given the flexibility of these connections, the design should be iterative in order to incorporate the connections stiffness in the determination of the fundamental mode and of the seismic forces. These approach is given in detail in the next chapter (§0).

The U-PLATE INERD CONNECTION proposed within the project may have two different configurations, as depicted in Figure 3.3. The difference consists in the position of the U-Plate and consequently on the loading configuration (parallel to the U or Perpendicular to the U). Moreover, the following parameters of U plate may be varied: the bend radius, the width (B), the thickness, and the type of steel. Figure 3.4 illustrates these parameters.

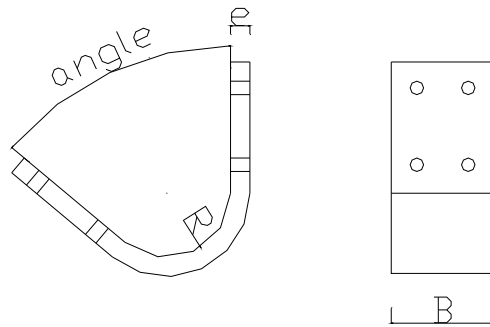
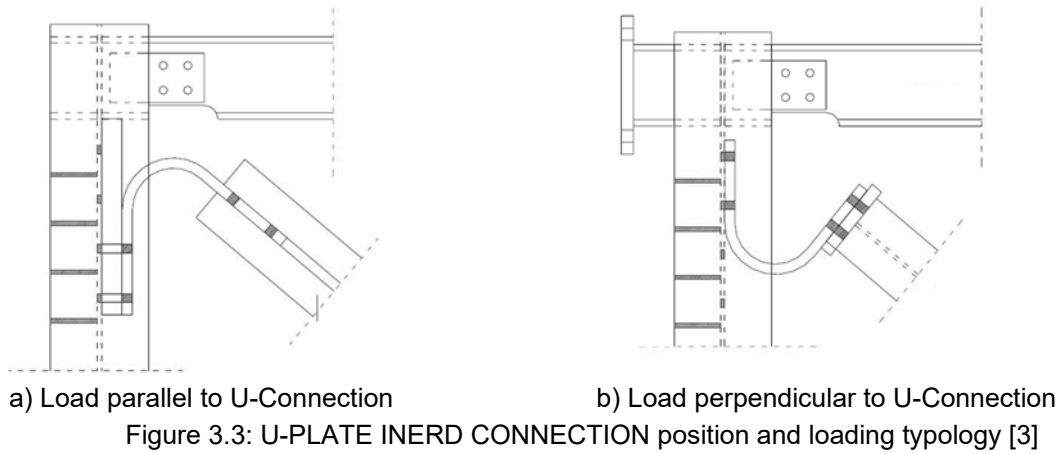


Figure 3.4: Geometric parameters for design of the U-PLATE [3]

3.2.2 Simulation of the U-PLATE INERD CONNECTION

A structural linear elastic model can be developed in any commercial available design software. In the present case study, plane CBF (Figure 3.5) was used in the analysis and modelled in the homemade software FineIG [5]. CBF members are designed and modelled as follows:

- Columns are continuous and pin-connected to the bases;
- Beams are pin-connected to the column;
- Braces are pin-connected to the columns;
- Storeys are not modelled, storey loads are applied on the beams.

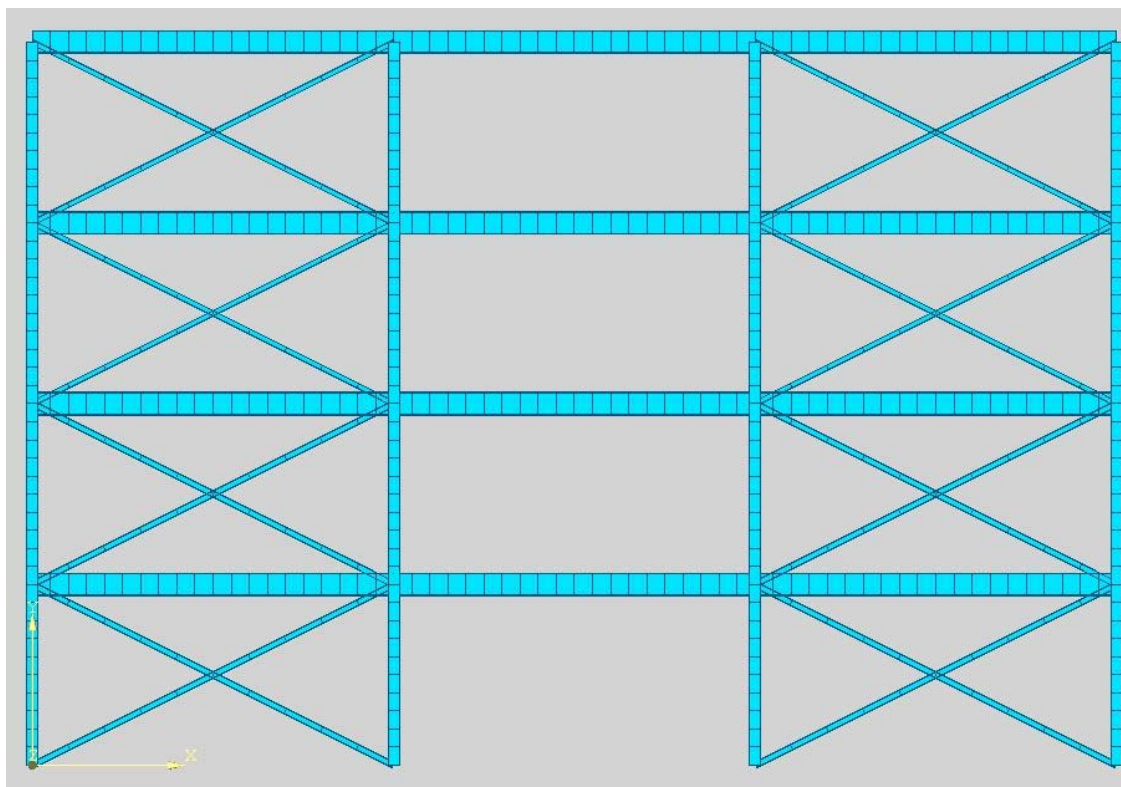


Figure 3.5: FE two-dimensional model

In what concerns the U-PLATE INERD CONNECTION, in a linear elastic model the simplest modelling technique consists in axial elastic spring (Figure 3.6). This spring is used in the connection between the braces and the columns. Because, the design of these connection is iterative, the initial stiffness can be assumed as rigid, in the first calculation. Then, with the selection of the U-PLATE INERD CONNECTION, the model should be improved with the connection axial stiffness. This procedure is further detailed in the next chapter.

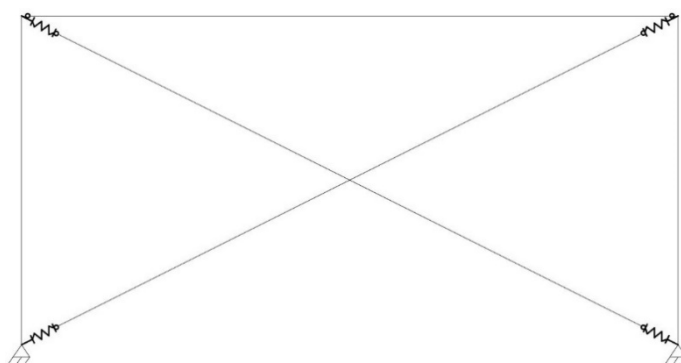


Figure 3.6: Simulation of the U-PLATE INERD CONNECTION in structural model

The current case study was developed by centreline-to-centreline (CL-to-CL) model. It is quick and easy to be defined, since the axis geometry of the frame is known at the beginning of the design process.

3.2.3 Design for static combinations

The design for the static loads, comprising permanent loads and variable loads (imposed loads), is performed previously to the seismic design. In CBF, except for the columns and beams participating in bracing systems, columns and beams are design for gravity loads. In the present case study, is assumed that the seismic design situation governs the design so that wind and snow load are neglected. These considerations are taken into account in the design for static combinations presented hereafter. In what concerns the columns and beams participating in bracing system, these are first design for the static combination and later verified in the seismic design situation.

3.2.3.1 Ultimate limit state results

The ultimate limit state load combination that governs the gravity members design is calculated according to Eq. (3.2).

$$\sum_{j>1} 1.35.G_{k,j} + \sum_{i>1} 1.5.Q_{k,i} \quad \text{Eq. (3.2)}$$

3.2.3.2 Member design

The results from the member design are presented in Table 3.4. As a simplification, it was assumed that all columns are equal (same profile). This is an assumption that may vary from designer/contractor to designer/contractor. In a weight optimized design, corner, edge and internal columns could be differentiated. However, in some situations homogeneity of structural response (e.g. similar connections) and production, all columns are assumed equal. In what respects the beams, these were differentiated according to the direction, remember Figure 3.1, as the loads on the beams varied significantly. In the design verifications according to [2] the following was considered:

- Columns buckling calculated assuming bracings effective (non-sway frame);
- Beams LTB disregarded as the beams are simply supported and the storey slab is assumed to stabilize the upper flange (compression flange).

Table 3.4: Verification of gravity members

Member	Section	Steel grade	N _{Ed} (kN)	M _{y,Ed} (kNm)	M _{z,Ed} (kNm)	Ratio
Secondary beam (Direction Y)	IPE360	S355	-	239	-	0.838
Main beam (Direction X)	IPE500	S355	-	647	-	0.986
Columns	HEB260	S355	-2638	-	-	0.943

3.2.3.3 Serviceability limit state checks

Table 3.5: Verification of member's deflection

Member	Section	Deflection	type	Adopted limit
Secondary beam (Direction Y)	IPE360	1/312	storey	1/300
Main beam (Direction X)	IPE500	1/339	storey	1/300

3.3 Seismic analysis

3.3.1 Seismic design situation

The building is recognized as regular in plan and in height conforming with the criteria in §4.1 of the EN 1998-1 [1]. Thus, the analysis was performed using planar models, one for each main direction. As the structure is perfectly symmetric only the accidental eccentricity (0.05L) is taken into account for the global torsion of the structure and the consequent amplification of the horizontal forces.

The seismic mass results from the gravity actions on the building and is quantified from the following combination of actions Eq. (3.3).

$$\sum G_{k,j} + \sum \psi_{E,i} Q_{k,i} \quad \text{Eq. (3.3)}$$

where:

$G_{k,j}$ are the gravity load effects in seismic design situation;

$\psi_{E,i}$ is the combination factor for variable load effect in seismic design situation;

$Q_{k,1}$ is the imposed load effects in seismic design situation;

3.3.2 Response Spectrum Analysis

As referred above, the flexibility of the U-PLATE INERD CONNECTION is significant and therefore, its behaviour influences the dynamic response of the structure. In order to select the connections to be used, it is necessary to estimate

the loads on the connections and this depends on the estimation of the seismic forces. For this reason, an iterative procedure is necessary. Thus, the first estimation of the structure fundamental mode of vibration is performed using approximation given by Eq. (3.4) as prescribed in §4.3.3 of the EN 1998-1 [1]. Then, the design pseudo acceleration and the base shear are determined using Eq. (3.5) to Eq. (3.7). In Table 3.6 are summarized the results of these calculations.

$$T_1 = C_t H^{2/3} \text{ with } C_t = 0.05 \quad \text{Eq. (3.4)}$$

$$a_g = \gamma_I a_{gR} \quad \text{Eq. (3.5)}$$

$$T_B \leq T \leq T_C: S_d(T) = a_g S \frac{2.5}{q} \quad \text{Eq. (3.6)}$$

$$F_b = S_d(T_1) m \lambda \quad \text{Eq. (3.7)}$$

Table 3.6: Estimation of the base shear – 1st iteration

H [m]	C _t	T ₁ [s]	a _g [m/s ²]	S _d (T ₁) [m/s ²]	λ	F _b [kN]
16.00	0.05	0.4	2.35	1.96	0.85	2122.1

The distribution of the seismic loads through the bracing systems is performed assuming equal lateral stiffness of all braced frames. Consequently, a uniform distribution of the base shear was considered amongst these frames. As referred above, the accidental eccentricity (0.05L) was taken into account for the global torsion of the structure. In Table 3.7 are given the forces per braced frame. Because the structure plan is a square and the brace frames are equally positioned in relation to the geometric centre, the distributed forces are equal in both directions.

Table 3.7: Distribution of seismic forces per braced frame

Frame	F _b [kN]	X [m]	L [m]	δ	F _b ' [kN]
1	1061.0	12	24	1.05	1114.1
4					
A					
D					

The distribution of the masses per story is performed based on the mass of each story and the height of the story to the ground, as expressed in Eq. (3.8). In Table 3.8 are given the forces per story.

$$F_i = F_b \frac{z_i m_i}{\sum z_j m_j} \quad \text{Eq. (3.8)}$$

Table 3.8: Distribution of the seismic forces per story

Storey	z_i [m]	$m \cdot z_i$ [ton.m]	F_i [kN]
1	4	1295	114.6
2	8	2589	229.1
3	12	3884	343.7
4	16	4823	426.7
	$\Sigma m \cdot z_i$	12591	

Then, with the seismic forces per story, the forces on each brace and correspondingly on the U-PLATE INERD CONNECTIONS can be estimated. The selection of the connection configuration is made based on force on the brace and on the results of the experimental tests realized within the INERD project [5]. Subsequently, the connection elastic stiffness is known and can be introduced in the calculation of the fundamental mode. From this step, the calculations of the latter are performed using numerical plane models, as illustrated in Figure 3.5. The detail selection and design of the members is given in the next chapter. It should be remarked, that the connection behaviour in Tension and in Compression differs. As a simplification, the stiffness of the connection was assumed equal for both loading cases, and the mean value from the test results was used.

The selection of the U-Connection configuration has an important constraint which is the angle between the column and the brace. As currently no design model is available for the U-Connection, this constrain limits significantly the selection of the connection configuration. In the present case, this angle is about 63° . Given the variability of the connection resistance with this angle, observed in the experimental tests of the INERD project, the connection properties cannot disregard the angle between column and brace. Accordingly, from the available configurations only one connection fits this practical requirement. It should be noted another conception could be considered adapting this angle through the reduction of the bracing system span and adding additional columns to the braced frames. In the case of several configurations are available, the described iterative procedure can be applied.

Hence, in the present case no iterative procedure to find the optimal solution was performed. Using the selected connection mechanical properties the braces profiles were determined. Then, using the actual bracings and U-Plate connection axial stiffness, the fundamental period of the was determined. In Table 3.9 are summarized the results of the calculation of the seismic forces using the EN 1998-1-1 [1] equation for estimation of the fundamental period and the seismic forces resulting from the fundamental period using the numerical model. These results show the importance of an accurate estimate of the fundamental period. The force

($N_{Ed,Brace}$) presented in Table 3.9 is the force in 1 brace, and consequently, the force used to design the U-PLATE INERD CONNECTION.

Table 3.9: Results of the iterative response spectrum analysis

Iteration	T_1 [s]	F_b [kN]	Storey	$F_{E,i}$ [kN]	$N_{Ed,Brace}$ [kN]	Comment
0	0.4	2122.1	1	114.6	311.4	Design criteria NOT OK. Insufficient connection resistance.
			2	229.1	279.4	
			3	343.7	215.3	
			4	426.7	119.3	
1	1.5	707.4	1	38.2	103.8	Design criteria OK.
			2	76.4	93.1	
			3	114.6	71.8	
			4	142.3	39.8	

3.4 Detailed design

3.4.1 Design properties of the U-PLATE INERD CONNECTION

In Table 3.10 are summarized the properties of the U-Plate connections tested within the INERD project [4]. These properties were used in the design and in the response spectrum analysis described above. As referred before, the connection behaviour differs if the load applied is compression or tension. Thus, in Table 3.10 an $F_{y,min}$ and $F_{y,max}$ are given. The first was used to select the connection configuration, and the second was used in the design of the non-dissipative members. These two values represent the limit of elasticity of the connection. The connection initial stiffness ($K_{ini,con}$) given is the average value between the connection initial stiffness in compression and in tension. The geometric configuration of each connection can be checked in [6].

Table 3.10: U-PLATE INERD CONNECTION mechanical properties [4]

Connection ID	$\alpha_{\text{Column-Brace}}$ [°]	$F_{y,\min}$ [kN]	$F_{y,\max}$ [kN]	$K_{\text{ini,con}}$ [kN/m]
Mola 2	45	98.0	133.0	9973.2
Mola 3	50	90.0	144.0	12825.8
Mola 4	50	153.0	217.0	16101.3
Mola 5	50	114.0	172.0	14908.7
Mola 6	30	63.0	96.0	5798.6
Mola 7	45	75.0	111.0	8577.1
Mola 8	50	77.8	130.0	6368.3
Mola 9	60	127.8	238.9	16812.0
Mola 10	51	127.8	260.0	15221.6
Mola 11	45	146.7	257.8	20915.8
Mola 12	51	205.6	390.0	22523.6

For the present case study, given the limitation on the column-brace angle, the final solution for the connections has only one option and is the following:

- 1st storey: Mola 9
- 2nd storey: Mola 9
- 3rd storey: Mola 9
- 4th storey: Mola 9

3.4.2 Damage limitation – limitation of interstorey drift

Assuming that the building has ductile non-structural elements the verification is:

$$d_r \cdot \nu \leq 0.0075h = 0.0075 \cdot 4000 = 30.0 \text{ mm} \quad \text{Eq. (3.9)}$$

Where $\nu = 0.5$ is the reduction factor according to §4.4.3.2 (1) of [1], h is the story height and d_r is the design interstorey drift. Table 3.11 includes the results from the analysis for each of the stories.

Table 3.11: Limitation of interstorey drift

Storey	1	2	3	4
$d_{e,top}$ (mm)	16.0	30.0	42.0	48.0
$d_{e,bottom}$ (mm)	0.0	16.0	30.0	42.0
$d_r = (d_{e,top} - d_{e,bottom}) q$ (mm)	48.0	42.0	36.0	18.0
$d_r v^*(1/(1-\theta))$ (mm)	30.0 = 30.0	24.6 < 30.0	20.2 < 30.0	9 < 30.0

3.4.3 Second order effects

The sensitivity to second order ($P-\Delta$) effects is estimated by the interstorey drift sensitivity coefficient θ given by Eq. (3.10), where P_{tot} and V_{tot} are the total gravity load at and above the storey considered in the seismic design situation and total seismic storey shear, respectively, at the storey under consideration. The calculated values of θ are listed in Table 3.12. The values given in the table are for each braced frame.

$$\theta = P_{tot} d_r / V_{tot} h \quad \text{Eq. (3.10)}$$

Table 3.12: 2nd order effects

Storey	1	2	3	4
$d_r = (d_{e,top} - d_{e,bottom}) q$ (mm)	48.0	42.0	36.0	18.0
P_{tot} / V_{tot}	6241 / 371	4654 / 333	3066 / 257	1479 / 142
h (mm)	4000	4000	4000	4000
θ	0.202 > 0.1	0.147 > 0.1	0.107 > 0.1	0.047 < 0.1

Only the value of θ for last storey is less than 0.1. For all other storeys second-order effects should be taken into account. As the values θ are smaller than 0.2, the second-order effects may be taken into account increasing the actions by the factor $1/(1-\theta)$. The results presented in Table 3.11 and in the next section are affected by this factor.

3.4.4 Final verification of dissipative U-PLATE INERD CONNECTION

Table 3.13 summarizes the final design check of the connection and the corresponding overstrength factor Ω . The latter was calculated using Eq. (3.11). The value of $F_{y,max}$ was used in order to assure that the brace buckling does not occur.

$$\Omega = \frac{F_{y,max}}{N_{Ed,Brace}} \quad \text{Eq. (3.11)}$$

Table 3.13: Verification of U-PLATE INERD CONNECTION

Storey	Connection ID	$N_{Ed,Brace}$ (kN)	$1/(1-\theta)*N_{Ed,Brace}$ (kN)	$F_{y,min}$ (kN)	$F_{y,max}$ (kN)	Ω
1	Mola 9	103.8	130.0	127.8	238.9	1.84
2	Mola 9	93.1	109.1	127.8	238.9	2.19
3	Mola 9	71.8	80.4	127.8	238.9	2.97
4	Mola 9	39.8	39.8	127.8	238.9	6.01

REMARK: The homogeneity criteria given in §6.7.3 (8) of the EN 1998-1-1 [1] was not satisfied. Again, this is due to the limitation on the connection configurations available for the present case study and consequently an optimization of the connection was not performed. In this situation, one the following procedure should be used: i) accept the value and verify by Push-over analysis that soft-storey does not occurs; ii) develop a new configuration to optimize the solution to be adopted for the 2nd level (at this stage, without a design model, testing of this configuration is required).

3.4.5 Capacity design of non-dissipative members

The columns shall be verified to resist design forces obtained from Eq. (3.12). The results for column verifications are presented in Table 3.14. The second-order effects were also included as described above. Note that only the edge and corner columns belong to bracing systems. The values presented in the table for the internal columns are for the gravity load design situation in seismic design situation affected by the second-order effects.

$$N_{col,Ed} = N_{Ed,G} + 1,1\gamma_{ov}\Omega_{min}(N_{Ed,E}) \quad \text{Eq. (3.12)}$$

Where:

$\gamma_{ov}=1.00$ is the material overstrength factor (test results were used in the design),
 $\Omega_{MIN} = 2.64$ as per Table 3.13.

Table 3.14: Column verification

Column	Column cross-section / Material	$N_{col,Ed}$ [kN]	$1/(1-\theta)*N_{col,Ed}$ [kN]	Utilization factor
Edge	HEB 260 / S355	-735	-921	0.329
Corner	HEB 260 / S355	-473	-593	0.212
Internal	HEB 260 / S355	-1138	-1425	0.510

Remark: Not that the most load columns are the internal columns. These columns do not participate in the bracing systems. For these columns the governing design situation is for gravity loads and not seismic action. The maximum utilization factor obtained was 0.94.

The design of the beams shall be verified to resist design forces obtained from Eq. (3.13) to Eq. (3.15). The results for beams verifications are presented in Table 3.15.

$$N_{Beam,Ed} = N_{Ed,G} + 1,1\gamma_{ov}\Omega_{min}(N_{Ed,E}) \quad \text{Eq. (3.13)}$$

$$M_{Beam,Ed} = M_{Ed,G} \quad \text{Eq. (3.14)}$$

$$V_{Beam,Ed} = V_{Ed,G} \quad \text{Eq. (3.15)}$$

Table 3.15: Beam verification

Beam	Beam cross-section / Material	$N_{Beam,Ed}$ [kN]	$1/(1-\theta)^*$ $N_{Beam,Ed}$ [kN]	$M_{Beam,Ed}$ [kN.m]	$1/(1-\theta)^*$ $M_{Beam,Ed}$ [kN.m]	Utilization factor
Main	<i>IPE 500 / S355</i>	-208.0	-261.5	303.4	380.0	0.551
Secondary	<i>IPE 360 / S355</i>	-208.0	-261.5	113.8	142.5	0.495

The bracings shall be verified to resist design forces obtained from Eq. (3.16). The results are presented in Table 3.16.

$$N_{Brace,Ed} = 1,1\gamma_{ov}\Omega_{min}(N_{Ed,E}) \quad \text{Eq. (3.16)}$$

Table 3.16: Brace verification

Storey	Brace cross-section / Material	$N_{Brace,Ed}$ [kN]	$1/(1-\theta)^*$ $N_{Brace,Ed}$ [kN]	Utilization factor
All	<i>HEA 140 / S355</i>	-209.8	262.8	0.882

3.5 Structural detailing

After fulfilment of all checks in §4, the U-PLATE INERD CONNECTIONS may be detailed. The detailed dimensions of the selected connection are presented in Figure 3.7.

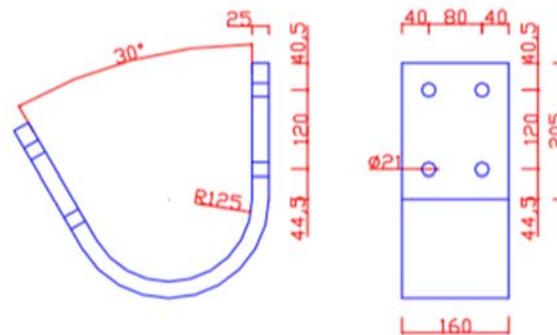


Figure 3.7: U-PLATE INERD CONNECTION (Mola 9) [4]

The braces are connected to the U-PLATE INERD CONNECTION by means of end-plate connection using fit bolts. The connection to the column is performed directly to the column web or flange, depending on the position of column (Figure 3.8).

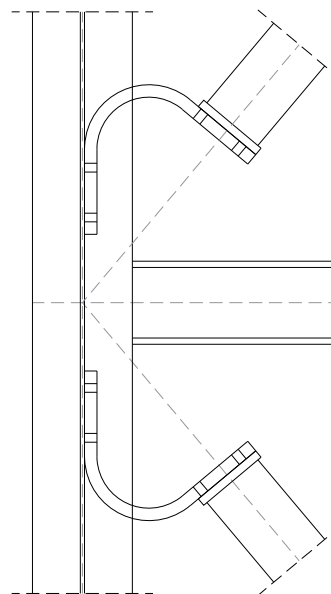


Figure 3.8: Double overlap connection between U-PLATE and Brace

3.6 References

1. Eurocode 8: Design of structures for earthquake resistance - Part 1: General rules, seismic actions and rules for buildings; EN 1998-1:2004.
2. EN1993-1-1, Eurocode 3: Design of steel structures - Part 1-1: General rules and rules for buildings. Brussels: Comité Européen de Normalisation (CEN); 2005.
3. Hot rolled products of structural steels – Part 2: Technical delivery conditions for non-alloy structural steels; EN 10025-2:2001.

4. INERD (CEC Agreement No7210-PR-316) – Two innovations for Earthquake resistant design, The INERD project, 2001-2004.
5. FINELG user's manual. Non-linear finite element analysis software. Version 9.3, July 2005.
6. Georgiev Tzv., Zhelev D., Raycheva L., Rangelov N., " INNOSEIS - Valorization of innovative anti-seismic devices", WORK PACKAGE 1 – DELIVERABLE 1.1, Volume with information brochures for 12 innovative devices in English, European Commission Research Programme of the Research Fund for Coal and Steel, (Article in Press).

4 FUSEIS BEAM LINKS

4.1 General

4.1.1 Introduction

This report presents a case study applying the FUSEIS beam links as lateral load resisting system. The Eurocode framework as well as the design guidelines have been applied for the design. After a general description of the case study it follows the general design with mentioning the most important design equations. The final design outcome for this specific structure is presented. A structural detailing solution is schematically sketched.

4.1.2 Description of building

4.1.2.1 Geometry and general assumptions

The case study considered herein is a high-rise office building with 8 storeys. The structural layout is regular both in plan and elevation. Dimensions are shown in Figure 4.1 and Figure 4.2. The storey height equals to 4 m. The number of bays in both directions is equal to 3, with an uniform bay width of 8 m. All buildings have composite slabs and secondary beams which transfer the loads to the main frames.

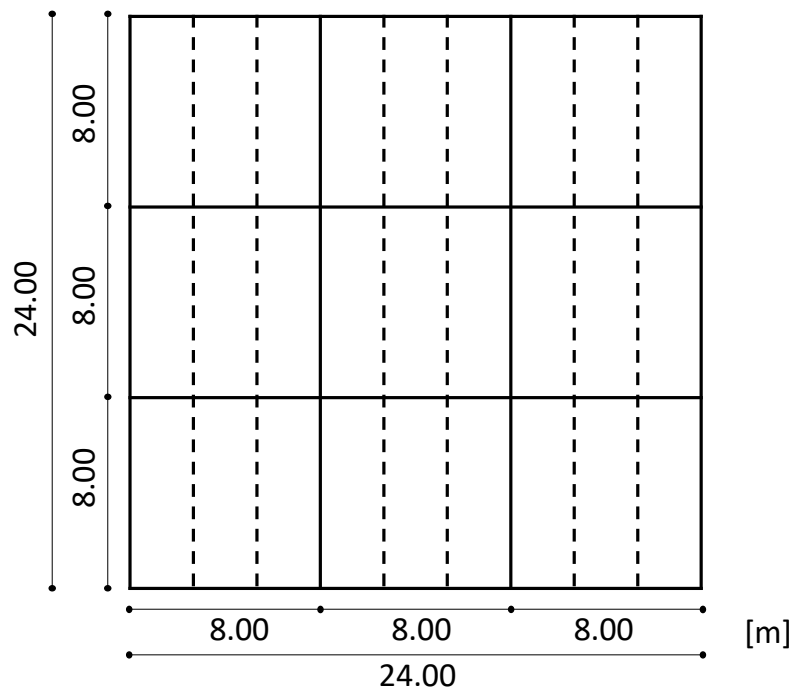


Figure 4.1: Floor plan of case study

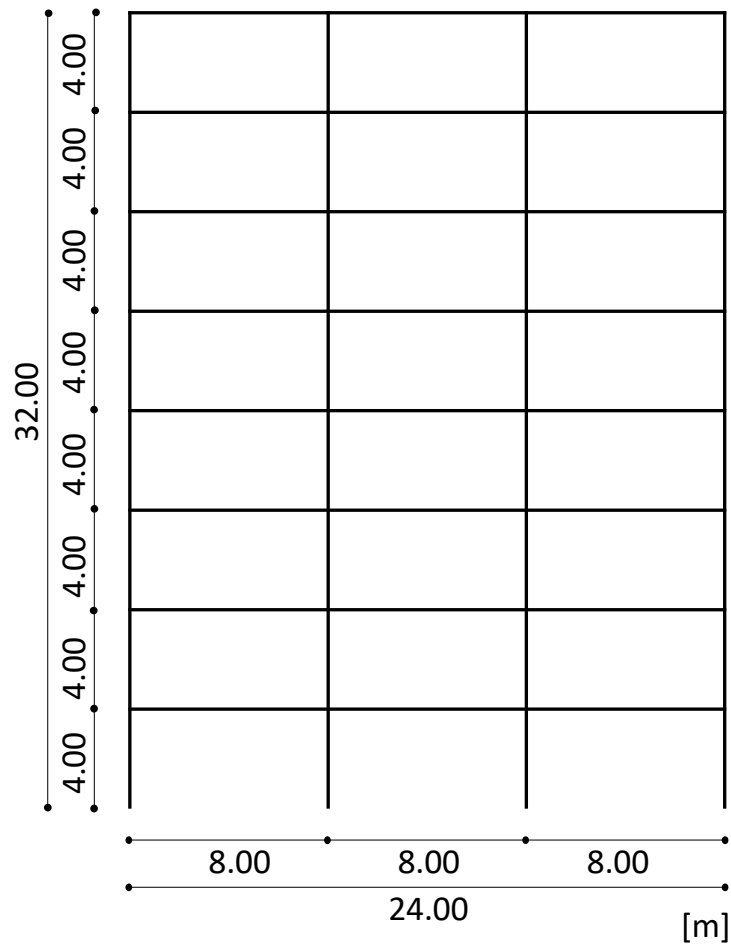


Figure 4.2: Side view of case study

4.1.2.2 Materials

Used materials – concrete and steel – are listed in Table 4.1. Standard C25/30 concrete has been used for the composite steel concrete slab. S355 steel has been used for almost all structural steel parts. Just for the FUSEIS beam links a lower steel grade of S235 has been used. This selection eases the capacity design and assures that the plastic hinge develops inside the FUSEIS beam link.

Table 4.1: Material properties

Concrete	C25/30, $g = 25 \text{ kN/m}^3$, $E = 31\,000 \text{ Mpa}$
Reinforcement	B500C
Structural steel	S235: Dissipative elements (FUSEIS beam links) S355: Non dissipative elements (beams and columns)

4.1.2.3 Loads and load combinations

The case study has been designed for vertical loads according to Eurocode 1, 3 and 4. Dead loads, superimposed loads and live loads have been considered as listed in Table 4.2. Table 4.3 summarizes the main assumptions for seismic loading conditions. Wind loads have been neglected assuming the seismic loads to be governing the lateral load resisting frame design. All relevant load cases and load combinations which have been considered for the design of the case study are listed in Table 4.4.

Table 4.2: Vertical loads

Dead loads	
Composite slab + steel sheeting	2.75 kN/m ²
Superimposed loads	
... for intermediate floors	0.70 kN/m ²
... for top floor	1.00 kN/m ²
Perimeter walls	4.00 kN/m
Live loads	
Offices (Class B):	3.00 kN/m ²
Movable partitions	0.80 kN/m ²

Table 4.3: Seismic loads

Elastic response spectrum	Type 1
Peak ground acceleration	$a_{gR} = 0.30g$
Importance class II	$\gamma_I = 1.0$ (Ordinary buildings)
Ground type	B ($T_B = 0.15$ s, $T_C = 0.50$ s)
Behavior factor q	5
Damping ratio	5 %
Factors of operating loads for seismic combination	$\phi = 1.00$ (roof), $\phi = 0.80$ (stories with correlated occupancies)
Seismic combination coefficient for the quasi-permanent value of variable actions	$\psi_2 = 0.30$

Table 4.4: Load cases and combinations used for the design of the case study.

Load cases	
Load case LC1	Dead loads (including $1.1 \cdot$ self weight)
LC2	Live loads
LC3, 4, ...	Seismic equivalent loads per relevant mode
Load combinations	
LCOMB1	$1.35 \cdot \text{LC1} + 1.5 \cdot \text{LC2}$
LCOMB2	$\text{LC1} + 0.3 \cdot \text{LC2}$
LCOMB3	$\text{LC1} + 0.24 \cdot \text{LC2}$
LCOMB4	Envelope of seismic loads in X-direction
LCOMB5	Envelope of seismic loads in Y-direction
LCOMB6	Envelope of seismic loads in both X- and Y-direction
LCOMB7	$1.0 \cdot \text{LC1} + 0.3 \cdot \text{LC2} + 1.0 \cdot \text{LCOMB6}$

4.2 Analysis and dimensioning

4.2.1 Simulation

The software RSTAB 8 has been used for the design of the case study. This software is widely spread in German design offices. The main advantages are, besides the highly user friendly workflow, the possibility of automatically combining loads according to Eurocode 1, checking for all relevant design equations contained in Eurocode 3, as well as conducting multi modal response spectrum analysis according to Eurocode 8.

Cross section selection for all steel members was assisted by the automatic design checks of RSTAB 8. Design equations which are not incorporated in automatic checks in the software, as e.g. Eurocode inter storey drift criteria, have been checked manually. Hereby an Excel work sheet has been developed, where the verification could be done automatically. RSTAB 8 allows to export the model and results into such an Excel worksheet.

Design for vertical loads has been conducted by the National Technical University of Athens (NTUA). The composite slabs were designed separately with the program SymDeck Designer, a software provided by the manufacturer, which takes into account construction phases both for the ultimate and serviceability limit states.

As the structural layout can be classified as regular both in plan and elevation, a planar model may be used applying the lateral force linear-elastic analysis

according to Eurocode 8. However the full 3D model has been used for the design presented in this report.

One FUSEIS beam link system has been applied for each lateral frame, as shown in Figure 4.3 (see also Figure 4.4 to Figure 4.6).

All girders and columns have been modelled as beam elements. The composite slabs are assumed to act as rigid diaphragm, what has been modelled by using rigid stiffening beams in each floor.

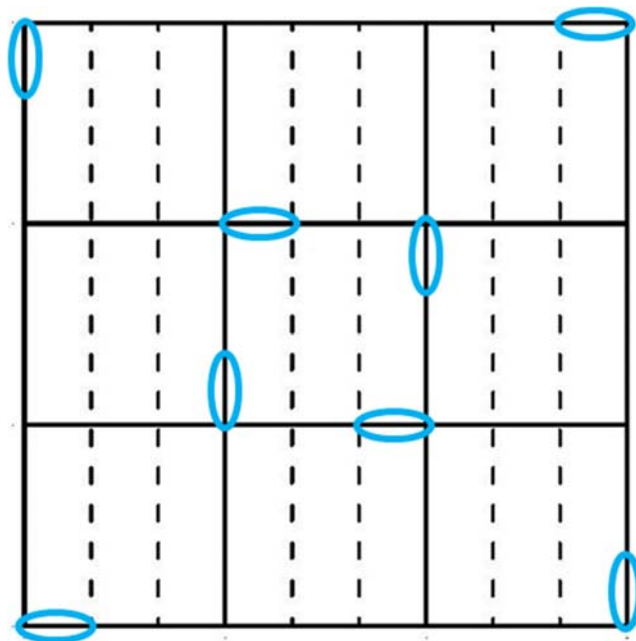


Figure 4.3: Positioning of FUSEIS beam link systems

4.2.2 Design for static and seismic combinations

4.2.2.1 Ultimate limit state results

Design checks according to Eurocode 3 have been automatically conducted by RSTAB. Cross section demand checks as well as stability failure (local and global buckling) have been considered. Profiles have been optimized until all design requirements have been fulfilled. Table 4.5 shows the final cross sections for each structural member. While the gravity load bearing frame is solely determined by vertical loads the FUSEIS beam link system is governed by the horizontal seismic loads. Moreover maximum demand to capacity ratios taken into account the most critical load combination as well as design equation are listed in Table 4.5.

Table 4.5: Final cross sections and exploitation ratios

Structural member	Profile	Exploitation
FUSEIS beam link system		
Column	HEB 400	0.69
Beam links storey 1	HEA 260	0.83
Beam links storey 2	HEA 240	0.64
Beam links storey 3	HEA 220	0.68
Beam links storey 4	HEA 220	0.63
Beam links storey 5	HEA 220	0.62
Beam links storey 6	HEA 200	0.65
Beam links storey 7	HEA 200	0.77
Beam links storey 8	HEA 200	0.96
Gravity load bearing frame		
Columns storey 1 & 2	HEB 300	0.71
Columns storey 3 & 4	HEB 260	0.70
Columns storey 5 & 6	HEB 220	0.53
Columns storey 7 & 8	HEB 200	0.32
Primary girder	IPE 500	0.40
Secondary girder	HEA 200	0.96

It should be mentioned that the profiles have been chosen not only on the base of Eurocode 3 verifications, but also due to the requirements contained in Eurocode 8 regarding strength, stiffness and capacity design. These requirements are listed in Section 4.3.3 of this document. Especially inter-storey drift limitations govern the design of the FUSEIS beam link system. Moreover, dissipative elements, and thus the FUSEIS beam links, need to satisfy demands of cross sectional class I, according to Eurocode 3.

4.2.2.2 Design outcome

The final design outcome is shown in Figure 4.4. Final cross sections have been already listed in Table 4.5. In total 5 Fuseis beam links have been used per storey, resulting in a distance of 80 cm between the centre lines of each beam link. In order to account for increased storey shear and to optimize the design, cross sections are increasing towards the bottom as can be seen in Figure 4.6. The distance between the column centre lines was chosen to 250 cm.

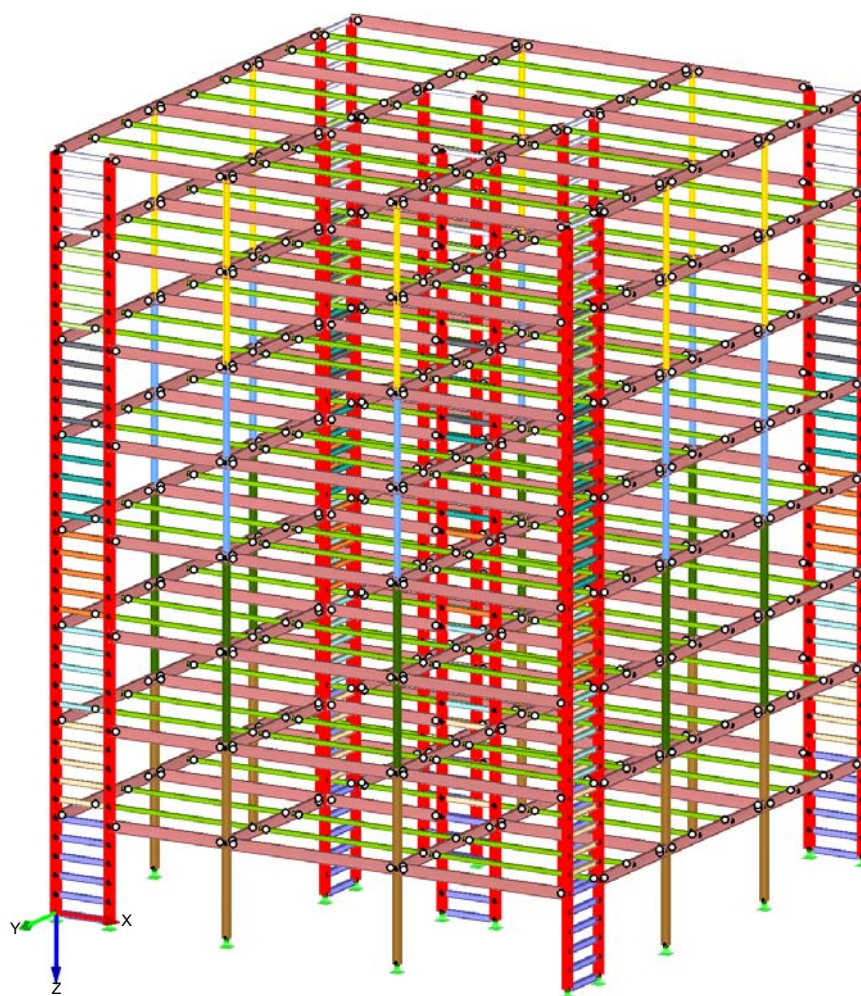


Figure 4.4: Isometric view of high-rise building

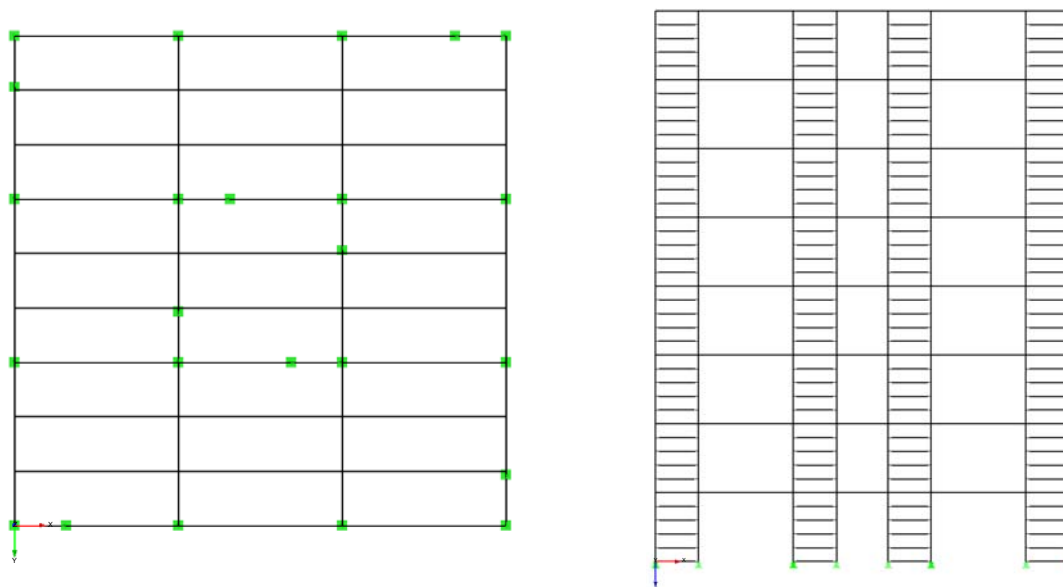


Figure 4.5: Top view (left) and side view (right)

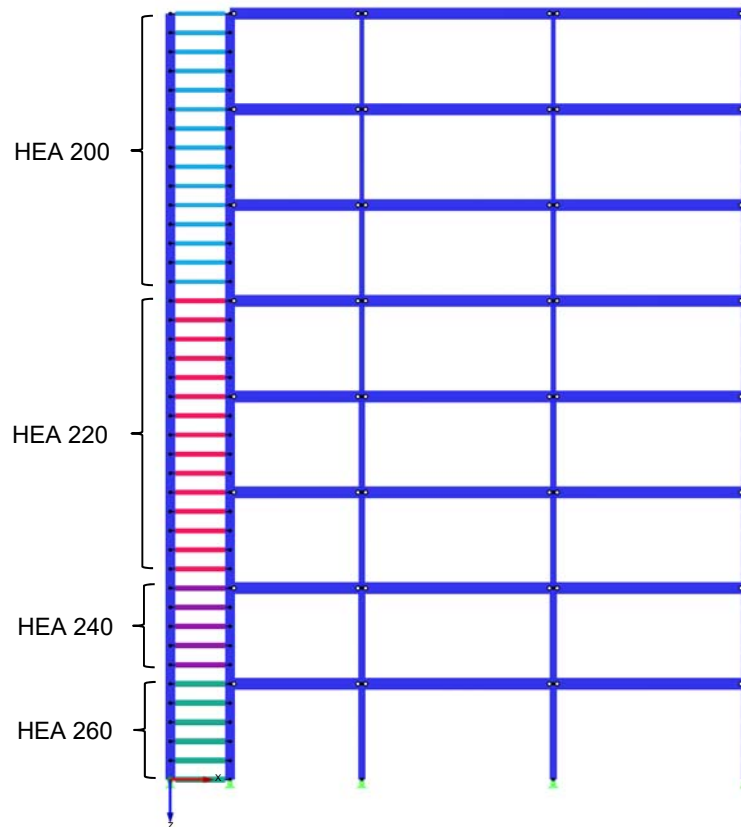


Figure 4.6: General design of FUSEIS beam link system – outer frame

Dynamic properties of the designed case study are listed in Table 4.6, which are period of vibration as well as effective mass participation factors for both directions. As can be seen, 1st and 2nd sway modes needed to be considered during design in order to account for more than 90% of modal masses. Due to the symmetrical application of FUSEIS beam link systems dynamic behaviour is extremely similar in both directions. All five relevant mode shapes are shown in Figure 4.7.

Table 4.6: Dynamic properties of high-rise case study.

Mode #	T [s]	$m_{eff,X} / m_{tot}$	$m_{eff,Y} / m_{tot}$	Remark
1	1.48	0.09	0.75	1 st sway mode y-direction
2	1.47	0.73	0.09	1 st sway mode x-direction
3	1.25	0.00	0.00	torsional mode
4	0.52	0.00	0.10	2 nd sway mode y-direction
5	0.50	0.12	0.00	2 nd sway mode x-direction
	Σ	0.94	0.94	

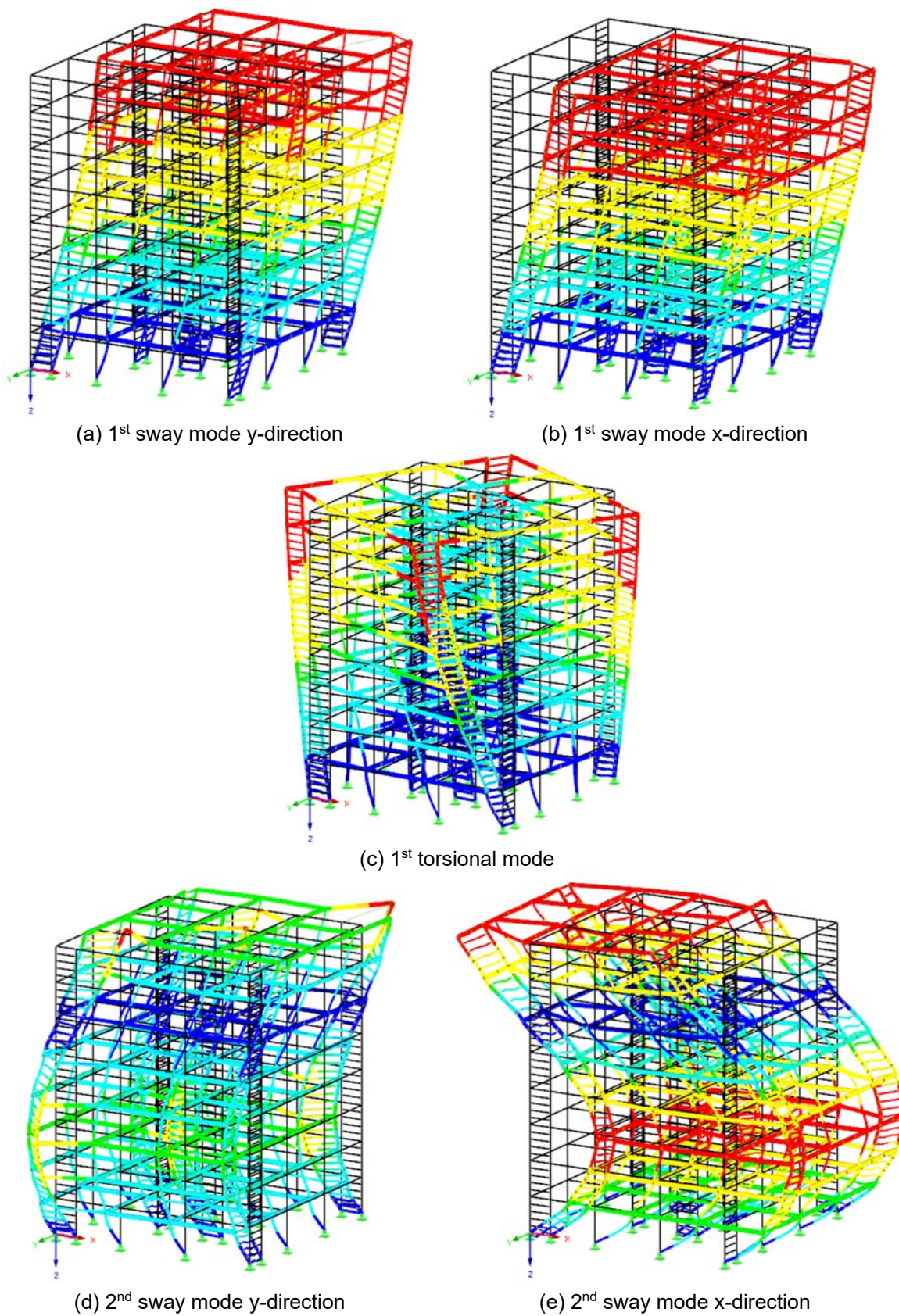


Figure 4.7: Mode shapes of high-rise case study.

4.3 Detailed design

4.3.1 Limitation of interstorey drift – Damage limitation

The criterion in accordance to section 4.4.3.2 of Eurocode 8-1 to limit damage for non-structural elements was verified. The following equation needs to be fulfilled.

$$d_r \cdot v \leq \{0.005; 0.0075; 0.01\} \cdot h \quad \text{Eq. (4.1)}$$

Since the building is assigned to importance class I, the reduction factor v is equal to 0.5 (4.4.3.2 (2) Eurocode 8-1). It is assumed that ductile non-structural elements are present in the building, thus according to Table 4.7 the limit value is equal to 0.0075.

Table 4.7: Interstorey drift limits for damage limitation of non-structural elements

Non-structural element characteristics	Limit value
Brittle elements	0.0050
Ductile elements	0.0075
Without or with non-interfering elements	0.0100

The design interstorey drift d_r is calculated by multiplying the interstorey drift d_e obtained from the linear elastic analysis with the chosen value of the behaviour factor q , according to section 4.3.4 of Eurocode 8-1. This interstorey drift must be lower than the allowed one, which equals to $0.0075 \cdot 4000 \text{ mm} / 0.5 = 60 \text{ mm}$. As can be seen in Table 4.8 and Table 4.9 respectively, this requirement is fulfilled in both directions. However, the inter-storey drift limitation was governing design and forced to choose a stiffer FUSEIS beam link system.

Table 4.8: Verification of interstorey drift limit – SLS – X-direction

Storey #	d_e [mm]	d_r [mm]	$d_{r,lim}$ [mm]	Ratio $d_r/d_{r,lim}$
1	10.7	53.5	60	0.89
2	8.3	41.5	60	0.69
3	9.0	45.0	60	0.75
4	8.4	42.0	60	0.70
5	8.0	40.0	60	0.67
6	7.2	36.0	60	0.60
8	6.1	30.5	60	0.51

Table 4.9: Verification of interstorey drift limit – SLS – Y-direction

Storey #	d_e [mm]	d_r [mm]	$d_{r,lim}$ [mm]	Ratio $d_r/d_{r,lim}$
1	11.1	55.5	60	0.93
2	8.9	44.5	60	0.74
3	9.4	47.0	60	0.78
4	8.4	42.0	60	0.70
5	7.6	38.0	60	0.63
6	6.7	33.5	60	0.56
7	5.3	26.5	60	0.44
8	3.3	16.5	60	0.28

4.3.2 Limitation of interstorey drift – P-delta effects (ULS)

According to section 4.4.2.2 of Eurocode 8-1 the second order coefficient calculated according to Eq. (4.2) must be checked. Second-order effects need to be taken into account if it is higher than 0.1 and it shall not exceed 0.3.

$$\theta = \frac{P_{tot} \cdot d_r}{V_{tot} \cdot h} \quad \text{Eq. (4.2)}$$

The evaluated sensitivity coefficients are calculated in Table 4.10 and Table 4.11 for both directions. As can be seen for some cases the coefficient is higher than 0.1, with a maximum value of about 0.16, however, much smaller than the limit value of 0.3. As some values exceed the limit of 0.1, second-order effects have been taken into account by directly accounting for it within the analyses.

Table 4.10: Verification of interstorey drift limit – ULS – X-direction

Storey #	$d_{r,x}$ [mm]	P_{tot} [kN]	V_{tot} [kN]	θ
1	0.93	25 899	2 315	0.150
2	0.74	22 591	2 025	0.116
3	0.78	19 289	1 846	0.118
4	0.70	16 006	1 823	0.092
5	0.63	12 722	1 640	0.078
6	0.56	9 446	1 494	0.057
7	0.44	6 177	1 241	0.038
8	0.28	2 912	859	0.018

Table 4.11: Verification of interstorey drift limit – ULS – Y-direction

Storey #	$d_{r,y}$ [mm]	P_{tot} [kN]	V_{tot} [kN]	θ
1	55.5	25 899	2 259	0.159
2	44.5	22 591	1 913	0.131
3	47.0	19 289	1 787	0.127
4	42.0	16 006	1 727	0.097
5	38.0	12 722	1 567	0.077
6	33.5	9 446	1 388	0.057
7	26.5	6 177	1 153	0.036
8	16.5	2 912	781	0.015

4.3.3 Design of dissipative devices

The horizontal beams in the FUSEIS beam link system are the primary dissipative zones where the energy dissipation capability is mainly located. Reduced beam sections (RBS) are recommended to clearly define the dissipative zones. Reduced beam sections (RBS) were designed according to EN 1998-3, see Figure 4.8. Geometrical boundary conditions are given in Eq. (4.3).

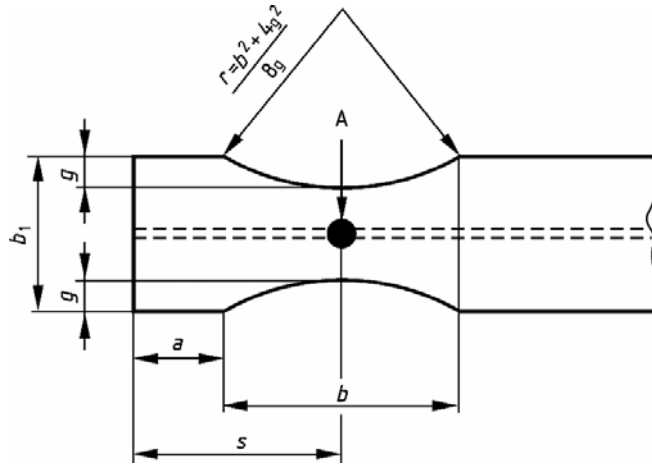


Figure 4.8: Geometrical characteristics of reduced beam section

$$\begin{aligned}
 a &= 0.6 \cdot b_f \\
 b &= 0.75 \cdot d_b \\
 g &= 0.20 \cdot b_f \text{ to } 0.25 \cdot b_f
 \end{aligned}
 \tag{4.3}$$

With

b_f = beam width

d_b = beam height

Due to the fact that beams can be modelled in RSTAB conveniently by directly choosing profiles from a library, e.g. HEA sections, and moreover that automatic design checks and profile optimization is based on these libraries, the original profiles were used - not taking into consideration the reduced beam section (RBS) explicitly. Instead, the yield strength of the FUSEIS beam link has been modified according to Eq. (4.4). With this modified yield strength RSTAB calculates internally beam section properties, representing the reduced beam section (RBS), which are then used for the design checks. The reduced stiffness was not taken into account, as it showed to be of negligible influence.

$$f_{y,mod} = \frac{W_{pl,RBS} * f_y}{W_{pl}} \quad \text{Eq. (4.4)}$$

With

$$W_{pl,RBS} = W_{pl} - 2 * g * t_f * (d_b - t_f)$$

4.3.4 Capacity design of non-dissipative members

4.3.4.1 Strong column weak beam criterion

According to 4.4.2.3 Eurocode 8-1 the plastic hinge must develop in the beam. The column must be capacity designed according to Eq. (4.5).

$$\sum M_{Rc} \geq 1.3 \cdot \sum M_{Rb} \quad \text{Eq. (4.5)}$$

The regular primary and secondary beams bearing the gravity loads are not intended to take part in the lateral force resisting system. Thus, they are pinned or partly-fixed to the columns so that Eq. (4.5) is fulfilled easily. For the FUSEIS beam links Eq. (4.5) is already taken into account during the design of the reduced beam sections (RBS). The verification of the ends of FUSEIS beam links at the most crucial spot – bottom of the FUSEIS beam link system – is listed in the following Table 4.12.

Table 4.12: Verification of strong column weak beam principle

M_{Rc} [kNm] (HEB 400, S355)	M_{Rb} [kNm] (HEA 260, S235)	$1.3 \cdot M_{Rb}$ [kNm]	Ratio $1.3 \cdot M_{Rb}/M_{Rc}$
1 147	216	281	0.24

4.3.5 Lateral torsional buckling

Lateral torsional buckling of the girders and beams are prevented by stabilisation due to the concrete plate, which is connected with the members by headed studs.

Overstrength of dissipative members due to the concrete plate has to be prevented by detailing of the connection joint. Lateral torsional buckling of FUSEIS beam links is assumed to be irrelevant, due to their short lengths.

4.3.6 FUSEIS columns

Columns shall be verified in compression whereby the force demands are to be calculated as follows (6.6.3 Eurocode 8-1):

$$N_{Ed} = N_{Ed,G} + 1.1 \cdot \gamma_{ov} \cdot \Omega \cdot N_{Ed,E} \quad \text{Eq. (4.6) (a)}$$

$$M_{Ed} = M_{Ed,G} + 1.1 \cdot \gamma_{ov} \cdot \Omega \cdot M_{Ed,E} \quad \text{(b)}$$

$$V_{Ed} = V_{Ed,G} + 1.1 \cdot \gamma_{ov} \cdot \Omega \cdot V_{Ed,E} \quad \text{(c)}$$

The factor Ω is calculated by the utilization rate of all beams in which dissipative zones are located:

$$\Omega = \min(\Omega_i); \quad \Omega_i = \frac{M_{pl,Rd,i}}{M_{Ed,i}} \quad \text{Eq. (4.7)}$$

Demand to capacity ratios for axial and shear force as well as bending moments for FUSEIS strong columns are listed for the most stressed columns in the following tables.

Table 4.13: Demand capacity ratios for FUSEIS strong columns – Axial force

N_{Ed} [kN]	$N_{pl,Rd}$ [kN]	$N_{Ed}/N_{pl,Rd}$
4 959	6 894	0.72

Table 4.14: Demand capacity ratios for FUSEIS strong columns – Shear force

	V_{Ed} [kN]	$V_{pl,Rd}$ [kN]	$V_{Ed}/V_{pl,Rd}$
Strong axis	542	2 977	0.18
Weak axis	67	1 434	0.05

Table 4.15: Demand capacity ratios for FUSEIS strong columns – Bending moment

	M_{Ed} [kNm]	$M_{pl,Rd}$ [kNm]	$M_{Ed}/M_{pl,Rd}$
Strong axis	671	1 119	0.60
Weak axis	133	381	0.35

4.3.7 FUSEIS beam links

To prevent that full plastic moment resistance and rotation capacity at plastic hinges at the beam links are not decreased by compression and shear forces, the following Equations shall be fulfilled (6.6.2 Eurocode 8-1):

$$\frac{M_{Ed}}{M_{pl,Rd}} \leq 1,0; \quad \frac{N_{Ed}}{N_{pl,Rd}} \leq 0,15; \quad \frac{V_{Ed}}{V_{pl,Rd}} \leq 0,5 \quad \text{Eq. (4.8)}$$

The shear force shall be calculated as follows:

$$V_{Ed} = V_{Ed,G} + V_{Ed,M} \quad \text{with} \quad V_{Ed,M} = \frac{2 \cdot M_{pl,Rd}}{L} \quad \text{Eq. (4.9)}$$

Demand to capacity ratios for axial and shear force as well as bending moments for FUSEIS beam links are shown in the following tables. As the shear force ratio is larger than 0.5, interaction has been taken into account for calculating the plastic moment resistance of the beam sections.

Table 4.16: Demand capacity ratios for FUSEIS beam links – Axial force

Storey #	N_{Ed} [kN]	$N_{pl,Rd}$ [kN]	$N_{Ed}/N_{pl,Rd}$
1	115	1 355	0.08
2	105	1 196	0.09
3	100	1 000	0.10
4	103	1 000	0.10
5	103	1 000	0.10
6	95	841	0.11
7	82	841	0.10
8	60	841	0.07

Table 4.17: Demand capacity ratios for FUSEIS beam links – Shear force

Storey #	V_{Ed} [kN]	$V_{pl,Rd}$ [kN]	$V_{Ed}/V_{pl,Rd}$
1	158	259	0.61
2	140	226	0.62
3	115	185	0.62
4	129	185	0.69
5	135	185	0.73
6	106	163	0.65
7	108	163	0.66
8	103	163	0.63

Table 4.18: Demand capacity ratios for FUSEIS beam links – Bending moment

Storey #	M_{Ed} [kNm]	$M_{pl,V,Rd}$ [kNm]	$M_{Ed}/M_{pl,Rd}$
1	119	137	0.87
2	37	109	0.34
3	26	83	0.32
4	33	75	0.44
5	39	70	0.56
6	38	61	0.62
7	38	60	0.63
8	37	63	0.59

4.3.8 Shear panel verification

The shear panel of the FUSEIS strong columns needs to be verified by the following Eq. (4.10).

$$V_{wp,Ed} < V_{wp,Rd} \quad \text{Eq. (4.10)}$$

$$V_{wp,Ed} = \frac{M_{b1,Ed} + M_{b2,Ed}}{z}$$

$$V_{wp,Rd} = 0,9 * V_{pl,Rd}$$

Demand to capacity ratios for the shear panel of the FUSEIS strong columns are shown in Table 4.19.

Table 4.19: Demand capacity ratios for FUSEIS strong columns – Shear panel verification

Storey #	$V_{wp,Ed}$ [kN]	$V_{wp,Rd}$ [kN]	$V_{Ed}/V_{pl,Rd}$
1	605	1 291	0.47
2	532	1 291	0.41
3	444	1 291	0.34
4	444	1 291	0.34
5	444	1 291	0.34
6	373	1 291	0.29
7	373	1 291	0.29
8	373	1 291	0.29

4.3.9 Seismic link classification

Design and detailing rules for frames with eccentric bracings having seismic links are discussed within 6.8.1 Eurocode 8-1. The FUSEIS beam links can also be considered as seismic links. Seismic links are classified based on their length into three categories:

- short links, which dissipate energy by yielding essentially in shear;
- intermediate links, in which the plastic mechanism involves bending and shear; and
- long links, which dissipate energy by yielding essentially in bending.

Table 4.20: Classification of seismic links by its length

Short links	Intermediate links	Long links
$e_s = 1.6 \cdot M_{p,link} / V_{p,link}$	$e_s < e < e_L$	$e > e_L = 3.0 \cdot M_{p,link} / V_{p,link}$

With

$$M_{p,link} = f_y \cdot b \cdot t_f \cdot (h - t_f) \quad \text{Eq. (4.11)}$$

$$V_{p,link} = \frac{f_y}{\sqrt{3}} \cdot t_w \cdot (h - t_f) \quad \text{Eq. (4.12)}$$

The classification into short, intermediate or long links of the FUSEIS beam links is checked for informational issues. In the case study design considered herein, all the beam links are to be classified into long links, besides the beam links at bottom story, which are classified as long links according to Table 4.20.

4.4 STRUCTURAL DETAILING

The FUSEIS beam link to FUSEIS strong column joint is formed as rigid to enable the Vierendeel girder behaviour. Joints are capacity designed according to Eurocode 3 and Eurocode 8 with sufficient overstrength, to assure plastification only occurring in the FUSEIS beam links. Bolted end-plate connections which enable an easy mounting and replacement of the beam links should be used. Such a connection is schematically shown in Figure 4.9. An exemplary detailing solution of the FUSEIS beam link system connected with the gravity load bearing framing system is shown in Figure 4.10.

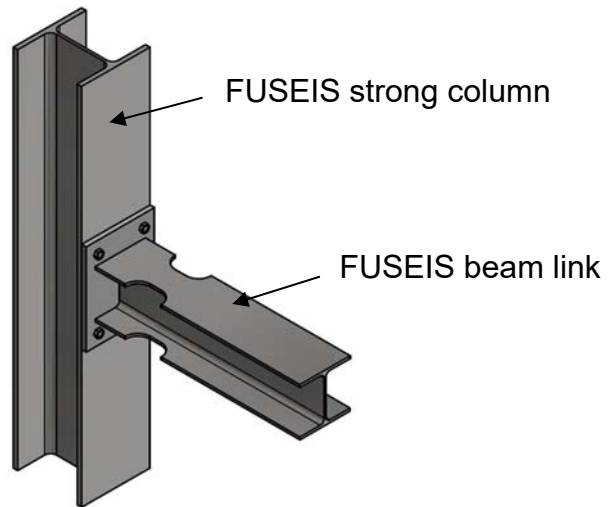


Figure 4.9: FUSEIS beam link system with bolted end-plate connection.

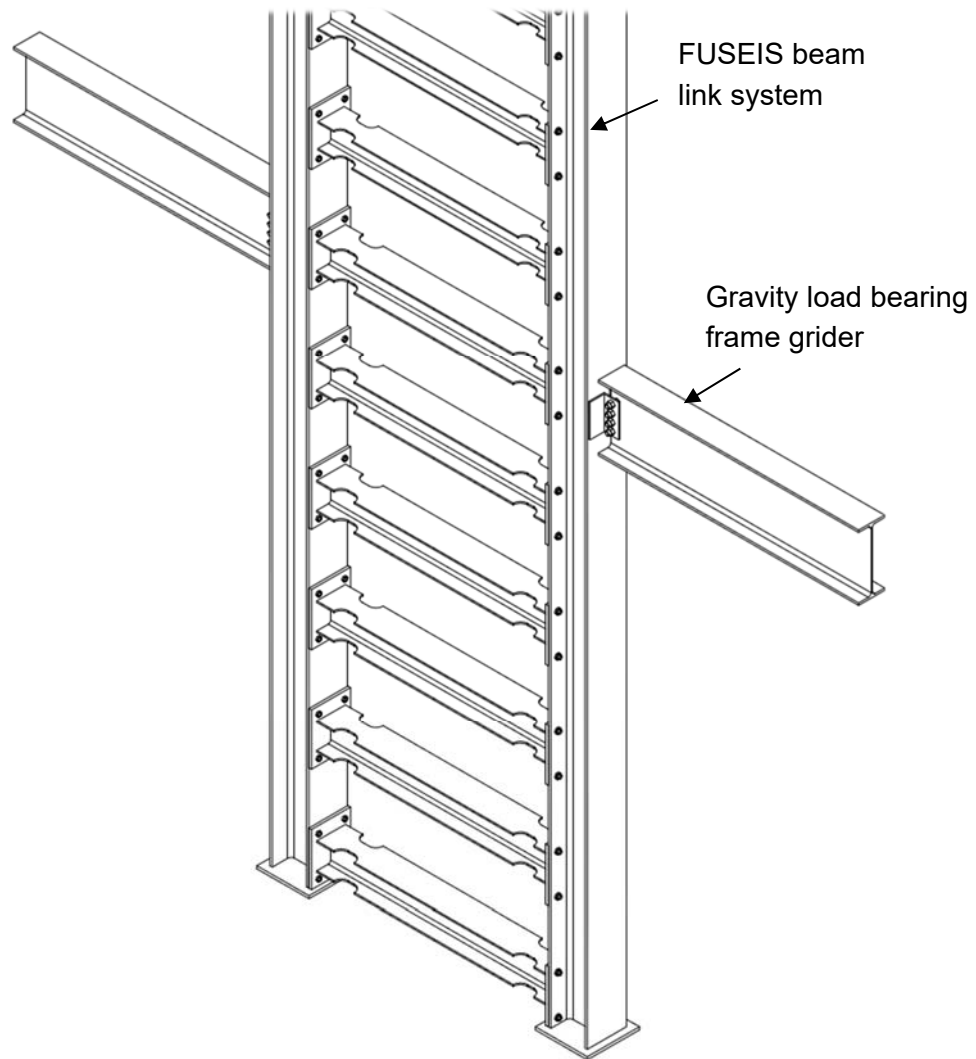


Figure 4.10: Schematical drawing of FUSEIS beam link system.

4.5 CONCLUSIONS

This design example of a high-rise office building shows how effectively the FUSEIS beam link system can be applied as solely lateral force resisting system. Fulfilling all relevant design equations and limitations can easily be achieved. Moreover, the FUSEIS beam link system can be designed similar as a conventional Moment Resisting Frame (MRF), which is already well known in design practice.

4.6 REFERENCES

- [1] Eurocode 0: Basis of structural design; EN 1990:2002 + A1:2005 + A1:2005/AC:2010.
- [2] Eurocode 1: Actions on structures - Part 1-1: General actions - Densities, self-weight, imposed loads for buildings; EN 1991-1-1:2002 + AC2009.
- [3] Eurocode 3: Design of steel structures - Part 1-1: General rules and rules for buildings; EN 1993-1-1:2005 + AC:2009.
- [4] Eurocode 4: Design of composite steel and concrete structures - Part 1-1: General rules and rules for buildings; EN 1994-1-1:2004
- [5] Eurocode 8: Design of structures for earthquake resistance - Part 1: General rules, seismic actions and rules for buildings; DIN EN 1998-1 + AC:2009, 2010.
- [6] Eurocode 8: Design of structures for earthquake resistance - Part 3: Assessment and Retrofitting of buildings; EN 1998-3:2004.
- [7] RSTAB 8, www.dlubal.com, 2017

5 FUSEIS PIN-LINK SYSTEM

5.1 General

5.1.1 Introduction

This case study refers to the detailed design of a 4-storey steel building incorporating the FUSEIS link system. A brief description of the FUSEIS pin link system is made in the beginning. Additional information about the system can be found in the document developed during the FUSEIS project [1], [2].

The design of the building was performed according to the provisions of the Eurocodes and the design guidelines presented within the INNOSEIS project.

5.1.2 Description of the FUSEIS pin link system

The FUSEIS pin link system consists of a pair of strong columns rigidly connected by multiple links (Figure 5.1). The links consists of two receptacle beams connected through a short steel pin. The receptacle beams can have an H or hollow section and they are welded to the column flanges. The joint between the receptacles and the pins, is formed through an end plate on which the threaded section of the pin is screwed (Figure 5.2).

Under strong lateral forces, plastic hinges will form on the ends of the pins, thus dissipating a large amount of energy, while leaving the rest of the structure undamaged. The pin section is reduced in the middle part of the pin to ensure that plastification will take place away from the connection area. Repair works are easy, since they are restricted to the pins which are not generally subjected to vertical loads, as they are placed between floor levels.

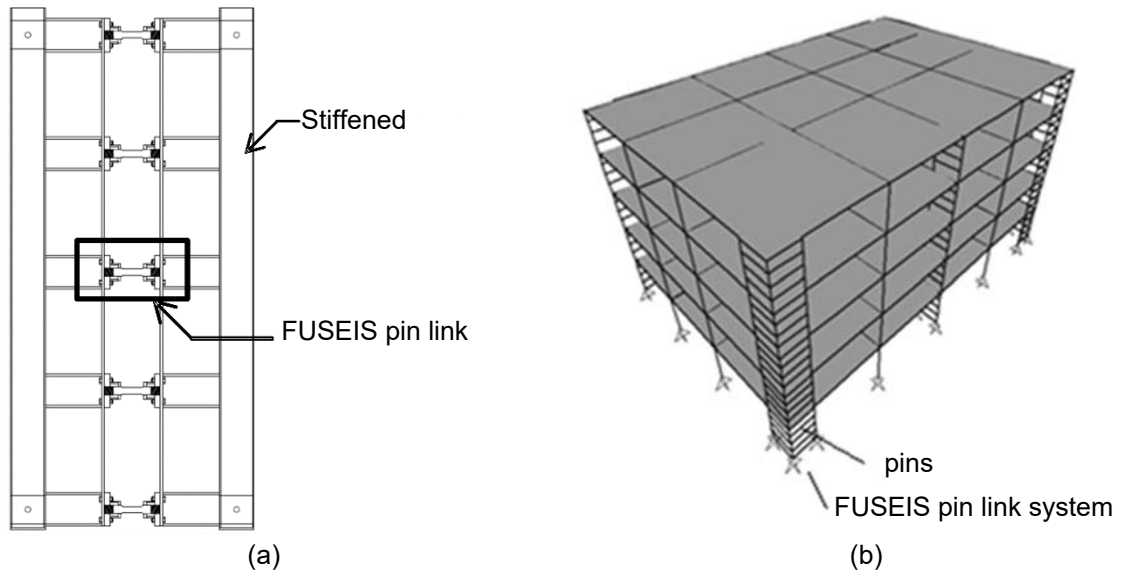


Figure 5.1: (a) FUSEIS pin link system configuration (b) Position of FUSEIS pin link system in a building

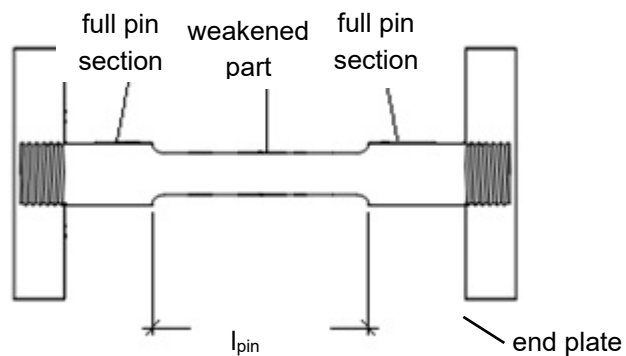


Figure 5.2: FUSEIS pin link

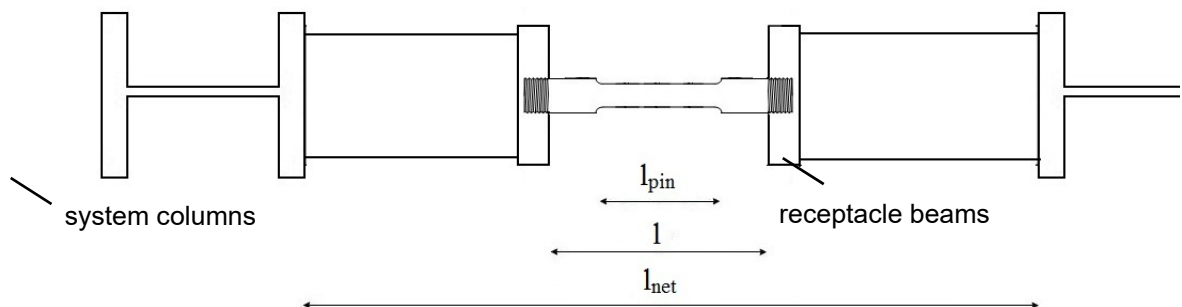


Figure 5.3: Typical plan view and dimensions of FUSEIS pin link system

Experimental investigations showed that the FUSEIS pin link system resists lateral loads as a vertical Vierendeel beam (Figure 5.4).

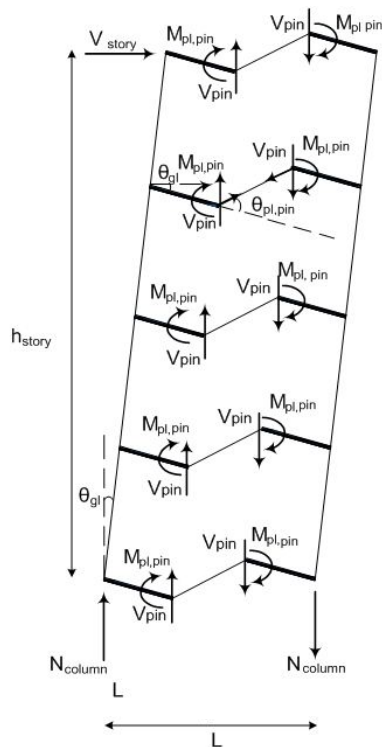


Figure 5.4: Vierendeel behaviour FUSEIS pin link system

5.1.3 Geometry and general assumptions

The building is a 4-storey composite building, consisting of four frames with three 8m bays in each direction (Figure 5.5). All the connections of the frames are pinned and two FUSEIS pin link systems are applied on each of the external frames in order to provide the required lateral resistance. The non-system columns are H shaped (HEB type), the main and the secondary floor beams composed of steel beams with IPE and HEA sections respectively, both acting compositely with the concrete slab.

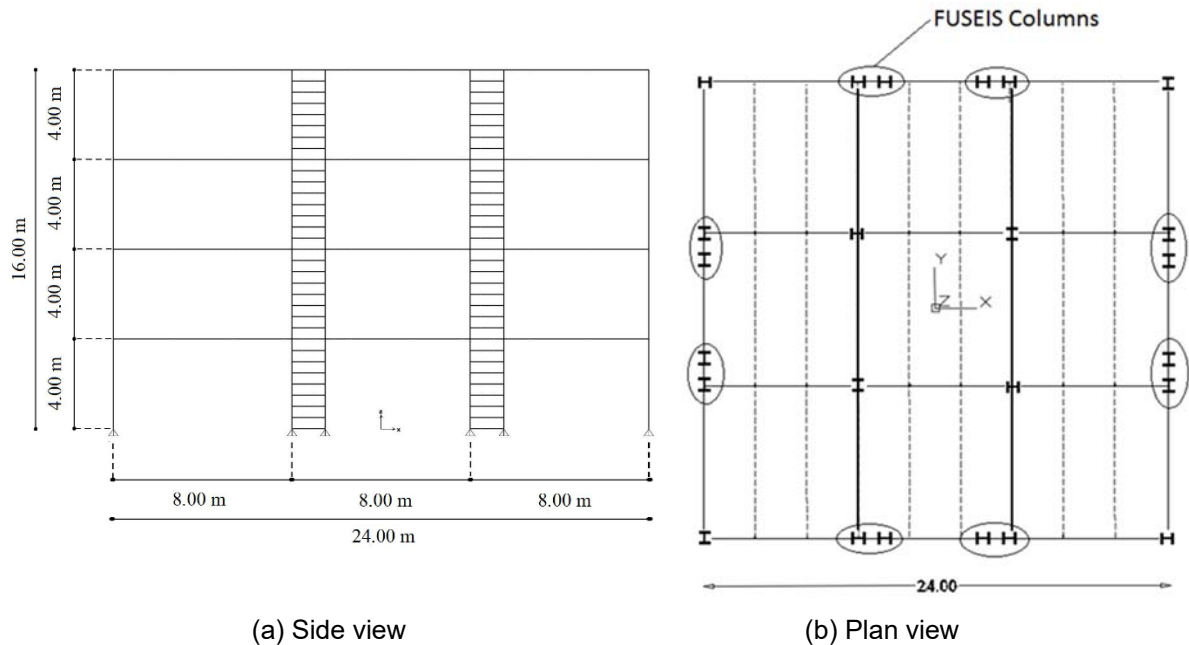


Figure 5.5: Side and plan view of the building - FUSEIS systems position

Gravity and seismic loads are summarised in Table 5.1, according to EN 1991-1-1 [9]. The behaviour factor is equal to 3, as proposed by the design guidelines.

Table 5.1: Loading assumptions

Vertical loads	
dead loads (composite slab + steel sheeting)	2.75 kN/m ²
superimposed loads for intermediate floors:	0.70 kN/m ²
superimposed loads for top floor:	1.00 kN/m ²
perimeter walls:	4.00 kN/m
total live load:	3.80 kN/m ² :
Design spectrum characteristics	
Elastic response spectra	Type 1
Peak ground acceleration	0.30g
Importance class II	$\gamma_I = 1.0$
Ground type	C
Behaviour factor	3
Seismic combination coefficient for the quasi-permanent value of variable actions	$\psi_2=0.30$

5.2 Basic and non-seismic design

5.2.1 Simulation

The modelling and design of the building, has been performed with the finite element software SAP2000v19 [6] The structural model is a linear-elastic model with beam elements, while no-section area elements were used for the correct distribution of the loads. The beam elements representing the FUSEIS pin links are divided into three parts with different cross sections in order to simulate the receptacle beams and the dissipative pin in the middle (Figure 5.7).

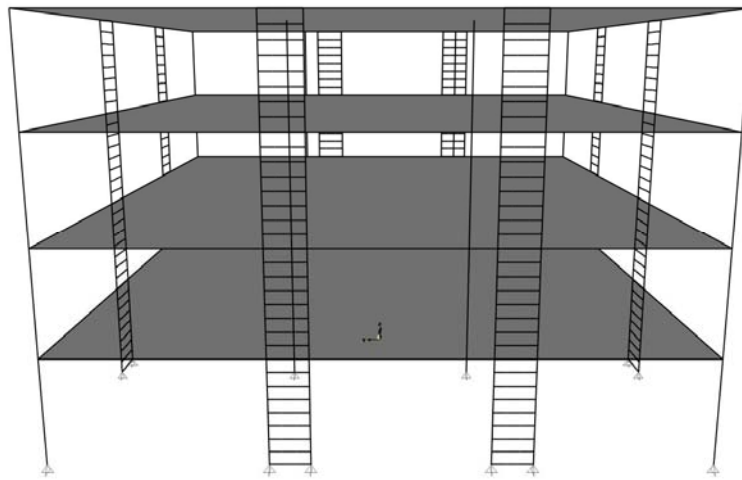


Figure 5.6: 3D view of the model in SAP2000

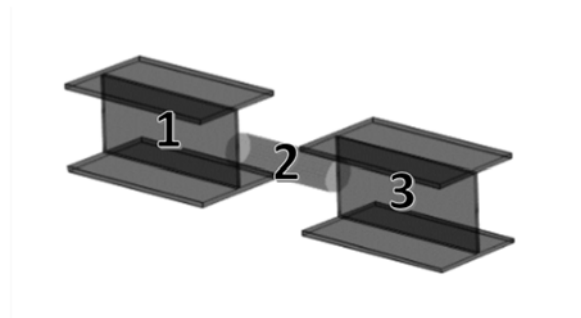


Figure 5.7: Simulation of FUSEIS pin link, division into three parts

5.2.2 Analysis and design

The columns and the beams of the main frame as well as the composite slabs, were designed both in the Ultimate Limit State (ULS) and the Serviceability Limit State (SLS) in accordance with the provisions of Eurocodes 3 and 4 [4], [8].

The profiles of all non-system members have been selected so that all the Eurocodes requirements are satisfied. When the programme automatic calculations were inadequate, e.g. for the design of the composite beams, hand calculations were used instead. The resulting cross section for the main beams was IPE500, for the secondary beams HEA200 and for the columns varied

between HEB200 and HEB280. For the design of the secondary beams, construction phases were critical, so temporary supports should be placed to reduce both bending deformation and section size.

The slabs are composite for all floors and were designed with the program SymDeck Designer, a software provided by the manufacturer, which takes into account construction phases both for the ultimate and serviceability limit states. The materials used are Fe320 for the steel sheet, C25/30 for concrete and B500C for reinforcing steel. The thickness of the steel sheet is 0.80mm and the longitudinal reinforcement is $\varnothing 8/100$.

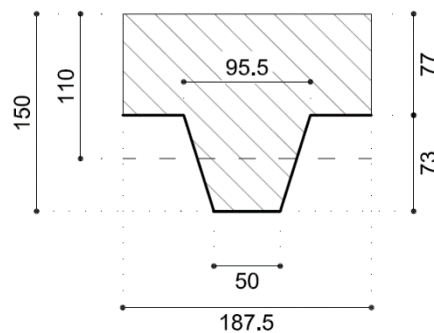
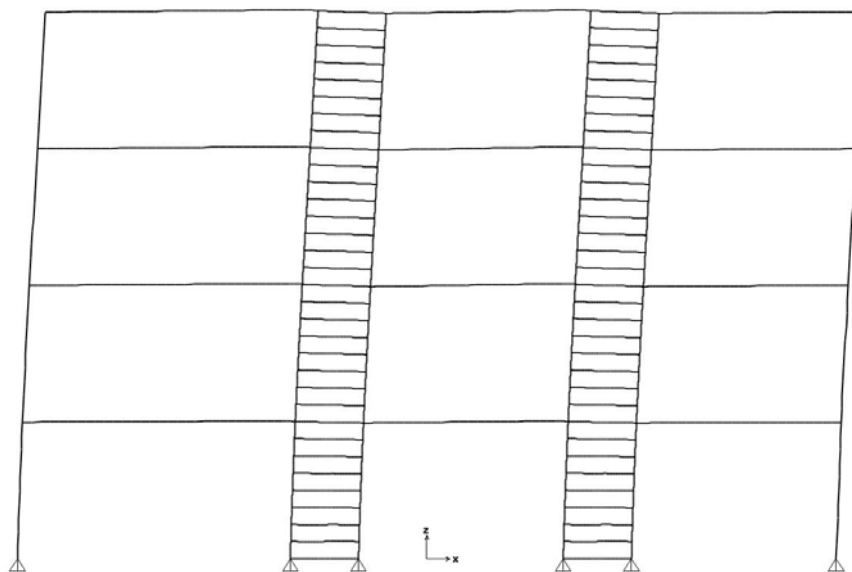
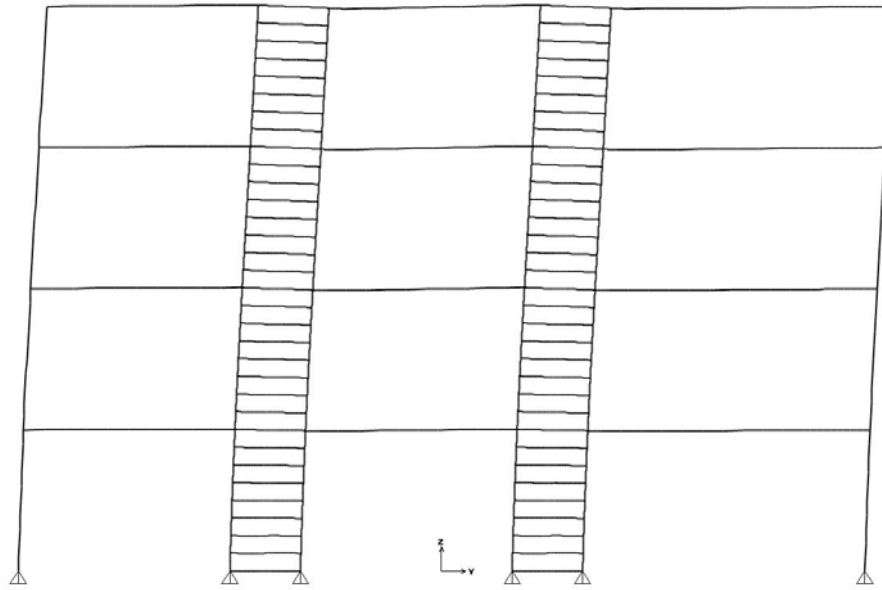


Figure 5.8: Composite slab section

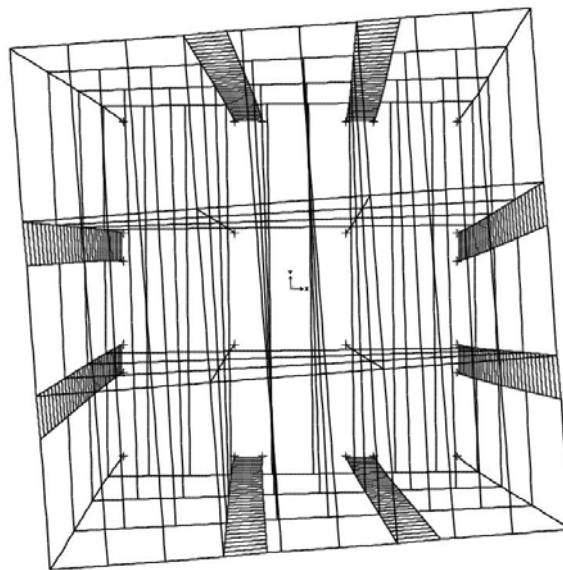
Multi - Modal Response Spectrum Analysis was carried out, to calculate the lateral loads and deformations and to dimension the FUSEIS systems. The first 5 modes were used to activate more than 90% of the mass. The first and the second modes were translational while the third was rotational, with their eigen periods and shapes given in Figure 5.9.



(a) 1st mode of vibration ($T_1=1.07s$)



(b) 2nd mode of vibration ($T_2=1.07s$)



(c) 3rd mode of vibration ($T_3=0.69s$)

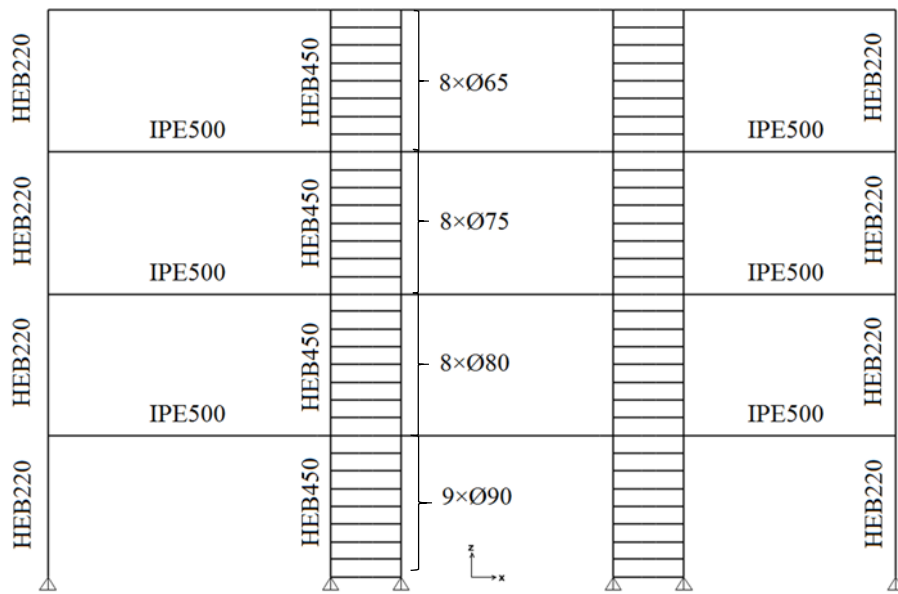
Figure 5.9: 1st, 2nd, 3rd mode shapes

The sections and configuration of the system were chosen after an iterative process. The FUSEIS systems consisted of a pair of strong columns (HEB450) at a central distance of 2.00m, the receptacle beams were HEA260, while nine links per storey were used, rigidly connected to the system columns. The dissipative elements of the links have steel grade S235, while the receptacle beams are S275, which is lower than the rest of the structural members (S355).

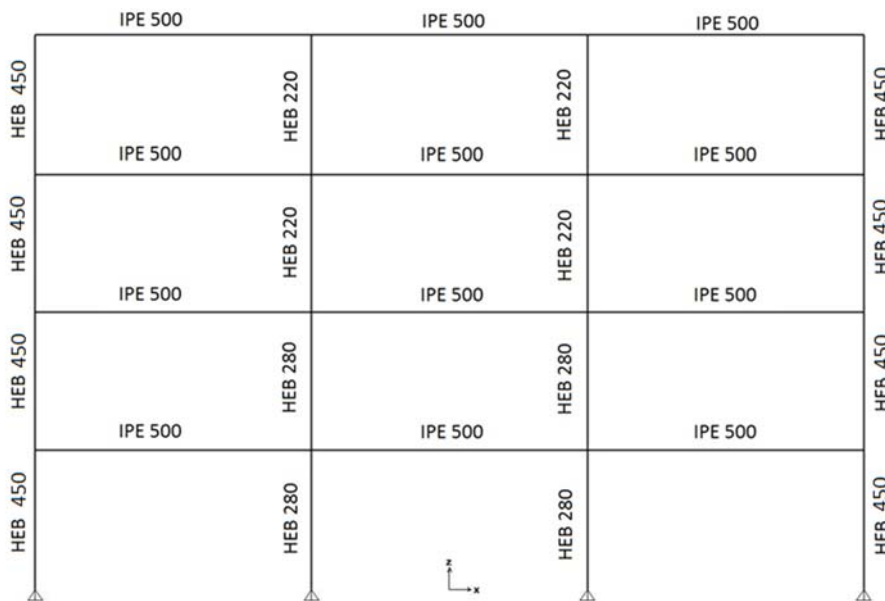
Table 5.2 summarizes the cross sections of the FUSEIS systems, starting from the foundation level.

Table 5.2: Cross sections of FUSEIS pin system (starting from ground floor)

Number of links	Full diameter section	Reduced diameter section	FUSEIS columns section	FUSEIS receptacle beams
×9	Ø105	Ø90	HEB450	HEA260
×8	Ø95	Ø80	HEB450	HEA260
×8	Ø90	Ø75	HEB450	HEA260
×8	Ø80	Ø65	HEB450	HEA260



(a) External frame sections



(b) Internal frame sections

Figure 5.10: Cross sections of the building

In order to ensure the development of a bending mechanism at the RDS (reduced diameter section) positions, the length l_{pin} was taken larger than the one calculated from Eq. (5.1), i.e. 300mm.

$$l_{pin} \geq \frac{4 \times M_{pl, pin, Rd}}{V_{pl, pin, Rd}} = \frac{4 \times W_{pl, pin}}{A_v / \sqrt{3}} \quad \text{Eq. (5.1)}$$

$M_{pl, pin, Rd}$	is the design plastic moment resistance of the weakened part of the pin
$V_{pl, pin, Rd}$	is the design shear resistance of the weakened part of the pin
l_{pin}	is the length of the weakened part of the pin (Figure 5.3)
$W_{pl, pin}$	is the plastic section modulus of the weakened part of the pin

5.3 Seismic analysis

5.3.1 Seismic design

The conventional method for calculating the seismic loads is by applying Multi - Modal Response Spectrum Analysis, according to Eurocode 8 [3]. In each direction, the number of modes taken into consideration is such, that the sum of the effective modal mass is greater than the 90% of the total mass. In order for the inelastic deformations to be considered, a behaviour factor must be introduced. The design guidelines propose a maximum value of the behaviour factor q equal to 3 for the FUSEIS pin link system.

In order to control the overall stability of the structure and the design of the ductile and non-ductile members under seismic loads, the conditions of §5.3.2-5.3.50 should be fulfilled, according to the design guide. Because the structure has similar stiffness and behaviour in both directions, only the results of x-direction are presented.

5.3.2 Limitation of inter-storey drift

Considering that the building has ductile non-structural members, Eq. (5.2) must be fulfilled.

Table 5.3 shows the results of the analysis and in both cases the check is verified in all storeys.

$$d_{r,v} \leq 0.0075h \quad \text{Eq. (5.2)}$$

Table 5.3: Limitation of inter-storey drift

Storey	u_x (mm)	d_{ex} (mm)	q^*d_{ex} (mm)	v^*d_{rx} (mm)	Check	0.0075h
1 st	11.9	11.9	35.6	17.8	\leq	30
2 nd	28.3	16.4	49.2	24.6	\leq	30
3 rd	46.8	18.5	55.5	27.7	\leq	30
4 th	65.0	18.2	54.7	27.4	\leq	30

5.3.3 Magnitude of 2nd order effects

The inter-storey drift coefficient θ may be calculated by a linear buckling analysis through the factor α_{cr} , the factor by which the design loading has to be increased to cause elastic instability in a global mode.

This check indicates whether the deformations of the structure are too big to ignore 2nd order effects. A linear buckling analysis was performed and the critical buckling factor α_{cr} , coefficient θ and checks derived from this analysis are presented in Table 5.4. According to EN1998-1 §4.4.2.2, when the inter-storey drift sensitivity coefficient θ , is limited to $\theta \leq 0.1$, 2nd order effects can be ignored.

Table 5.4: Magnitude of 2nd order effects

α_{cr}	$\theta = q / \alpha_{cr}$	Check	limit	Seismic load multiplier
46	0.065	\leq	0.1	1.00

5.3.4 Dissipative elements verifications

The FUSEIS systems were designed based on the results of the most unfavourable seismic combination 1.0G+0.3Q+E. In order to ensure a uniform dissipative behaviour, the overstrength values Ω of the reduced sections were checked to differ less than 25%. A factor $\max\Omega/\min\Omega=1.18$ was calculated. Table 5.5 to Table 5.8 summarize the results of all dissipative element verifications. As shown, the bending moment check was the most critical, with maximum utilization factor equal to 90%. Additionally, it was derived from the shear check, that no reduction of bending moment resistance was needed due to high shear force.

Table 5.5: Check of axial forces

Reduced diameter pins Φ (mm)	N_{Ed} (kN)	$N_{pl,pin,Rd}$ (kN)	$\frac{N_{Ed}}{N_{pl,pin,Rd}} \leq 0.15$
Ø90	0.52	1495.00	0.000
Ø80	0.58	1181.24	0.000
Ø75	4.43	1038.20	0.004
Ø65	4.16	779.82	0.005

Table 5.6: Check of shear forces

Reduced diameter pins Φ (mm)	$V_{CD,Ed}$ (kN)	$V_{pl, pin, Rd}$ (kN)	$\frac{V_{CD,Ed}}{V_{pl, RBS/pin, Rd}} \leq 0.5$
Ø90	188.00	863.14	0.22
Ø80	133.17	681.98	0.20
Ø75	109.67	599.40	0.18
Ø65	70.50	450.21	0.16

Table 5.7: Check of bending moments

Reduced diameter pins Φ (mm)	M_{Ed} (kNm)	$M_{pl, pin, Rd}$ (kNm)	$\frac{M_{Ed}}{M_{pl, pin, Rd}} \leq 1.00$
Ø90	24.44	28.20	0.87
Ø80	17.93	19.98	0.90
Ø75	14.52	16.45	0.88
Ø65	9.17	10.58	0.87

Considerably large rotations developed in FUSEIS pins during seismic excitation. Therefore, it is necessary to limit these rotations accordingly.

$$\theta_{pin} = \frac{L}{l_{pin}} \times \theta_{gl} \leq \theta_{ULS, pin} \quad \text{Eq. (5.3)}$$

Where

L is the axial distance between the FUSEIS columns (Figure 5.4)

l_{pin} is the length of the weakened part of the pin (Figure 5.3)

θ_{gl} is the rotation of the FUSEIS system as shown in (Figure 5.4)

$\theta_{ULS, pin}$ is equal to 14%

The results in Table 5.8 show that all rotations are well below the limit value.

Table 5.8: Check of chord rotation

Storey number	θ_{pin} (mrad)	check	$\theta_{pl, pin}$ (mrad)
1 st	59.38	\leq	140
2 nd	81.96	\leq	140
3 rd	92.45	\leq	140
4 th	91.21	\leq	140

5.3.5 Non-dissipative elements verifications

The non-dissipative elements i.e. the system columns, the receptacle beams, the full section pins and their connections were capacity designed for increased internal forces.

5.3.5.1 System columns

The utilization factors of the system columns were calculated according to the provisions of EN1993-1-1 [4]. The increased forces were calculated according to the following equations:

$$N_{CD,Ed} = N_{Ed,G} + 1.1 \times \alpha \times \gamma_{ov} \times \Omega \times N_{Ed,E} \quad \text{Eq. (5.4)}$$

$$M_{CD,Ed} = M_{Ed,G} + 1.1 \times \alpha \times \gamma_{ov} \times \Omega \times M_{Ed,E} \quad \text{Eq. (5.5)}$$

$$V_{CD,Ed} = V_{Ed,G} + 1.1 \times \alpha \times \gamma_{ov} \times \Omega \times V_{Ed,E} \quad \text{Eq. (5.6)}$$

where,

$N_{Ed,G}$, $M_{Ed,G}$, $V_{Ed,G}$ are the internal forces due to the non-seismic actions of the seismic combination

$N_{Ed,E}$, $M_{Ed,E}$, $V_{Ed,E}$ are the internal forces due to the seismic action

$\Omega = \min \Omega_i = \min \left\{ \frac{M_{pl,RBS,pin,Rd,i}}{M_{Ed,i}} \right\}$ is the minimum overstrength factor

γ_{ov} is the material overstrength factor (suggested value 1.25)

$\alpha=1.5$ is an additional factor only used for the FUSEIS pin link system, to ensure that pin links will yield first

In any case, the increment factor ($1.1 \times \gamma_{ov} \times \Omega$ or $1.1 \times \alpha \times \gamma_{ov} \times \Omega$) shall not exceed the behaviour factor q .

The utilization factors of the system columns were calculated according to the provisions of EN1993-1-1 and were as high as 100% for both cases.

5.3.5.2 Full pin sections and receptacles

The moment resistance of the full pins sections was verified at the contact area with the face plates. The utilization factors for pin sections and receptacles are shown in Table 5.9.

a) Receptacle beams

The receptacle beams shall be capacity designed, to ensure that they will not yield prior to the reduced diameter section pin, according to Eq. (5.8):

$$\frac{M_{CD,Ed}}{M_{pl,rec,Rd}} \leq 1.0 \quad \text{Eq. (5.7)}$$

$$M_{CD,Ed} = \frac{I_{net}}{I_{pin}} M_{pl,pin,Rd} \quad \text{Eq. (5.8)}$$

where,

$M_{pl,pin,Rd}$ is the design plastic moment resistance of the weakened part of the pin

$M_{CD,Ed}$ is the capacity design bending moment

I_{net} is the total length of the link between the column flanges (Figure 5.3)

$M_{pl,rec,Rd}$ is the design bending moment resistance of the receptacle beam

b) Full pin section

To ensure that the full cross section of the pins will not yield prior to the reduced sections, the moment resistance of the full cross section shall be verified to be greater than the capacity design moment $M_{CD,Ed}$, calculated as shown in Eq. (5.9).

$$\frac{M_{CD,Ed}}{M_{pl,Rd}} \leq 1.0 \quad \text{Eq. (5.9)}$$

$$M_{CD,Ed} = \frac{I}{I_{pin}} M_{pl,pin,Rd} \quad \text{Eq. (5.10)}$$

where,

I for FUSEIS beam link system is the length between the face plates of the columns and for FUSEIS pin links is the length between the face plates of the receptacles (Figure 5.3)

$M_{pl,Rd}$ is the design bending moment resistance of the full beam/pin section

Table 5.9: Utilization factors of the full pin sections and receptacles

Full diameter pins Φ (mm)	$M_{CD,Ed}$ (kNm)	$M_{pl,Rd}$ (kNm)	$\frac{M_{CD,Ed}}{M_{pl,Rd}} \leq 1.00$
Ø105	37.60	44.91	0.84
Ø95	26.63	33.37	0.80
Ø90	21.93	28.20	0.78
Ø80	14.10	19.98	0.71
Receptacle HEA260	145.70	252.95	0.58

c) Connection between the FUSEIS links and the columns

The joints between the FUSEIS links and the system columns, are formed as fully welded. To ensure that these connections will have enough overstrength to yield after the plastification of the links, they are capacity designed according to Eq. (5.11) and Eq. (5.12) and the results for a typical connection are given in Table 5.10.

$$M_{CD,con,Ed} = 1.1 \times \gamma_{ov} \frac{L_{net}}{l_{pin}} M_{pl,pin,Rd} \quad \text{Eq. (5.11)}$$

$$V_{CD,con,Ed} = 1.1 \times \gamma_{ov} \frac{2 \times M_{pl,pin,Rd}}{l_{pin}} \quad \text{Eq. (5.12)}$$

Table 5.10: Welded connection design

Design moment (kNm)	Design force (kN)	Stiffeners Thickness (mm)	Beam welds	Utilization factor
155	255	8	$a_r=8\text{mm}$ $a_w=5\text{mm}$	0.98

5.4 Structural detailing

After fulfilment of all checks the FUSEIS links may be detailed. Their final design is presented in Figure 5.12 and Figure 5.13. The lengths of each part of the FUSEIS links are the same along the height of the building. Only the diameter of the pin is variable, as shown in Table 5.2.

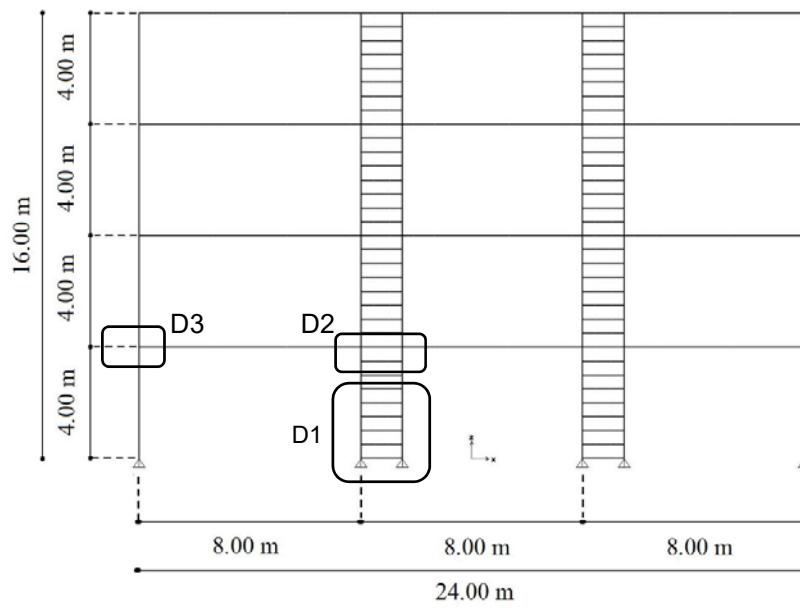


Figure 5.11: Side view of building

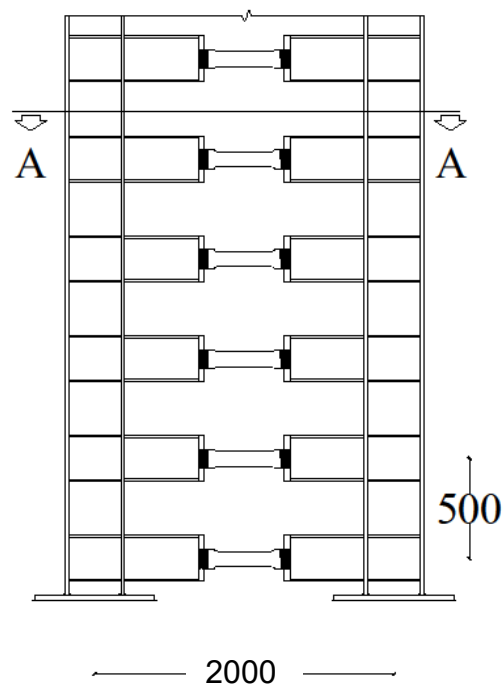


Figure 5.12: Detail D1

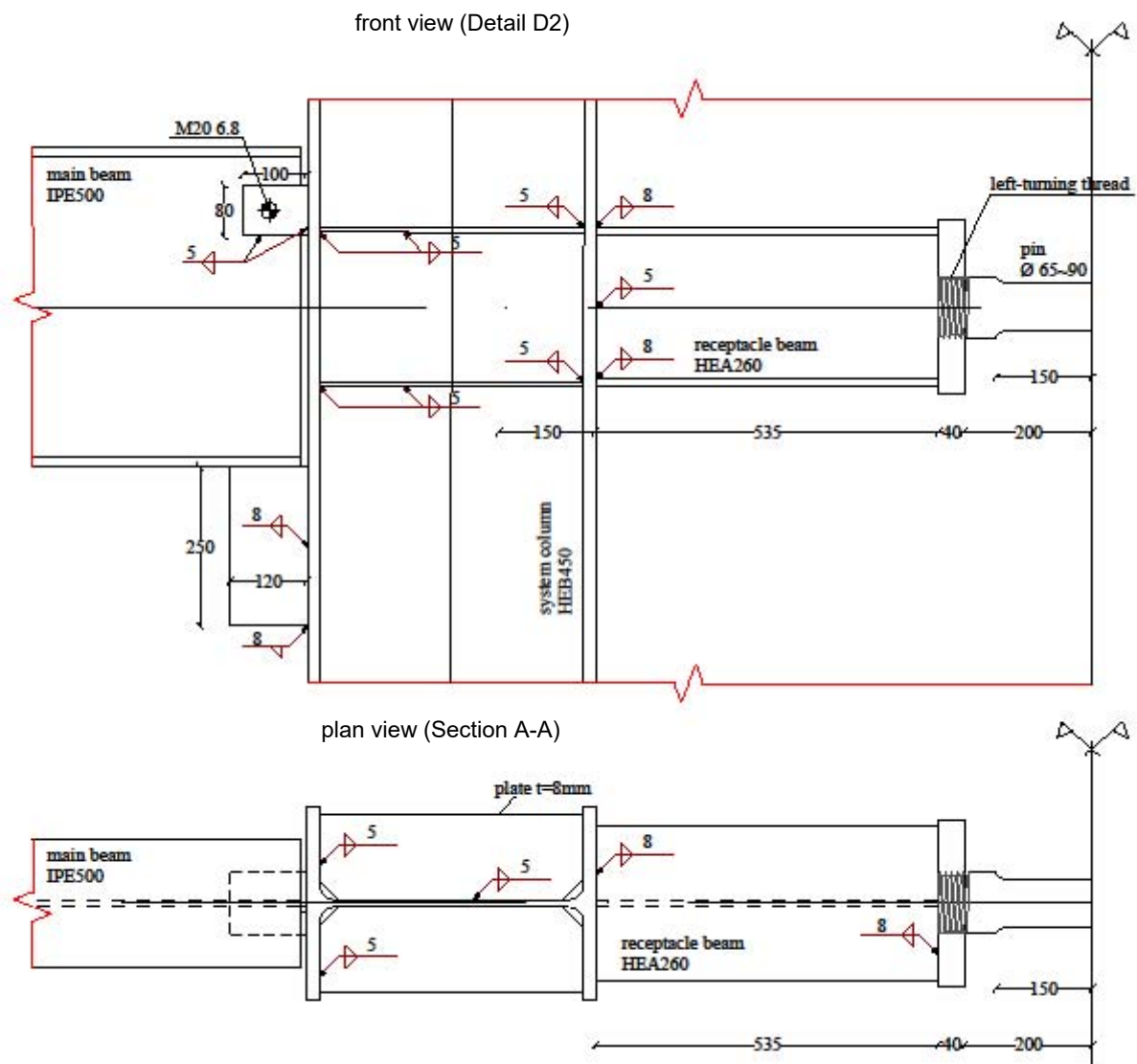


Figure 5.13: Side view and plan view of a typical FUSEIS horizontal link

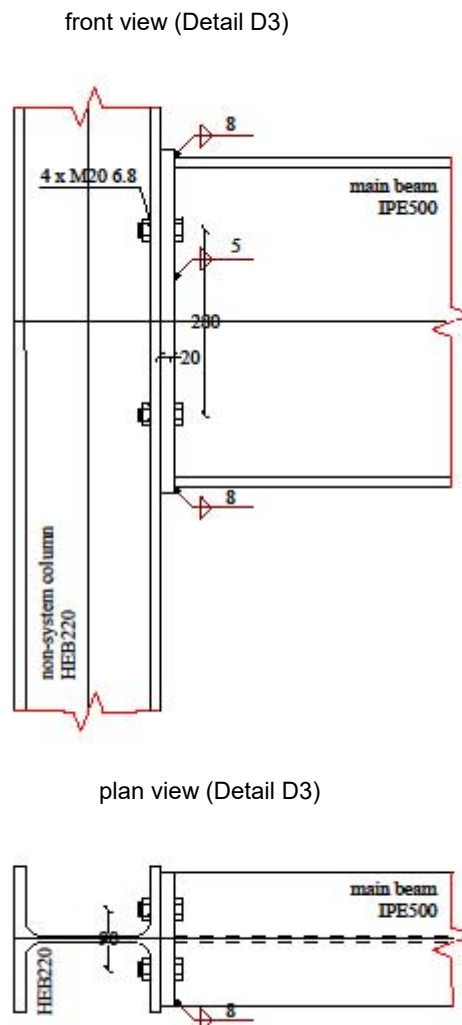


Figure 5.14: Beam to column connection of the main frame

5.5 References

1. Vayas, I., Karydakis, Ph., Dimakogianni, D., Dougka, G., Castiglioni, C. A., Kanyilmaz, A. et al. Dissipative devices for seismic resistant steel frames - The FUSEIS Project, Design Guide. Research Programme of the Research Fund for Coal and Steel 2012.
2. I. Vayas, Ph. Karydakis, D. Dimakogianni, G. Dougka, Castiglioni, C. A., Kanyilmaz, A. et al. Dissipative devices for seismic-resistant steel frames (FUSEIS). Research Fund for Coal and Steel, European Commission; EU 25901 EN 2013.
3. EN1998-1-1, Eurocode 8: Design of structures for earthquake resistance – Part 1-1: General rules, seismic actions and rules for buildings. Brussels: Comitee Europeen de Normalisation (CEN); 2003.
4. EN1993-1-1, Eurocode 3: Design of steel structures - Part 1-1: General rules and rules for buildings. Brussels: Comitee Europeen de Normalisation (CEN); 2003.

5. FEMA – 356: Prestandard and Commentary for the seismic rehabilitation of Buildings. Washington; 2000.
6. SAP2000, CSI, Computers and Structures Inc., www.csiberkeley.com.
7. EN1994-1-1: Eurocode 4: Design of composite steel and concrete structures. Part 1-1: General rules and rules for buildings. Brussels: Comité Européen de Normalisation (CEN); 2005.
8. EN 1993-1-8: Eurocode 3: Design of steel structures. Part 1-8: Design of joints. Brussels: Comité Européen de Normalisation (CEN); 2004.
9. EN1991-1-1, Eurocode 1: Actions on structures

6 BOLTED FUSEIS BEAM SPLICE

The case study which presents the implementation of dissipative bolted FUSEIS beam splices is elaborated in section 2. The report presents the mid-rise case study (4-storey) equipped with FUSEIS bolted beam splices and INERD pin connections in both main directions of the buildings. The reader is kindly invited to go back in the text and follow the case study there.

7 WELDED FUSEIS BEAM SPLICE

7.1 General

7.1.1 Introduction

This case study refers to the seismic design of new eight-story composite concrete and steel office buildings. It aims to demonstrate the implementation of the welded FUSEIS beam splice. The elaborated case study comprises the conceptual design, modelling and analysis by linear response spectrum analysis methods (RSA), detailed design of main dissipative and non-dissipative members as well as basic structural detailing of welded beam splice.

7.1.2 Description of the building

7.1.2.1 Geometry, materials and general assumptions

The case study deals with an eight-story frame building with three 8 m bays in both directions. The gravity frames are composed of beams and columns, located at each structural axis. Lateral forces are resisted by the moment resistant frames with welded FUSEIS beam splices (MRF-WFBS) in the Y direction and by conventional concentrically braced frames (CBF) in the X direction. In this respect, beam-to-column joints and column bases are assumed as fully fixed in the Y direction and nominally pinned in the X direction. The floor plan and elevation of the building are illustrated in Figure 7.1 to Figure 7.4. Figure 7.5 gives the dimensions assigned to the concrete slab. The elements and materials used herein are:

In the Y direction – MRF-WFBS

- IPE450 composite beams (S275 steel grade and C25/30, A500 NR concrete)
- HEA200 composite beams (S355 steel grade and C25/30, A500 NR concrete) – resist vertical loads only
- Columns with S355 steel grade (strong moment of inertia)

In the X direction – CBF

- IPE500 beams (S355 steel grade)
- Columns with S355 steel grade (weak moment of inertia)
- CBF bracings which are assumed to function in tension only (highlighted in blue Figure 7.1 in and Figure 7.2).

The welded FUSEIS beam splices are placed near the null moment sections defined by the gravity loading. The reinforced beam zone adjacent to the welded FUSEIS beam splices (red segments in Figure 7.1) consists in the reinforcement of

the IPE450 composite beam with welded web and flange plates. Diaphragms are assumed rigid, thus neglecting membrane (in-plane) deformations.

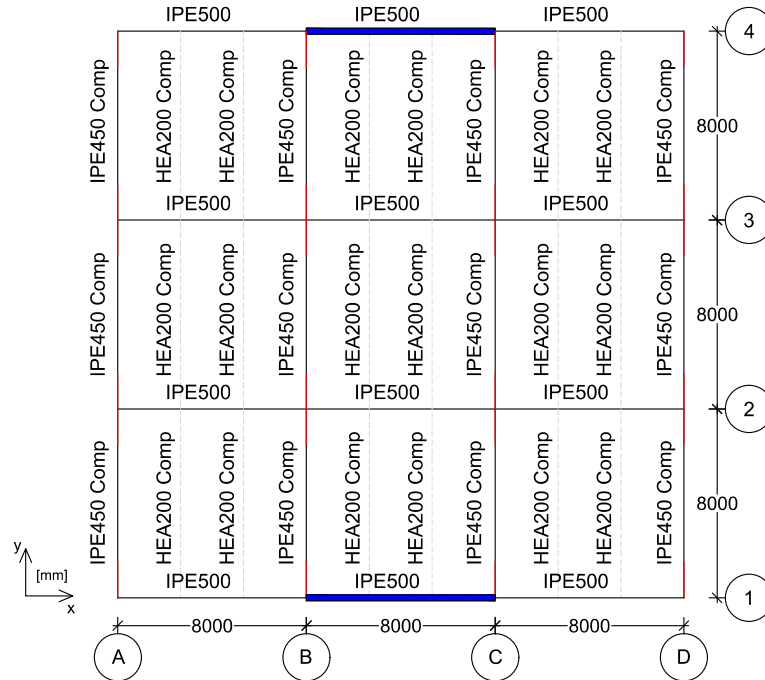


Figure 7.1: Plan view of case study building

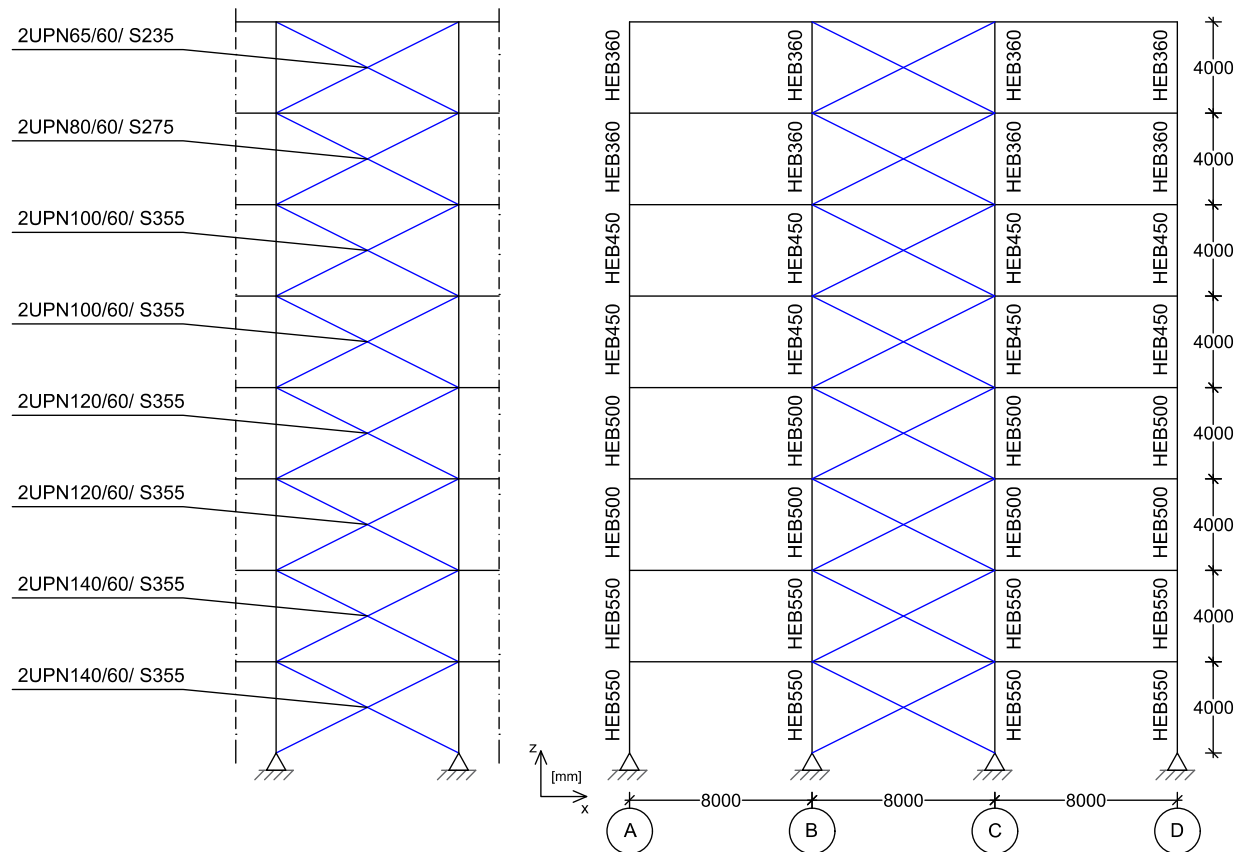


Figure 7.2: Exterior side view of the case study building (X direction)

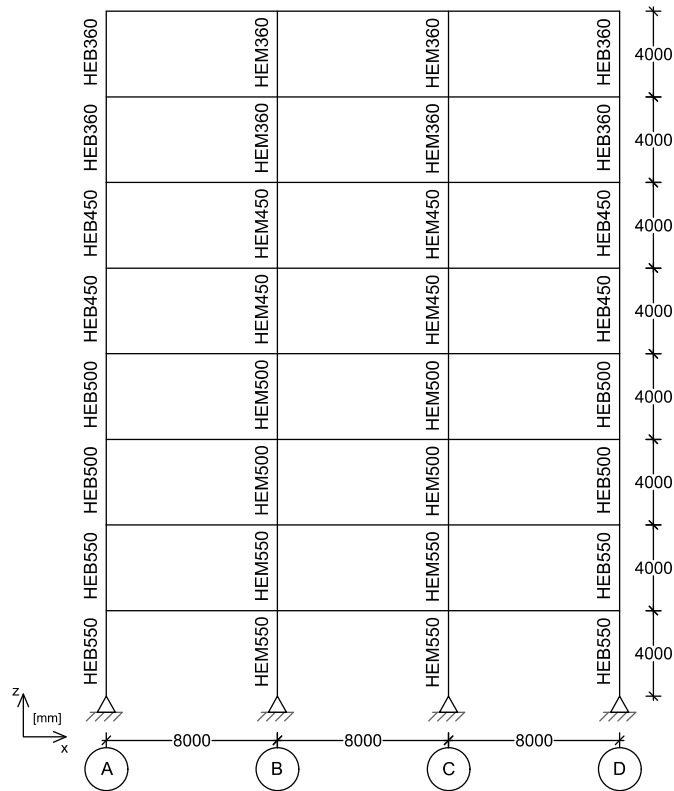


Figure 7.3: Interior side view of the case study building (X direction)

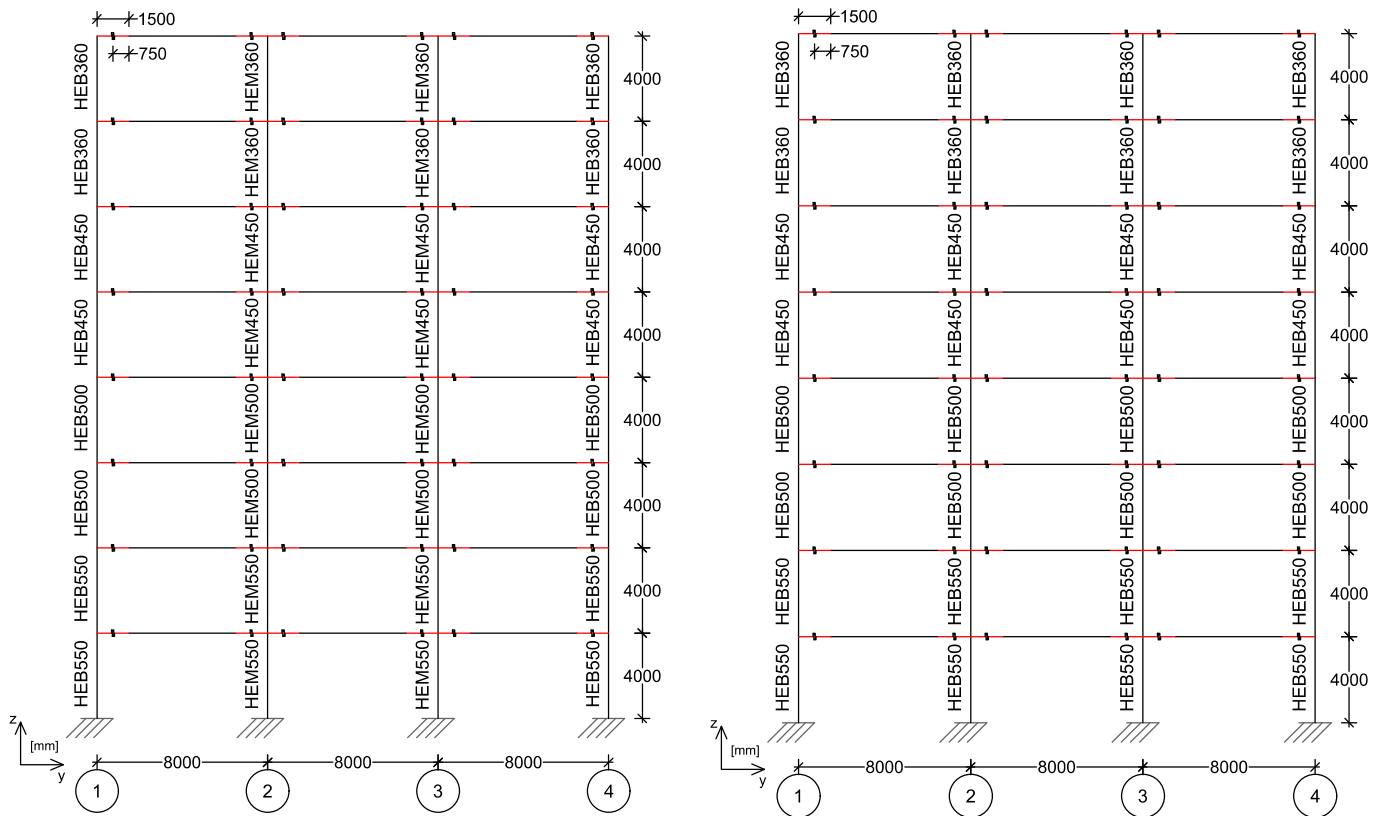


Figure 7.4: Exterior and interior side views of the case study building (Y direction)

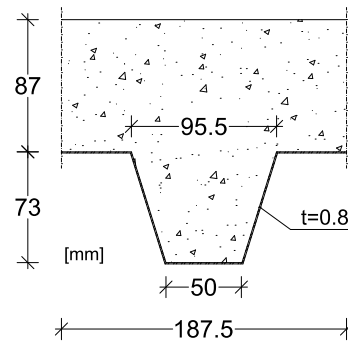


Figure 7.5: Representation of the composite slab (thickness of the profile steel sheet – 0.8 mm)

7.1.2.2 Loads and load combinations

The gravity loads and seismic action parameters are summarized in Table 7.1, whereas Table 7.2 presents the coefficients for the various load combinations.

Table 7.1: Quantification of the applied gravity loads and seismic action parameters

Vertical loads		
Load Class	Type of load	Value
Dead Load	Composite slab with profile sheeting	3.00 kN/m
Superimposed loads	Services, ceiling and raised floors	0.70/1.00 kN/m ² ¹
	Perimeter walls	4.00 kN/m
Live loads	Office (Class B)	3.00 kN/m ² ²
	Movable partitions	0.80 kN/m ²
Seismic action		
Importance factor (Class II)	$\gamma_I=1.00$	
Soil acceleration	$a_{gr}=0.30g$	
Soil type	C	
S_{max}	1.15	
T_B	0.20 s	
T_C	0.60 s	
T_D	2.00 s	
Damping ratio	5%	
Behavior factor	4	

¹ 0.70 kN/m² for the first floor and 1.00 kN/m² for the roof

² The roof is considered as accessible and, according to the paragraph 6.3.4.1(2) of [1], this has the same live load value as the service floor.

Table 7.2: Coefficients used for the load combinations

Coefficient	Value
γ_G	1.35
γ_Q	1.50
Ψ_2 Office (Class B)	0.30
Ψ_2 Roof	0.00
φ Correlated floors	0.80
φ Roof	1.00

The seismic masses are calculated according to Eq. (7.1) and presented in Table 7.3.

$$\sum_{j>1} G_{k,j} + \sum_{i>1} \Psi_{2,i} \cdot \varphi_i \cdot Q_{k,i} \quad \text{Eq. (7.1)}$$

Table 7.3: Quantification of seismic masses

Seismic mass of the first 7 floors		2325.40 t
Concrete and metal deck self-weight + Composite IPE and HEA + IPE500 (Gk1,1-7)	$(3.00 \cdot 24.00 \cdot 24.00 + 73.01 + 59.63 + 85.72) / 9.81$	198.41 t
Utilities, ceiling, floor finishing (Gk2,1-7)	$0.70 \cdot 24.00 \cdot 24.00 / 9.81$	41.10 t
Perimeter walls (Gk3,1-7)	$4.00 \cdot 4.00 \cdot 24.00 / 9.81$	39.14 t
Partitions (Qk1,1-7)	$0.80 \cdot 0.30 \cdot 0.80 \cdot 24.00 \cdot 24.00 / 9.81$	11.27 t
Imposed loads (Qk2,1-7)	$0.80 \cdot 0.30 \cdot 3.00 \cdot 24.00 \cdot 24.00 / 9.81$	42.28 t
Seismic mass floor of the roof		257.12 t
Concrete and metal deck self-weight + Composite IPE and HEA + IPE500 (Gk1,8)	$(3.00 \cdot 24.00 \cdot 24.00 + 73.01 + 59.63 + 85.72) / 9.81$	198.41 t
Utilities, ceiling, floor finishing (Gk2,8)	$1.00 \cdot 24.00 \cdot 24.00 / 9.81$	58.72 t
Imposed loads (Qk1,8)	$0.00 \cdot 1.00 \cdot 24.00 \cdot 24.00 \cdot 3.00 / 9.81$	0.00 t
Columns and CBF mass		107.42 t
Total		2689.94 t

7.2 Basic and non-seismic design

7.2.1 Preliminary design of the welded FUSEIS beam splices and reinforcing zones

To assess the MRF-WFBS resistance to seismic action based on the linear response spectrum analysis, initial dimensions of the welded FUSEIS beam splice components must be defined. Following the recommendations in [2] and [3], the user shall begin with the preliminary design of the gravity members based on the ultimate and serviceability limit state criteria, assuming a building without welded FUSEIS beam splices. Then, subjecting the conventional structure to a linear response spectrum analysis, the user acquires an initial idea of the building performance under earthquake loading, thus estimating approximately the acting moment that the welded FUSEIS beam splice will have to resist. Finally, all other components' preliminary dimensions may be subsequently derived. Table 7.4 presents the acting moment estimated based on the conventional structure and the dimensions chosen for the flange plate of the fuses. Table 7.5 gives the computed dimensions for the rest of the components. Figure 7.6 indicates the location of the welded FUSEIS beam splice and the span of the reinforced beam cross section. Finally, Figure 7.7 illustrates the definition of each dimension.

Table 7.4: Preliminary design of the flange plate of the fuses

Floor	$M_{Ed,est}$ [kNm]	Lever arm (z) [m]	$N_{f,est}$ [kN]	Flange plate dimensions ($b_f \cdot t_f$) [mm ²]
1	193	0.569	340	170*12 (S235)
2	238	0.569	419	170*12 (S235)
3	239	0.569	420	170*12 (S235)
4	224	0.569	394	170*12 (S235)
5	201	0.568	354	170*10 (S235)
6	176	0.568	310	170*10 (S235)
7	131	0.568	231	170*8 (S235)
8	78	0.567	137	170*8 (S235)

where:

$M_{Ed,est}$ Estimated design moment for the welded beam splices
 $N_{f,est} = M_{Ed,est} / Z$ Estimated design axial force for the flange plate of the fuse

Table 7.5: Dimensions adopted for the rest of the components

Component	Criteria	Assigned dimension		Material
Gap (g)	Approximately 10% of the beam cross-section height	50 mm for all fuses		-
Free length (L_0)	Rotation capacity, buckling of the fuse flange plate	200 mm for all fuses		-
Upper layer rebar (Φ_{upper})	Must remain elastic, at least twice the mechanical area of the flange plate (i.e. $2 \cdot A_r \cdot f_{sd}/f_{yd}$ where $f_{sd}=235$ MPa and $f_{yd}=500$ MPa)	12 Φ 16 mm for all fuses		A500
Lower layer rebar (Φ_{lower})	Must remain elastic	170*8	12 Φ 12 mm	A500
		170*10	8 Φ 12 mm	
		170*12	8 Φ 10 mm	
Web plate of the fuses ($h_w \cdot t_w$)	Capacity design of the fuse resisting moment	2 plates of 170*8 mm ² for all fuses		S235
Reinforcing flange plates ($b_{r,f} \cdot t_{r,f}$)	Reinforced cross section must remain elastic	240*10 mm ² for all fuses		S275
Reinforcing web plates ($h_{r,w} \cdot t_{r,w}$)	Reinforced cross section must remain elastic	2 plates of 200*10 mm ² for all fuses		S275
Beam	-	IPE450		S275

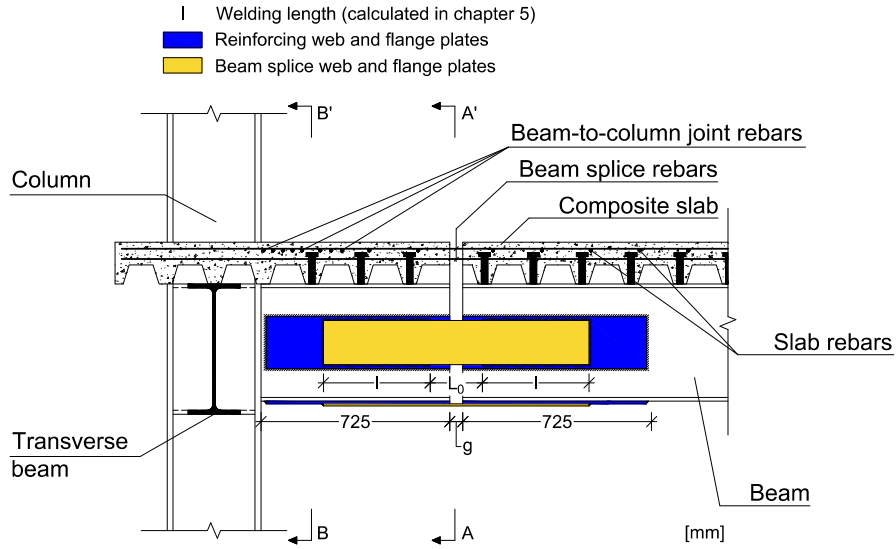
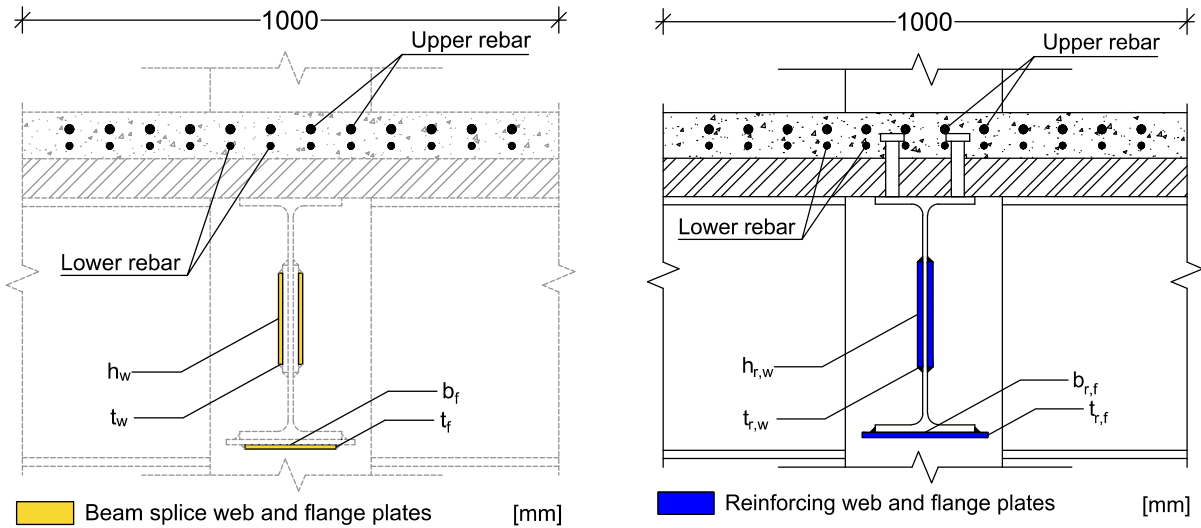


Figure 7.6: Location of the welded FUSEIS beam splice and span of the reinforced zone



Cross section A-A'

Cross section B-B'

Figure 7.7: Illustration of the dimensions of each component

7.2.2 Simulation

The building is modelled with frame type elements only, using the SAP2000 software [4]. The types of connections assigned for the beam-column joints and the base of the columns were already described in section 7.1.2.1. Diaphragm constraint is applied on each floor. The composite beams are modelled by means of the section designer command offered by SAP2000 [4]. The welded FUSEIS beam splice stiffness and strength properties were determined according to [2, 3]. Bracings are assumed to be tension-only. According to [5], braced systems should be modelled with one bracing only and not both diagonals which form the X cross.

It should be noted that the equivalent number of bracings at each floor on each side of the structure shown subsequently in Figure 7.8 to Figure 7.10 is equal to one, since one of them were assigned null axial stiffness for both tension and compression situations. These bracings were only applied to consider their mass.

7.2.3 Design for static combinations

Given that the welded FUSEIS beam splices are placed strategically approximately at the null moment sections defined by gravity loads, these are in principle safety checked for static combinations. Nevertheless, this will be shown subsequently for demonstration purposes. Additionally, it is considered herein that the seismic design situation governs the design of the welded FUSEIS beam splices, therefore wind combination is not assessed.

7.2.3.1 Ultimate limit state results

The ultimate limit state load combination that governs the gravity members design is calculated according to Eq. (7.2).

$$\sum_{j>1} 1.35 \times G_{k,j} + \sum_{i>1} 1.5 \times Q_{k,i} \quad \text{Eq. (7.2)}$$

The results from the member verification are presented in Table 7.6.

Table 7.6: Verification of gravity members

Member	HEA composite	IPE composite	IPE500	Internal column	External column	Welded Beam Splice
Section	HEA200	IPE450	IPE500	HEM360	HEB360	170*8 mm ²
Steel grade	S355	S275	S355	S355	S355	S235
M _{y,Rd+} [kNm]	382	918	779	-	-	163
M _{y,Rd-} [kNm]	184	*				
N _{Rd} [kN]	-	-	-	-11317	-6411	-
N _{Ed} [kN]	-	-	-	-1463	-784	-
M _{y,Ed+} [kNm]	173	124	670	≈ 0	≈ 0	39
M _{y,Ed-} [kNm]	131	*				
M _{z,Ed} [kNm]	-	-	-	≈ 0	≈ 0	-
Ratio+	0.45	0.14 ^a	0.86	0.13 ^b	0.12 ^c	0.24 ^d
Ratio-	0.71	*				

a, b, c Section was designed to increase the global stiffness of the structure

d In elastic regime

* Negative moments are resisted by the reinforced cross section in IPE composite beams

7.2.3.2 Serviceability limit state checks

The serviceability limit state load combination is calculated according to Eq. (7.3).

$$\sum_{j>1} G_{k,j} + \sum_{i>1} \psi_0 \times Q_{k,i} \quad \text{Eq. (7.3)}$$

The results from the member verification are presented in Table 7.7.

Table 7.7: Verification of member's deflection

Member	Displacement [mm]	Deflection	Limit adopted	Ratio
HEA composite	17	1/476	1/250	0.52
IPE450 composite	2	1/4347	1/250	0.06
IPE500	28	1/288	1/250	0.87

7.2.4 Seismic analysis

7.2.4.1 Seismic design situation

The building is recognized as regular in plan and in height. Theoretically the center of masses and the center of rigidity coincide. To account for uncertainties in the location of masses and thus the rotational component of the seismic motion, additional accidental mass eccentricity (§4.3.3.3.3 [5]) with a value of 1200 mm (5% of 24000 mm) was introduced in both directions. The mass eccentricity effects were considered by defining two static load cases T_x and T_y , simulating rotation. To account for the torsional effects, the story seismic forces in both main directions were calculated based on the lateral force method (§4.3.3.2 [5]). The final seismic design situation accounting for accidental torsional effects was derived by Eq. (7.4) and Eq. (7.5).

$$E = E_x + 0.3E_y \pm T \quad \text{Eq. (7.4)}$$

$$E = 0.3E_x + E_y \pm T \quad \text{Eq. (7.5)}$$

where:

T is considered as $T_x + T_y$;

T_x and T_y are accidental torsional effects of applied story seismic force with eccentricity of 5% in X and Y direction, respectively;

E_x and E_y are the analysis results without accidental torsion by applying RSA in X and Y direction, respectively.

The seismic combination is calculated according to Eq. (7.6).

$$\sum_{j>1} G_{k,j} + \sum_{i>1} \psi_2 \times Q_{k,i} + E \quad \text{Eq. (7.6)}$$

where:

$G_{k,j}$ are the gravity load effects in seismic design situation;

$Q_{k,i}$ are the movable load effects in seismic design situation;

ψ_2 is given in Table 7.2;

E is the effect of the seismic action including accidental torsional effects.

7.2.4.2 Response spectrum analysis

Multi-modal RSA was performed. The first, second and third natural modes of vibrations are presented in Figure 7.8 to Figure 7.10, respectively. They correspond to the X and Y translational and the torsional mode. The results from the analysis are summarized in Table 7.8. The table indicates that additional translational modes were needed to activate more than 90% of the total mass.

Table 7.8: Participating mass ratio and periods

Mode no.	Type	Period [s]	Participating mass in direction X	Participating mass in direction Y
1	Y	2.026	0.000	0.773
2	X	1.966	0.776	0.000
3	TORSION	1.358	0.000	0.000
4	X	0.672	0.146	0.000
5	Y	0.654	0.000	0.109
6	TORSION	0.459	0.000	0.000
7	X	0.393	0.040	0.000
8	Y	0.356	0.000	0.047
Sum of participating mass			0.962	0.928

According to [5] for a period higher than T_c the spectrum acceleration must be equal or greater than the lower bound. Therefore, the response spectrum is

corrected by the lower bound limit and it affects the spectral accelerations related to the first and second periods.

Translation in Y

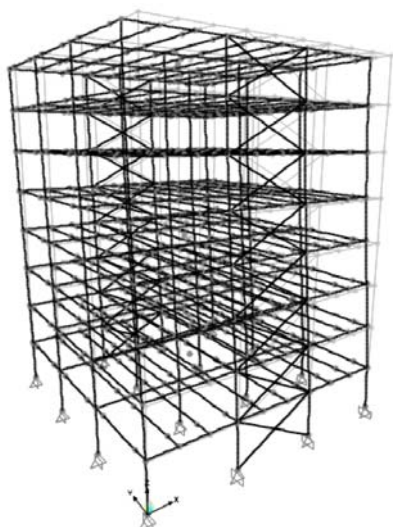


Figure 7.8: First mode of free vibration,
 $T_1 = 2.026$ s

Translation in X

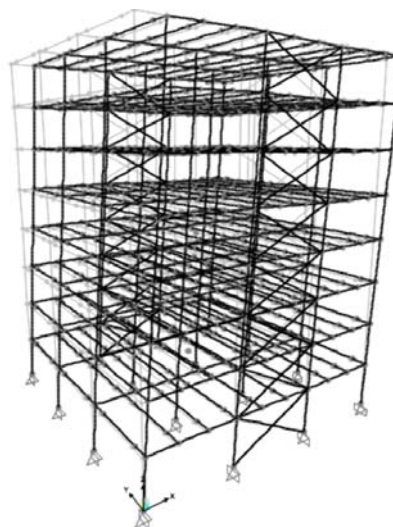


Figure 7.9: Second mode of free vibration,
 $T_2 = 1.966$ s

Torsional

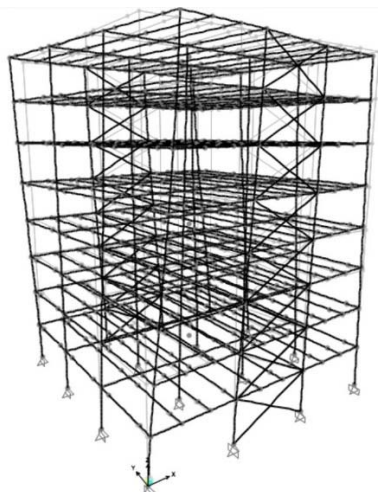


Figure 7.10: Third mode of free vibration,
 $T_3 = 1.358$ s

7.3 Detailed design

7.3.1 Damage limitation – limitation of inter-story drift

Assuming that the building has ductile non-structural elements, the verifications is:

$$d_r \cdot v \leq 0.0075h = 0.0075 \cdot 4 = 0.030 \text{ m} \quad \text{Eq. (7.7)}$$

where $\nu = 0.5$ is the reduction factor according to §4.4.3.2 (1) of [5], h is the story height and d_r is the design inter-story drift. Table 7.9 and Table 7.10 include the results from the analysis of each story.

Table 7.9: Inter-story drift for the X direction

Earthquake in the X direction			
Story	$d_{r,max}$ [m]	$d_{r,max} \cdot \nu$ [m]	≤ 0.030
1	0.010	0.023	True
2	0.018	0.023	True
3	0.020	0.025	True
4	0.019	0.025	True
5	0.017	0.026	True
6	0.015	0.024	True
7	0.012	0.022	True
8	0.007	0.018	True

Table 7.10: Inter-story drift for the Y direction

Earthquake in the Y direction			
Story	$d_{r,max}$ [m]	$d_{r,max} \cdot \nu$ [m]	≤ 0.030
1	0.029	0.015	True
2	0.056	0.028	True
3	0.060	0.030	True
4	0.059	0.029	True
5	0.053	0.027	True
6	0.045	0.022	True
7	0.037	0.018	True
8	0.022	0.011	True

where $d_{r,max}$ is the maximum design inter-story drift value within each directional earthquake combination, obtained by the product between the elastic inter-story drift and the behavior factor.

7.3.2 Second order effects

The second order effects are considered by the inter-story drift sensitivity coefficient θ given by Eq. (7.8), where P_{tot} and V_{tot} are the total gravity load at and above the story considered in the seismic design situation and the total seismic story shear at the story under consideration, respectively. Table 7.11 and Table 7.12 give the calculated values of θ for directional earthquake combination X and Y, respectively.

$$\theta = \frac{P_{tot} \cdot d_r}{V_{tot} \cdot h} \quad \text{Eq. (7.8)}$$

Table 7.11: 2nd order effects in X direction

Earthquake in the X direction								
Story	d _{r,x} [m]	d _{r,y} [m]	P _{tot} [kN]	h [m]	V _x [kN]	V _y [kN]	Θ _x [rad]	Θ _y [rad]
1	0.044	0.009	26393	4.000	1598	451	0.168<0.200	0.117<0.200
2	0.045	0.016	22986	4.000	1492	443	0.160<0.200	0.197<0.200
3	0.049	0.018	19578	4.000	1306	412	0.170<0.200	0.201>0.200
4	0.047	0.017	16179	4.000	1198	385	0.148<0.200	0.167<0.200
5	0.050	0.016	12780	4.000	1042	348	0.142<0.200	0.133<0.200
6	0.046	0.013	9392	4.000	947	322	0.107<0.200	0.088<0.200
7	0.043	0.011	6004	4.000	750	254	0.080<0.200	0.058<0.200
8	0.036	0.006	2633	4.000	473	192	0.046<0.200	0.020<0.200

Table 7.12: 2nd order effects in Y direction

Earthquake in the Y direction								
Story	d _{r,x} [m]	d _{r,y} [m]	P _{tot} [kN]	h [m]	V _x [kN]	V _y [kN]	Θ _x [rad]	Θ _y [rad]
1	0.013	0.029	26393	4.000	486	1481	0.166<0.200	0.119<0.200
2	0.013	0.054	22986	4.000	454	1405	0.158<0.200	0.207>0.200
3	0.015	0.061	19578	4.000	398	1278	0.168<0.200	0.217>0.200
4	0.014	0.057	16179	4.000	365	1147	0.146<0.200	0.188<0.200
5	0.015	0.052	12780	4.000	317	1025	0.140<0.200	0.150<0.200
6	0.014	0.043	9392	4.000	288	903	0.105<0.200	0.005<0.200
7	0.013	0.035	6004	4.000	227	723	0.079<0.200	0.068<0.200
8	0.011	0.021	2633	4.000	143	435	0.048<0.200	0.030<0.200

The tables show that some θ values were slightly above 0.2. Second order effects should therefore be considered by an amplification factor of $1/(1-\theta)$, with the maximum θ value obtained. Furthermore, a pushover analysis (POA) shall also be performed to compliment the RSA method. However, since the intent of the present document is to provide the design process through RSA method only, the POA is not presented. For further information regarding the POA, please refer to [2].

7.3.3 Final verification of the welded FUSEIS beam splices

The bending moment, shear and axial resistances of the welded FUSEIS beam splice should fulfill §7.8.3 (2) and (7) of [3]. The equations to satisfy §7.8.3 (2) of [3] are:

$$\frac{M_{Ed}}{M_{FUSE,pl,Rd}} \leq 1.00 \quad \text{Eq. (7.9)}$$

$$\frac{N_{Ed}}{N_{FUSE,pl,Rd}} \leq 0.15 \quad \text{Eq. (7.10)}$$

$$\frac{V_{Ed}}{V_{FUSE,pl,Rd}} \leq 0.50 \quad \text{Eq. (7.11)}$$

where:

$V_{Ed} = V_{Ed,G} + V_{Ed,M}$ with $V_{Ed,M}$ being the shear force obtained by capacity design;

M_{Ed} and N_{Ed} are the design moment and axial force;

$M_{FUSE,pl,Rd}$, $N_{FUSE,pl,Rd}$ and $V_{FUSE,pl,Rd}$ are the plastic moment, axial and shear resistance of the fuse, determined based on [2];

Table 7.13 gives the moment verification of the welded FUSEIS beam splice and the check for the homogeneous dissipative behavior. Excluding 8th floor's Ω value to ease the structural detailing of the welded FUSEIS, the homogenous indicator presents a value of 1.27 which is assumed as acceptable. Table 7.14 gives the shear force verification.

Table 7.13: Moment verification of the fuses and check for homogeneous dissipative behavior

Floor	Fuse type [mm ²]	M _{Ed} [kNm]	M _{Rd-} [kNm]	M _{Rd+} [kNm]	α^+	α^-	$\Omega = \frac{M_{FUSE,pl,Rd}}{M_{Ed}}$	$\frac{\max \Omega}{\min \Omega} \leq 1.25$
1	170*12	186	273	423	0.46	0.53	1.46	1.27
2	170*12	233	273	423	0.46	0.53	1.17	
3	170*12	237	273	423	0.46	0.53	1.15	
4	170*12	224	273	423	0.46	0.53	1.21	
5	170*10	198	227	365	0.40	0.45	1.14	
6	170*10	175	227	365	0.40	0.45	1.29	
7	170*8	129	163	293	0.32	0.32	1.25	
8	170*8	81	163	293	0.32	0.32	2.00	

where:

$\alpha = M_{FUSE,pl,Rd}/M_{beam,pl,Rd}$ and $\Omega = M_{FUSE,pl,Rd}/M_{Ed}$.

Table 7.14: Shear force verification of the fuses

Floor	Fuse type [mm ²]	V _{Ed} [kN]	V _{Rd} [kN]	Ratio
1	170*12	150	369	0.41
2	170*12	150	369	0.41
3	170*12	150	369	0.41
4	170*12	150	369	0.41
5	170*10	134	369	0.36
6	170*10	134	369	0.36
7	170*8	112	369	0.30
8	170*8	107	369	0.29

7.3.4 Final verification of the conventional bracings

The verification of conventional bracings follows the design rules speculated in section 6.7 of [5]. Table 7.15 gives the normalized slenderness verification. Table 7.16 presents the axial force verification and the check for homogeneous dissipative behavior.

Table 7.15: Normalized slenderness verification

Floor	Bracing type	$L_{cr,y}$ [m]	$L_{cr,z}$ [m]	i_y [m]	i_z [m]	$1.30 < \bar{\lambda}_y < 2.00$	$1.30 < \bar{\lambda}_z < 2.00$
1	2UPN140/60/	4.472	8.944	0.055	0.072	1.10 ^e	1.60
2	2UPN140/60/	4.472	8.944	0.055	0.072	1.10 ^e	1.60
3	2UPN120/60/	4.472	8.944	0.046	0.069	1.30	1.70
4	2UPN120/60/	4.472	8.944	0.046	0.069	1.30	1.70
5	2UPN100/60/	4.472	8.944	0.039	0.068	1.50	1.70
6	2UPN100/60/	4.472	8.944	0.039	0.068	1.50	1.70
7	2UPN80/60/	4.472	8.944	0.031	0.065	1.70	1.60
8	2UPN65/60/	4.472	8.944	0.025	0.064	1.90	1.50

where:

$L_{cr,y}$ and $L_{cr,z}$ are the buckling length for the moment of inertia of the bracing along y (in-plane) and z direction (out-of-plane), respectively.

i_y and i_z are the radius of gyration for the moment of inertia of the bracing along y (in-plane) and z direction (out-of-plane), respectively;

$\bar{\lambda}_y$ and $\bar{\lambda}_z$ are the normalized slenderness for the moment of inertia of the bracing along y (in-plane) and z direction (out-of-plane), respectively;

^e Section was assigned to mobilize the necessary axial force.

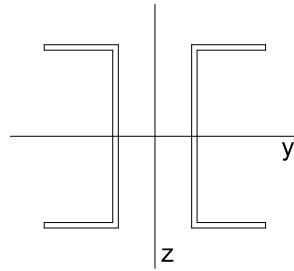


Figure 7.11: Schematic representation of the y and z axis

Table 7.16: Axial force verification of the bracings and check for homogeneous dissipative behavior (tension-only)

Floor	Bracing type	Steel	N_{pl} [kN]	N_{Ed} [kN]	Ratio	$\Omega = \frac{N_{pl}}{N_{Ed}}$	$\frac{\max \Omega}{\min \Omega} \leq 1.25$
1	2UPN140/60/	S355	1445	1327	0.92	1.09	1.17
2	2UPN140/60/	S355	1445	1293	0.90	1.12	
3	2UPN120/60/	S355	1205	1121	0.93	1.08	
4	2UPN120/60/	S355	1205	1033	0.86	1.17	
5	2UPN100/60/	S355	955	871	0.91	1.10	
6	2UPN100/60/	S355	955	792	0.83	1.21	
7	2UPN80/60/	S275	616	598	0.97	1.03	
8	2UPN65/60/	S235	423	359	0.85	1.18	

7.3.5 Capacity design of non-dissipative elements and members

The capacity design of non-dissipative elements and members (columns and reinforcing zones) should be done according to §7.8.3 (3) and (4) of [3]. The design forces are therefore obtained from Eq. (7.12) to Eq. (7.14).

$$N_{CD,Ed} = N_{Ed,G} + 1.1 \cdot \gamma_{ov} \cdot \Omega \cdot N_{Ed,E} \quad \text{Eq. (7.12)}$$

$$M_{CD,Ed} = M_{Ed,G} + 1.1 \cdot \gamma_{ov} \cdot \Omega \cdot M_{Ed,E} \quad \text{Eq. (7.13)}$$

$$V_{CD,Ed} = V_{Ed,G} + 1.1 \cdot \gamma_{ov} \cdot \Omega \cdot V_{Ed,E} \quad \text{Eq. (7.14)}$$

Table 7.17 present the verification of the reinforcing zone.

Table 7.17: Moment verifications of the reinforcing zone

Section	M_{Ed} [kNm]	M_y [kNm]	Ratio
Reinforcing zone (RZ)	288	822	0.35
Current beam section immediately after the RZ	138	657	0.21

where M_y is the yield moment.

Table 7.18 present the verification of the inner and outer governing columns of the welded FUSEIS beam splice moment resisting frames. Table 7.19 gives the CBF column verification.

Table 7.18: Safety check of conditional inner and outer columns of the MRF-WFBS

Column	Section	M_{Ed} [kNm]	V_{Ed} [kN]	N_{Ed} [kN]	Ratio
Inner	HEM550	1151	280	2721	0.44
	HEM500	511	246	2037	0.21
	HEM450	415	204	1347	0.19
	HEM360	329	152	654	0.19
Outer	HEB550	776	178	3751	0.56
	HEB500	281	133	2618	0.20
	HEB450	221	107	1547	0.17
	HEB360	165	77	620	0.17

Table 7.19: Safety check of conditional column of the CBF

Column	Section	N_{Ed} [kN]	$N_{Rd,M}$ [kN]	Ratio
CBF	HEB550	5661	8778	0.64
	HEB500	3852	8300	0.46
	HEB450	2283	7548	0.30
	HEB360	916	6229	0.15

where $N_{Rd,M}$ is the reduced axial resistance due to bending moment-axial force interaction.

7.4 Structural detailing

The internal forces and moments transition from the flange and web fuse plates of the welded FUSEIS beam splice to the adjacent reinforcing zone is achieved by means of welds. These are designed such that the flange and web fuse plates mobilize their maximum resistance. Table 7.20 gives the design of the web plates' welds. Table 7.21 shows the safety check of the flange plate's welds. Lastly, Table 7.22 illustrates the verification of the reinforcing plates' welds, assuming the mobilization of the plates' maximum axial resistance.

Table 7.20: Design of the web fuse plates' weld thickness

I [mm]	V_{Ed} [kN]	M_{Ed} [kNm]	Weld thickness [mm]
410	185	63	5

Table 7.21: Verification of the flange fuse plate's weld thickness

Flange [mm ²]	I [mm]	N _{Ed} [kN]	f _{w,Ed} [kN/m]	Weld thickness [mm]	f _{w,Rd} [kN/m]	Ratio
170*8	410	320	323	5	1039	0.31
170*10	410	400	404	7	1455	0.28
170*12	410	479	484	7	1455	0.33

Table 7.22: Verification of the reinforcing plates' weld thickness

Plate	N _{Ed} [kN]	f _{w,Ed} [kN/m]	Weld thickness [mm]	f _{w,Rd} [kN/m]	Ratio
Flange	660	423	7	1637	0.26
Web	550	353	7	1637	0.22

Shear connectors were designed to mobilize full connection at the positive critical moment section of the composite beams, which resulted in two $\Phi 25$ mm connectors ($f_u = 450$ MPa, $h_{sc} = 120$ mm) spaced by 187.5 mm along the composite beams. Design of conventional transverse rebar and concrete compression verifications were subsequently performed. The resulting rebar quantity is equal to $\Phi 12//187.5$ mm. The rebar near the beam-column joint were determined according to annex C of [5]. Table 7.23 presents the final dimensions adopted for the beam splices.

Table 7.23: Final beam splice dimensions

Fuse type		170*12	170*10	170*8
Applied at floor(s)	-	1-4	5-6	7-8
Fuse web plate S235	mm ²	2x 170*8	2x 170*8	2x 170*8
Fuse flange plate S235	mm ²	170*12	170*10	170*8
Reinforcing web plate S275	mm ²	2x 200*10	2x 200*10	2x 200*10
Reinforcing flange plate S275	mm ²	240*10	240*10	240*10
Welds: fuse web plate	mm	5	5	5
Welds: fuse flange plate	mm	7	7	5
Welds: fuse web and flange plate welding length (Figure 7.12)	mm	410	410	410
Welds: reinforcing web plate	mm	7	7	7
Welds: reinforcing flange plate	mm	7	7	7
Gap	mm	50	50	50
Free length	mm	200	200	200

Figure 7.13: Structural detailing of the welded FUSEIS beam splice (170*8 mm² fuse – top view)

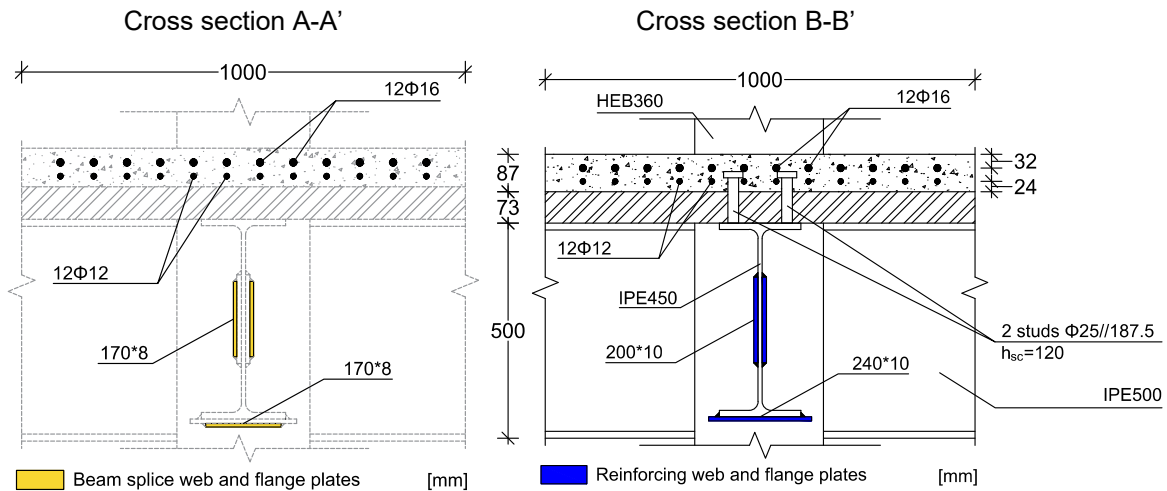


Figure 7.14: Cross section A-A' and B-B' from Figure 7.12

7.5 References

- [1] EN1991-1-1, Eurocode 1: Actions on structures - Part 1-1: General actions - Densities, self-weight, imposed loads for buildings. Brussels: Comitee Europeen de Normalisation (CEN); 2002.
- [2] Calado, L., Proença, J.M., Sio, J., "INNOSEIS – Valorization of innovative anti-seismic devices", WORK PACKAGE 1 – DELIVERABLE 1.1, Volume with information brochures for 12 innovative devices in English, European Commission Research Programme of the Research Fund for Coal and Steel, (Article in Press).
- [3] Calado, L., Proença, J.M., Sio, J., "INNOSEIS – Valorization of innovative anti-seismic devices", WORK PACKAGE 3 – DELIVERABLE 3.2, Volume with pre-normative design guidelines for innovative devices, European Commission Research Programme of the Research Fund for Coal and Steel, (Article in Press).
- [4] SAP2000, CSI, Computers and Structures Inc., www.csiberkeley.com.
- [5] EN1998-1-1, Eurocode 8: Design of structures for earthquake resistance – Part 1-1: General rules, seismic actions and rules for buildings. Brussels: Comitee Europeen de Normalisation (CEN); 2003.

8 REPLACEABLE BOLTED LINKS

8.1 Introduction

Conventional seismic design philosophy is based on dissipative response, which implicitly accepts damage of the structure under the design earthquake and leads to significant economic losses. Repair of the structure is often impeded by the permanent (residual) drifts of the structure. In order to reduce the repair costs and downtime of a structure hit by an earthquake, and consequently obtain a more rational design approach in the context of sustainability, the concepts of removable dissipative members and re-centring capability of the structure are employed. These concepts are implemented in a dual structure, obtained by combining steel eccentrically braced frames (EBFs) with removable bolted links with moment resisting frames (MRFs). The bolted links are intended to provide the energy dissipation capacity and to be easily replaceable, while the more flexible MRFs would provide the necessary re-centring capability to the structure.

This case study presents the conceptual design, modelling and analysis by linear response spectrum analysis methods [2-4] and basic structural detailing of a new mid/high-rise steel office building implementing replaceable bolted links.

8.2 Description of building

8.2.1 Geometry and general assumptions

The case study presented hereafter consists in designing and analysing an eight-story building with dual EBFs with replaceable bolted links. The plan view for the building is presented in Figure 8.1a. The number of bays in both directions is 3, with a span length of 8m. The height of each story is 4m. The main lateral load resisting system is composed of four MRFs and two EBFs on transversal direction and two MRFs and two EBFs on longitudinal direction. The external frames on transversal direction consist of dual steel frames, combining two moment resisting frames (MRFs) (which provide the necessary re-centring capability to the structure, assuring the restoring forces after an earthquake) with one central eccentrically braced frame (EBF) with replaceable bolted links, which are intended to provide the energy dissipation capacity and to be easily replaceable (Figure 8.1b). These are the plane frames that will be further designed and analysed. All the other frames are gravitational loads resisting systems (with pinned HE200A composite steel-concrete beams). The main beams, columns and braces are made of European I-sections (IPE, HEA, HEB and HEM type), while the replaceable links are made of welded I-sections. The material used for structural elements is S355 steel.

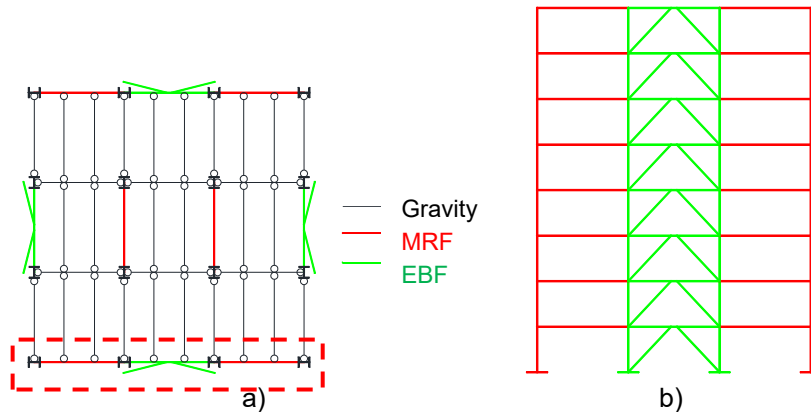


Figure 8.1: Structure description: a) plane configuration, b) frame elevation.

Table 8.1 includes the assumptions for gravity and seismic loads. The gravity loads were applied as uniform distributed loads on the secondary beams and reduced to concentrated loads on the main frames. The dead load takes into account the composite slab and steel sheeting, resulting 2.75 kN/m^2 . There were considered superimposed loads from services, ceilings and raised floors of 0.7 kN/m^2 at intermediate floors and 1.0 kN/m^2 at last floor. A 4.0 kN/m permanent load was taken into account for perimeter walls. The live load considers the occupancy of the building (offices - class B) and movable partition walls, resulting 3.8 kN/m^2 . All gravitational loads assigned to the analysed frames correspond to half the bay (4m). Type 1-C spectrum was selected for design considering peak ground accelerations of $0.3g$ (Figure 8.2) and high ductility class (DCH). A behaviour factor $q=4$ was adopted.

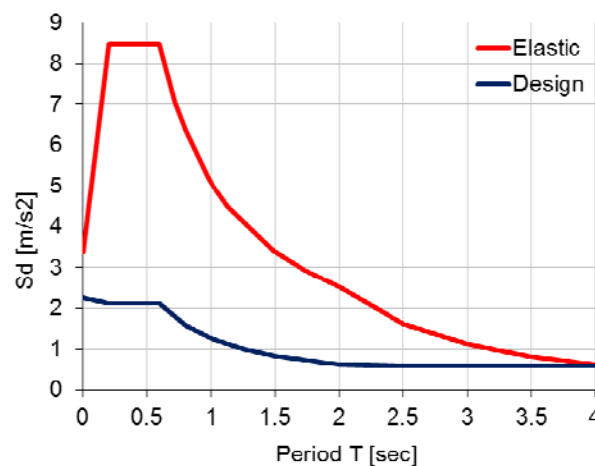


Figure 8.2: Elastic and design response spectra.

Table 8.1: Site details

Vertical loads	
Dead loads (composite slab + steel sheeting)	2.75 kN/m ²
Superimposed loads (Services, ceiling, raised floor)	0.7 kN/m ² - intermediate floors 1.0 kN/m ² – last floor
Perimeter walls	4.0 kN/m ²
Live loads – (office class B + movable partition)	3.00+0.8=3.8 kN/m ²
<ul style="list-style-type: none"> DCH design: 	
Elastic response spectra	Type 1
Peak ground acceleration	a _{gR} =0.3g
Importance class II	γ _I = 1.0 (Ordinary buildings)
Ground type	C (T _B = 0.2 s, T _C = 0.60 s)
Proposed behaviour factor q (DCH)	4
Damping ratio	5%
Seismic combination coefficient for the quasi-permanent value of variable actions	ψ ₂ =0.30

8.2.2 Modelling for linear elastic analysis

The modelling, analysis and design of the buildings, was performed with the finite element program SAP2000 [5]. The structural model was a linear-elastic 2D model. Rigid diaphragms were assigned at each level to account for the effect of reinforced concrete slabs. The structural masses (in tons) corresponding to half of the floor area (12x24m) were assigned in the frames' structural nodes, since only the external frames resist lateral loads (Figure 8.3).

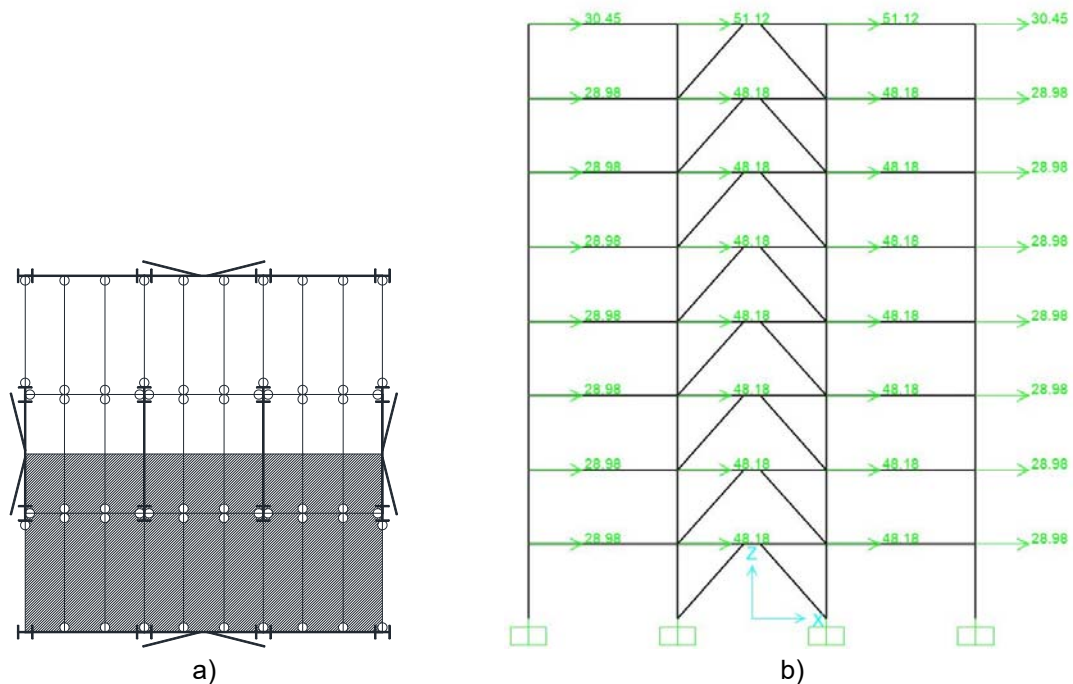


Figure 8.3: Structural masses: a) tributary area and b) assigned in structural nodes of 2D model.

8.3 Persistent design situation

8.3.1 Ultimate Limit State

MRFs were designed from fundamental Ultimate Limit State (ULS) load combination $1.35 \cdot G_k + 1.5 \cdot Q_k$, where G_k are permanent loads (dead load) and Q_k are variable loads (live load). IPE330 sections were obtained for beams, HE200B sections for columns.

8.3.2 Serviceability Limit State

Beams deflections were checked from fundamental load combination $1.0 \cdot G_k + 1.0 \cdot Q_k$. They had to be increased to IPE360 to have deflections less than $L/350$ (22.86mm).

8.4 Response spectrum analysis

Multi-modal response spectrum analysis was performed and the results are summarized in Table 8.2, presenting the modes that activated more than 90% of the mass.

Table 8.2: Participating mass ratio

Mode No	Eigen Period (s)	Participating mass ratio (%)	Total (%)
1	<u>1.126</u>	71.58	94.85
2	0.385	17.76	
3	0.221	5.51	

8.5 Global imperfections and 2nd order effects

Global imperfections were considered in the structural analysis, according to EN1993-1-1 [6], through equivalent lateral forces, from combination $1.35 \cdot G_k + 1.5 \cdot Q_k$.

These forces were computed based on total gravitational loads and initial global imperfection ϕ , level by level, and considered in every load combination further on. Lateral equivalent forces were 8.7 kN for current levels and 8.9 kN for roof level.

Second order effects were not accounted for in design because the inter-story drift sensitivity coefficient θ , computed according to EN1998-1-1 [7], was found to be smaller than 0.1.

8.6 Seismic design

A capacity design of dual structures, obtained by combining steel eccentrically braced frames with replaceable bolted links and moment resisting frames, should be performed using general code-based approach [7], but some additional criteria need to be considered.

8.6.1 Ultimate Limit State - Dissipative elements design

Shear links are the dissipative elements of the system. They were designed from welded (h x b x t_f x t_w) class 1 I-sections.

The links were designed to be replaceable, by using a flush end-plate link-beam connection that was kept elastic. This means that the connection had a design shear force $V_{j,Ed}$ and bending moment $M_{j,Ed}$ corresponding to a fully yielded and strain hardened link, computed as follows:

$$V_{j,Ed} = \gamma_{sh} \gamma_{ov} V_{p,link} \quad \text{Eq. (8.1)}$$

$$M_{j,Ed} = \frac{V_{j,Ed} e}{2} \quad \text{Eq. (8.2)}$$

where γ_{ov} is 1.25 and γ_{sh} is adopted as 1.8 for DCH.

In order to achieve the connection over-strength, very short dissipative members were adopted ($e=0.8M_{p,link}/V_{p,link}$). Therefore, links had lengths of 0.9 m.

Link sections were obtained from the following governing seismic load combination: $1.0 \cdot G_k + 0.3 \cdot Q_k + 1.0 \cdot A_{Ed}$ (where A_{Ed} is seismic action) and are presented in the following tables:

Table 8.3: Links sections

Story	Link section	Ω_i	Min Ω_i	Ω
1	490x260x20x8	2.44	1.96	2.45
2	490x260x20x8	2.41		
3	440x230x20x7	2.09		
4	440x230x20x7	2.31		
5	390x200x20x6	1.96		
6	390x200x20x6	2.29		
7	330x210x16x5	2.25		
8	250x190x14x4	1.97		

A homogeneous dissipative behaviour was ensured between links (25%). The structural over-strength was computed as [7]:

$$\Omega = \gamma_{ov} \Omega_i \quad \text{Eq. (8.3)}$$

$$\Omega_i = \gamma_{sh} \frac{V_{p,link,i}}{V_{Ed,i}} \quad \text{Eq. (8.4)}$$

8.6.2 Ultimate Limit State – Non - dissipative elements design

EBFs columns, braces and beams are the non-dissipative elements of the system and were designed from the seismic load combination that provides over-strength

(Ω) to these elements with respect to dissipative ones: $1.0 \cdot G_k + 0.3 \cdot Q_k + \Omega \cdot A_{Ed}$. The sections are presented below:

Table 8.4: Elements sections

Story	Braces	Beams	Columns
1	HE320B	HE500A	HE340M
2	HE320B	HE500A	HE340M
3	HE300B	HE450A	HE300M
4	HE280B	HE450A	HE300M
5	HE280B	HE400A	HE300B
6	HE260B	HE400A	HE300B
7	HE240B	HE340A	HE280B
8	HE200B	HE260A	HE280B

8.6.3 Limitation of inter-story drift

Considering that the building has ductile non-structural elements the following Eq. (8.5) is checked.

$$d_r \cdot v \leq 0.0075 \cdot h = 0.0075 \cdot 4000 = 30\text{mm} \quad \text{Eq. (8.5)}$$

Where d_r is the design inter-storey drift, $v=0.5$ is a reduction factor on the design displacements due to the importance class of the building (ordinary buildings) and h is the story height. Table 8.5 includes the results of the analysis; the check is verified for all stories with values lower than the limit value 30 mm.

Table 8.5: Limitation of inter-story drift

Story	Drift [mm]
1	7.2
2	10.0
3	12.6
4	14.2
5	15.5
6	16.3
7	17.0
8	16.7

8.6.4 Dual configurations

The duality of the structure was checked by verifying that the MRFs were able to resist at least 25% of the total seismic force [8-10]:

$$F_y^{MRF} \geq 0.25 (F_y^{MRF} + F_y^{EBF}) \quad \text{Eq. (8.6)}$$

$$F_y^{EBF} = \frac{L}{H} V_{p,link} \quad \text{Eq. (8.7)}$$

$$F_y^{MRF} = \frac{4M_{pl,b}}{H} \quad \text{Eq. (8.8)}$$

where: F_y^{MRF} is the yield strength of MRF, F_y^{EBF} is the yield strength of EBF, L is the frame span, H is the frame story height, $V_{p,link}$ is the shear strength of the link and $M_{pl,b}$ is the beam plastic moment.

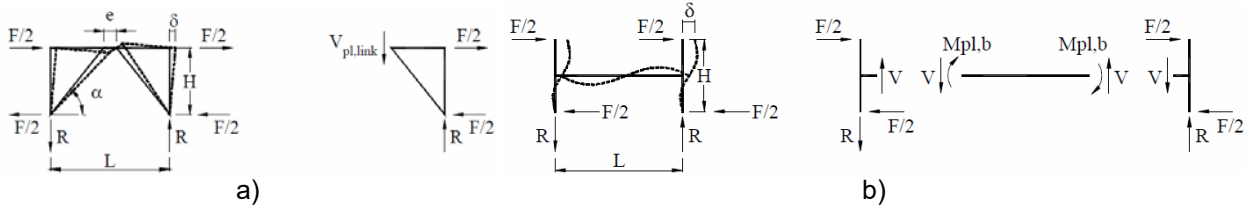


Figure 8.4: Basic one-story a) EBF and b) MRF components [10].

In order to have dual frames, the MRFs beams were increased as follows:

Table 8.6: MRFs beams

Story	Sections
1	IPE450
2	IPE450
3	IPE400
4	IPE400
5	IPE360
6	IPE360
7	IPE360
8	IPE360

8.6.5 Weak beam-strong column

Columns were increased in order to satisfy the “weak beam-strong column” condition:

$$\sum M_{Rc} \geq 1.3 \sum M_{Rb} \quad \text{Eq. (8.9)}$$

where: $\sum M_{Rc}$ is the sum of upper and lower columns moment resistance and $\sum M_{Rb}$ is the moment resistance of the MRF beam.

The final sections of MRFs column from elastic design are the following:

Table 8.7: MRFs columns

Story	Sections
1	HE260B
2	HE260B
3	HE240B
4	HE240B
5	HE220B
6	HE220B
7	HE220B
8	HE220B

Frame sections after elastic design are the following:

Table 8.8: Frame sections

Story	Links	Braces	Beams	Columns	MRFs beams	MRFs columns
1	490x260x20x8	HE320B	HE500A	HE340M	IPE450	HE260B
2	490x260x20x8	HE320B	HE500A	HE340M	IPE450	HE260B
3	440x230x20x7	HE300B	HE450A	HE300M	IPE400	HE240B
4	440x230x20x7	HE280B	HE450A	HE300M	IPE400	HE240B
5	390x200x20x6	HE280B	HE400A	HE300B	IPE360	HE220B
6	390x200x20x6	HE260B	HE400A	HE300B	IPE360	HE220B
7	330x210x16x5	HE240B	HE340A	HE280B	IPE360	HE220B
8	250x190x14x4	HE200B	HE260A	HE280B	IPE360	HE220B

8.6.6 Re-centring verification

In order to verify the re-centring capability of eccentrically braced frames with replaceable links, it was checked that the ultimate displacement of the EBFs (δ_u^{EBF}) at ultimate limit state (ULS) (where the plastic deformation capacity of the link $\gamma_{pl,u}$ is considered to be 0.11 rad) is smaller than the yield displacement of the MRFs (δ_y^{MRF}), meaning the yielding in MRFs is prevented up to the attainment of ultimate deformation capacity in the EBFs with replaceable links. This was done analytically, using formulas below [10]:

$$\delta_u^{EBF} = \delta_y^{EBF} + \delta_{pl}^{EBF} = \frac{F_y^{EBF}}{K^{EBF}} + \frac{e}{L} \frac{H}{e} \gamma_{pl,u} < \delta_y^{MRF} = \frac{F_y^{MRF}}{K^{MRF}} \quad \text{Eq. (8.10)}$$

$$K^{EBF} = \frac{K_{link}^{EBF} K_{br}^{EBF}}{K_{link}^{EBF} + K_{br}^{EBF}} \quad \text{Eq. (8.11)}$$

$$K_{link}^{EBF} = \frac{L}{H^2} (L - e) \frac{G A_s}{e} \quad \text{Eq. (8.12)}$$

$$K_{br}^{EBF} = 2 \frac{E A}{I_{br}} \cos^2 \alpha \quad \text{Eq. (8.13)}$$

$$K^{MRF} = \frac{4}{H^2 \left(\frac{L}{6E I_b} + \frac{H}{12E I_c} \right)} \quad \text{Eq. (8.14)}$$

where δ_y^{EBF} is the yield displacement of the EBF, δ_p^{EBF} is the plastic displacement of the EBF, K^{EBF} is the EBF stiffness, e , L and H are illustrated in Figure 8.4, $\gamma_{pl,u}$ is the plastic deformation capacity of the link, K^{MRF} is the MRFs stiffness, K_{link}^{EBF} is the link's stiffness, K_{br}^{EBF} is the braces stiffness, G is the shear modulus, A_s is the link shear area, E is the Young's modulus, A is brace cross-section area, l_{br} is the brace length and α is the brace angle.

This analytical procedure should be used as a pre-design of re-centring capability, being recommended for low-rise structures, where lateral deformation of the structure is dominated by a shear-type response. It could also be used as pre-design for mid-rise and high-rise buildings (where a global bending behaviour may arise in elevation), but re-centring is strongly recommended to be checked through pushover (PO) and/or time-history analyses.

Because using formulas is an approximate and simplified approach, nonlinear static and/or dynamic analyses are recommended for all structures in order to check the re-centring capability.

After running the PO analysis on the frame designed on the base of elastic analysis, yielding was observed in MRFs before the attainment of ultimate deformation capacity in the EBFs with replaceable links. Therefore, the steel grade for MRFs was increased to S690 and some sections were reduced as follows (changes are shown in bold):

Table 8.9: Final frame sections

Story	Links	Braces	Beams	Columns	MRFs beams	MRFs columns
1	490x260x20x8	HE320B	HE500A	HE300M	IPE360	HE220B
2	490x260x20x8	HE320B	HE500A	HE300M	IPE360	HE220B
3	440x230x20x7	HE300B	HE450A	HE260M	IPE360	HE220B
4	440x230x20x7	HE280B	HE450A	HE260M	IPE360	HE220B
5	390x200x20x6	HE280B	HE400A	HE260B	IPE360	HE220B
6	390x200x20x6	HE260B	HE400A	HE260B	IPE360	HE220B
7	330x210x16x5	HE240B	HE340A	HE240B	IPE360	HE220B
8	250x190x14x4	HE200B	HE260A	HE240B	IPE360	HE220B

Further on, it is observed that no yielding in any other structural element appears before reaching 0.15 rad in links (Figure 8.5). When peak link rotation reaches 0.15 rad, full plastic mechanism is attained with plastic rotations in other links ranging between 0.066 rad and 0.149 rad.

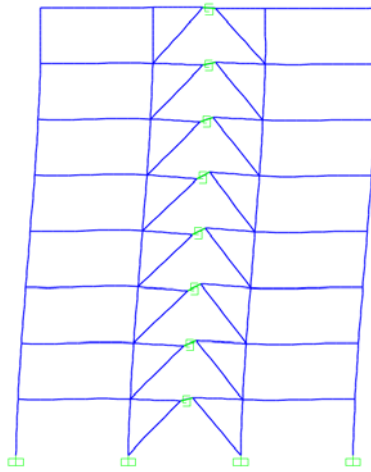


Figure 8.5: Deformed frame under PO with modal distribution, at a lateral top displacement of 0.48m.

The objective of having no yielding in the MRFs before the attainment of the Significant Damage (SD) deformation in the replaceable links (0.14 rad) of the EBFs is accomplished, representing the basic design requirement for dual frames with replaceable dissipative members. MRFs provide the re-centring of the frame until the links ultimate deformation (0.15 rad).

8.6.7 Links removal and frame re-centring

In what concerns the link removal and re-centring of frames, static nonlinear staged construction analysis from SAP2000 was used. The steps of the analysis are the following:

1. the frame is loaded with gravitational forces and afterwards with lateral forces (until reaching ultimate deformation in links),
2. it is unloaded,
3. the links are removed storey by storey, starting from the first level to the top [11].

After the elimination of the last link, the structure comes back to its initial position (see Figure 8.6).

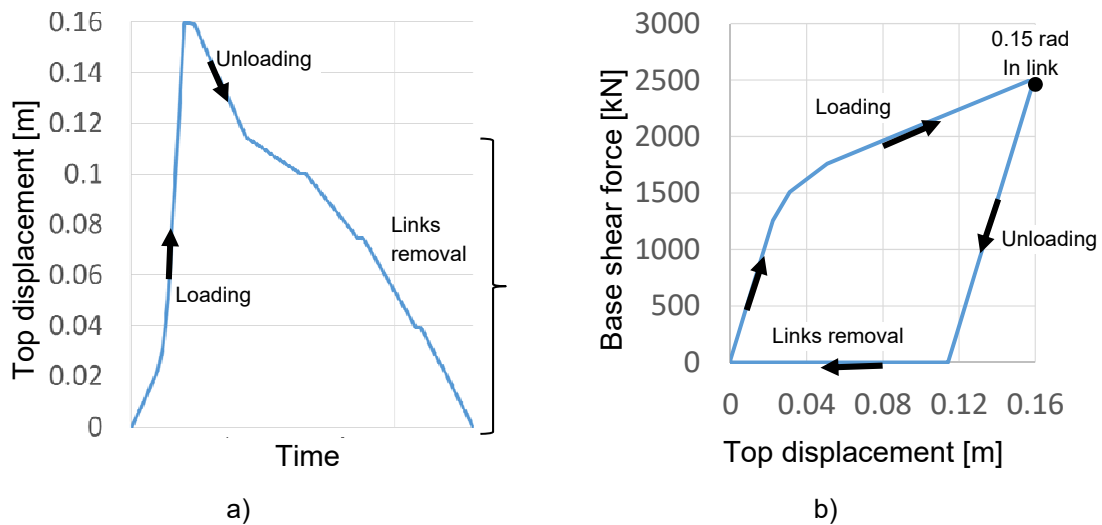


Figure 8.6: Frame response during loading, unloading, and link removal: a) top displacement in time and b) base shear force vs. top displacement.

The technically easiest way to release the forces in links is by flame cutting the web and flanges of the link [12] if large permanent drifts occur or by unbolting otherwise, on a storey by storey basis [13], as proved by the adopted procedure for the test structure in the DUAREM project [1].

8.7 Structural detailing

This type of dual EBF frames may be conceived adopting different solutions of interaction between the replaceable link and the reinforced concrete slab (Figure 8.7). One may be realised so that the beam containing the replaceable link is totally disconnected from the reinforced concrete slab. This solution prevents any damage to the reinforced concrete slab. Another solution may be realised so that the beam containing replaceable links is connected to the slab in a conventional way. Some damage may occur in the reinforced concrete slab at the interface with the replaceable link, needing local repair after a strong earthquake.

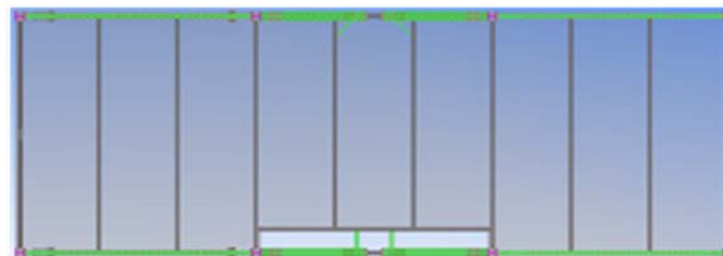


Figure 8.7: Floor layout

The reinforced concrete slab may be designed as a one way slab, on the longitudinal direction, casted over corrugated steel sheeting used as formwork.

The ends of the links may be fixed at the upper flange by the slab and at the lower flange by L fly-braces, in conventional solution, and at both flange by L braces, in the disconnected solution (Figure 8.8).

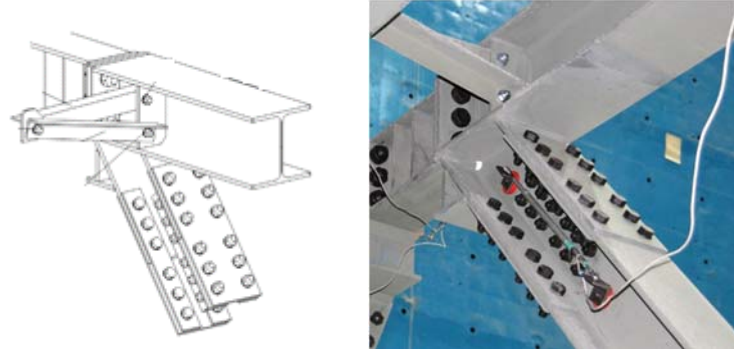


Figure 8.8: Link end braces

The secondary beams are pinned composite beams. Shear studs should be present on the main beams, except in the zones near the joints and over the links and there should be a gap between the reinforced concrete slab and the steel columns, ensured by strips of polystyrene board in order to prevent transferring of forces between slab and columns (Figure 8.9).

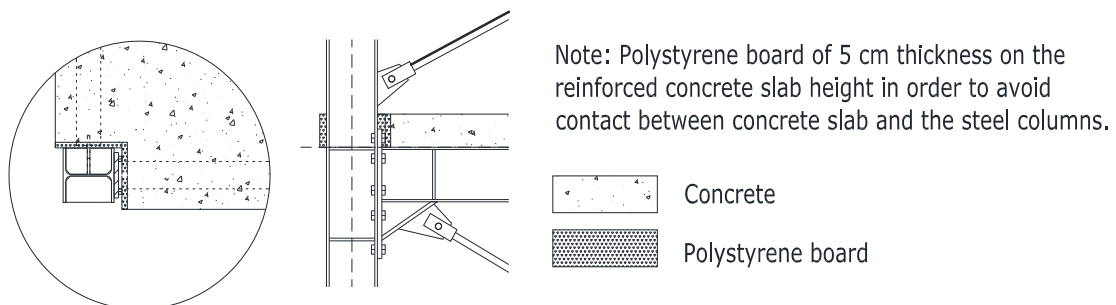


Figure 8.9: Details of gap between r.c. slab and steel columns

The extended full-strength end plate MRF beam to column connection (Figure 8.10), with haunch and bolts, should be designed to resist forces and moments larger than the ones corresponding to the formation of plastic hinges at the ends of the beam.

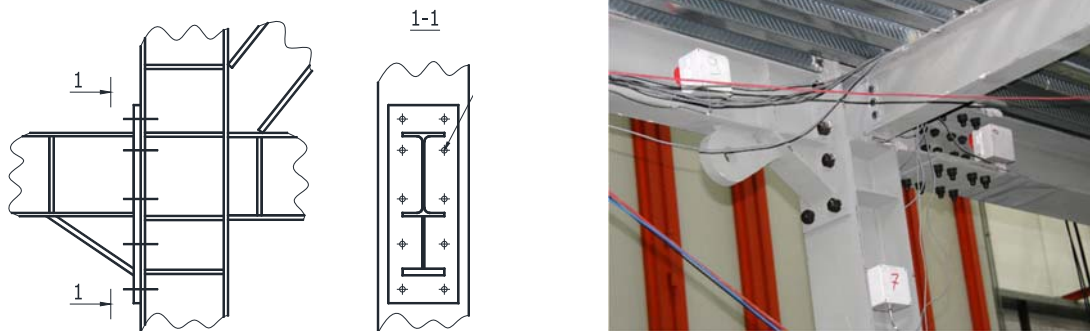


Figure 8.10: Beam to column connection

For the bolted links to be replaceable, the flush end plate connection (Figure 8.11) should be designed to remain in the elastic range (considering an elastic distribution of the internal bolt rows forces). Contact surfaces should be class B (blasted with shot or grit with zinc paint), providing a coefficient of friction of at least 0.4 and bolts should be preloaded.

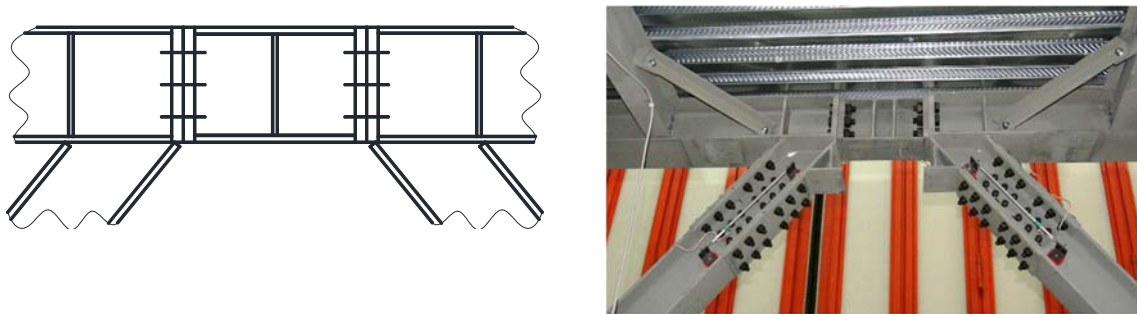


Figure 8.11: Link flush end plate connection

Table 8.10 summarizes the results from verification checks.

Table 8.10: Link flush end-plate connection

Story	End plate	Bolts	Design forces and moments		Resistance	
			V_{Ed}	M_{Ed}	V_{Rd}	M_{Rd}
1	510x260x30	6x2 M30 10.9	1735	781	2466	820
2	510x260x30	6x2 M30 10.9	1735	781	2466	820
3	460x260x30	5x2 M30 10.9	1357	611	2020	618
4	460x260x30	5x2 M30 10.9	1357	611	2020	618
5	410x240x30	5x2 M30 10.9	1024	461	2181	549
6	410x240x30	5x2 M30 10.9	1024	461	2181	549
7	350x230x30	4x2 M30 10.9	725	326	1598	379
8	270x230x30	3x2 M30 10.9	434	195	1147	222

8.8 References

1. Ioan A., Stratan A., Dubina D., Poljansek M., Molina F. J., Taucer F., Pegon P., Sabau G., Experimental validation of re-centring eccentrically braced frames with removable links, *Engineering Structures* 113 (2016) 335–346;
2. Dubina D., Stratan A., Chesoi (Ioan) A., “Design Recommendations for Dual Moment - Eccentric Braced Frames with Replaceable Links”, EUROSTEEL 2017, September 13–15, 2017, Copenhagen, Denmark (in print);
3. Dubina D., Stratan A., Chesoi (Ioan) A., Design of steel dual frames with replaceable bolted links eccentric bracing systems, 1st EU-Sino Workshop on Earthquake-resistance of Steel Structures, Shanghai, China, October 27, 2016;
4. Stratan A., Chesoi (Ioan) A., Dubina D., Design criteria and modelling of re-centring dual eccentrically braced frames, COMPDYN 2017, 6th ECCOMAS Thematic Conference on Computational Methods in Structural Dynamics and Earthquake Engineering, M. Papadrakakis, M. Fragiadakis (eds.), Rhodes Island, Greece, 15–17 June 2017;
5. SAP2000, CSI, Computers and Structures Inc., www.csiberkeley.com
6. EN1993-1-1. Eurocode 3: Design of steel structures - Part 1-1: General rules and rules for buildings. Brussels: Comitee Europeen de Normalisation (CEN); 2003.
7. EN1998-1-1, Eurocode 8: Design of structures for earthquake resistance – Part 1-1: General rules, seismic actions and rules for buildings. Brussels: Comitee Europeen de Normalisation (CEN); 2003.
8. NEHRP (2003). NEHRP Recommended provisions for new buildings and other structures (FEMA 450). Part 1: Provisions and Part 2: Commentary. Building Seismic Safety Council, National Institute of Building Sciences, Washington, D.C.;
9. P100-1/2013 (2013). Seismic design code – Part 1: Rules for buildings;
10. Stratan A., Dinu F., Dubina D., “Replacement of bolted links in dual eccentrically braced frames”, 14th European Conference on Earthquake Engineering, August 30 – September 3, 2010, Ohrid, Republic of Macedonia;
11. A. Ioan, A. Stratan, D. Dubina, M. D’Aniello and R. Landolfo, “Seismic performance and re-centring capability of dual eccentrically braced frames with replaceable links”, 8th International Conference on Behavior of Steel Structures in Seismic Areas Shanghai, China, July 1-3, 2015;
12. Stratan, A., Ioan, A., Dubina, D. 2012. Re-centring capability of dual eccentrically braced frames with removable bolted links. STESSA 2012 (Behaviour of Steel Structures in Seismic Areas) Conference, 9-11 January 2012, Santiago, Chile, pp. 723-728;
13. Ioan, A., Stratan, A., Dubina, D. 2012. Evaluation of restoring capacity of dual steel EBFs with removable links. The 8th International PhD & DLA Symposium, 29-30 October, 2012, Pecs, Hungary.

9 REPLACEABLE SHEAR PANELS

9.1 General

9.1.1 Introduction

This case study refers to the seismic design of new high-rise steel office buildings. It aims at demonstration of implementation of the frames with replaceable shear panels. The case study elaborated refers to conceptual design, modelling and analysis by linear response spectrum analysis methods (RSA), detailed design of main dissipative and non-dissipative members and basic structural detailing of replaceable shear panels.

9.1.2 Description of building

9.1.2.1 Geometry and general assumptions

The case study deals with an eight-storey frame building with three 8m bays in both directions. The gravity frames are composed of beams and columns, located at each structural axis. The shear panels are the main horizontal load resisting systems, located in the middle of each facade as shown in Figure 9.1. Additional vertical elements (stanchions) are needed in order to border the shear panel. The height of the story is considered 4 m.

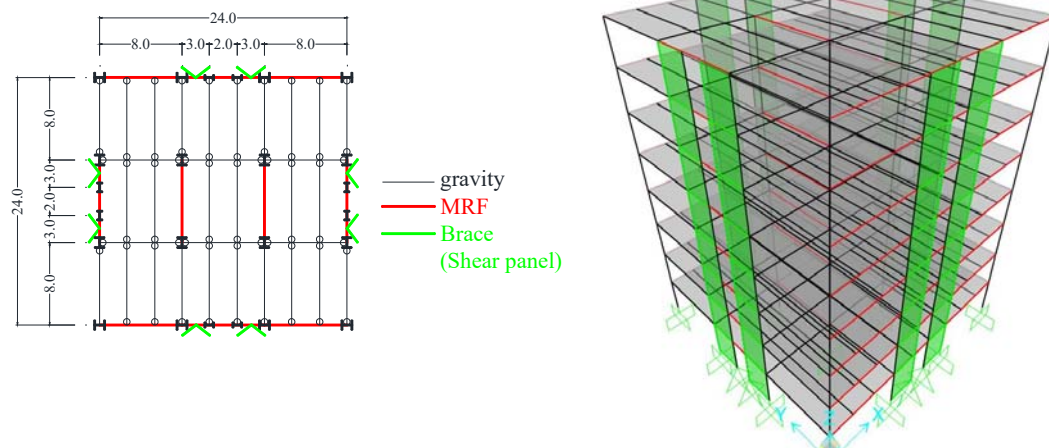


Figure 9.1: Floor plan and elevation

Hot rolled HEB profiles for columns and IPE profiles for beams are used for all gravity frames. Composite action with the concrete slab is not considered. The shear panels are loaded primarily with shear forces resulting from the seismic action (or wind load) and the rest of the frame columns carry the gravity loads. The shear panels had lower steel grade (S235) than the rest of the structural members (S355). The beams production was not considered to be fully controlled,

so that the properties of the beam material had to comply with EN1993-1-1 [1] recommendations with $\gamma_{ov} = 1.25$.

Table 9.1 includes the gravity and seismic loads taken into account. The gravity loads were applied as uniform distributed loads on the secondary beams. The dead load takes into account the slab and steel sheeting, resulting a value of 2.75 kN/m^2 . There were considered some superimposed loads from services, ceilings and raised floors of 0.7 for intermediate floors and 1 for last floor, respectively. A 4.0 kN/m was taken into account for perimeter walls. The live load takes into account de destination of the buildings (offices - class B) and movable partition walls, resulting a value of 3.8 kN/m^2 .

Type 1-C spectrum [2] (Figure 9.2a) was selected for design considering a high seismicity case, having a peak ground accelerations of 0.3 and a high ductility class structure (Figure 9.2b). Because no recommendation for reduction factor, q , is given in EN1998 [2], and based on previews research [3], [4] a value of 5 was taken into consideration.

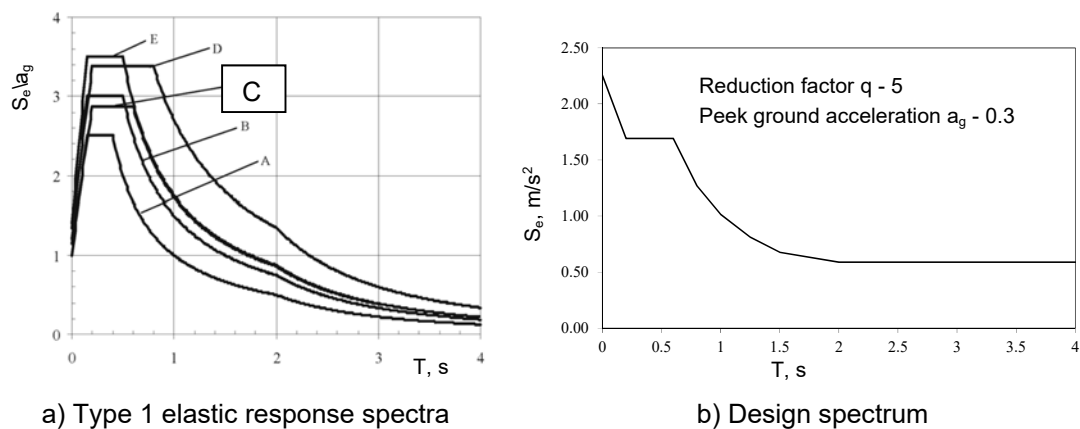


Figure 9.2: Response spectrum [3]

Table 9.1: Loads and actions

Vertical loads	
Dead loads (composite slab + steel sheeting)	2.75 kN/m ²
Superimposed loads (Services, ceiling, raised floor)	0.7 kN/m ² - intermediate floors 1.0 kN/m ² – last floor
Perimeter walls	4.0 kN/m
Live loads – (office cl. B +movable partition)	3.00+0.800=3.8 kN/m ²
Seismic load	
Elastic response spectra	Type 1
Peak ground acceleration	$a_g=0.3g$
Importance class II	$\gamma_I = 1.0$ (Ordinary buildings)
Ground type	C ($T_B = 0.2$ s, $T_C = 0.60$ s)
Proposed behaviour factor q (DCH)	5
Damping ratio	5%
Seismic combination coefficient for the quasi-permanent value of variable actions	$\psi_2=0.30$

For preliminary design, in order to determine the size of the panels, the shear panels are replaced with tension only diagonals (further denoted as equivalent braces) (Figure 9.3). For determining the size of the boundary elements (HBE and VBE), the panels are modelled with 10 inclined pin ended strips [8]. This structure is then designed according to [2], [5] and [6].

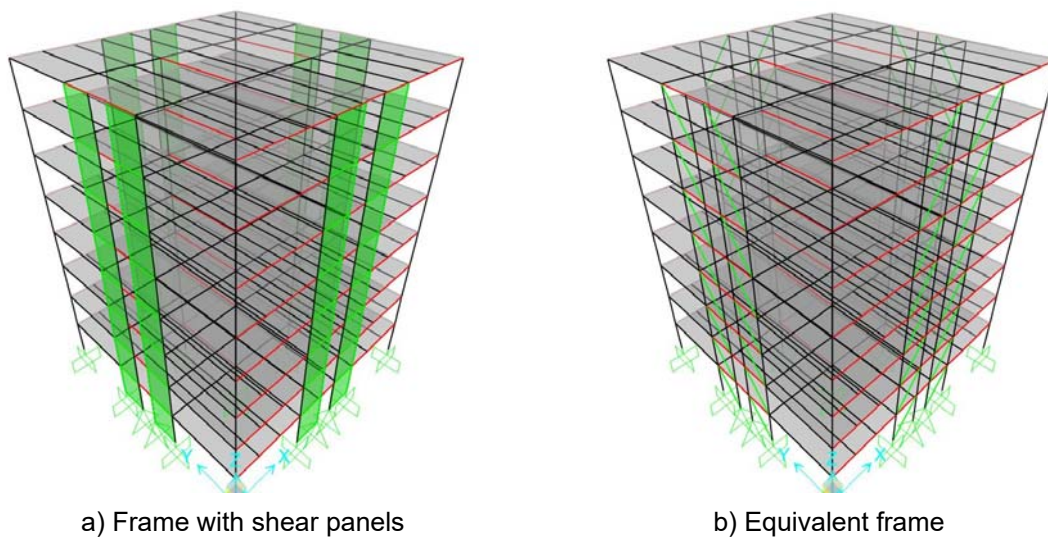


Figure 9.3: Preliminary design

9.1.2.2 Modelling for linear elastic analyses

The modelling of the building was performed with the finite element software SAP2000 [7]. The structural model is a linear-elastic 3D model with beam elements (Figure 9.4). Rigid diaphragms were assigned at each level to account for the effect of reinforced concrete slabs. The structural masses were taken into

account from loads.

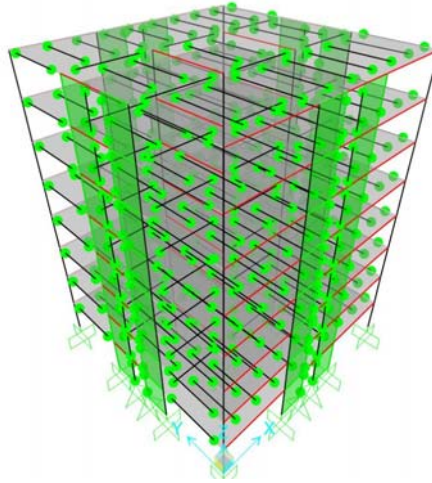


Figure 9.4: Modelling of 8 story structure for liner analysis

On transversal direction (X), the lateral load resisting system is located in the exterior frames. In these frames, all joints between gravity floor beams and columns are considered rigid with exception of the stanchions which are double pinned. For interior frames, all joints between gravity floor beams and columns are considered pinned.

On Y direction the lateral load resisting system is, also, located in the exterior frames, but in this case just the beam-to-column joints in the braced span are rigid, while the MRF joints are pinned. For the interior frames, only the interior spans have rigid beam-to-column joints, while the rest are pinned.

The elements simulating the equivalent braces are defined through constant RHS-shape section and joined to the frame by simple pin connections. The elements simulating the 10 pin ended strips are defined through constant curcular bars. For designing the Diaphragm action of floor and roof concrete decks is simulated by diaphragm constraint.

The current case study was developed by centreline-to-centreline (CL-to-CL) model. It is quick and easy to be defined, since the axis geometry of the frame is known at the beginning of the design process.

9.1.3 Persistent design situation

As the shear panels are not designed to account for gravitational loads, the moment resisting frames were designed at ultimate and serviceability limit state under persistent design situation.

9.1.3.1 Ultimate Limit State

MRFs were designed from fundamental design load combination without taking into account the shear panels. Figure 9.5 presents the resulted structural elements.

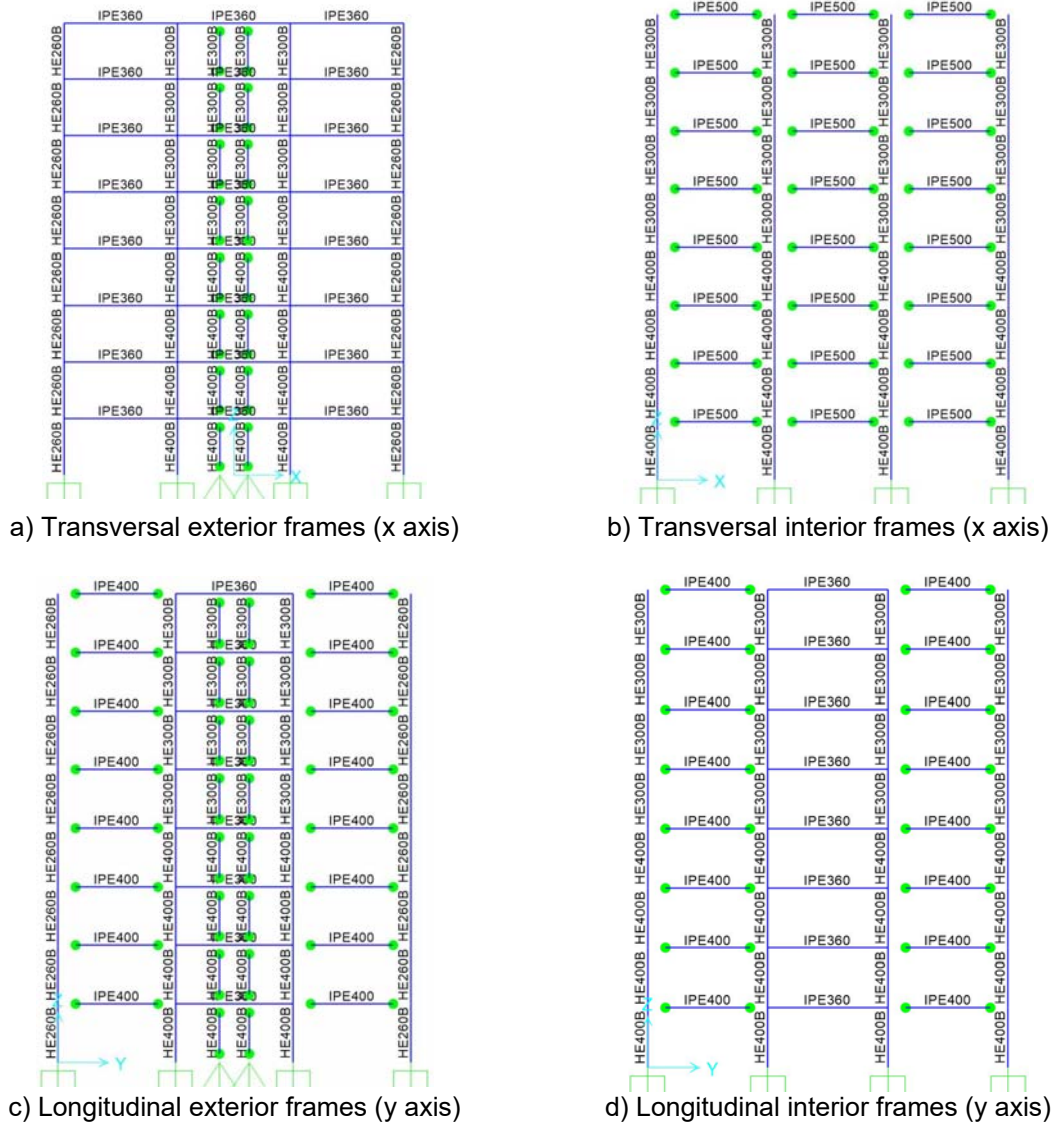


Figure 9.5: 8 story gravity frames

9.1.3.2 Serviceability Limit State

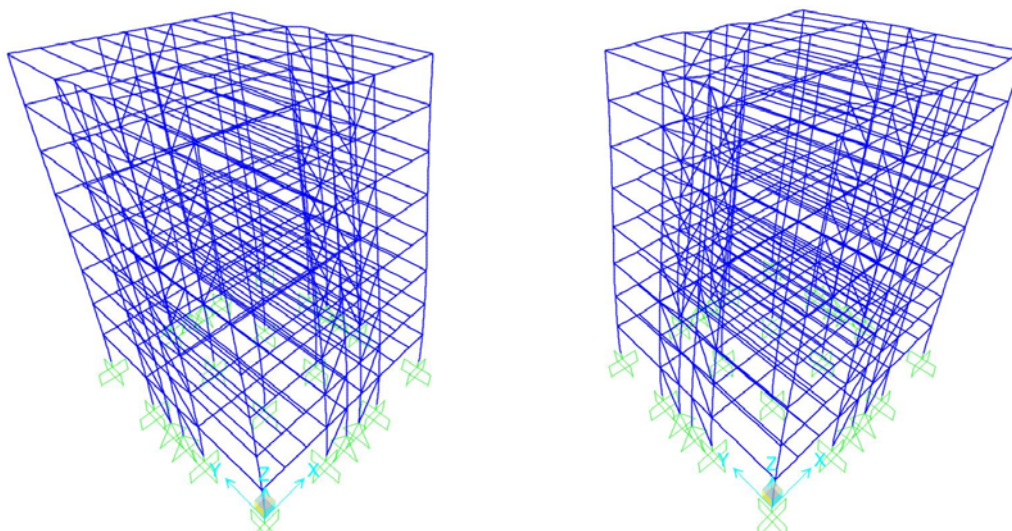
Beams deflections were checked from fundamental load combination and found to be less than the limit taken into account, $L/250$, see Table 9.2

Table 9.2: Beam deflection

Frame	Beam	Max. deflection	L/250
Transv. ext.	IPE360	17.7	<u>32</u>
Transv. int.	IPE500	20.5	
Long. ext.	IPE400	20.0	
Long. int.	IPE400	21.8	
Secondary beams	IPE360	30.8	

9.1.4 Response spectrum analysis

Multi-modal response spectrum analysis was performed and the results are summarized in Table 9.3, presenting the modes (Figure 9.6) that activated more than 90% of the mass.



a) Mode 1 – translation on Y

b) Mode 2 – translation on X

Figure 9.6: 1st and 2nd modes of vibration

Table 9.3: Participating mass ratio

Mode No	Eigen Period (s)	Participating mass in direction X (%)	Participating mass in direction Y (%)
1	0.677	-	73
2	0.64	74.4	-
4	0.25	6	-
18	0.20	-	17
19	0.184	8.5	-
21	0.16	2.2	-
Sum of participating masses		91.1	90

9.1.5 Global imperfections and 2nd order effects

Global imperfections of $H_i=2.46$ KN were not considered in the structural analysis, according to EN1993-1-1 [3]. These forces were computed based on total gravitational loads and initial global imperfection ϕ , level by level.

Second order effects were not accounted for in design because the inter-story drift sensitivity coefficient θ , computed according to EN1998-1-1 [3], found to be 0.085 smaller than 0.1.

9.1.6 Seismic design

9.1.6.1 Ultimate Limit State - Dissipative elements design

The equivalent braces and shear panel boundary beams were designed to resist the forces of the most unfavourable seismic combination. The resulted equivalent brace areas are presented in Table 9.4. In order to satisfy a homogeneous dissipative behaviour, the 25% limit between the maximum overstrength Ω_{\max} and the minimum value Ω_{\min} , was ensured (Table 9.5).

Table 9.4: Equivalent brace areas

Story	A_{brace} [mm ²]
1,2,3	3200
4,5,6	2376
7	1810
8	1195

Table 9.5: Homogeneity of equivalent braces and MRF beams

Element	Ω_{\min}	Ω_{\max}	Homogeneity
Brace	1.56	2.00	21%
MRF beam	1.16	1.4	17.5%

Additionally, the minimum moments of inertia, $I_{b,\text{req}}$, about an axis taken perpendicular to the plane of the web (Eq. (9.1)), of shear panels boundary beams was checked [6] (see Table 9.6).

$$0.0031 \cdot \frac{\Delta t_w \cdot L^4}{L} h \quad \text{Eq. (9.1)}$$

Table 9.6: Checking of shear panels boundary beam

Story	t_w (par. 0)	Beam	$I_{b,\text{req}}$	I_b
1,2,3	2.00	IPE 360	3.0E+07	2.3E+08
4,5,6	1.50	IPE 360	1.9E+07	2.3E+08
7	1.20	IPE 360	2.0E+07	2.3E+08
8	1.00	IPE 360	5.3E+07	2.3E+08

9.1.6.2 Ultimate Limit State – Non-dissipative element design

The non-dissipative elements, columns and stanchions, where checked with the most unfavourable seismic combination, to ensure that the failure of the shear panels occurs first.

Additionally, minimum moments of inertia, $I_{c,req}$, about an axis taken perpendicular to the plane of the web, was checked [6] (see Table 9.7). If there is different section for column and stanchions, the de average moment of inertia can be used for checking.

$$0.003 \cdot t_w \cdot \frac{h^4}{L} \quad \text{Eq. (9.2)}$$

Table 9.7: Checking of shear panels boundary columns

Story	Columns	Stanchions	I_c	$I_{c,req}$
1,2,3	HE 400 B	HE 400 B	5.8E+08	5.3E+08
4,5,6	HE 400 B	HE 400 B	5.8E+08	4.0E+08
7	HE 400 B	HE 400 B	5.8E+08	3.2E+08
8	HE 400 B	HE 300 B	4.1E+08	2.3E+08

9.1.6.3 Limitation of inter-story drift

Considering that the building has ductile non-structural elements the inter-story drift is limited to 0.0075, in accordance with EN 1998-1 [3]. The inter-story drifts (Table 9.8) were computed with Eq. (9.3) using story displacements taken from Sap2000 [7] from the combination of loads given in Eq. (9.4):

$$(d_{e,top} - d_{e,bottom}) / h < 0.0075 \quad \text{Eq. (9.3)}$$

$$1 \cdot G + v \cdot q \cdot E \quad \text{Eq. (9.4)}$$

Where $v = 0.5$ is a reduction factor on the design displacements due to the importance class of the building (ordinary buildings), $q=5$ is the behaviour factor, $h=4$ is the story height, $d_{e,top}$ and $d_{e,bottom}$ are top and bottom displacement of considered story.

Table 9.8: Inter-story drifts

Frame	Inter-story drift
Transv. ext.	0.006
Long. ext.	0.0065

9.1.6.4 Shear panels

After design, the equivalent braces are converted into shear panels having the thickness, t_w (Table 9.9, panel thicknesses are the same on height, in both directions), calculated with the Eq. (9.5).

$$t_w = \frac{2 \cdot A_{brace} \cdot \Omega \sin \phi}{L \cdot \sin 2\alpha} \quad \text{Eq. (9.5)}$$

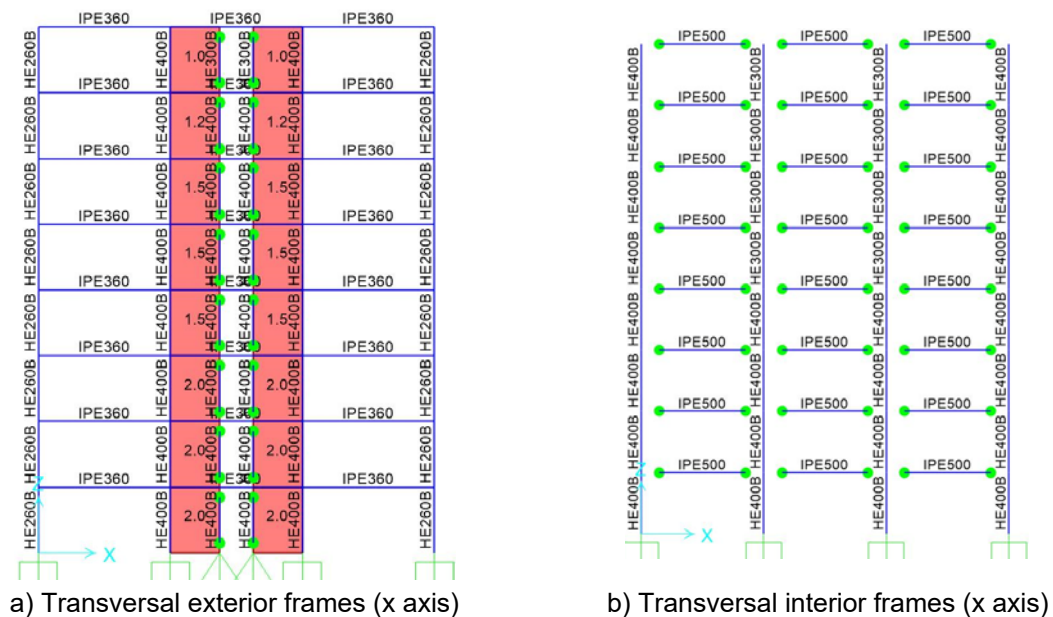
Where:

- θ is angle between the vertical and the longitudinal axis of the equivalent brace;
- L is the distance between VBE centrelines;
- α is the angle of inclination of the tension field in the shear panels, taken as 40° ;
- Ω is the system overstrength factor.

Table 9.9: Shear panels

Story	Area of equivalent brace	Panel thickness, t_w , mm
1	3200	2.0
2	3200	2.0
3	3200	2.0
4	2376	1.5
5	2376	1.5
6	2376	1.5
7	1810	1.2
8	1195	1.0

The result of design process is show in Figure 9.7.



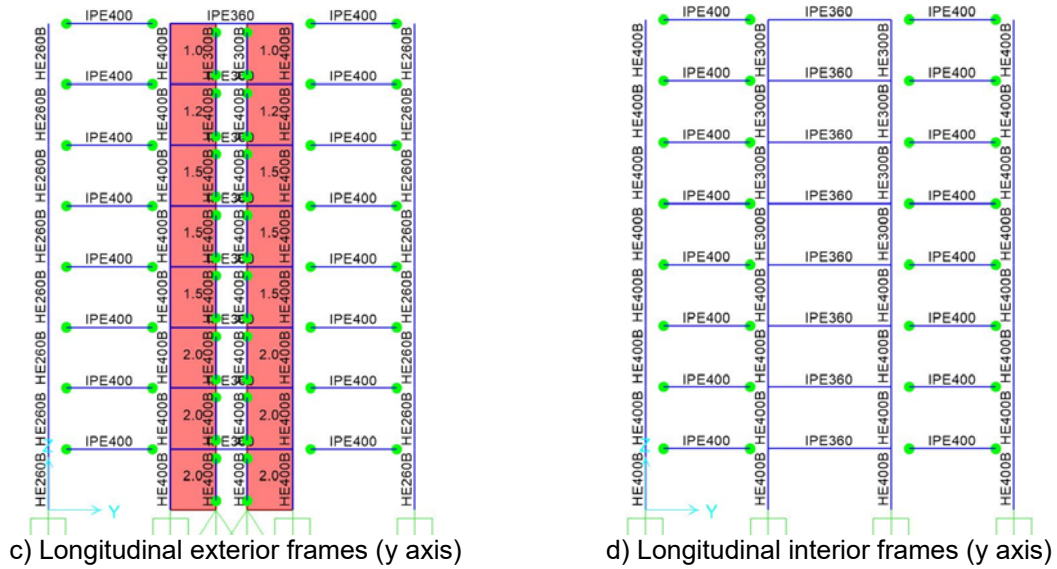
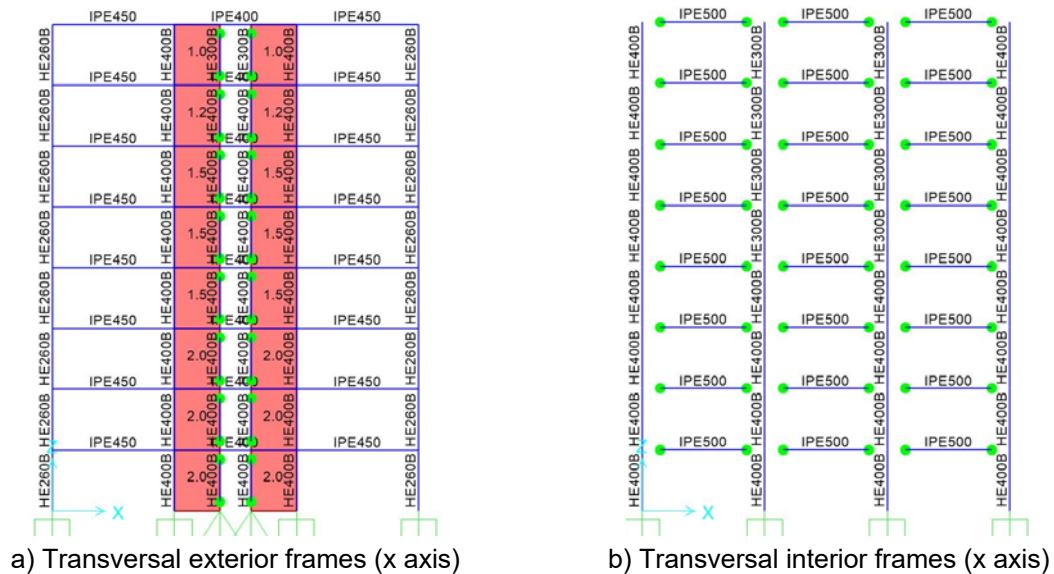


Figure 9.7: 8 story structure

9.1.6.5 Dual configurations

The duality of the structures was checked, in both directions, by verifying that the MRFs is be able to resist at least 25% of the total seismic force. Some adjustments were needed for the structural elements. Figure 9.8 presents the final section for the structural elements.



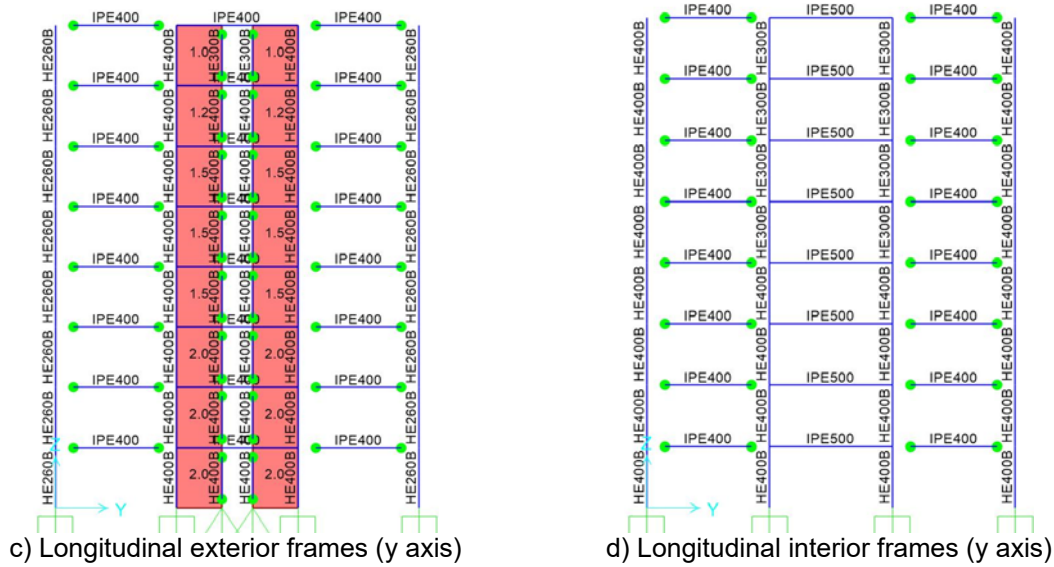


Figure 9.8: Dual 8 story structure

9.1.6.6 Weak beam-strong column

The “weak beam-strong column” condition was checked and found to comply with recommendation given in EN 1998-1-1 [3].

$$\sum M_{Rc} \geq 1.3 \sum M_{Rb} \quad \text{Eq. (9.6)}$$

Where: $\sum M_{Rc}$ is the sum of upper and lower columns moment resistance and $\sum M_{Rb}$ is the moment resistance of the MRF beam.

9.1.7 Re-centring verification

In order to verify the re-centring capacity of the structure it is recommended to use detailed nonlinear static analysis. 2 types on analysis can be performed:

- push-over analysis where the structure is loaded till failure, calculate the target displacement corresponding to ultimate limit state and check the plastic mechanism at ULS if the damage is isolated in the dissipative members;
- load laterally the structure till ULS, unload it and remove the dissipative members in order to see if the structure recovers its initial position.

9.2 Structural detailing

In the following are presented the structural detailing of the structure connections and the shear panel corner detail for 1st story transversal frame (Figure 9.9).

The MRF beam-to-column connection was designed using 27 mm extended end plate with 675x225 hunch and M24 10.9 class bolts (Figure 9.10a). The shear

panel main beam-to-column connection was designed using 24 mm extended end plate and M24 10.9 class bolts (Figure 9.10b). Stanchion-to-main beam connections were designed bolted using 20 mm flush end plate and M20 10.9 class bolts (Figure 9.10c). Bottom horizontal boundary element to column connection was done using bolted flush end plate with M20 10.9 class bolts (Figure 9.10d). The connection between shear panel and boundary elements was designed using 10 mm welded fin plates to the boundary elements and M16 slip-resistant 8.8 class bolts (Figure 9.10e). 13 bolts were needed for horizontal direction 17 bolt for horizontal one. An additional 4 mm strengthening plate was welded on the bolted area of the shear panels in order to avoid failure by shear and bearing (Figure 9.10e).

All pinned beam to column connection were designed using welded gusset plate on the connecting element and bolts.

The tests carried out at UPT ([3] and [4]) have proven that bolted connections in shear and bearing (category C) between the shear panel and boundary elements, realized by fit bolts, exhibit satisfactory fatigue behaviour, provide enough overstrength and allow the removal of the damaged shear panel after the re-centring of the building.

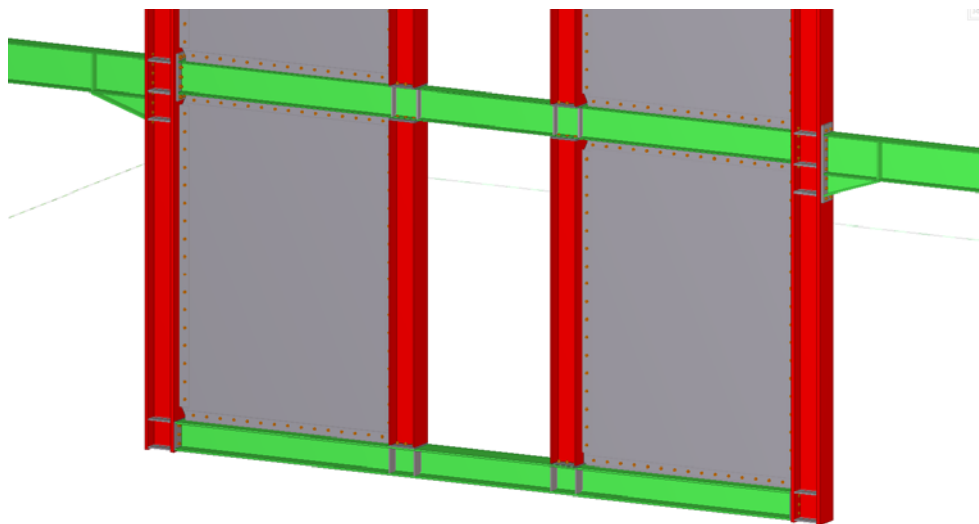


Figure 9.9: Overview of joints

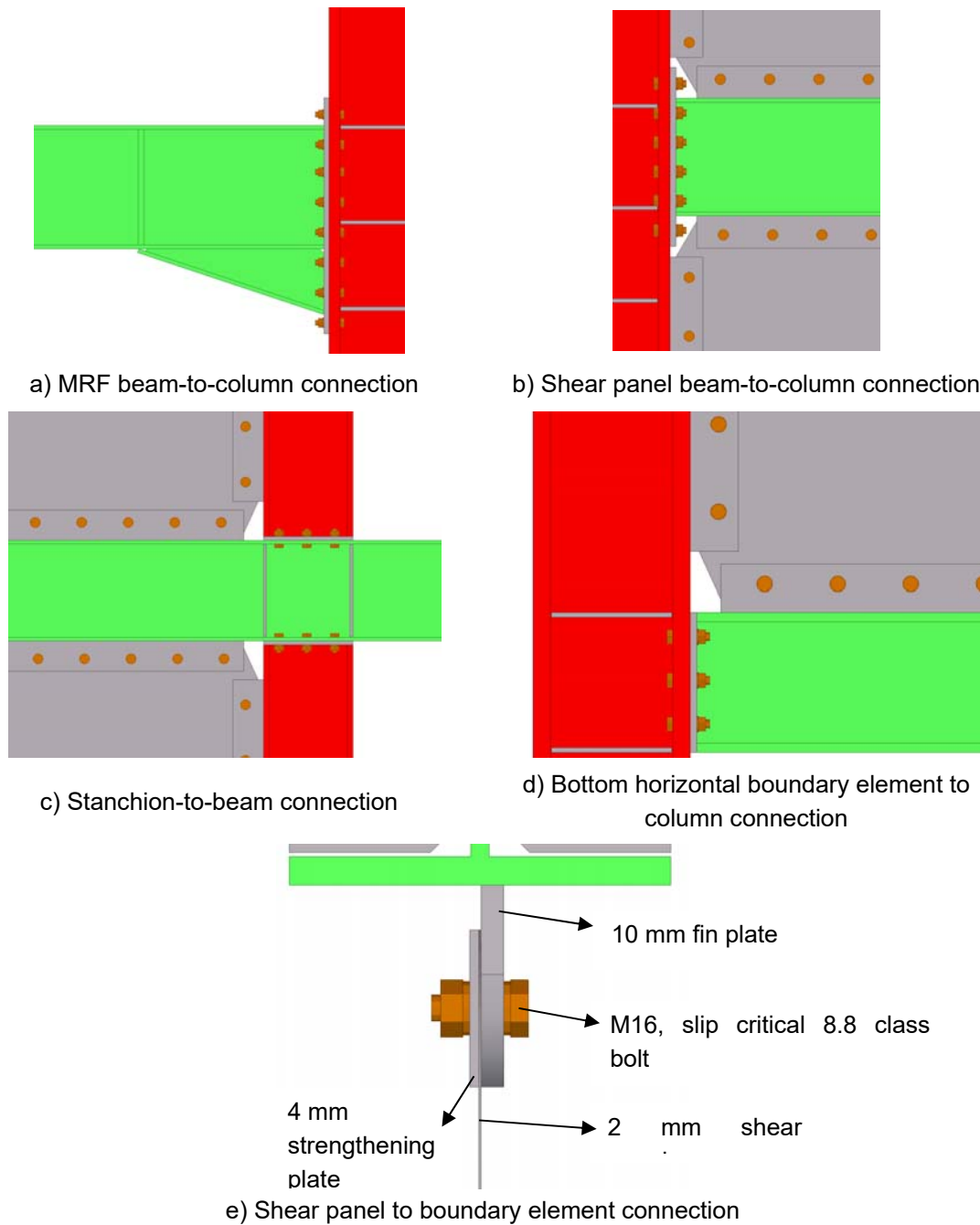


Figure 9.10: Overview of joints

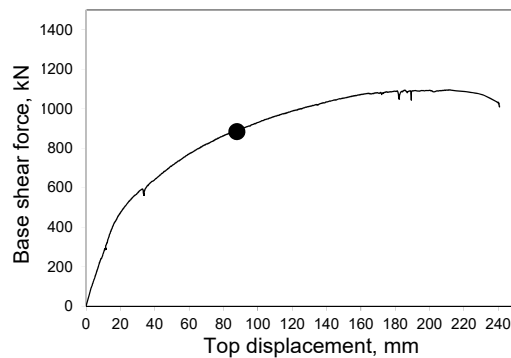
The presented corner detail of the shear panels has proven to have satisfactory behaviour during experimental tests (Figure 9.11a), even if, from 2% top drift (black dot in Figure 9.11c), crack started to develop (Figure 9.11b).



a) Corner detail



b) Fracture of panel



c) Capacity curve

Figure 9.11: Experimental test on frame with rigid connection

9.3 References

1. EN1993-1-1. Eurocode 3: Design of steel structures - Part 1-1: General rules and rules for buildings. Brussels: Comité Européen de Normalisation (CEN); 2003.
2. EN1998-1-1, Eurocode 8: Design of structures for earthquake resistance – Part 1-1: General rules, seismic actions and rules for buildings. Brussels: Comité Européen de Normalisation (CEN); 2003.
3. Dubina D., Dinu F. Experimental evaluation of dual frame structures with thin-walled steel panels. Thin-Walled Structures 2013; 78:57-69.
4. Neagu C. Multi-story building frames stiffened with dissipative shear wall: PHD Thesis; Ed. Politehnica; University Politehnica Timisoara; Romania, 2011.
5. EN 1993-1-8: Eurocode 3: Design of steel structures. Part 1-8: Design of joints. Brussels: Comité Européen de Normalisation (CEN); 2004.
6. AISC 341-16. Seismic provisions for structural steel buildings; American Institute for Steel Construction: 2016.
7. SAP2000. CSI: Computers and Structures Inc., www.csiberkeley.com.
8. Georgiev Tzv., Zhelev D., Raycheva L., Rangelov N., " INNOSEIS - Valorization of innovative anti-seismic devices", WORK PACKAGE 1 – DELIVERABLE 1.1, Volume with information brochures for 12 innovative devices in English, European Commission Research Programme of the Research Fund for Coal and Steel, (Article in Press).

10 CBF-MB

10.1 General

10.1.1 Introduction

This case study refers to the seismic design of new four-storey steel office buildings. It aims at demonstration of the implementation of the Concentrically Braced Frames with Modified Braces (CBF-MB). The case study elaborated, refers to conceptual design, modelling and analysis by linear response spectrum analysis methods (RSA), detailed design of main dissipative and non-dissipative members and basic structural detailing of CBF-MB.

10.1.2 Description of building

10.1.2.1 Geometry and general assumptions

The case study deals with a four-storey frame building with three 8m bays in both directions. The gravity frames are composed of beams and columns, located at each structural axis. Nominally pinned beam-to-column joints and pinned column bases are assumed. The CBF-MBs are the main horizontal load resisting systems, located in the middle of the first and the third bay as shown in Figure 10.1.

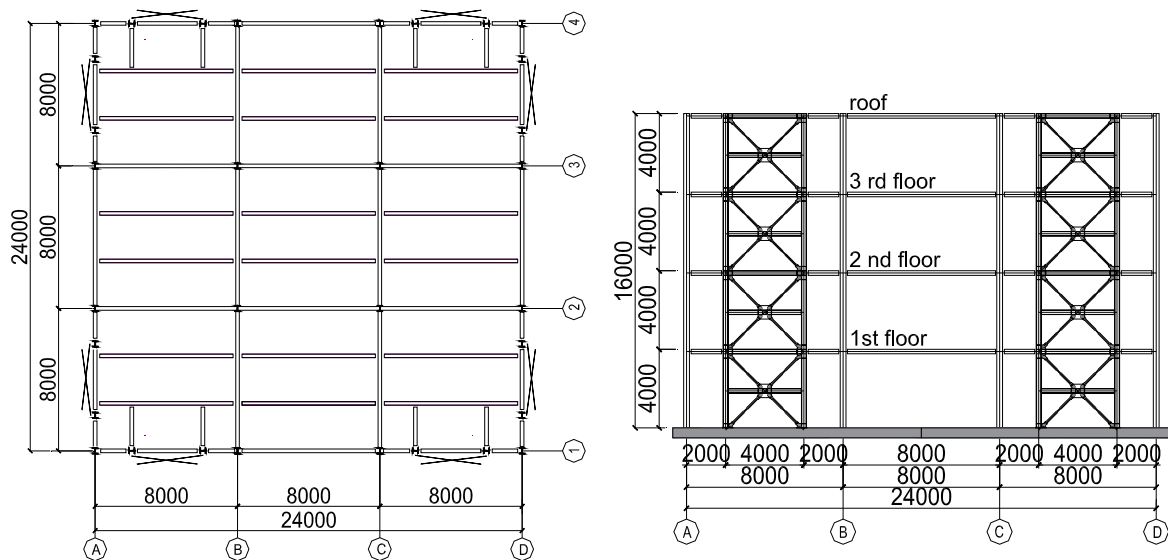


Figure 10.1: Floor plan and elevation

Hot rolled HEA and HEB profiles for columns and IPE profiles [2] for floor beams are used for all gravity frames. Both, floors and roof slabs are designed with steel

beams and concrete deck. Composite action with the concrete slab is not considered. However, dowels connecting main and secondary beams to the concrete deck are used to provide structural integration and floor diaphragm action. Diaphragms are assumed as rigid, thus neglecting membrane (in-plane) deformations.

Each CBF-MB consists of two columns, floor beams, splitting beams and braces. It is integrated in the centre of each side bay, as shown in Figure 10.1. In this way columns of the CBF are loaded primarily with axial forces resulting from the seismic action (or wind load) and the rest of the frame columns carry the gravity loads.

10.1.2.2 *Materials*

Steel grade S235 is used for the design of modified braces (dissipative elements) The adopted steel grades for CBF columns are S275 and S355. CBF-MB floor beams and splitting beams are designed with steel grade S275.

Gravity frame is designed by conventional approach and steel grades S275 and S355 are used. Floor slabs are designed by Hi-Bond metal decking used for formwork only, concrete C25/30 and reinforcing steel B500B are assumed.

10.1.2.3 *Loads and load combinations*

Table 10.1 summarizes the adopted gravity loads and seismic action parameters. Top floor loads are adopted as for non-occupied roof. It is assumed that snow load intensity is less than the imposed roof load and the altitude of construction site is below 1000 meters. Consequently, the snow load is excluded from the seismic design situation.

Table 10.1: Loads and actions

Vertical loads	
Concrete and metal deck self-weight	2.75 kN/m ²
Utilities, ceiling, floor or roof finishing:	
– First, second and third floor	0.70 kN/m ²
– Roof	1.00 kN/m ²
Facades:	0.60 kN/m ²
Tributary facade height (4 m for first storey and 4 m for roof including parapet wall).	
Partitions, only at office floors	0.80 kN/m ²
Imposed loads 1 st , 2 nd , 3 rd floor (category B):	3.00 kN/m ²
Imposed loads roof (category H):	0.75 kN/m ²

Seismic action	
Design response spectrum for elastic analysis	Type 1
Reference peak ground acceleration	$a_{g,R} = 0.30g$
Importance class II (Ordinary building)	$\gamma_I = 1.0$
Ground type	$B (T_B = 0.15 \text{ s}, T_C = 0.50 \text{ s})$
Behaviour factor q	5.0
Damping ratio	5%
Factors for storey occupancy	$\varphi = 0.80$
Seismic combination coefficient	
First, second and third floor	$\psi_2 = 0.30, \psi_E = 0.24$
Roof	$\psi_2 = 0.00, \psi_E = 0.00$

The seismic masses are calculated according to Eq. (10.1) and presented in Table 10.2.

$$\sum_{j>1} G_{k,j} + \sum_{i>1} \psi_{E,i} \cdot Q_{k,i} \quad \text{Eq. (10.1)}$$

Table 10.2: Seismic masses

Seismic mass floor 1 to 3 = 315.4 t (for each one)	
Concrete and metal deck self-weight – ($G_{k1,1}$)	$2.75 \times 24.0 \times 24.0 / 9.81 = 161.5 \text{ t}$
Utilities, ceiling, floor finishing – ($G_{k2,1}$)	$0.70 \times 24.0 \times 24.0 / 9.81 = 41.1 \text{ t}$
Facades – ($G_{k3,1}$)	$0.60 \times 4.0 \times 4.0 \times 24.0 / 9.81 = 23.5 \text{ t}$
Partitions – ($G_{k4,1}$)	$0.80 \times 24.0 \times 24.0 / 9.81 = 47.0 \text{ t}$
Imposed loads – ($Q_{k,1}$). Ψ_E	$3.0 \times 24.0 \times 24.0 \times 0.24 / 9.81 = 42.3 \text{ t}$
Seismic mass roof = 243.7 t	
Concrete and metal deck self-weight – ($G_{k1,2}$)	$2.75 \times 24.0 \times 24.0 / 9.81 = 161.5 \text{ t}$
Utilities, ceiling, floor finishing – ($G_{k2,2}$)	$1.00 \times 24.0 \times 24.0 / 9.81 = 58.7 \text{ t}$
Facades – ($G_{k3,2}$)	$0.60 \times 4.0 \times 4.0 \times 24.0 / 9.81 = 23.5 \text{ t}$
Imposed loads – ($Q_{k,2}$). Ψ_E	$0.75 \times 24.0 \times 24.0 \times 0.0 / 9.81 = 0.0 \text{ t}$
Steel skeleton seismic mass = 148 t	

Seismic masses for the building are summarized in Table 10.3.

Table 10.3: Seismic masses by floor

Floor 1 to 3 mass = 315.4 t	Roof mass = 243.7 t	Skeleton mass = 140.8 t
Total seismic mass = 1330.7 t		

10.2 Basic and non-seismic design

10.2.1 Preliminary selection of modified braces

The modified braces provide the primary source of stiffness and dissipation capacity for the CBF-MB system so their design differs from the ordinary brace design. Initially brace shape and first-estimation cross sections need to be chosen. The user should expect that several iterations would have to be done. The cross-sections to be defined are illustrated in Figure 10.2 and the choice of their recommended lengths is demonstrated in Table 10.4. The recommendations of [5, 6] have been followed.

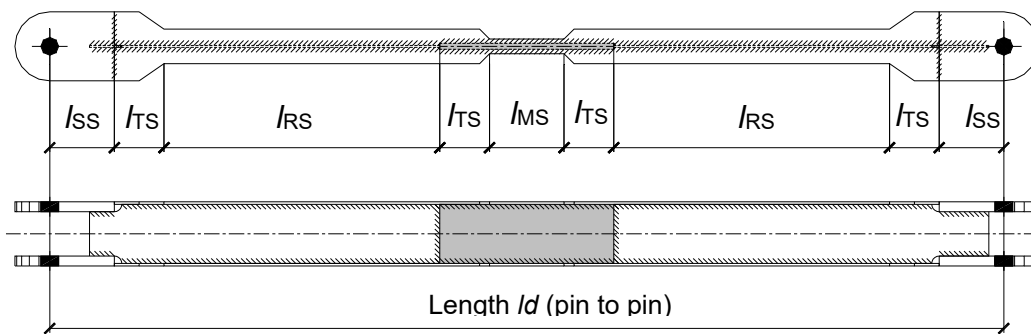


Figure 10.2: Definition of the cross-sections within a modified brace member

Table 10.4: Choice of specific lengths in modified braces

Specific length (mm)	Recommendations according to [5], [6]	A particular value in this example (mm)			
l	NA	5656			
		storey			
		1	2	3	4
l_d	$(0.375 - 0.40)l$	2150	2150	2190	2190
l_{MS}	$l_{MS} = (0.067 \div 0.085)l_d$	180	160	150	145
l_{TS}	~ 100	100	100	100	100
l_{SS}	Preference of designer	130	130	130	130
l_{RS}	$l_{RS} \approx (0.3)l_d$	655	665	690	693

Where:

l is the system length of the diagonal,

l_d is the pin-to-pin length of the brace,

l_{MS} is the length of the modified section,

l_{TS} is the length of the transition section,

l_{SS} is the length of the strong section,

l_{RS} is the length of the reduced section,

MS, RS, SS and TS are abbreviations for modified section, reduced section, strong section and transition section respectively.

As stated in [5] and [6], some relations between the area and section modulus of reduced section and modified section should be achieved to ensure that yielding in tension and flexural plastic strains due to buckling occurs in different zones along the modified brace length. The preliminary selection of the brace flange and web geometry is demonstrated in Table 10.5. The MB cross sections will be described by abbreviations for example F85.6W150.5-M180.36-T14 that should be interpreted as explained below.

- For reduced section: F (flange) 85.6 width 85 mm, thickness 6 mm; W (web) 150.5 width 150 mm, thickness 5 mm;
- For modified section: M (modified section) 180.36 length 180 mm, flange width 36 mm – T14 (web thickness of MS) 14 mm.

Table 10.5: Choice of Area and Section modulus in modified braces

Storey	Abbreviation of the MB	Recommendations according to [5], [6]	Value adopted in the particular example
1 st storey	F85.6W150.5-M180.36-T14	$A_{MS}/A_{RS} \geq 1.4$	$A_{MS} = 25.3 \text{ cm}^2$
			$A_{RS} = 17.7 \text{ cm}^2$
			$A_{MS}/A_{RS} = 1.43$
		$W_{pl,RS}/W_{pl,MS} \geq 2.0$	$W_{MS} = 11.2 \text{ cm}^3$
			$W_{RS} = 22.6 \text{ cm}^3$
			$W_{pl,RS}/W_{pl,MS} = 2.01$
2 nd storey	F75.6W130.4-M160.36-T12	$A_{MS}/A_{RS} \geq 1.4$	$A_{MS} = 19.9 \text{ cm}^2$
			$A_{RS} = 14.2 \text{ cm}^2$
			$A_{MS}/A_{RS} = 1.4$
		$W_{pl,RS}/W_{pl,MS} \geq 2.0$	$W_{MS} = 8.6 \text{ cm}^3$
			$W_{RS} = 17.4 \text{ cm}^3$
			$W_{pl,RS}/W_{pl,MS} = 2.03$
3 rd storey	F70.5W105.3-M150.38-T10	$A_{MS}/A_{RS} \geq 1.4$	$A_{MS} = 14.3 \text{ cm}^2$
			$A_{RS} = 10.2 \text{ cm}^2$
			$A_{MS}/A_{RS} = 1.41$
		$W_{pl,RS}/W_{pl,MS} \geq 2.0$	$W_{MS} = 6.2 \text{ cm}^3$
			$W_{RS} = 12.5 \text{ cm}^3$
			$W_{pl,RS}/W_{pl,MS} = 2.0$

4 th storey	F60.4W75.2,5- M145.33-T9	$A_{MS}/A_{RS} \geq 1.4$	$A_{MS} = 9.4 \text{ cm}^2$
			$A_{RS} = 6.7 \text{ cm}^2$
			$A_{MS}/A_{RS} = 1.41$
		$W_{pl,RS}/W_{pl,MS} \geq 2.0$	$W_{MS} = 3.7 \text{ cm}^3$
			$W_{RS} = 7.3 \text{ cm}^3$
			$W_{pl,RS}/W_{pl,MS} = 1.98 \approx 2.0$

Where:

A_{MS} is the modified section area,

A_{RS} is the reduced section area.

$W_{pl,RS}$ is the reduced section plastic modulus,

$W_{pl,MS}$ is the modified section plastic modulus.

10.2.2 Preliminary check of brace slenderness

Since there is modified section inserted in the mid-length, then the real buckling length $l_{cr} = \mu \cdot l_d$ will be longer than l_d . The effective length l_{cr} may be obtained by FE elastic buckling analysis or by Eq. (10.2).

$$\mu = l_{cr} / l_d = 0.88 K_L^{(0.033)} \cdot K_I^{(0.1 \ln(K_L) - 0.36)} \quad \text{Eq. (10.2)}$$

Where:

$K_L = L_{RS} / L_{MS}$ is the section length ratio,

$K_I = I_{MS} / I_{RS}$ is the inertia moment ratio,

I_{MS} is the moment of inertia of the modified section,

I_{RS} is the moment of inertia of the reduced section,

μ is a parameter that modifies the geometric brace length l_d to buckling length l_{cr} .

Hereafter Eq. (10.2) is used and the results are presented in Table 10.6. According to [1] braces of CBFs with X-configuration must have non-dimensional slenderness in the range of $1.3 \leq \bar{\lambda}_{eff} \leq 2.0$. The effective slenderness is defined by Eq. (10.3).

$$\lambda_{eff} = \mu \cdot l_d / i_{RS} \quad \text{Eq. (10.3)}$$

Where i_{RS} is the minor radius of gyration of the reduced section.

Table 10.6: Modified braces slenderness

Storey	Modified Brace	K_L	K_I	μ	L_{cr} (m)	λ_{eff}	$\bar{\lambda}_{eff}$
1	F85.6W150.5-M180.36-T14	3.639	0.120	1.497	3.219	172.7	1.84
2	F75.6W130.4-M160.36-T12	4.156	0.151	1.391	2.991	173.4	1.85
3	F72.5W104.3-M150.40-T10	4.600	0.195	1.299	2.845	169.5	1.80
4	F60.4W75.2,5-M145.33-T9	4.779	0.217	1.265	2.770	188.5	2.00

10.2.3 Simulation

The structural linear elastic model was formed according to the rules given in [5, 6] by the software SAP 2000 [8]. All gravity columns are modelled as continuous and pin-connected to the bases. All joints between gravity floor beams and columns are nominally pinned as well.

CBF-MB members are designed and modelled as follows. CBF-MB columns are continuous. The joints between splitting beams and columns are assumed to be rigid and full-strength so they are modelled as continuous while the joints between beams and CBF-MB columns are assumed nominally pinned. The elements simulating the modified braces are defined through constant H-shape section with characteristics of the reduced section and joined to the frame by simple pin connections. CBF-MB column bases were designed and detailed as pinned which is considered the most practical approach for this type of system. The elastic analysis requires a tension-only diagonal model [1]. Diaphragm action of floors and roof concrete decks is simulated by diaphragm constraint.

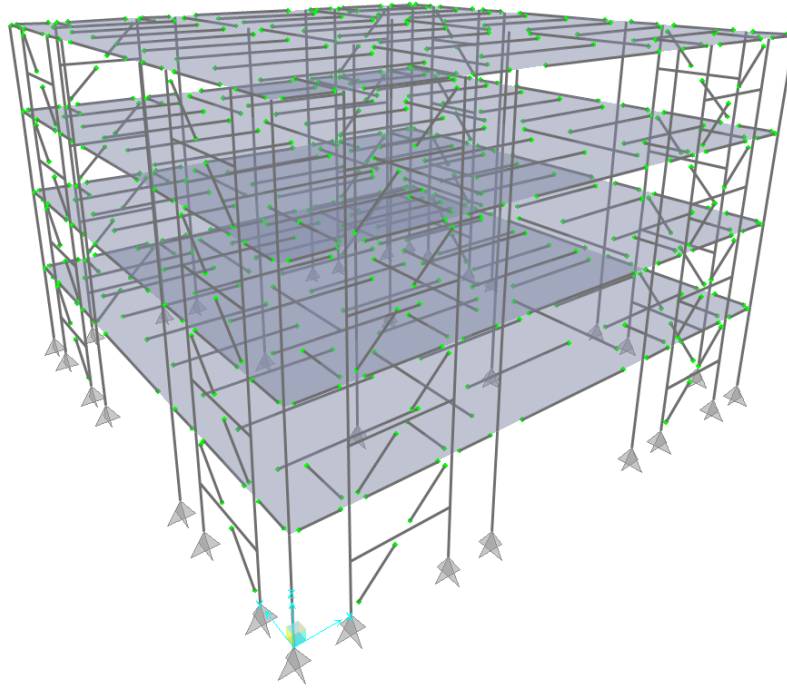


Figure 10.3: FE three-dimensional model

The current case study was developed by centreline-to-centreline (CL-to-CL) model. It is quick and easy to be defined, since the axis geometry of the frame is known at the beginning of the design process.

10.2.4 Design for static combinations

Distinctive feature of the structural configuration demonstrated in this case study is the fact that the proposed seismic resistant system (CBF-MB) is arranged so as to be almost released from gravity loads, excluding its self-weight and small tributary dead and imposed loads. It is easy to be checked that the seismic design situation governs the design of CBF-MB system, therefore wind combination will not be considered hereafter.

10.2.4.1 Ultimate limit state results

The ultimate limit state load combination that governs the gravity members design is calculated according to Eq. (10.4).

$$\sum_{j>1} 1.35.G_{k,j} + \sum_{i>1} 1.5.Q_{k,i} \quad \text{Eq. (10.4)}$$

10.2.4.2 Member design

The results from the member design are presented in Table 10.7.

Table 10.7: Verification of gravity members

Member	Section	Steel grade	N_{Ed} (kN)	$M_{y,Ed}$ (kNm)	$M_{z,Ed}$ (kNm)	Ratio
Secondary roof beam	IPE300	S275	-	130	-	0.791
Main roof beam	HEA340	S275	-	361	-	0.773
Secondary floor beam	IPE360	S275	-	230	-	0.861
Main floor beam	HEA400	S275	-	605	-	0.936
Internal column from base to level 8.0m	HEB300	S275	-2564	-	-	0.866
External column from base to level 8.0m	HEA240	S275	-1155	-	-	0.888
Internal column from level 8 to roof level	HEA240	S275	-1145	-	-	0.837
External column from base to roof level	HEA200	S275	-519	-	-	0.630

10.2.4.3 Serviceability limit state checks

Table 10.8: Verification of member's deflection

Member	Section	Deflection	type	Adopted limit
Secondary roof beam	IPE300	1/230	roof	1/200
Main roof beam	HEA340	1/261	roof	1/200
Secondary floor beam	IPE360	1/255	floor	1/250
Main floor beam	HEA400	1/256	floor	1/250

10.3 Seismic analysis

10.3.1 Seismic design situation

The building is recognized as regular in plan and in height. Theoretically the centre of masses and the centre of rigidity coincide. In order to account for uncertainties in the location of masses and for the rotational component of the seismic motion, additional accidental mass eccentricity (§4.3.3.3.3 [1]) with value of 1200 mm (5% of 24000 mm) was introduced in both directions. The mass eccentricity effects were taken into account by defining two static load cases M_x and M_y , simulating rotation. In order to account for the torsional effects, the storey seismic forces in both main directions were calculated based on the lateral force method (§4.3.3.2 [1]). It was done by introducing quake load pattern, floor diaphragm constraints and eccentricity of 5% in SAP 2000 [8]. The final seismic design situation that

accounts for accidental torsional effects was derived by Eq. (10.5) as recommended by P. Fajfar [7].

$$E = SRSS (Ex \pm Mx, Ey \pm My) \quad \text{Eq. (10.5)}$$

where:

Ex and Ey are the results of analysis without accidental torsion by applying RSA in X and Y direction, respectively;

Mx and My are the accidental torsional effects of applied storey seismic force with eccentricity of 5% in X and Y direction, respectively;

SRSS is the square root of sum of the squares combination.

The global rotational effect was assessed as about 6.0% to 6.5% amplification of the seismic effects (internal forces and displacements), depending on the storey.

The seismic combination that governs the CBF-MB braces design is calculated according to Eq. (10.6).

$$\sum_{j=1}^4 G_{k,j} + E + 0.3Q_{k,i} \quad \text{Eq. (10.6)}$$

where:

$G_{k,j}$ are the gravity load effects in seismic design situation;

E is the effect of the seismic action including accidental torsional effects;

$Q_{k,1}$ is the first floor imposed load effects in seismic design situation;

10.3.2 Response Spectrum Analysis

Multi-modal RSA was performed. The first and the second natural modes of vibrations are presented on Figure 10.4. They are dominantly translational. The third mode of vibration is rotational as shown on Figure 10.5. The results from the analysis are summarized in Table 10.9. The first and the second modes activate less than 90% of the total mass. It is observed that at least 5 modes of free vibration have to be included in the modal analysis in order to activate more than 90% of the seismic mass.

Table 10.9: Participating mass ratio and periods

Mode No	Eigen Period (s)	Participating mass in direction X (%)	Participating mass in direction Y (%)
1	1.1113	79.7	-
2	1.1109	-	79.9
3	0.681	-	-
4	0.398	14.7	-
5	0.394	-	14.6
Sum of participating masses		94.4	94.5

According to [1] when $T_c \leq T$ the spectrum acceleration has to be greater or equal to the lower bound. Since the first mode dominates the response, the check may be done by Eq. (10.7):

$$S_d(T) = \frac{V_{tot}}{P_{tot}} \geq \beta \cdot a_g, \quad \text{Eq. (10.7)}$$

where V_{tot} is the total base shear from the response spectrum analysis, P_{tot} is the total vertical load, corresponding to the seismic design situation and $\beta = 0.2$ is the lower bound factor for the horizontal design spectrum. The check proves that there is no need to increase the base shear (Table 10.10).

Table 10.10: Check of the lower bound for the horizontal design spectrum

V_{tot} (kN)	P_{tot} (kN)	V_{tot} / P_{tot}	βa_g
920	13 362	0.0689	0.060

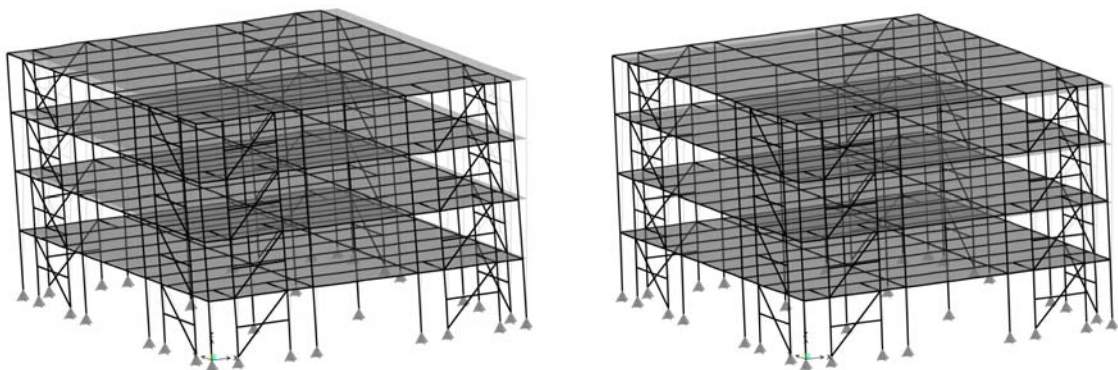


Figure 10.4: First and second mode of free vibration, $T_1 = 1.1113$ s, $T_2 = 1.1109$ s

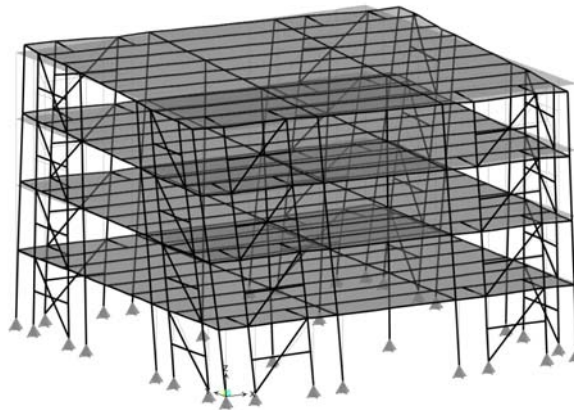


Figure 10.5: Third mode of free vibration, $T_3 = 0.681$ s

10.4 Detailed design

10.4.1 Damage limitation – limitation of interstorey drift

Assuming that the building has ductile non-structural elements the verification is:

$$d_r \cdot v \leq 0.0075h = 0.0075 \cdot 4000 = 30.0 \text{ mm}, \quad \text{Eq. (10.8)}$$

Where $v = 0.5$ is the reduction factor according to §4.4.3.2 (1) of [1], h is the story height and d_r is the design interstorey drift. Table 10.11 includes the results from the analysis for each of the stories.

Table 10.11: Limitation of interstorey drift

Storey	1	2	3	4
$d_{e, \text{top}}$ (mm)	8.1	17.4	27.6	37.1
$d_{e, \text{bottom}}$ (mm)	0.0	8.1	17.4	27.6
$d_r = (d_{e, \text{top}} - d_{e, \text{bottom}}) q$ (mm)	40.5	46.5	51.0	47.5
$d_r v$	$20.3 < 30$	$23.3 < 30$	$25.5 < 30$	$23.8 < 30$

10.4.2 Second order effects

The sensitivity to second order ($P-\Delta$) effects is estimated by the interstorey drift sensitivity coefficient θ given by Eq. (10.9), where P_{tot} and V_{tot} are the total gravity load at and above the storey considered in the seismic design situation and the total seismic storey shear at the storey under consideration, respectively. The calculated values of θ are listed in Table 10.12.

$$\theta = P_{\text{tot}} d_r / V_{\text{tot}} h \quad \text{Eq. (10.9)}$$

Table 10.12: 2nd order effects

Storey	1	2	3	4
$d_r = (d_{e, \text{top}} - d_{e, \text{bottom}}) q$ (mm)	40.5	46.5	51.0	47.5
$P_{\text{tot}} / V_{\text{tot}}$	13119 / 940	9437/767	6148/554	2699/338
h (mm)	4000	4000	4000	4000
θ	0.146 > 0.1	0.145 > 0.1	0.130 > 0.1	0.082 < 0.1
$1/(1-\theta)$	1.172	1.170	1.150	1.089

The values of θ for first three storeys are more than 0.10 but less than 0.20, so corresponding to §4.4.2.2 (2) of [1], the second-order effects should be considered in the design with factoring the seismic load effects by $1/(1-\theta)$.

10.4.3 Final verification of dissipative members

The non-dimensional slenderness of the brace $\bar{\lambda}_{\text{eff}}$ should be limited to $1.3 \leq \bar{\lambda}_{\text{eff}} \leq 2.0$ as stated in §6.7.3 (1) of [1]. The yield resistance $N_{pl,Rd}$ of the modified brace should fulfil §6.7.3 (5) of [1] and should be obtained by Eq. (10.10). It should be noted that in the current example $\gamma_{M0} = 1.05$ and $\gamma_{M1} = 1.05$.

According to §6.7.3 (8) of [1] the maximum and minimum overstrength Ω should not differ more than 25% providing homogeneous dissipative behaviour of the diagonals. Since the initial brace cross-sections are not changed after the verifications in sections 10.4.1 and 10.4.2, the normalized slenderness is not changed and the valid results are shown in Table 10.6. The rest verifications are presented in Table 10.13, where the design forces N_{Ed} include torsional effects and are scaled by $1/(1-\theta)$ to account for the second order effects.

$$N_{pl,Rd} = A_{RS} \cdot f_y / \gamma_{M0} \quad \text{Eq. (10.10)}$$

Table 10.13: Verification of braces and check for homogeneous dissipative behaviour

Storey	Brace cross section	A_{RS} (cm ²)	N_{Ed} (kN)	$N_{pl,Rd}$ (kN)	$\Omega = \frac{N_{pl,Rd}}{N_{Ed}}$	$\frac{\max \Omega}{\min \Omega} < 1.25$
1	F85.6 W150.5-M180.36-T14	17.7	387.0	396.1	1.023	1.13
2	F75.6W130.4-M160.36-T12	14.2	307.7	317.8	1.033	
3	F70.5W105.3-M150.38-T10	10.2	225.4	228.3	1.013	
4	F60.4W75.2,5-M145.33-T9	6.7	130.8	149.9	1.146	

10.4.4 Transition stage

The splitting beam should be designed as per the recommendations of [5, 6]. The transition stage (“just before buckling” stage) is introduced because it is characterized with additional bending moments and axial forces (load case UNB) that occur within the storey H-frame – Figure 10.6. That internal effect is to be accounted for into design. It is simulated in the model for elastic analysis by introducing unbalanced forces integrally in all four stories simultaneously.

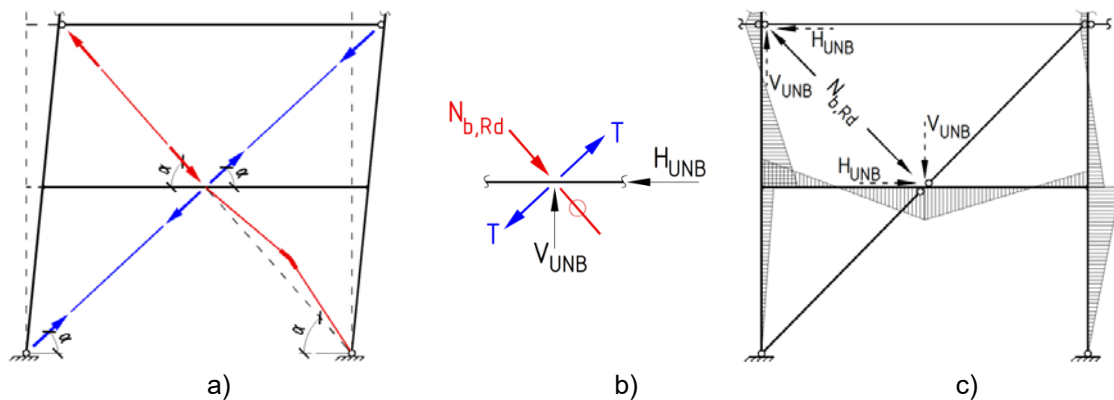


Figure 10.6: a) Transition stage (“just before buckling”); b) Unbalanced forces; c) Internal moments (M_{UNB}) resulting from the unbalanced forces (load case UNB)

The unbalanced forces are calculated based on Eq. (10.11), Eq. (10.12), Eq. (10.13) and the results are presented in Table 10.14.

$$V_{UNB} = N_{b,Rd} \cdot \sin \alpha \quad \text{Eq. (10.11)}$$

$$H_{UNB} = N_{b,Rd} \cdot \cos \alpha \quad \text{Eq. (10.12)}$$

$$N_{b,Rd} = \chi \cdot A_{RS} \cdot f_y / \gamma_{M1} \quad \text{Eq. (10.13)}$$

Table 10.14: Unbalanced forces in splitting beams

Storey	Brace cross sections	A_{RS} (cm ²)	$\bar{\lambda}_{eff}$	Buckling curve	χ	$N_{b,Rd}$ (kN)	V_{UNB} (kN)	H_{UNB} (kN)
1	F85.6 W150.5-M180.36-T14	17.7	1.84	“c”	0.226	89.5	63.3	63.3
2	F75.6W130.4-M160.36-T12	14.2	1.85	“c”	0.224	71.2	50.3	50.3
3	F70.5W105.3-M150.38-T10	10.2	1.80	“c”	0.235	53.7	37.9	37.9
4	F60.4W75.2,5-M145.33-T9	6.7	2.00	“c”	0.196	29.4	20.8	20.8

10.4.5 Capacity design of non-dissipative members

CBF-MB columns shall be verified to resist design forces obtained from Eq. (10.14) to Eq. (10.16). The results for column verifications are presented in Table 10.15.

$$N_{col,Ed} = N_{Ed,G} + 1.1\gamma_{OV}\Omega_{min}\rho(N_E + N_{UNB}) \quad \text{Eq. (10.14)}$$

$$M_{col,Ed} = M_{Ed,G} + 1.1\gamma_{OV}\Omega_{min}\rho(M_E + M_{UNB}) \quad \text{Eq. (10.15)}$$

$$V_{col,Ed} = V_{Ed,G} + 1.1\gamma_{OV}\Omega_{min}\rho(V_E + V_{UNB}) \quad \text{Eq. (10.16)}$$

Where:

$\gamma_{OV}=1.25$ is the material overstrength factor according to §6.2 (3) of [1],

$\Omega_{MIN}=1.013$ as per Table 10.13,

$\rho = 1.15$ is factor accounting for the available overstrength of the system, when DCH is adopted (see [6]).

Note that the second order effect is considered by increasing the seismic loads with $1/(1-\theta)=1.172$.

Table 10.15: CBF columns verification

Storey	Column cross-section / Material	$N_{col,Ed}$	$M_{col,Ed}$	Utilization factor
1	HEA 300 / S355	-1487	100	0.764
2	HEA 300 / S355	-968	70	0.529
3	HEA 240 / S275	-560	58	0.732
4	HEA 240 / S275	-222	43	0.395

Splitting beams shall be verified to resist design forces obtained from Eq. (10.17) to Eq. (10.19). The results for splitting beams verifications are presented in Table 10.16.

$$N_{sb,Ed} = N_{Ed,G} + 1.1\gamma_{OV}\Omega_{min}\rho(N_E + N_{UNB}) \quad \text{Eq. (10.17)}$$

$$M_{sb,Ed} = M_{Ed,G} + 1.1\gamma_{OV}\Omega_{min}\rho(M_E + M_{UNB}) \quad \text{Eq. (10.18)}$$

$$V_{sb,Ed} = V_{Ed,G} + 1.1\gamma_{OV}\Omega_{min}\rho(V_E + V_{UNB}) \quad \text{Eq. (10.19)}$$

Table 10.16: Splitting beam verification

Storey	Splitting beam cross-section / Material	$N_{sb,Ed}$	$M_{sb,Ed}$	Utilization factor	$\bar{\lambda}_{LT}$
1	HEA 240 / S275	-88	99	0.603	0.36
2	HEA 240 / S275	-76	90	0.545	0.36
3	HEA 240 / S275	-54	81	0.485	0.36
4	HEA 240 / S275	-28	66	0.387	0.36

Floor beams shall be verified to resist design forces obtained from Eq. (10.20) to Eq. (10.22). The results are presented in Table 10.17.

$$N_{b,Ed} = N_{Ed,G} + 1.1\gamma_{OV}\Omega_{\min}\rho(N_E + N_{UNB}) \quad \text{Eq. (10.20)}$$

$$M_{b,Ed} = M_{Ed,G} + 1.1\gamma_{OV}\Omega_{\min}\rho(M_E + M_{UNB}) \quad \text{Eq. (10.21)}$$

$$V_{b,Ed} = V_{Ed,G} + 1.1\gamma_{OV}\Omega_{\min}\rho(V_E + V_{UNB}) \quad \text{Eq. (10.22)}$$

Table 10.17: Floor beam verification

Storey	Floor beam cross-section / Material	$N_{b,Ed}^3$	$M_{b,Ed}$	Utilization factor
1	HEA 240 / S275	-443	43.3	0.531
2	HEA 240 / S275	-355	43.3	0.467
3	HEA 240 / S275	-255	43.3	0.395
4	HEA 240 / S275	-168	32.6	0.281

The splitting beam shall be designed so that avoiding lateral-torsional buckling by satisfying Eq. (10.23). Results are presented in Table 10.16.

$$\bar{\lambda}_{LT} \leq 0.40 \quad \text{Eq. (10.23)}$$

The cross sections of splitting beam and columns shall be chosen to satisfy Eq. (10.24) in accordance with §4.4.2.3 (4) of [1].

$$2.M_{Rc} \geq 1.3M_{Rb}, \quad \text{Eq. (10.24)}$$

In that particular case it is obvious that Eq. (10.24) is fulfilled.

10.5 Structural detailing

After fulfilment of all checks in §10.4 the modified diagonals may be detailed. Their final design is presented in Figure 10.7 to Figure 10.10.

³ It is recommended that axial beam force is calculated based on the diagonal plastic resistance in tension, additionally scaled by $1.1\gamma_{OV}\rho$. The axial force from the 3D model is non-realistic since the floor diaphragm constraint was implemented.

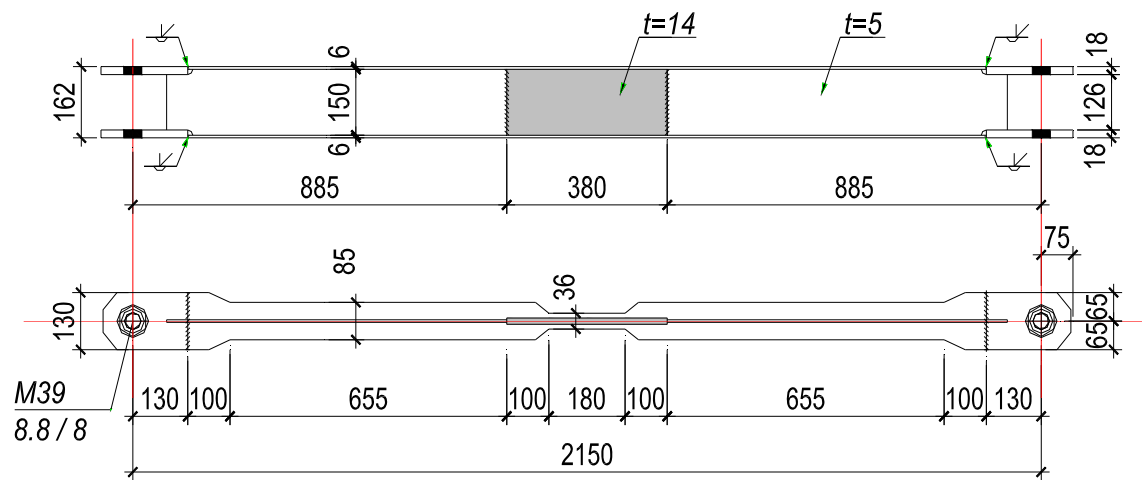


Figure 10.7: Overview of modified brace member F85.6 W150.5-M180.36-T14 at the first storey

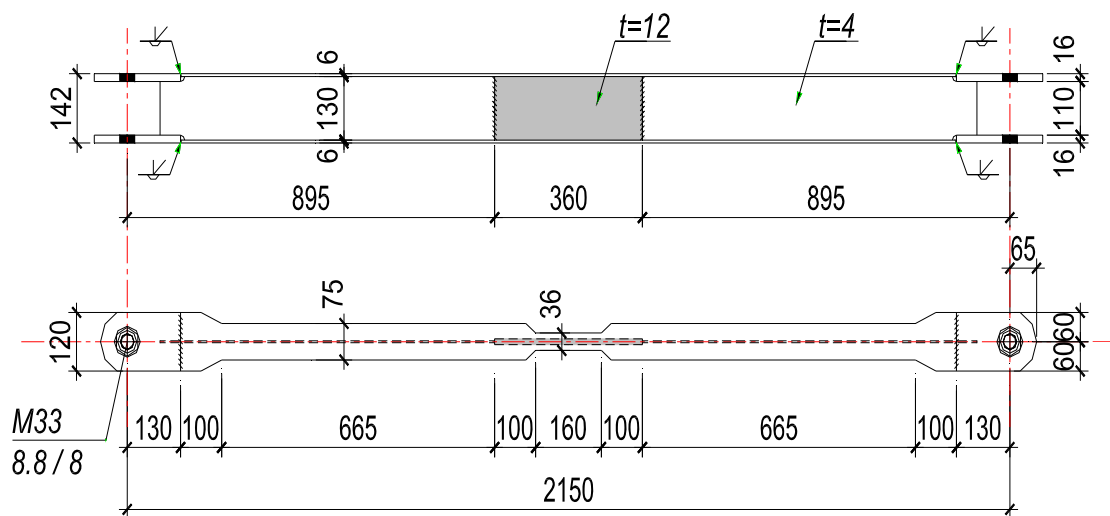


Figure 10.8: Overview of modified brace member F75.6W130.4-M160.36-T12 at the second storey

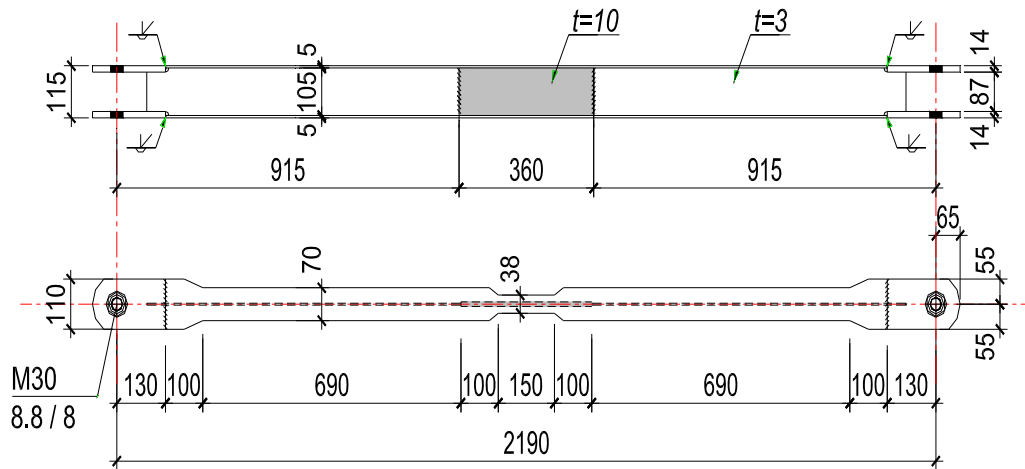


Figure 10.9: Overview of modified brace member F70.0W105.5-M150.38-T10 at the third storey

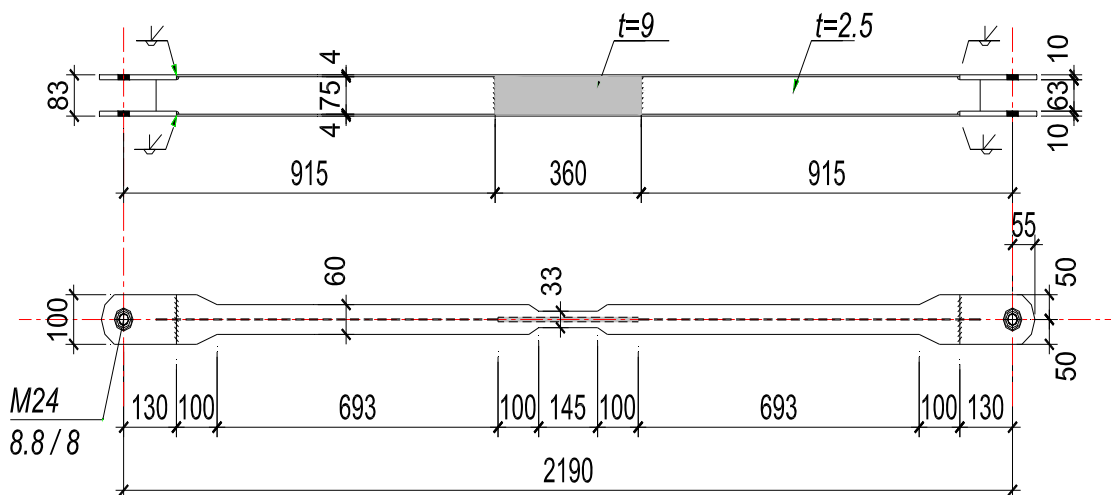


Figure 10.10: Overview of modified brace member F60.4W75.2,5-M145.33-T9 at the fourth storey

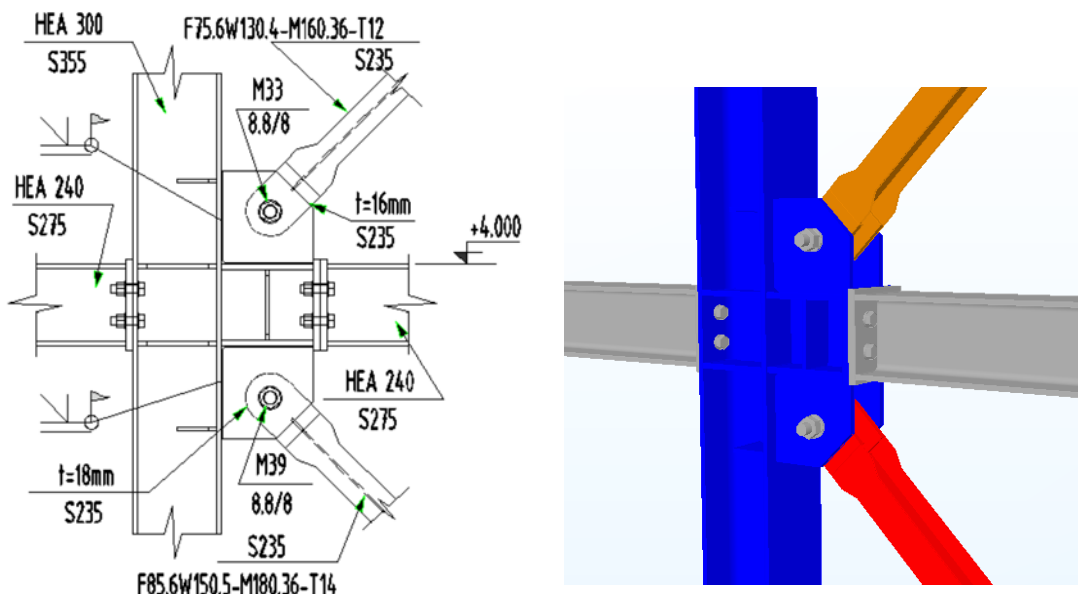
The connection between modified braces and the gusset plate should be designed by bolts. The tests carried out [9] have proven that bolted connections in shear and bearing (category A), realized by fit bolts, exhibit satisfactory fatigue behaviour and provide enough overstrength, therefore, in the context of §6.5.5 (6) of [1], are recommended to be used for CBF-MBs. Their dimensioning should fulfil §6.5.5 (3) and (5) of [1]. Table 10.18 summarizes the results from verification checks. It is worth noting that the design force for bolted connection should be obtained by Eq. (10.25). The factor p that accounts for the available overstrength of the system is not included since the mentioned overstrength is generated apart from the brace and it will not affect the connection.

Table 10.18: Bolted connection design

Storey	$N_{pl,Rd}$ (kN)	$N_{con,Ed}$ (kN)	Bolt diameter /grade	Plate thickness (mm) / steel grade	Bolt shear resistance (kN)	Plate bearing resistance (kN)	Utilizati on factor
1	396.1	545	M39 /8.8	18 / S235	917	607	0.898
2	317.8	437	M33 /8.8	16 / S235	657	456	0.958
3	228.3	314	M30 /8.8	14 / S235	543	363	0.865
4	149.4	206	M24 /8.8	10 / S235	347	207	0.994

$$N_{con,Ed} = 1.1\gamma_{OV} N_{pl,Rd} = 1.375N_{pl,Rd} \quad \text{Eq. (10.25)}$$

The braces are connected to the gusset plate by means of fit bolts. In order to provide some erection tolerances, the connection between the gusset plate and the column are designed by full penetration field welds. The final design of the joints between the braces and the floor beam and the braces and the splitting beam at the first storey are illustrated in Figure 10.11.



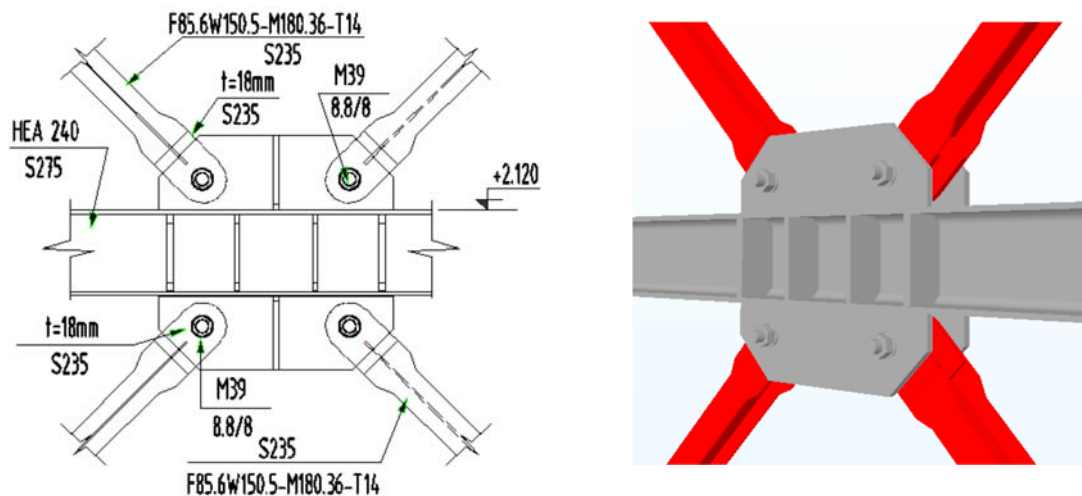


Figure 10.11: Overview of CBF-MB joints

10.6 References

1. Eurocode 8: Design of structures for earthquake resistance - Part 1: General rules, seismic actions and rules for buildings; EN 1998-1:2004.
2. Hot rolled products of structural steels – Part 2: Technical delivery conditions for non-alloy structural steels; EN 10025-2:2001.
3. EN1993-1-1, Eurocode 3: Design of steel structures - Part 1-1: General rules and rules for buildings. Brussels: Comitee Europeen de Normalisation (CEN); 2005.
4. EN1993-1-8, Eurocode 3: Design of steel structures - Part 1-8: Design of Joints. Brussels: Comitee Europeen de Normalisation (CEN); 2005.
5. Georgiev Tzv., Zhelev D., Raycheva L., Rangelov N., "INNOSEIS - Valorization of innovative anti-seismic devices", WORK PACKAGE 1 – DELIVERABLE 1.1, Volume with information brochures for 12 innovative devices in English, European Commission Research Programme of the Research Fund for Coal and Steel, (Article in Press).
6. Georgiev Tzv., Rangelov N., Raycheva L., Raykov St., INNOSEIS - Valorization of innovative anti-seismic devices", WORK PACKAGE 3 – DELIVERABLE 3.2, Volume with pre-normative design guidelines for innovative devices, European Commission Research Programme of the Research Fund for Coal and Steel, (Article in Press).
7. Fajfar P., Kreslin M., "Modelling and Analysis, Chapter 4 of EC8-1", EUROCODE 8 Background and Applications, Dissemination of information for training – Lisbon, 10-11 February 2011.
8. SAP2000, CSI, Computers and Structures Inc., www.csiberkeley.com.
9. Tzvetan Georgiev, „Improvement of X-CBF hysteresis behaviour by introduction of MCS”, 8th Hellenic National Conference on Steel Structures, Tripoli, Greece, 2-4 October 2014, page 75.

11 SSCD

11.1 General

11.1.1 Introduction

This case study refers to the seismic design of a new four-story steel structure with four reinforced concrete shear walls. The steel structure is made up of a pendular system (beams hinged to the column) so that it is supposed that it carries only the vertical loads. In order to limit the seismic shear transmitted to the reinforced concrete wall, they are connected to the steel structure through the Steel Self-Centering Devices (SSCDs). In this way also the structure is able to recenter after the seismic event. Given the strong nonlinear behavior of such system, nonlinear analyses are used to design them.

11.1.2 Description of the building

The commercial case study building is located in Mirandola (Emilia-Romagna, MO), city strongly affected by structural damages after the 2012 earthquake event. The building presents an hybrid structure, with the following main components (Figure 11.1):

- **r.c. shear walls** in correspondence of the four corner stair cases devoted to sustain horizontal seismic action;
- **internal steel pinned frames** used to sustain vertical loads;
- **SSCD hysteretic systems** for the (horizontal) connection between r.c. walls and steel frames, opportunely designed and sized to make the building able to force high-intensity seismic events.

The global dynamic behaviour of the building has been deeply analyzed through both linear and nonlinear analyses executed on a three dimensional model realized using SAP2000 software, allowing to better understand its effective structural response. The design procedure adopted for all the three main components of the building (i.e. r.c. shear walls, steel frame and SSCD) is *iterative*: the mechanical and geometrical properties of the different elements (mainly SSCD and shear walls) strongly influence the behaviour and the stiffness performance of the structure, this last moreover governing the dynamic performance of the building both in the linear and nonlinear fields. Preliminary *linear analyses* have been executed for the pre-sizing of the different components; the design – as well as the model - has been then refined through nonlinear analyses.

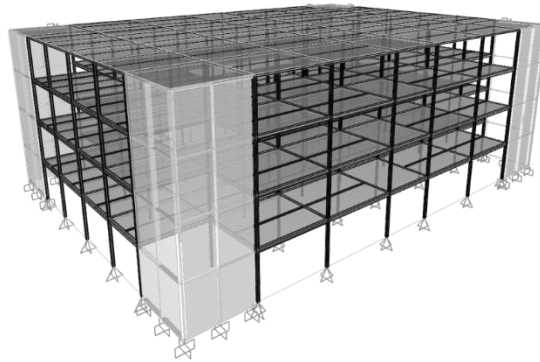


Figure 11.1: Three dimensional schematization of the case study building.

The overall plan dimensions of the building are equal to 50x36 m; the building presents 4 storey with interstorey height equal to 4.50 m. The ground, 1st and 2nd floors house commercial activities, while at the basement a car par is present. Four stair cases are located in correspondence of the four corners of the building. Due to the presence of internal ramps, some differences in the disposition of structural elements and storey slabs among basement (level P1) and the other floors (P2, P3 and P4), as simply schematized in Figure 11.2, are present, with resulting different mass distributions. The storey slabs are organized in the same way at different levels with maximum length equal to 6.0 m. Figure 11.3 shows the typical section of the building.

The pinned steel frame, used to only sustain static vertical loads of different storey, present columns located at distance between 6.0 and 8.0 m, with hinged connections to the foundation system; in correspondence of the r.c. walls, a “gap” of 10 cm has been introduced in order to practically separate the steel and the r.c. components of the building. Secondary beams have been also introduced to reduce the free length of horizontal storey, decreasing in such a way their deformability. For the frames, steel grade S275 was used.

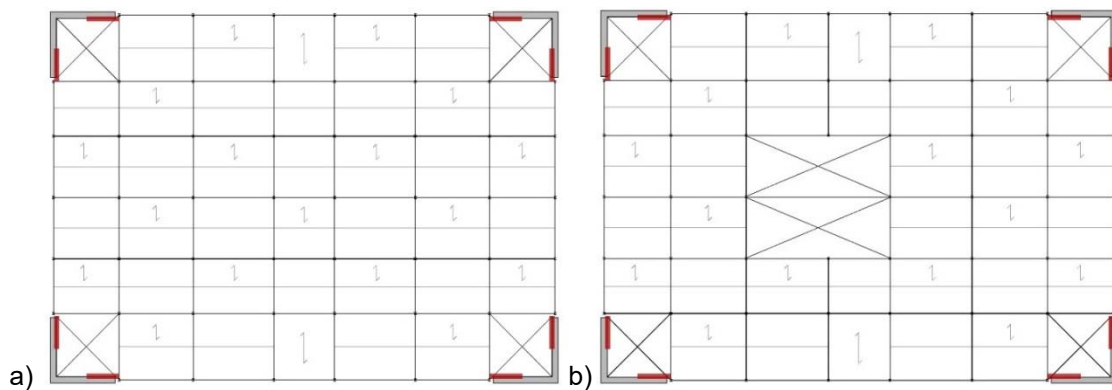


Figure 11.2: Typical plan dispositions: a) P1, b) P2 and P3.

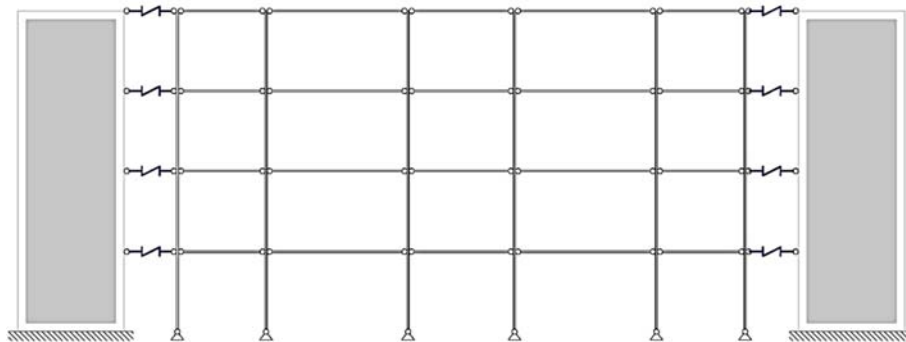


Figure 11.3: Typical section of the designed system.

The r.c. shear walls have been designed, according to EN1998-1:2005 [1], as *large lightly reinforced walls*, characterized by high transversal dimensions and limited inelastic behaviour under design seismic action. In the present case, the r.c. walls are designed to sustain the maximum reactions due to the connected SSCD. Concrete class C25/30 and steel reinforcing bars B450C have been adopted.

The SSCD systems have been introduced to adsorb and to dissipate the seismic energy, limiting the displacements and the deformation of the building. The design philosophy is based on the concentration of nonlinear deformations in correspondence of such dissipative systems under seismic action, with r.c. walls and steel frames that still remain in the elastic field.

The horizontal disposition of SSCD allows to strictly separate the steel frames from the r.c. walls: in this way, the displacement of the storeys during the seismic event is allowed avoiding the direct contact between the storeys and the walls. The presence of relative displacements without contact/friction between steel frame and r.c. walls guarantee the correct behaviour of the SSCD.

The initial length of the dissipative systems has been assumed equal to 3.5 m (corresponding to the one of the prototypes experimentally tested and presented in Braconi et al. [9]); steel grade S355JR was used for all the components of the SSCD except for the dissipative elements, characterized by low yielding strength.

11.2 Preliminary design

11.2.1 Determination of actions

Static and seismic loads were determined in relation to the actual Italian Standard for Constructions prescriptions (D.M.14/01/2008 [2]). Figure 11.4 shows the response spectra adopted for linear analyses.

- $G_1 = 1,90 \text{ kN/m}^2$ *Permanent load of the interstorey floor slab (dead)*
- $G_2 = 2,45 \text{ kN/m}^2$ *Permanent load of the interstorey floor slab*
- $G_1 = 0.15 \text{ kN/m}^2$ *Permanent load of the roof floor slab (dead)*

- $G_2 = 0.20 \text{ kN/m}^2$ *Permanent load of the roof floor slab*
- $Q_k = 5.00 \text{ kN/m}^2$ *Live load for commercial activities (interstorey)*
- $Q_k = 1.20 \text{ kN/m}^2$ *Snow load (roof)*
- $V_N = 50 \text{ years}$ *Nominal life of the building*
- $C_U = 1.5$ *Use coefficient*
- $V_R = V_N C_U = 75$ *Reference life for seismic action*

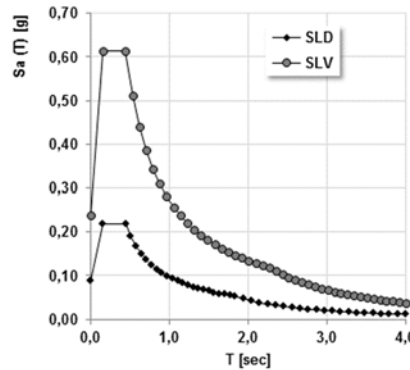


Figure 11.4: Response spectra according to D.M.14/01/2008 for SLV and SLD.

11.2.2 Pre-sizing of structural elements – Pinned steel frames

The steel frames are designed to sustain only vertical load. The profiles have been consequently selected only considering vertical acting loads, for both beams (under flexure) and columns (under axial force). The design of beam sections has been executed adopting the following maximum bending action:

$$M_{ed} = \frac{q l^2}{8} \quad \text{Eq. (11.1)}$$

Adopting, for the evaluation of q , the following combination (SLU):

$$q = \gamma_{G1} G_1 + \gamma_{G2} G_2 + \gamma_{Q1} Q_{k1} + \gamma_{Q2} \psi_{02} Q_{k2} \quad \text{Eq. (11.2)}$$

As a consequence, following the prescriptions of D.M.14/01/2008 [2] the equations below can be used to evaluate the minimum section to adopt:

$$M_{b,Rd} = \frac{W_{el} f_{yk}}{\gamma_{M0}} \quad \text{Eq. (11.3)}$$

$$W_{el,min} = \frac{M_{ed} \gamma_{M0}}{f_{yk}} \quad \text{Eq. (11.4)}$$

For what concerns columns, the minimum section is provided by the following equation, considering for the determination of N_{ed} the loads acting on a surface of dimensions equal to 6x8 m:

$$A_{min} = \frac{N_{ed} \gamma_{M0}}{f_{yk}} \quad \text{Eq. (11.5)}$$

Table 11.1 summarizes the profiles adopted for the elements of the steel frames.

Table 11.1: Elements profiles in relation to design.

Element	L [m]	q [kN/m]	Profile
Interstorey beam	6.0	40.94	HEB220
Interstorey beam	8.0	40.94	HEB280
Roof beam	6.0	6.9	HEB160
Roof beam	8.0	6.9	HEB160
Columns			HEB220

11.2.3 Pre-sizing of structural elements – SSCD

An initial length equal to 3.50 m has been adopted, based on the results of experimental investigations. The transversal sections of the carter, piston, sliding frame and pre-tensioned elements were then evaluated, contributing to the multilinear elastic behaviour of the SSCD system and allowing to determine the slope of the bilinear force/displacement curve. The parameters influencing the dissipative behaviour (i.e. the ones related dissipative elements) were initially neglected, introducing them only when the structure shifts in the nonlinear field. In the first step, all the SSCD at different levels were assumed to be equal. The data used for the determination of the force/displacement bilinear elastic curve (Figure 11.5) are summarized in Table 11.2.

To introduce the dissipative systems in the SAP2000 model of the building, a *multilinear* elastic schematization can be then adopted.

Bilinear Elastic F/d curve		
k_{el}	144,658	kN/mm
k_{pe}	28,886	kN/mm
F_y	634,822	kN
d_y	4,388	mm
F_u	938,765	kN
d_u	14,911	mm

Table 11.2: Initial parameters of the F/d curve of the SSCD systems.

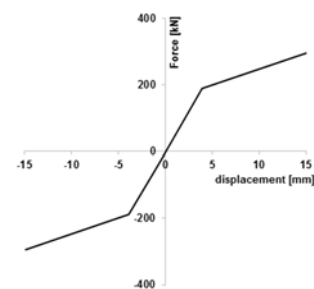


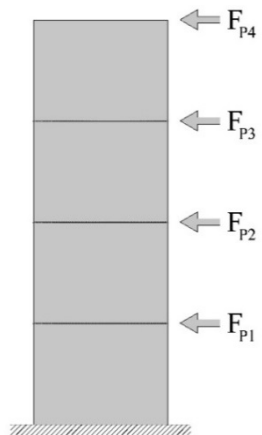
Figure 11.5: bilinear elastic curve of the SSCD

11.2.4 Pre-sizing of structural elements – r.c. shear walls

The length of r.c. shear wall was assumed equal to 6.0 m, according to the architectural design; the thickness can be determined to provide the r.c. walls with an elastic behaviour during the seismic event. A preliminary sizing of r.c. walls has been then executed considering the elastic seismic action (unitary behaviour factor for SLV): this means that the SSCD behave as “rigid components” that do not dissipate the seismic action, transferring it as a whole directly to the walls.

A static equivalent analysis has been executed, considering the r.c. wall as a cantilever beam with concentrated loads, with maximum stresses in correspondence of the base of the element (shear and bending actions). The design force and resulting shear and bending actions are summarized in Table 11.3. The design of the r.c. wall has been executed in order to avoid the development of plastic hinge in correspondence of base section. According to EN1998-1:2005 [1] and D.M.14/01/2008 [2] the following prescriptions shall be moreover respected.

Table 11.3: Static forces for $q=1$, resulting design actions and schematization adopted for the r.c. walls.

	F_h [kN]	Storey	z_i [m]	Design actions	
	23838,1	P1	4,5	V_{ed}	4935 kN
		P2	9	M_{ed}	30964
		P3	13,5		
		P4	18		
	W_i [kN]	F_i [kN]			
	15449,74	F_{P1}	969,63		
	13590,34	F_{P2}	1705,86		
	14214,94	F_{P3}	2676,38		
	2420,58	F_{P4}	607,66		

The thickness of the section b_w shall be higher than the maximum between 150 mm and $h_s/20$, being h_s the free height of the interstorey, shifting in the present case into:

$$b_w \geq 225 \text{ mm} \quad \text{Eq. (11.6)}$$

Longitudinal reinforcements, positioned in correspondence of all the sides of the wall with spacing lower than 300 mm shall be opportunely connected; the diameter of longitudinal reinforcements shall satisfy the following relationship:

$$\phi_1 \leq \frac{b_w}{10} \quad \text{Eq. (11.7)}$$

The two extreme confined portions of the section shall have length l_c equal to:

$$l_c = 0,20 l_w \geq 1,5 b_w = 1,20 m \quad \text{Eq. (11.8)}$$

The vertical reinforcements in correspondence of confined zones shall satisfy the following equation:

$$1\% \leq \rho \leq 4\% \quad \text{Eq. (11.9)}$$

Considering all the prescriptions above listed, a thickness equal to 600 mm, reinforcement of diameter 24 mm with spacing equal to 100 mm in confined portions and 250 mm in the other parts were used.

11.2.5 Modelling and structural analysis of the case study

11.2.5.1 Linear model and analysis

The response spectra used for the dynamic modal analyses of the building, determined in relation to the location and considering soil of category “C”, are presented in Figure 11.4. The study of the results of linear dynamic analysis allows to better characterize the structural behaviour of the building, that is similar in the two main directions X and Y (i.e. similar vibration periods, modal shapes), exhibiting a flexural behaviour and high participating mass (Figure 11.6).

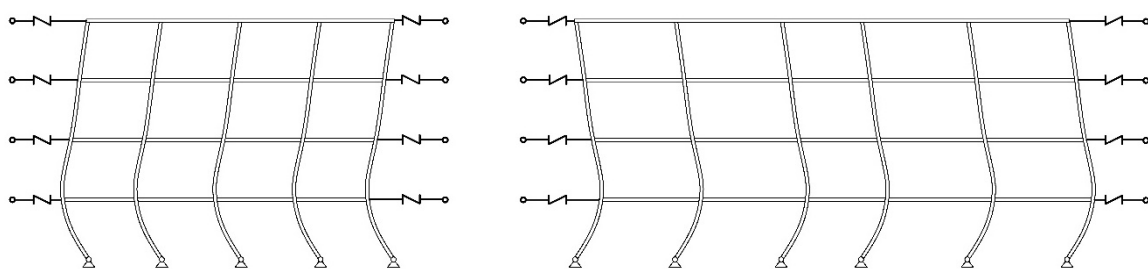


Figure 11.6: First modal shape associated to Y and X directions.

The horizontal displacement of the building is directly related to the activation of the SSCD in the considered direction, with elastic forces proportional to the displacement of the different storey.

In order to optimize the structural behaviour of the system, a modal deformed shape as much as possible *uniform*, aiming to remain more or less “vertical” above the first floor, has been pursued: in this way, all the SSCD system shall behave

with the same level of forces and deformations, with related displacements near to zero for all the storey above the first one (Figure 11.7).

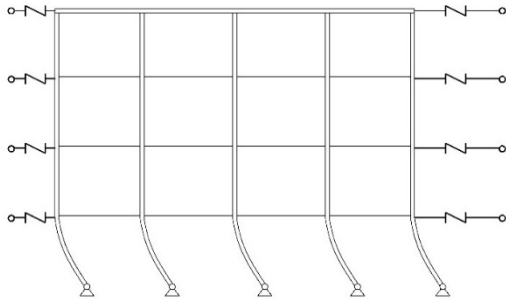


Figure 11.7: Desired modal deformation.



Figure 11.8: Independent mass corresponding to the different floors: scheme adopted.

The desired deformation can be obtained acting on the elastic stiffness of the SSCD devices (k_{el}): the variation of such parameter for the dissipative devices of the different floors allows to modify the global behaviour of the building. The “control parameters” assumed are the displacements x_i of the building in correspondence of SSCD of different levels (x_1, x_2, x_3, x_4): varying the ratios between displacements, the relative k_{el} can be modified to achieve the desired modal shape deformation.

In the first design phase, the stiffness k_{el} has been modified directly acting on the length of the piston L_P , keeping unchanged the other characteristics. The modification of the elastic parameters of the dissipative devices has been followed by linear modal analyses with iterative procedure until the desired configuration is obtained. It's necessary to evidence that, in the particular considered case study, due to the reduced stiffness of the columns - not able to realize a strong connection between different storey - each floor behaves as “independent” floor (i.e. masses with independent behaviour, Figure 11.8). If each storey is independent from one another, its own motion is directly governed by simple relationship; the vibration period of the single mass of the generic i -th floor is provided by:

$$T_i = 2\pi \sqrt{\frac{m_i}{k_i}} \quad \text{Eq. (11.10)}$$

If all the storeys shall behave in a similar way (i.e. with the same displacement), it's necessary to impose them to have the same vibration period. Since the seismic mass of each floor is given, the relative ratio among the different stiffness of the SSCD shall be evaluated (Table 11.4). In the present case, considering that the seismic masses of the first three levels are about the same, adopted SSCD are the same for levels P1, P2 and P3; different systems are used for P4. With the values

of stiffness presented in Table 11.4 the modal deformed shape presented in Figure 11.9 have been obtained, very close to the desired “vertical configuration”. Table 11.5 shows the results of linear modal analysis in the final selected configuration.

Table 11.4: Stiffness of the different SSCD in relation to the results of linear dynamic analysis.

Storey	z_i [m]	m_i [kN]	k_{el} SSCD [kN/mm]
P1	4,50	15449,74	144,66
P2	9,00	13590,34	144,66
P3	13,50	14214,94	144,66
P4	18,00	2420,58	48,02

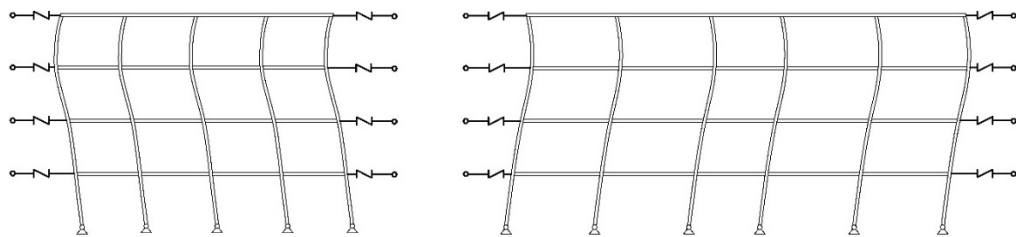


Figure 11.9: Modal deformed shape corresponding to first modes in Y and X directions.

Table 11.5: Modal analysis results.

Mode	Period [s]	% Mass X	% Mass Y	% Mass Z	% Resulting Mx	% Resulting My
1	0,315126	0,00	81,36	0,00	0,00	81,36
2	0,313854	84,10	0,00	0,00	84,10	81,36
3	0,284094	0,00	17,47	0,00	84,10	98,82
4	0,276967	15,59	0,00	0,00	99,69	98,82

The actions on the SSCD during the elastic phase can be estimated considering seismic action for Damage Limitation limit state (SLD), allowing to evaluate the maximum expected displacement for each one of the SSCD; base actions in correspondence of r.c. shear walls can be determined and compared to the ones initially considered, with the eventual optimization of the element’s thickness. The final design of SSCD can be then executed determining the transversal area of dissipative elements, before neglected, directly influencing β parameter, the global dissipated energy and the shape of the F/d curve. The main characteristics of the designed SSCD applied to different levels are summarized in Table 11.6, Table 11.7 and Table 11.8; Figure 11.10 shows the corresponding flag-shaped curves.

Table 11.6: Geometrical and mechanical properties of pre-tensioned cables.

Pre-tensioned cables					
		P1, P2, P3		P4	
Number of elements	n	2		2	
Diameter	ϕ	22	mm	12	mm
Transversal area	A_{PTE}	380,13	mm ²	113,10	mm ²
Global transversal area	$A_{PTE,tot}$	760,27	mm ²	226,19	mm ²
Yielding strength	$f_{y,PTE}$	1670,00	N/mm ²	1670,00	N/mm ²
Pre-tension percentage	$\rho_{PTE}=f_{PTE}/f_{y,PTE}$	0,50		0,50	
Pre-tension strength	f_{PTE}	835,00	N/mm ²	835,00	N/mm ²
Pre-tension force	F_{PTE}	634,82	kN	188,87	kN
Length	L_{PTE}	3500	mm	3500	mm
Elastic modulus	E_{PTE}	196000	N/mm ²	196000	N/mm ²
Maximum elongation	d_{PTE}	14,91	mm	14,91	mm

Table 11.7: Geometrical and mechanical properties of dissipative elements.

Dissipative Elements (Steel Grade BO40)					
		P1, P2, P3		P4	
Number of elements	n	4		4	
Transversal area	A_{ED}	120	mm ²	80	mm ²
Global transversal area	$A_{ED,tot}$	480	mm ²	320	mm ²
Yielding strength	$f_{y,ED}$	240	N/mm ²	240	N/mm ²
Yielding force	$F_{y,ED}$	115,2	kN	76,8	kN
Ultimate elongation	$A_{gt,ED}$	24,67	%	24,67	%
Length of reduce transversal area	L_{ED}	170	mm	170	mm

Table 11.8: Parameters of SSCD for levels P1, P2 and P3.

Flag Shaped F/d curve		
	P1, P2, P3	P4
k_{el}	144,658 kN/mm	48,237 kN/mm
k_{pe}	28,886 kN/mm	9,588 kN/mm
F_y	634,822 kN	188,873 kN
d_y	4,388 mm	3,9155 mm
F_u	938,765 kN	294,295 kN
d_u	14,911 mm	14,911 mm
$\alpha = k_{pe}/k_{el} =$	0,200	0,199
$\beta = F_{y,ED}/F_{PTE} =$	0,181	0,407

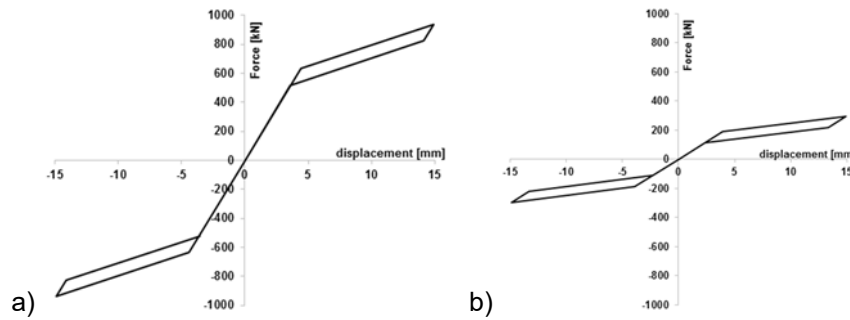


Figure 11.10: Flag-shaped curves for SSCD of levels: a) P1, P2 and P3; b) P4.

In order to introduce the SSCD in the numerical model of the building, link elements with a specific flag-shaped constitutive relationship have been used. The SSCD model is made up of two different elements working in parallel (Figure 11.11): the first one characterized by a “*multilinear elastic*” relationship defining the first two branches of the curve with stiffness equal to k_{el} and k_{pe} , yielding force F_y and maximum displacement d_u (Figure 11.12a), the second one defined as “*plastic*” characterizes the hysteretic cycles of dissipative elements through the parameter k_{DE} and the corresponding F_{yDE} (Figure 11.12b).

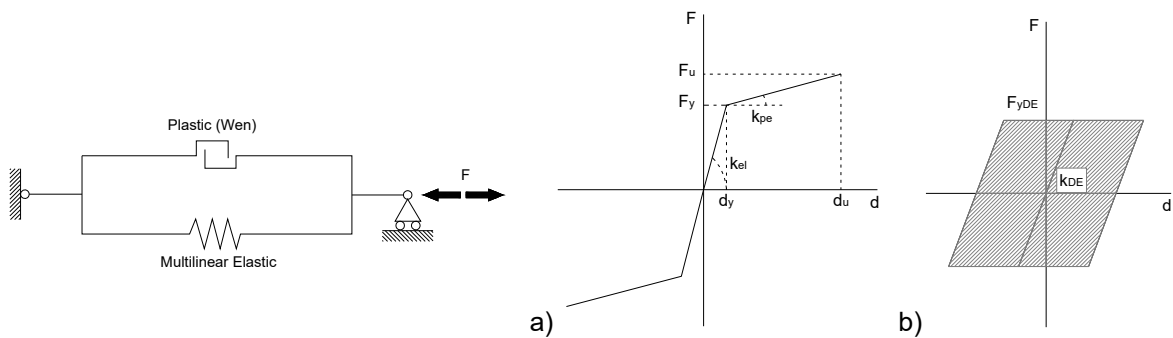


Figure 11.11: Simplified model of the SSCD with two NL Link element in parallel.

Figure 11.12: a) Multilinear Elastic and b) plastic constitutive laws.

11.2.5.2 Nonlinear modelling and nonlinear dynamic analyses

Nonlinear dynamic analyses have been further executed to deeply investigate the structural behaviour of the building in the post-elastic phase. According to the design approach used for the considered building, all the “non-dissipative” elements (i.e. pinned steel frame and r.c. shear walls) remain in the elastic field, while all the plastic behaviour is concentrated in the SSCD. Incremental dynamic analyses (IDA) have been executed according to the procedure proposed by Vamvatsikos and Cornell [12], foreseeing the steps listed below:

1. Determination of the unscaled accelerograms to be used: $a_1(t_i)$;
2. Determination of the Scale Factor (SF) to be applied to the unscaled accelerogram: $a_\lambda = \lambda a_1$.
3. Determination of the Intensity Measure (IM), function of the unscaled accelerogram that monotonically increases with the scale factor λ (i.e. the PGA – peak ground acceleration, the Spectral Acceleration corresponding to the first period and so on).
4. Determination of the Damage Measure (DM), parameter characterizing the structural response of the building during seismic events (for example the maximum base shear V_b , the maximum interstorey drift, and so on).
5. Determination of the IDA Curve, that is a graphical representation of the DM towards the parameter IM considered for the selected accelerogram.

In the present case, the PGA is selected as IM parameter.

Two DM are adopted: the maximum interstorey drift d_{rmax} and the maximum displacement of the SSCD systems d_{dmax} . The reaching of the Damage Limitation limit state (SLD) is associated to the achievement of the maximum interstorey drift according to D.M. 14/01/2008 [2] to guarantee the effective use of the building:

$$d_r \leq 0,01 h \quad \text{Eq. (11.11)}$$

Being h the interstorey heights. In this case, the relationship shifts into:

$$d_r \leq 45 \text{ mm} \quad \text{Eq. (11.12)}$$

The Life Safety limit state (SLV) is associated to axial deformation of the SSCD systems higher than the maximum allowed elongation, corresponding to the yielding condition of pre-tensioned cables and the loss of re-centering capability. This limit can be imposed equal to:

$$d_{SSCD} \leq 14,91 \text{ mm} \quad \text{Eq. (11.13)}$$

It's necessary to highlight that such limitation does not perfectly correspond to the reaching of an "ultimate" collapse limit state, since, from a static point of view, the SSCDs are still able to provide to the structure with sufficient residual strength towards collapse. The problem mainly consists in the loss of the re-centering capability, that otherwise still maintains reduced dissipative capacity. Probably, the SLV condition is not contemporarily reached by all the SSCD systems, with the following loss of efficacy of only some of them. Seven accelerograms have been

used for the execution of IDA. The considered IM has been scaled considering different SF for the different accelerograms up to 0.40g (Table 11.9).

Table 11.9: Scale factors adopted for the different accelerograms.

Seismic event	PGA _{max}	0,05 g	0,10 g	0,15 g	0,20 g	0,25 g	0,30 g	0,35 g	0,40 g
0520ME	0,2591	0,193	0,386	0,579	0,772	0,965	1,158	1,351	1,544
0529ME	0,2672	0,187	0,374	0,561	0,749	0,936	1,123	1,310	1,497
SPC1	0,3127	0,160	0,320	0,480	0,640	0,799	0,959	1,119	1,279
SPC2	0,2508	0,199	0,399	0,598	0,797	0,997	1,196	1,396	1,595
SPC3	0,2855	0,175	0,350	0,525	0,701	0,876	1,051	1,226	1,401
SPC4	0,3374	0,148	0,296	0,445	0,593	0,741	0,889	1,037	1,186
SPC5	0,2507	0,199	0,399	0,598	0,798	0,997	1,197	1,396	1,596

Figure 11.13 and Figure 11.14 represent the summary of the results of IDA executed adopting the 7 different accelerograms. Analysing the results coming from the IDAs, it is evident that the maximum elongation of dissipative devices (d_{dmax}) is strongly influenced by the considered accelerograms: up to IM equal to 0.15g a similar behaviour is visible, while increasing levels of IM correspond to increasing difference in the obtained results. Similar considerations can be executed also for the maximum interstorey drift (d_{rmax}), related to SLD. This fact is mainly due to the different frequency content of different seismic input; to partially reduce this effect, the average results of the seven accelerograms, according to what foreseen by D.M.14/01/2008 have been considered. Average values of DM evidence the ability of the designed structure to highly satisfy the requirement imposed for SLD for PGA up to 0.30g, while in the case of SLV the maximum PGA is within the range 0.25g (satisfaction) and 0.30g (overcoming of SLV limitation). Residual displacements have been also evaluated to test the efficacy of the model (Table 11.10): residual displacements are lower than the 2% of the maximum exhibited interstorey displacements, value that can be considered allowable to guarantee the re-centering capability of the system.

As visible from Figure 11.14, P1, P2 and P4 levels presented similar behaviour for increasing levels of PGA while P3 is characterized by higher displacement. The yielding limit of the four curves is, more or less, the same and within the range [0.10g; 0.15g], defining a quite regular behaviour of the building.

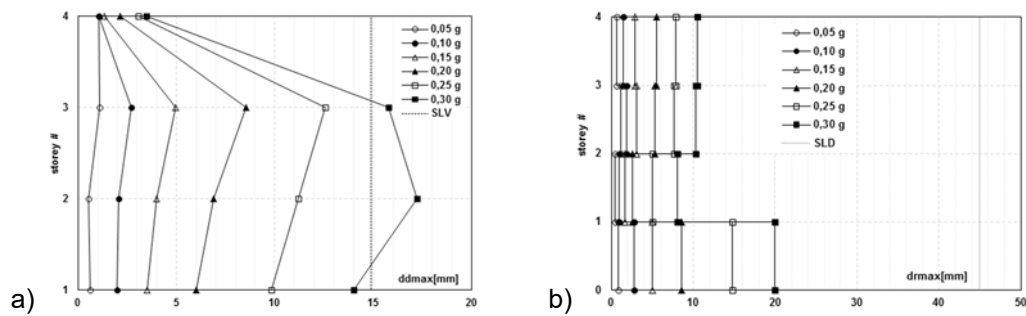


Figure 11.13: Average results of 7 inputs: a) max displacement of SSCD (SLV) and b) max interstorey displacement (SLD).

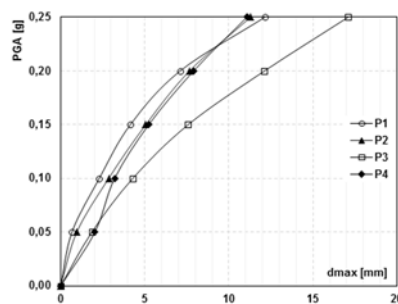


Figure 11.14: Result of IDA in terms of displacement of different storeys towards PGA (average of 7 accelerograms).

Table 11.10: Residual average displacements for the building (PGA equal to 0.25g).

storey #	d_r [mm]	d_{rmax} [mm]	d_r [%]
P1	0,08	14,79	0,55
P2	0,09	5,03	1,89
P3	0,08	7,65	1,02
P4	0,16	7,90	2,07

The execution of safety checks in correspondence of all the structural elements constituting the building, according to what foreseen by actual standard and in correspondence of PGA respectively equal to 0.25g for SLV, led to several modifications in the profiles of elements, according to what briefly summarized in Table 11.11 for steel sections. No changes were otherwise required for the dimensions and reinforcement of r.c. walls.

Table 11.11: New element profiles after the execution of safety checks

Element	Preliminary profile	Modification	Reason
Interstorey steel beams	HEB280	HEA340	Flexural behaviour
Roof steel beams	HEB160	HEB180	Flexural behaviour
Column	HEB220	HEB240	Buckling

11.2.6 Optimization of proposed solution

Results of nonlinear analyses globally evidenced that the structural behaviour of the system is mainly influenced by the maximum elongation of SSCD, directly characterizing the achievement of SLV, while interstorey displacement, related to the satisfaction of SLD condition, are usually strongly below the imposed limitation and don't represent a limit for the determination of the effective capacity of the system.

The modification of SSCD can be then executed in order to increase the structural capacity of the building for the satisfaction of SLV limitation for IM higher than 0.25g, directly acting on different parameters. The following possibilities have been then taken into consideration.

11.2.6.1 Case 1 – Increase of SSCD length

Since the parameter that strongly influences the displacement of the SSCD system is the length of the dissipative devices, several modifications have been introduced and tested, adopting the maximum external length of the device equal to 5.30 m and the length of the pre-tensioned cables equal to 5.10 m, respect to the initial one equal to 3.50 m (from experimental tests on the SSCD prototype). Several modifications have been introduced in the design of SSCD, keeping constant the characteristics of dissipative elements and the ratios between SSCD at different levels only acting on the piston length (Figure 11.15). Considering the results as presented in Figure 11.16, the increase of the SSCD length don't significantly affect the behaviour of the structure, since the maximum allowable PGA remains equal to 0.25g. This is mainly due to the fact that the increase of the length is related to the decrease of the linear stiffness (Figure 11.15). As a consequence, additional parameters shall be modified to increase the capacity of the whole structure.

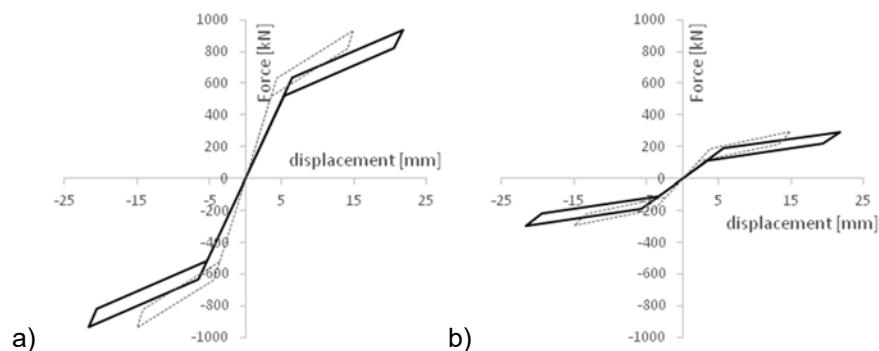


Figure 11.15: First modification (SSCD length): modified flag-shaped curves for a) levels P1, P2 and P3, b) P4.

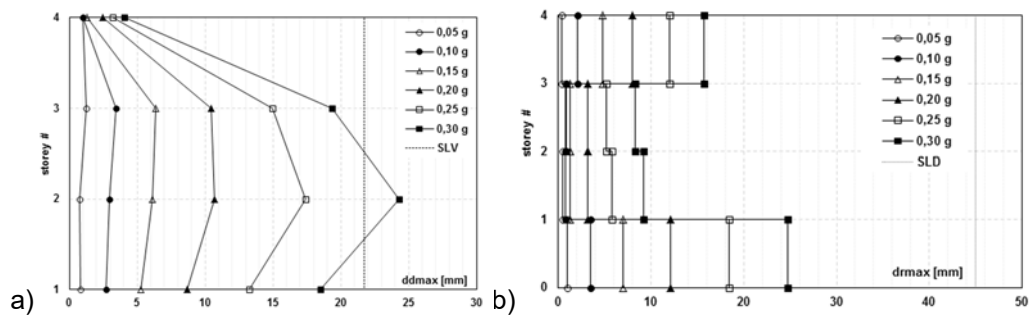


Figure 11.16: Average IDA for a) maximum displacement of SSCD (SLV) and b) interstorey displacement (SLD) – case 1.

11.2.6.2 Case 2 – Increase of pre-tensioned cables diameter

The second possibility consists in the modification of pre-tensioned cables' diameter increasing them by 4.0 mm; the global length of the SSCD is, also in this case, increased respect to the initial one up to 5.30 m. The target SLV displacement, since the diameter does not affect this parameter, remains equal to 21.93 mm. The modification of the cables' diameter directly influences the yielding and ultimate forces, as well as the stiffness of both the elastic and post-elastic branches of the flag-shaped curve (Figure 11.17).

As visible, the coupling of the modifications of SSCD length and cables' diameter is able to increase the effective structural capacity of the system, with maximum allowable PGA equal to 0.30 g without the overcoming of SLV. No modifications at SLD can be observed.

The comparison between the 1st and the 2nd cases do not evidence significant differences for IM lower or equal to 0.15g: this means that below 0.15g the influence of pre-tensioned cable is not relevant and that they still remain in the elastic field, with F_Y of SSCD between [0.15g; 0.20g]. increasing the PGA the influence of cables becomes higher, influencing the post-elastic behaviour of SSCDs.

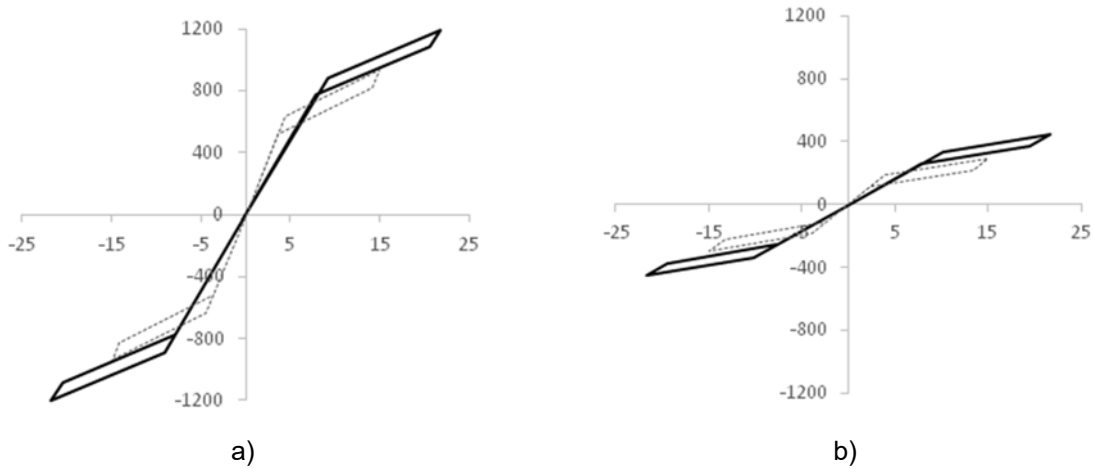


Figure 11.17: modification (SSCD length and cables' diameter): flag-shaped curves for a) levels P1, P2 and P3, b) P4.

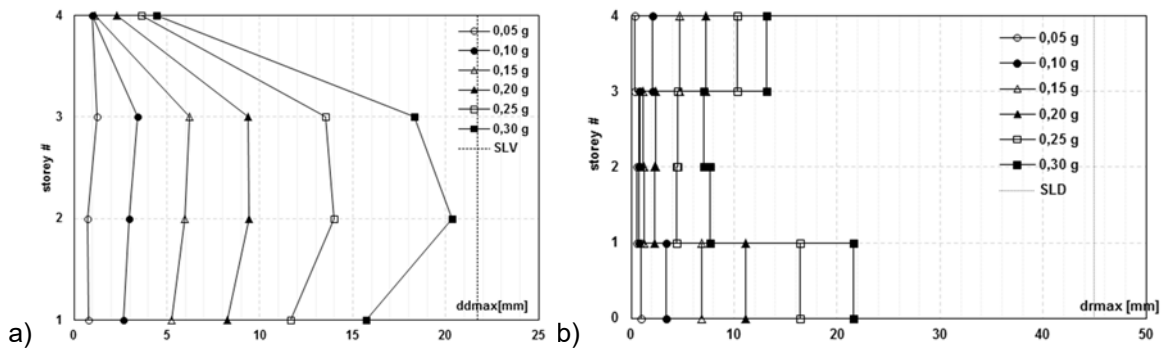


Figure 11.18: Average IDA for a) maximum displacement of SSCD (SLV) and b) interstorey displacement (SLD) – case 2.

11.2.6.3 Case 3 – Increase of dissipative elements – $\beta=0,50$

The flag-shaped curves of considered SSCD systems are related to β coefficients, respectively equal to 0.18 for P1, P2 and P3 and to 0.40 for P4. Increasing the dissipative capacity of the building, the global capacity of the structure can be also increased.

In this third case, to evaluate the efficacy of such parameter, the initial length of the SSCD (3.50 m) is adopted, increasing the dimension of dissipative elements up to achieve $\beta=0.50$, without the alteration of other characteristics (Figure 11.19).

As evidenced by Figure 11.20 this solution has relevant efficacy, with maximum allowed PGA at SLV equal to 0.35g, with reduced maximum interstorey displacements (about half of initial ones). Since the stiffness of the SSCD is not modified, interstorey displacements are reduced, moreover the lower size of the device allows lower costs and more easiness in the assembly.

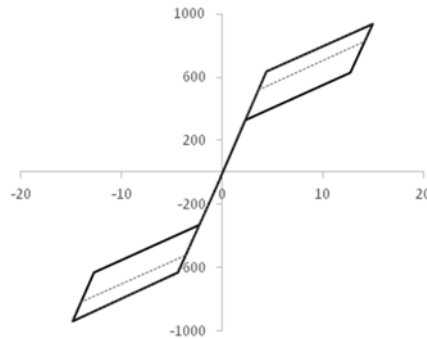


Figure 11.19: 3rd modification (β coefficient 0.50): flag-shaped curves for levels P1, P2 and P3.

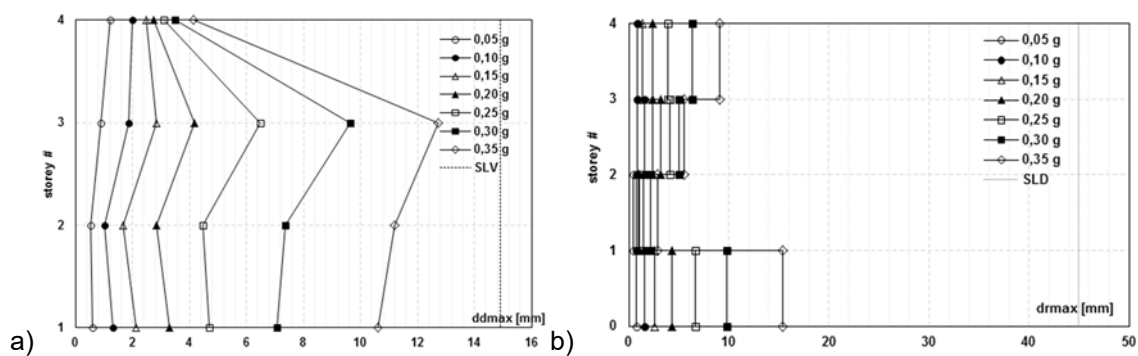


Figure 11.20: Average IDA for a) maximum displacement of SSCD (SLV) and b) interstorey displacement (SLD) – case 3.

11.2.6.4 Case 4 – Increase of dissipative elements – $\beta=0,75$

Considering the positive effects of case 3, β coefficient has been then increased up to 0.75 in the case of P1, P2 and P3 (Figure 11.21) keeping unaltered 0.40 for the case of P4. According to Braconi et al. [9] in order to save the re-centering capability of the system, β shall be maintained lower than 0.90: case 4) represents consequently the upper condition for the system.

An additional increase of the structural capacity can be observed, up to maximum PGA equal to 0.40g (Figure 11.22) and lower interstorey displacements.

A significant variation of the structural behaviour respect to case 3) can be also observed, with significant contribution of SSCD of levels P3 and P1 (and not P2 like in the previous case); the contribution of SSCD at level P4 is higher respect to previous cases considered, with increase of the global dissipated energy.

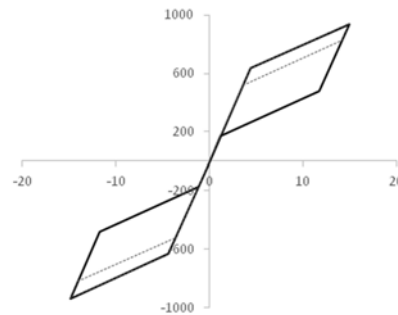


Figure 11.21: 4th modification (β coefficient 0.75): flag-shaped curves for levels P1, P2 and P3.

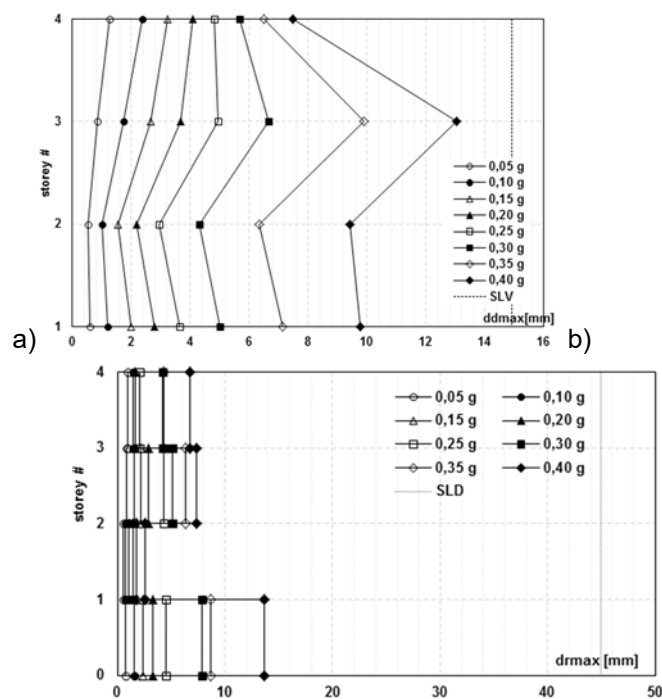


Figure 11.22: Average IDA for a) maximum displacement of SSCD (SLV) and b) interstorey displacement (SLD) – case 4.

11.2.6.5 Case 5 – Increase of dissipative elements – $\beta=1.25$

The increase of β coefficient over 0.90 leads, according to experimental tests' results, to the loss of the typical flag-shaped behaviour of dissipative elements: as visible from Figure 11.23, residual displacement in this case are relevant. The most evident result of IDA is that the increase of the dissipative elements' section reduces the global capacity of the building, with maximum allowable PGA equal to 0.30g (Figure 11.24): this means that, over a certain limit, the increase of the size of dissipative elements is not useful to increase the structural performance of the building. SLD condition is highly assessed.

The higher elongations are achieved in correspondence of the SSCD of P4 (roof level), that, in all the other considered cases, are the loss conditioned: this is

responsible for the decrease of the global capacity for SLV. This aspect is also evidenced by the capacity curve of the different levels (Figure 11.25): despite the curve relative of P4 shows yielding in correspondence of PGA equal to 0.10g, the curves of the other three level exhibit a more or less linear behaviour: this means that the building reaches its maximum limit at level P4 with the other SSCD in the elastic field.

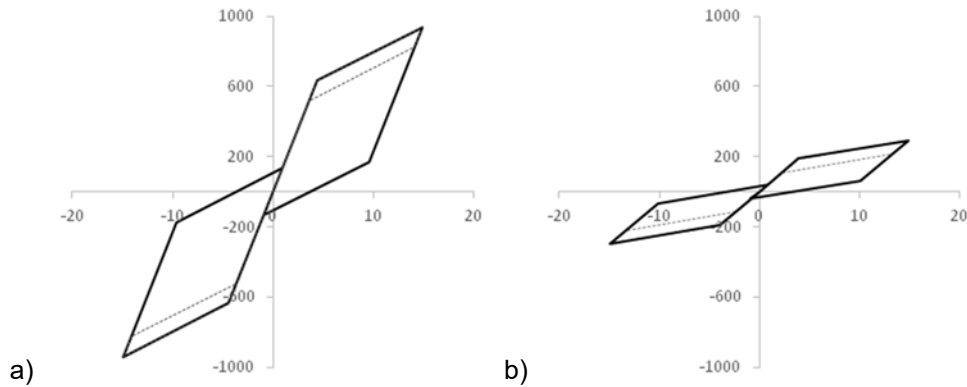


Figure 11.23: 5th modification (β coefficient 1.25): flag-shaped curves for levels a) P1, P2 and P3, b) P4.

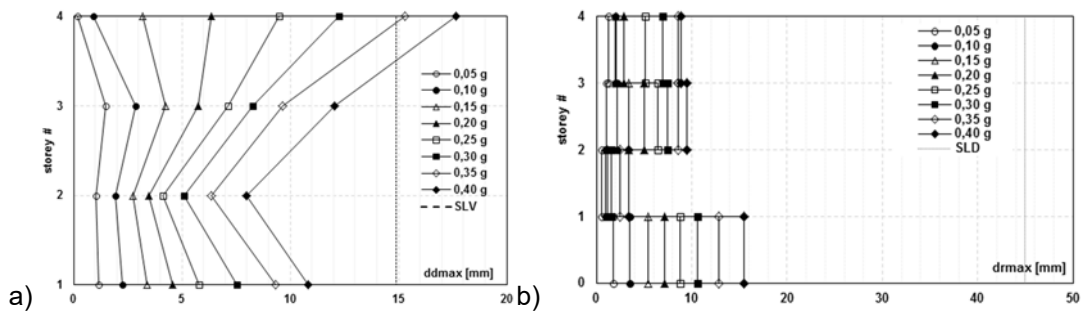


Figure 11.24: Average IDA for a) maximum displacement of SSCD (SLV) and b) interstorey displacement (SLD) – case 5.

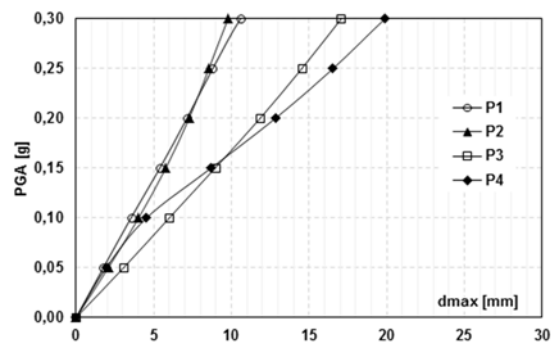


Figure 11.25: Capacity curves for the different storeys – case 5.

Residual displacements have been finally evaluated: for β values higher than 1.0, the SSCD loss the re-centering capacity, leaving the building exposed to residual displacements, whose average values for PGA equal to 0.30g is summarized in Table 11.12. As visible, the re-centering capability of the structure is not provided (residual displacements up to 25%).

Table 11.12: Average residual values of the steel structure for PGA=0.30g.

storey #	$\beta=1.25$			$\beta=2.00$		
	d_r [mm]	d_{rmax} [mm]	d_r [%]	d_r [mm]	d_{rmax} [mm]	d_r [%]
P1	0,54	10,56	5,08	0,64	11,75	5,48
P2	0,40	1,54	25,85	0,76	1,61	47,26
P3	0,59	7,45	7,98	0,75	8,06	9,36
P4	0,24	6,93	3,41	0,37	9,53	3,87

Similar considerations can be also made in the case of β coefficient equal to 2.0, once again with the increase of the size of dissipative elements and the loss of flag-shaped behaviour (Figure 11.26).

In this case, the structural capacity of the system (Figure 11.27) is higher than adopting $\beta=1.25$, with maximum allowable PGA equal to 0.40g, but with high residual displacements (Table 11.12).

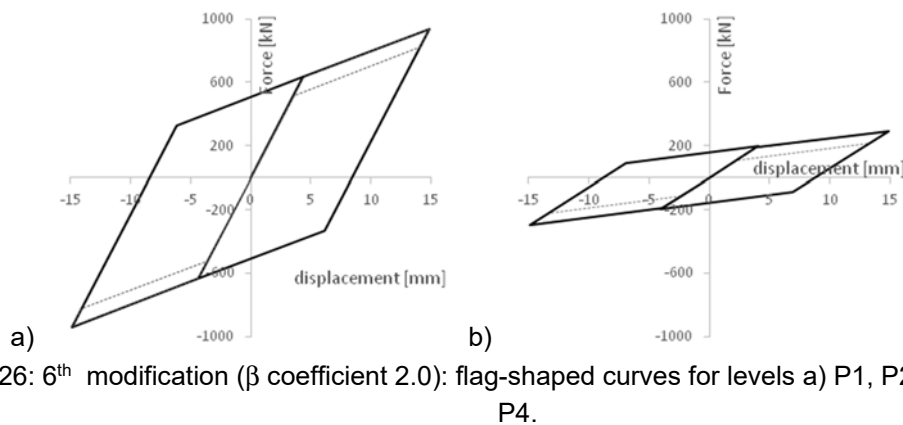


Figure 11.26: 6th modification (β coefficient 2.0): flag-shaped curves for levels a) P1, P2 and P3, b) P4.

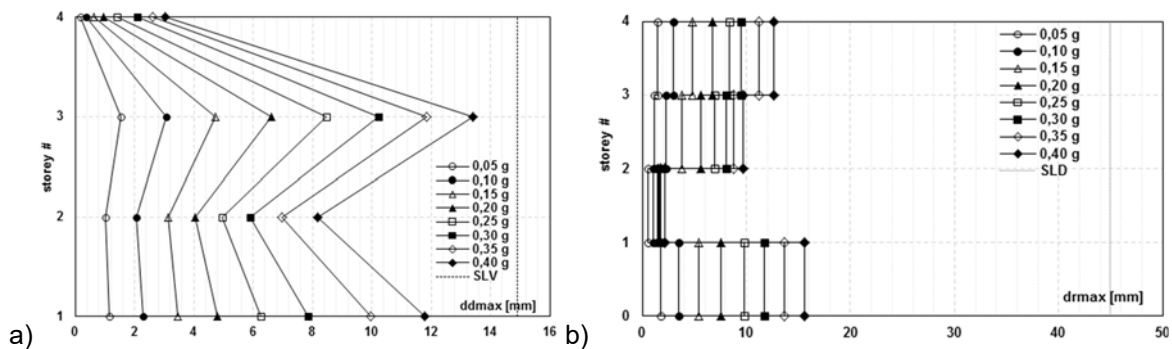


Figure 11.27: Average IDA for a) maximum displacement of SSCD (SLV) and b) interstorey displacement (SLD) – $\beta=2.0$.

11.3 Conclusions

The proposed SSCD system, designed inside the STEELRETRO research project (Braconi et al. [8]) to combine the dissipative capacity of “traditional” systems with the re-centering capability, has been used for the design of a commercial hybrid r.c./steel commercial building. The design procedure, as widely presented is iterative and include both linear and nonlinear analyses.

The “original” prototype of the system, with mechanical and geometrical properties described in Braconi et al. [9], allowed to design the building for seismic action with maximum PGA equal to 0.25g, in agreement with the requirements of actual standards for both the SLD and SLV and providing a good re-centering capacity, with very limited residual displacements.

The modification of parameters such as the length of the device, the diameter of the cables and the size of the dissipative elements of the SSCD allow to improve the structural performance of the building, as widely demonstrated. Otherwise, the need to keep the energy dissipation coefficient β lower than 0.90 was evidenced: higher β are associated to higher maximum allowable PGA levels (for SLV) but to the loss of the re-centering capacity.

The optimization of the system can be achieved through the application of parametric investigations aiming to determine the characteristics values of SSCD systems – such as mainly the length of pre-tensioned cables and the transversal area of dissipative elements – to be used in relation to the effective requirements of the building.

The horizontal location of the SSCD (as connection between r.c. walls and steel frames) allows the direct control of the structural behaviour of the building and the possibility to optimize the modal deformed shape in order to have, such as in the considered case, equal displacements in correspondence of all the storeys.

The comparison between the numerical results of the analyses and the data coming from the experimental tests evidence that the simplifications adopted in the

model (such as, for example the neglecting of friction and of dissipative elements in the determination of equivalent stiffness) lead to a percentage error that mainly influences the quantity of dissipated energy. On the other hand, very low differences between analysis and experimental tests have been revealed for what concerns the estimation of residual displacements.

The most significant limit of the SSCD system is related to the reduced displacement capacity, able to sustain maximum 25 mm. The quantity of dissipated energy is related to the displacements and to the forces acting on the device: the displacement can be increased with the increase of the dimension of pre-tensioned cables or with the length of the device – the last one difficult to be applied. The dissipative capacity of the SSCD can be increase with higher size of the dissipative elements, keeping the β coefficient lower than 0.90.

It's moreover necessary to underline that the absence of specific standards determining the parameters needed for the characterization of the dissipative devices do not allow to directly compare the behaviour of a “traditional” system with the one of a building with dissipative protection system. The SSCD proposed device has been designed and checked considering both the static and the seismic condition, but the effective determination of performance levels according to SLO, SLD, SLV and SLC is not clear, as well as the definition of the effective behaviour factor q , assumed in the present case equal to 1.0.

11.4 References

- [1] EN1998-1:2005 - *Eurocode 8 –Design of structures for earthquake resistance, Part 1: General Rules, seismic action and rules for buildings.*
- [2] NTC (2008) Norme tecniche per le Costruzioni. Gazzetta Ufficiale n. 29, February 4, 2008, Suppl. Ordinario n.30, Italy (in Italian).
- [3] FEMA (2000a) - *FEMA-350 - Recommended seismic design criteria for new steel moment-frame buildings.*
- [4] Christopoulos C., Filiatrault A. *Principles of passive supplemental damping and seismic isolation.* IUSS Press, Pavia, 2006.
- [5] Christopoulos C., Tremblay R., Kim H., Lacerte M. *Dissipative Bracing System for the Seismic Resistance of Structures: Development and Validation*, ASCE Journal of Structure Engineering 134, Special Issue: Design and Analysis of Structures with Seismic Damping Systems, 96-107, 2008.
- [6] Kam W.Y., Pampanin S., Palermo A., Carr A.J. (2008) - *Design Procedure and Behaviour of Advanced Flag-Shape (AFS) MDOF Systems*, 2008 New Zealand Society of Earthquake Engineering (NZSEE) Conference, 11-13 April 2008, Wairakei, Nuova Zelanda.
- [7] Kam W.Y., Pampanin S., Palermo A., Carr A.J. (2010) - *Self-centering structural systems with combination of hysteretic and viscous energy dissipations*, Earthquake Engineering and Structural Dynamics **39** (10), 1083-1108.
- [8] Braconi A., Tremea A., Lomiento G., Bonessio, N., Braga F., Hoffmeister B., Gundel M., Karamanos S.A., Varelis G., Obiala R., Tsintzons P., Vasilikis D., Lobo J. B., Bartlam P., Estanislau S. C., Nardini L., Morelli F., Salvatore W., Dubina D., Dogariu A., Bordea S., Bortone G., Signorini N., Fianchisti G., Fulop L., STEEL solutions for seismic RETROfit and

- upgrade of existing constructions, RFSR-CT-2007-00050 project - Final Report, European Commission, Bruxelles, 2010.
- [9] Braconi A., Morelli F., Salvatore W. *Development, design and experimental validation of a steel self centering device (SSCD) for seismic protection of buildings*. Bulletin of Earthquake Engineering 10 (6), 1915-1941, 2012.
- [10] Uang C.M., Bertero V.V. (1990) - *Evaluation of seismic energy in structures*, Earthquake Engineering & Structural Dynamics **19** (2), 77-90.
- [11] Banushi G. Un modello semianalitico del comportamento meccanico di un dissipatore autocentrante per la protezione sismica delle strutture, Tesi di Laurea, Facoltà di Ingegneria, Università di Pisa, 2010.
- [12] Vamvatsikos D., Cornell C.A. *Incremental dynamic analysis*, Earthquake Engineering and Structural Dynamics 31, 491-514, 2002-.

12 TRSH

12.1 General

In the present study, a specific design procedure for the implementation of TRiangular Shaped Hysteretic (TRSH) devices in “V-bracing” systems of multi-story steel structures is proposed and applied to a high-rise (8 storeys) case-study building located in a moderate ($\text{PGA}=0.20\text{g}$) seismic area. In particular, since TRSH elements are categorized as anti-seismic devices, the EN 1993-1 (CEN, 2005-1) and EN 1998-1 (CEN, 2005-2) performance requirements are slightly modified in order to accomplish also EN 15129 (CEN, 2009) provisions. Moreover, the identified solution, thanks to an optimized layout of the TRSH devices, is shown to ensure a complete protection of the case-study structure during the seismic excitation.

12.2 Design rules

The philosophy behind the proposed design procedure aims at pursuing two main goals: (1) during the seismic excitation, the main structure (beams and columns) remain in the elastic range; (2) yielding and dissipation mechanisms occur only in TRSH elements (that are easily replaceable).

12.2.1 General

The design methodology, described in the following, is based on the provisions of EN 1993-1 (CEN, 2005-1), EN 1998-1 (CEN, 2005-2), and EN 15129 (CEN, 2009). In particular, some clauses of EN 1998-1-1 were appropriately rearranged to cover also the provisions given in EN 15129.

The proposed procedure consists of two steps: (1) a preliminary structural layout is defined by means of a simple analytical calculation (equivalent lateral loads method); (2) a linear multimodal response spectrum analysis is carried out in order to assess the suitability of the proposed structural layout against the EN 1998-1 performance requirements (the final solution is usually identified iteratively). Two different approaches can be adopted for the second step:

1. multimodal response spectrum analysis with consideration of the elastic stiffness k_1 of the TRSH devices and an appropriate q-factor;
2. Multimodal response spectrum analysis with consideration of the equivalent stiffness k_{eff} of the TRSH devices with appropriate q-factor.

In the following the structural design taken into account first approach is shown.

It is worth noting that for a more accurate design, the EN 15129 strongly recommends to perform nonlinear time-history analyses when the equivalent damping ratio related to hysteretic energy dissipation is higher than 15 %.

12.2.2 Preliminary design

Assuming that the gravitational loads at Ultimate Limit States (ULS) combination ($1.3G_1 + 1.5G_2 + 1.5Q$) are entrusted to the main frame (beams and columns), at each story level of the building, the TRSH bracing system is preliminary designed in order to withstand alone the overall lateral seismic load. In this regard, according to EN 1998-1 (§ 4.3.3.2.2 - 4.3.3.2.3, CEN, 2005-2), a rough approximation of the lateral seismic load (inertia force) acting at the i -th floor level F_i can be obtained from a simple analytical calculation (equivalent lateral loads method):

$$F_i = F_b \cdot \frac{z_i \cdot m_i}{\sum z_j \cdot m_j} \quad \text{Eq. (12.1)}$$

where:

$F_b = S_a(T_1) \cdot m \cdot \lambda$	seismic base-shear;
$S_a(T_1) = \left(\frac{1}{q}\right) \cdot S_{ae}(T_1)$	inelastic spectrum;
$S_{ae}(T_1)$	reference elastic spectrum;
$q = 3.0$	assumed behavior factor;
$T_1 = C_t \cdot H^{3/4}$	fundamental period of the building.

Once known the inertia forces F_i , the shear load acting at the base of column elements at each story level $F_{b,i}$ can be calculated (sum of inertia forces at upper story levels) and the TRSH device shall be designed in order to accomplish the following verification:

$$F_{Rd,t,i} = n_i \cdot F_{y,t,i} \geq \gamma_x \cdot \gamma_b \cdot F_{b,i} \quad \text{Eq. (12.2)}$$

where $F_{Rd,t,i} = n_i \cdot F_{y,t,i}$ is the design resisting force of the TRSH device (being $F_{y,t,i}$, and n_i respectively the yielding force, and the number of triangular elements composing the device). $\gamma_x = 1.2$ is the reliability factor and $\gamma_b = 1.1$ is the partial factor for the device acc. to EN 15129 (CEN, 2009).

In case of frame with V bracings, it is worth noting that both the tension and compression diagonals shall be taken into account and element cross-sections should be chosen in order fulfill the following checks:

$$N_{Ed,b,i} = \frac{F_{b,i} \cdot \cos \alpha}{2} \leq 0.5 \cdot N_{Rd,b,i} \quad \text{Eq. (12.3)}$$

$$\lambda_{b,i} = \sqrt{A_{b,i} \cdot f_y / N_{cr,b,i}} \leq 2.0 \quad \text{Eq. (12.4)}$$

where $N_{Ed,b,i}$ is the axial action effect; $N_{Rd,b,i}$, $N_{cr,b,i}$ are respectively the design axial resisting force and the critical buckling load of brace the elements; $\lambda_{b,i}$ is the a-dimensional slenderness of the same (2.0 is the limit for "V bracing systems" according to EN 1993-1 (CEN, 2005-1).

12.2.3 Design for linear elastic analysis

12.2.3.1 Multi-modal response spectrum analysis

In the current state of the art, a building with TRSH bracing system may be simulated with linear-elastic elements with appropriate lateral stiffness (for the calculation of elastic stiffness of TRSH devices see the relevant Information Brochure-INNOSEIS, 2017). Both dissipative and non-dissipative structural elements shall be verified with reference to the seismic load combination ($G_1 + G_2 + \psi Q + E$). In this regard, the conventional method for the calculation of internal forces due to the seismic action (E) is Multi-Modal Response Spectrum Analysis, where the number of modes of vibration considered in each direction is such that the sum of the effective mass is at least equal to 85% of the total mass and there are no modes with mass participating $> 5\%$. The design spectrum shall be defined with a maximum behavior factor equal $q = 3.0$, which was obtained from preliminary Pushover analyses (see the Information Brochure-INNOSEIS, 2017).

12.2.3.2 Limitation of interstory drift

Limitation of interstory drift ensures the protection of non-structural elements under seismic loading and provides an estimation of the damage for different performance levels. It leads the selection and the distribution of stiffness within the structure and eventually the size and type of the TRSH system.

Assuming that the building has ductile non-structural elements the following verification relevant of the maximum interstorey d_r shall be fulfilled:

$$d_r \cdot v \leq 0.0075 \cdot h \quad \text{Eq. (12.5)}$$

where $v = 0.5$ is a reduction factor on the design displacements due to the importance class of the building (ordinary buildings) and h is the story height.

In linear analysis the displacements induced by the design seismic action d_s shall be calculated on the basis of the elastic deformations d_e of the structural system through the expression:

$$d_s = q \cdot d_e \quad \text{Eq. (12.6)}$$

In case the capacity ratios of the dissipative elements (Ω) are low, the calculation of the design interstory drift based on d_s is conservative and a therefore reduction factor (q_Ω) equal to the capacity ratio of the devices may be employed as follows:

$$d_s = q \cdot q_\Omega \cdot d_e \quad \text{Eq. (12.7)}$$

The design interstory drift d_r is defined as the difference of the average lateral displacements at the top and bottom of the story under consideration. Depending on the type of the non – structural elements (brittle materials, ductile or not connected) and the importance class of the building, the design interstory drift d_r is compared to the corresponding values of the Code. The optimal design is achieved when the maximum interstory drifts of the structure are close to the limit values. Since the horizontal displacements are multiplied by the behavior factor the limitation of interstory drift does not depend on it.

12.2.3.3 Second order effects

The possible influence of 2nd order effects shall be controlled by the limitation of the interstory drift sensitivity coefficient θ below the limit values of the Code. Coefficient θ is calculated as:

$$\theta = \frac{P_{tot} \cdot d_r}{V_{tot} \cdot h_{story}} \quad \text{Eq. (12.8)}$$

where P_{tot} is the total gravity load at and above the considered story, V_{tot} is the seismic story shear, d_r is the interstorey drift, and h_{story} is the interstorey height.

Alternatively, the interstory drift sensitivity coefficient θ may be calculated more accurately by a linear buckling analysis through the factor α_{cr} , the factor by which the design loading would have to be increased to cause elastic instability in a global mode. The analysis is carried out under conditions of the constant gravity loads of the seismic combination (1,0·G+0,3· ϕ ·Q) and produces the buckling modes. The modes that move the building at x and y directions are chosen and the correspondent α_{cr} values are calculated as follows:

$$\alpha_{cr} = \frac{1}{\theta} = \frac{F_{cr}}{F_{Ed}} \quad \text{Eq. (12.9)}$$

where F_{cr} is the elastic critical buckling load for global instability mode based on initial elastic stiffnesses and F_{Ed} is the design loading for the seismic combination. To take into consideration the inelastic displacements of the building, α_{cr} shall be divided by the q factor. The values of θ in this case are:

$$\theta = \frac{q}{\alpha_{cr}} \quad \text{Eq. (12.10)}$$

The relevant EC3-1 (CEN, 2005-1) provisions require for buildings that the interstory drift sensitivity coefficient is limited to $\theta \leq 0.1$, if second order effects are ignored. If $0.1 < \theta < 0.2$, second-order effects may approximately be taken into account by multiplying the relevant seismic action effects by a factor equal to $1/(1 - \theta)$. If $0.2 < \theta < 0.3$ a more accurate second order analysis applies. In any case it shall be $\theta < 0.3$.

2.3.4 Dissipative elements (TRSH devices)

At each generic i -th story level it shall be verified that: the seismic action $F_{Ed,i}$, taking into account $\gamma_x = 1.2$ as reliability factor and $\gamma_b = 1.1$ as partial safety factor for TRSH devices, does not exceed its design resistance $F_{Rd,t,i}$ (see EN 15129, section 4.1.2):

$$F_{Rd,t,i} = n_i \cdot F_{y,t,i} \geq \gamma_b \cdot \gamma_x \cdot F_{Ed,i} \quad \text{Eq. (12.11)}$$

Moreover, to achieve a uniform dissipative behavior at each storey level, it should be checked that the maximum over-strength ratio Ω of TRSH elements over the entire structure do not differ from the minimum value Ω more than 25%:

$$\frac{\max \Omega_i}{\min \Omega_i} \leq 1.25 \quad \text{Eq. (12.12)}$$

where $\Omega_i = (n_i \cdot F_{y,t,i})/F_{Ed,i}$.

In all above checks, in safety favour, upper and lower bound design properties of TRSH devices (provided by the manufacturer) should be considered.

12.2.3.4 Non-dissipative elements

In order to ensure that the yielding occurs only in the TRSH elements, non-dissipative structural members (beams, columns and braces) shall be capacity designed for increased values of internal forces compared to the ones derived from the analyses with the most unfavourable seismic combination:

$$\begin{cases} N_{Rd} \geq N_{Ed,G} + 1,1 \cdot \gamma_{ov} \cdot \Omega \cdot N_{Ed,E} \\ M_{Rd} \geq M_{Ed,G} + 1,1 \cdot \gamma_{ov} \cdot \Omega \cdot M_{Ed,E} \\ V_{Rd} \geq V_{Ed,G} + 1,1 \cdot \gamma_{ov} \cdot \Omega \cdot V_{Ed,E} \end{cases} \quad \text{Eq. (12.13)}$$

where:

- N_{Rd} (M_{Rd} , V_{Rd}) is the axial (bending or shear accordingly) design resistance of the structural element;
- $N_{Ed,G}$ ($M_{Ed,G}$, $V_{Ed,G}$) is the axial (bending or shear accordingly) force acting on the structural element due to the non-seismic actions;
- $N_{Ed,E}$ ($M_{Ed,E}$, $V_{Ed,E}$) is the axial (bending or shear accordingly) force acting on the structural element due to the design seismic action;
- γ_{ov} is the overstrength factor ($\gamma_{ov} = 1,25$ for steel S355);
- $\Omega = \min(N_{Rd,i}/N_{Ed,E,i})$ over all the bracing diagonals.

12.3 High-rise case-study building

Equations, element properties, design recommendations, critical checks and proposed behaviour factor (q-factor), included in the Information Brochure (INNOSEIS, 2017)), are verified hereafter through numerical analyses on a 3D high-rise case-studies building equipped with the TRSH devices. Both dissipative and non-dissipative elements of the resisting frame are preliminary designed with a simplified analytical procedure (equivalent lateral loads method, see Section 12.2.2). Eventually a multi-modal response spectrum analysis is carried out and relevant results are verified by means of structural checks prescribed in EC8 (see Section 2.3) in to in order to assess the suitability of the proposed structural design (the final solution is usually defined iteratively). All numerical analyses are carried out by means of the commercial software SAP2000 v.19 (CSI, 2016).

12.3.1 Description of the building frame

12.3.1.1 Geometry

Both front-view and planar geometries of the considered case-study frame are represented in Figure 12.1.

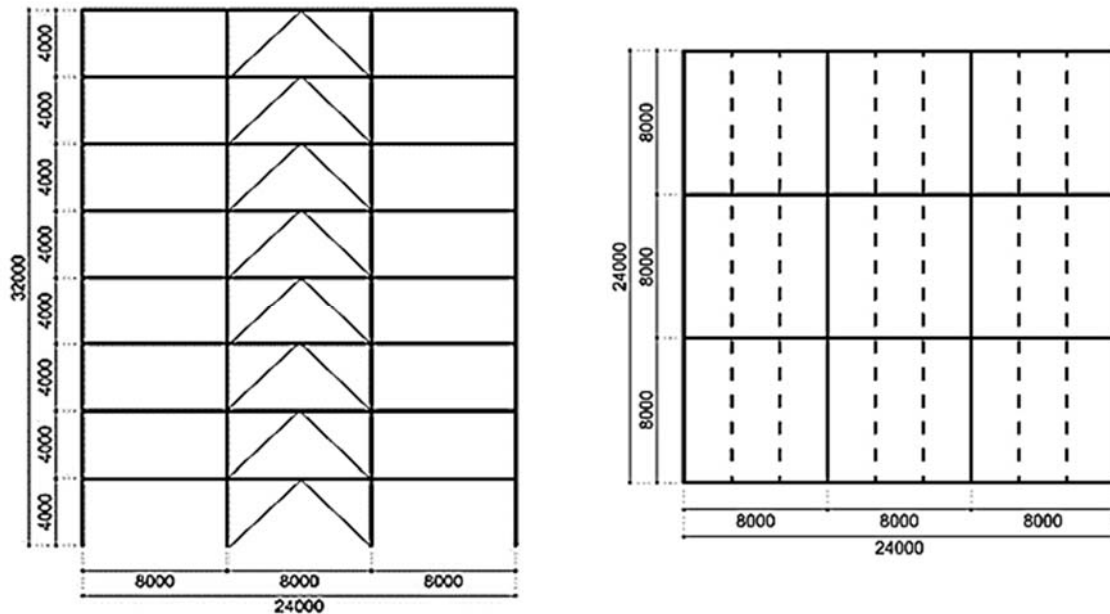


Figure 12.1: Front (left) and planar (right) geometry views of the case-studies building frame

12.3.1.2 Load analysis

The following Dead Loads (G) have been assumed in structural calculations:

- steel self-weight: 78.5 kN/m^3 ;
- composite slab: $g_{2,c} = 2.75 \text{ kN/m}^2$ (concrete self-weight 25.0 kN/m^3 , steel sheeting height 73 mm , thickness 1 mm , slab thickness 150 mm , equivalent uniform slab thickness 110 mm);
- services, ceilings, raised floors: $g_{2,if} = 0.70 \text{ kN/m}^2$ for intermediate floors, $g_{2,tf} = 1.00 \text{ kN/m}^2$ for top floor;
- perimeter walls (1.00 kN/m^2): $g_{2,per} = 4.00 \text{ kN/m}$.

Live Loads (q) have been estimated as:

- offices (class B): $q = 3.00 \text{ kN/m}^2$
- movable partitions ($\leq 2.00 \text{ kN/m}^2$): $q_{add} = 0.80 \text{ kN/m}^2$
- total live load: $q_{add} = 3.80 \text{ kN/m}^2$
- coeff. for the seismic combinations: $\psi_2 = 0.60$
- roof accessible and snow load neglected.

Seismic Loads (E) have been defined through the EC8 reference elastic spectrum assuming:

- importance factor: $\gamma_I = 1.0$;
- peak ground acceleration: $a_{gR} = 0.20g$;
- ground Type B, Type 1 spectrum: $S = 1.2$, $T_B = 0.15s$, $T_C = 0.50s$, $T_D = 2.00s$;
- vertical ground acceleration not accounted for.

12.3.2 Preliminary design

The non-dissipative elements of the resisting frame (beams and columns) are preliminary designed in order to withstand ($N_{Rd} \geq N_{Ed}$, $V_{Rd} \geq V_{Ed}$, and $M_{Rd} \geq M_{Ed}$) alone the gravitational loads at Ultimate Limit States (ULS) combination ($1.3G_1 + 1.5G_2 + 1.5Q$). The columns are supposed completely restrained at the base while beams hinged to the columns. The resulting beams and columns cross-sections are reported in Table 12.1.

Table 12.1: Beam and column cross-section at each storey level

storey level	column	beam	steel
1	SHS 340X340X20	IPE 450	S 355
2	SHS 340X340X20	IPE 450	S 355
3	SHS 300X300X16	IPE 450	S 355
4	SHS 300X300X16	IPE 450	S 355
5	SHS 220X220X16	IPE 450	S 355
6	SHS 220X220X16	IPE 450	S 355
7	SHS 180X180X16	IPE 450	S 355
8	HEB 300	IPE 450	S 355

The TRSH dissipative bracing system is then preliminary designed according to the procedure described in Section 12.2.2. Assuming a behaviour factor $q = 3.0$ (see Information Brochure-INNOSEIS, 2017), the base-shear $F_b(T_1)$ is calculated as:

$$T_1 = C_t \cdot H^{\frac{3}{4}} = 1.01s \quad \text{Eq. (12.14)}$$

$$S_a(T_1) = S_{ae}(T_1)/q = 0.10g \quad \text{Eq. (12.15)}$$

$$F_b(T_1) = m_{tot} \cdot \lambda \cdot S_a(T_1) = 2777.1kN \quad \text{Eq. (12.16)}$$

Resulting inertia F_i ($F_i = F_b \cdot (z_i \cdot m_i) / (\sum z_j \cdot m_j)$) and shear $F_{b,i}$ forces on column elements at each storey level are reported in Table 12.2.

Table 12.2: Mass and inertia force distribution at each storey level

storey level	m_i [kg]	F_i [kN]	$F_{b,i}$ [kN]	$\gamma_x \cdot \gamma_b \cdot F_{b,i}$ [kN]
1	354000	77.1	2777.1	3665.7
2	354000	154.3	2699.9	3563.9
3	354000	231.4	2545.6	3360.2
4	354000	308.6	2314.2	3054.8
5	354000	385.7	2005.7	2647.5
6	354000	462.8	1620.0	2138.3
7	354000	540.0	1157.1	1527.4
8	354000	617.1	617.1	814.6

The TRSH devices to be installed at the i -th storey level are chosen among real devices prototypes experimentally tested within the European LESSLOSS project (LESSLOSS, 2007). Lower and upper bound design properties of the TRSH have to be provided by the device manufacturer and then the number triangular plates n_i can be determined as:

$$n_i = \frac{\gamma_x \cdot \gamma_b \cdot F_{b,i}}{F_{y,LBDP,t,i}} \quad \text{Eq. (12.17)}$$

where $F_{y,LBDP,t,i}$ is the lower bound design property of the yielding force $F_{y,t,i}$ of the single dissipative element, $\gamma_x = 1.2$ is the reliability factor and $\gamma_b = 1.1$ the partial factor for the TRSH device.

Resulting design parameters of TRSH devices at each story level are reported in Table 12.3 (note that two TRSH devices are installed at each storey level – one along each horizontal direction).

Table 12.3: Layout of TRSH devices at each storey level

storey level	TRSH type	$F_{y,t,i}$ [kN]	$F_{u,t,i}$ [kN]	$k_{el,i}$ [kN/m]	n [-]	$F_{y,t,i}$ [kN]	$F_{u,t,i}$ [kN]	$k_{el,i}$ [kN/m]
1	TR250(7)-S355J2	50	59	5000	2x37	2x1850	2x2183	2x185000
2	TR250(7)-S355J2	50	59	5000	2x36	2x1800	2x2124	2x180000
3	TR250(7)-S355J2	50	59	5000	2x34	2x1700	2x2006	2x170000
4	TR250(7)-S355J2	50	59	5000	2x31	2x1550	2x1829	2x155000
5	TR250(7)-S355J2	50	59	5000	2x27	2x1350	2x1593	2x135000
6	TR250(7)-S355J2	50	59	5000	2x22	2x1100	2x1298	2x110000
7	TR250(7)-S355J2	50	59	5000	2x16	2x800	2x944	2x80000
8	TR250(7)-S355J2	50	59	5000	2x9	2x450	2x531	2x45000

Moreover, the cross-section of brace-elements are chosen in order to fulfil the requirements related to both axial resistance and non-dimensional slenderness

(see Section 12.2.2). Relevant design parameters are reported in Table 12.4 (note that two bracing systems are installed at each storey level – one along each horizontal direction).

Table 12.4: Bracing elements cross-sections at each storey level

storey level	cross section	$N_{Ed,i}$ [kN]	$N_{Rd,i}$ [kN]	l_0 [m]	$N_{cr,i}$ [kN]	$\lambda_{b,i}$ [-]
1	2x(2UPN300)	981.8	2x(2x3795)	5.26	2x(2x943.5)	2.0
2	2x(2UPN300)	954.6	2x(2x3795)	5.26	2x(2x943.5)	2.0
3	2x(2UPN300)	900.0	2x(2x3795)	5.26	2x(2x943.5)	2.0
4	2x(2UPN300)	818.2	2x(2x3795)	5.26	2x(2x943.5)	2.0
5	2x(2UPN300)	709.1	2x(2x3795)	5.26	2x(2x943.5)	2.0
6	2x(2UPN300)	572.7	2x(2x3795)	5.26	2x(2x943.5)	2.0
7	2x(2UPN300)	409.1	2x(2x3795)	5.26	2x(2x943.5)	2.0
8	2x(2UPN300)	218.2	2x(2x3795)	5.26	2x(2x943.5)	2.0

The structural layout resulting from the preliminary design is represented in Figure 12.2.

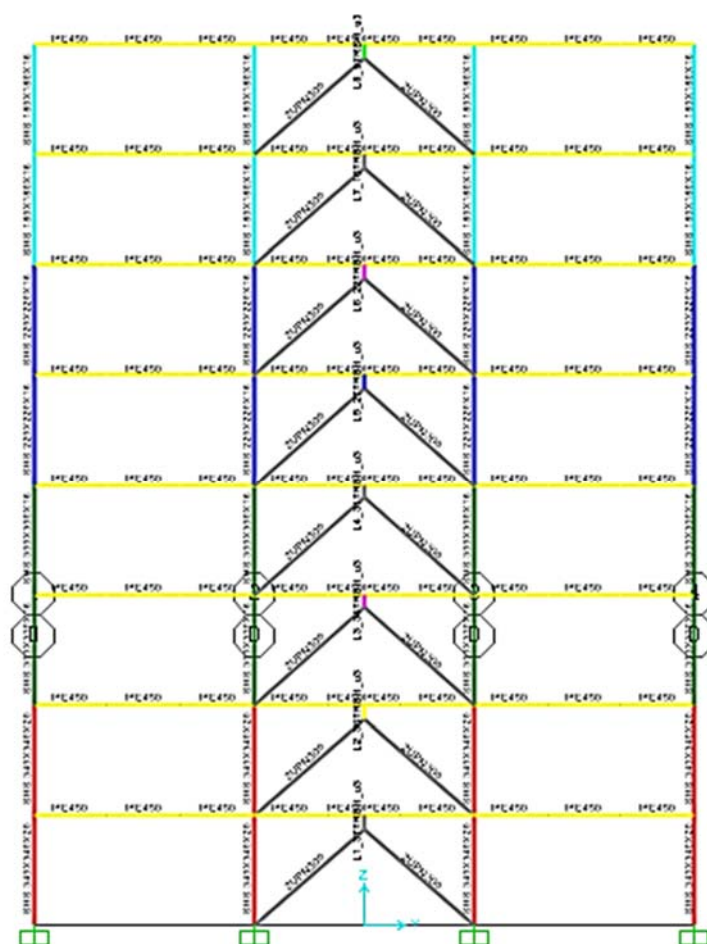


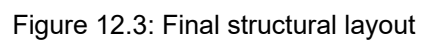
Figure 12.2: Structural layout resulting from the preliminary design

12.3.3 Linear elastic analysis

A linear elastic analysis is carried out in accordance with the EN 1998-1-1 provisions (CEN, 2005-2) described in Section 12.2.3. In particular, both dissipative and non-dissipative structural elements are verified with reference to the seismic load combination ($G_1 + G_2 + \psi Q + E$). Since the solution initially defined through the preliminary design does not satisfy some EC8 verifications, the final structural layout is identified by changing iteratively only the configuration of TRSH devices until the configuration reported in Table 12.5 and represented in Figure 12.3 is reached.

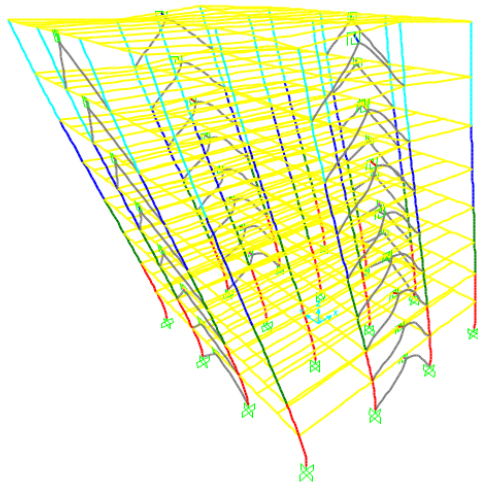
Table 12.5: Final layout of TRSH devices at each storey level

storey level	TRSH type	$F_{y,t,i}$ [kN]	$F_{u,t,i}$ [kN]	$k_{el,i}$ [kN/m]	n [-]	$n \cdot F_{y,t,i}$ [kN]	$n \cdot F_{u,t,i}$ [kN]	$n \cdot k_{el,i}$ [kN/m]
1	TR250(7)-S355J2	50	59	5000	2X11	2X550	2X649	2X55000
2	TR250(7)-S355J2	50	59	5000	2X17	2X850	2X1003	2X85000
3	TR250(7)-S355J2	50	59	5000	2X16	2X800	2X944	2X80000
4	TR250(7)-S355J2	50	59	5000	2X14	2X700	2X826	2X70000
5	TR250(7)-S355J2	50	59	5000	2X13	2X650	2X767	2X65000
6	TR250(7)-S355J2	50	59	5000	2X11	2X550	2X649	2X55000
7	TR250(7)-S355J2	50	59	5000	2X10	2X500	2X590	2X50000
8	TR250(7)-S355J2	50	59	5000	2X6	2X300	2X354	2X30000

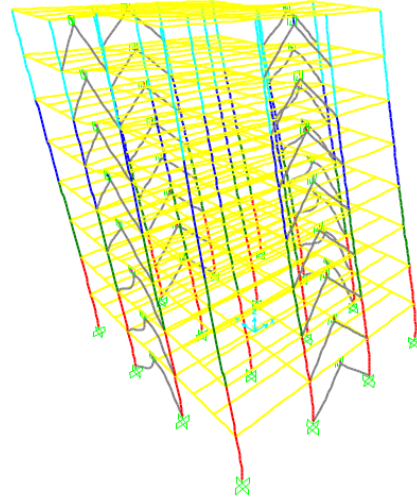


A multi-modal response spectrum analysis has been performed taking into account inertia seismic loads relevant to the first mode shapes (Figure 12.4) that jointly activate at least the 90% of the total mass of the building along both horizontal directions.

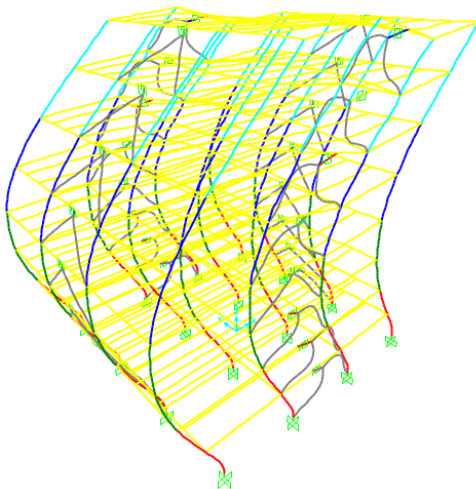
Mode 1



Mode 2



Mode 3



Mode 4

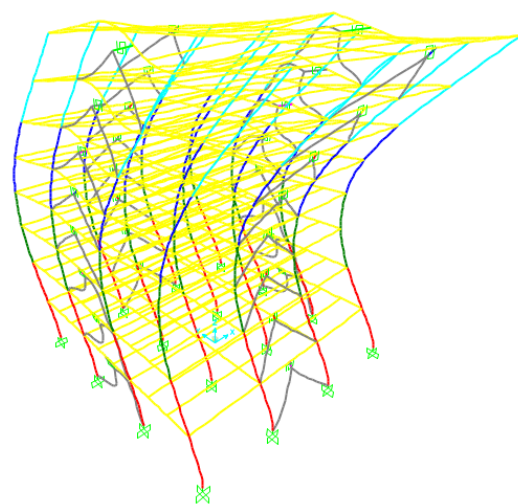


Figure 12.4: Mode shapes considered in response-spectrum analysis

Relevant modal parameters are summarized in Table 12.6. It is worth noting that the CQC rule has been used to combine modal results while the SRSS rule for the directional combination (seismic spectrum loads are simultaneously applied along both horizontal directions).

Table 12.6: Periods and participating mass ratios of considered mode shapes

Mode n°	Period [s]	Part. mass X [%]	Part. mass Y [%]	Sum X [%]	Sum Y [%]
1	2.21	77	0	77	0
2	2.21	0	77	77	77
3	0.78	14	0	91	77
4	0.78	0	14	91	91

12.3.3.2 Limitation of interstory drift

Assuming that the building is equipped with ductile non-structural elements, the following limitation of the maximum interstory drift d_r has been verified (see Section 12.2.3):

$$d_r \cdot v \leq 0.0075 \cdot h = 30\text{mm} \quad \text{Eq. (12.18)}$$

As witnessed by results reported in Table 12.7, this requirement is fulfilled at each storey level.

Table 12.7: Results of interstory drift verifications at each storey level

Storey level	$d_{e,top,X}$ [mm]	$d_{e,top,Y}$ [mm]	$d_{e,bottom,X}$ [mm]	$d_{e,bottom,Y}$ [mm]	$d_r = q \cdot d_{e,top} - d_{e,bottom} $ [mm]	$d_r \cdot v$ [mm]
1	9	9	0	0	38.2	19.1
2	21	21	9	9	50.9	25.5
3	33	33	21	21	50.9	25.5
4	46	46	33	33	55.2	27.6
5	57	57	46	46	46.7	23.3
6	69	69	57	57	50.9	25.5
7	79	79	69	69	42.4	21.2
8	88	88	79	79	38.2	19.1

12.3.3.3 Verification of second order effects

The possible influence of 2nd order effects has been controlled by the limitation of the interstory drift sensitivity coefficient θ below the limit values of the Code (see Section 12.2.3):

$$\theta = \frac{P_{tot} \cdot d_r}{V_{tot} \cdot h_{story}} \quad \text{Eq. (12.19)}$$

Since in six cases $0.1 < \theta < 0.2$ (Table 12.8), the second-order effects are taken into account by multiplying the seismic action by the factor $1/(1 - \theta)$.

Table 12.8: Results of 2nd order effects verification at each storey level

Storey level	P_{tot} [kN]	d_r [mm]	V_{tot} [kN]	h_{story} [mm]	θ [-]	$1/(1 - \theta)$ [-]
1	27878	38.2	1647	4000	0.16	1.19
2	24346	50.9	1591	4000	0.19	1.24
3	20815	50.9	1404	4000	0.19	1.23
4	17289	55.2	1237	4000	0.19	1.24
5	13764	46.7	1101	4000	0.15	1.17
6	10264	50.9	983	4000	0.13	1.15
7	6764	42.4	803	4000	0.09	1.10
8	3269	38.2	487	4000	0.06	1.07

3.3.4 Verification of dissipative elements

It has been verified that, along both horizontal directions, the maximum seismic action ($\gamma_x \cdot \gamma_b \cdot F_{Ed,i}$) on the TRSH device has not exceeded the design resistance $F_{Rd,t,i}$ of the element (see Section 12.2.3):

$$F_{Rd,t,i} = n_i \cdot F_{y,t,i} \geq \gamma_x \cdot \gamma_b \cdot F_{Ed,i} \quad \text{Eq. (12.20)}$$

This requirement is fulfilled at each storey level as witnessed by results reported in Table 12.9

Table 12.9: Resistance verification of TRSH elements at each storey level

Storey level	TRSH type	n [-]	$n \cdot F_{y,t,i}$ dir. X [kN]	$n \cdot F_{y,t,i}$ dir. Y [kN]	$\gamma_x \cdot \gamma_b \cdot F_{Ed,i}$ dir. X [kN]	$\gamma_x \cdot \gamma_b \cdot F_{Ed,i}$ dir. Y [kN]
1	TR250(7)-S355J2	2X11	2X550	2X550	357.7	357.7
2	TR250(7)-S355J2	2X17	2X850	2X850	654.2	654.2
3	TR250(7)-S355J2	2X16	2X800	2X800	606.3	606.3
4	TR250(7)-S355J2	2X14	2X700	2X700	525.8	525.8
5	TR250(7)-S355J2	2X13	2X650	2X650	481.0	481.0
6	TR250(7)-S355J2	2X11	2X550	2X550	418.0	418.0
7	TR250(7)-S355J2	2X10	2X500	2X500	353.1	353.1
8	TR250(7)-S355J2	2X6	2X300	2X300	221.9	221.9

Moreover, to achieve a uniform dissipative behavior among all storey levels, the following requirement related to the distribution of the over-strength ratios Ω of the TRSH elements over the entire structure has been verified (see Section 12.2.3):

$$\frac{\max \Omega_i}{\min \Omega_i} \leq 1.25 \quad \text{Eq. (12.21)}$$

where $\Omega_i = (n_i \cdot F_{y,t,i}) / (\gamma_x \cdot \gamma_b \cdot F_{Ed,i})$.

This requirement is fulfilled as witnessed by relevant results reported in Table 12.10

Table 12.10: TRSH devices over-strength factor verification

Storey level	Ω_i dir. X [-]	Ω_i dir. Y [-]	$\max(\Omega_i)/\min(\Omega_i)$ dir. X [-]	$\max(\Omega_i)/\min(\Omega_i)$ dir. Y [-]
1	2.03	2.03		
2	1.72	1.72		
3	1.74	1.74		
4	1.76	1.76		
5	1.78	1.78	1.18	1.18
6	1.74	1.74		
7	1.87	1.87		
8	1.78	1.78		

It is worth noting that the over strength factor used for structural checks of non-dissipative element is $\Omega = 1.72$ (the minimum among obtained values).

3.3.5 Verification of non-dissipative elements

In order to ensure that the yielding occurs only in TRSH devices, non-dissipative structural members (beams, columns, and braces) have been verified according to capacity design requirements (see Section 12.2.3):

$$\begin{cases} N_{Rd} \geq N_{Ed,G} + 1,1 \cdot \gamma_{ov} \cdot \Omega \cdot N_{Ed,E} \\ M_{Rd} \geq M_{Ed,G} + 1,1 \cdot \gamma_{ov} \cdot \Omega \cdot M_{Ed,E} \\ V_{Rd} \geq V_{Ed,G} + 1,1 \cdot \gamma_{ov} \cdot \Omega \cdot V_{Ed,E} \end{cases} \quad \text{Eq. (12.22)}$$

Results relevant to elements under maximum axial load, shear load, and bending moment are respectively reported from Table 12.11 to Table 12.13.

Table 12.11: Verification of non-dissipative element under max axial load

element type	N_{Rd} [kN]	$N_{Ed,G} + 1,1 \cdot \gamma_{ov} \cdot \Omega \cdot N_{Ed,E}$ [kN]
column – SHS 340X340X20	7903	3178.9
column – SHS 300X300X16	5618	2220.7
column – SHS 220X220X16	4044	1345.1
column – SHS 180X18X16	3448	543.1
beam – IPE450	-	-
brace – 2UPN300	3795	418.1

Table 12.12: Verification of non-dissipative element under max shear load

element type	$V_{Rd,X}$ [kN]	$V_{Rd,Y}$ [kN]	$V_{Rd,Z}$ [kN]	$V_{Ed,G} + 1,1 \cdot \gamma_{ov} \cdot \Omega \cdot V_{Ed,E}$ [kN]		
				dir. X	dir. Y	dir. Z
column – SHS 340X340X20	2654.7	2654.7	-	46.4	46.4	-
column – SHS 300X300X16	1873.9	1873.9	-	17.5	17.5	-
column – SHS 220X220X16	1374.2	1374.2	-	12.1	12.1	-
column – SHS 180X18X16	1124.3	1124.3	-	8.7	8.7	-
beam – IPE450	-	-	1034.0	-	-	141.6
brace – 2UPN300	-	-	-	-	-	-

Table 12.13: Verification of non-dissipative el. under max. bend. moment

element type	$M_{Rd,X}$ [kNm]	$M_{Rd,Y}$ [kNm]	$M_{Rd,Z}$ [kNm]	$M_{Ed,G} + 1,1 \cdot \gamma_{ov} \cdot \Omega \cdot M_{Ed,E}$ [kNm]		
				dir. X	dir. Y	dir. Z
column – SHS 340X340X20	1271.2	1271.2	-	150.2	150.2	-
column – SHS 300X300X16	655.9	655.9	-	30.6	30.6	-
column – SHS 220X220X16	338.1	338.1	-	19.8	19.8	-
column – SHS 180X18X16	219.8	219.8	-	14.9	14.9	-
beam – IPE450	-	-	549.3	-	-	353.7
brace – 2UPN300	-	-	-	-	-	-

12.4 Conclusions

In the present study, a specific design procedure for the implementation of TRSH devices in “V-bracing” systems of steel structures is proposed and applied to a 3D case-study high-rise (8 storeys) building located in a moderate (PGA=0.20g)

seismic area. The preliminary design of the resisting frame is defined by means of a simple analytical procedure (equivalent lateral loads method) and then the proposed structural layout is assessed in a multi-modal response spectrum analysis. The final solution, usually obtained iteratively adjusting the preliminary design, is shown to widely fulfil all the requirements relevant to both dissipative and non-dissipative structural elements provided by EC8-1 (CEN, 2005-2).

Since based on simple calculations, the proposed method can be easily adopted by practitioners; however, for a more accurate design, the EN 15129 strongly recommends performing nonlinear time-history analyses when the equivalent damping ratio related to hysteretic energy dissipation is higher than 15%.

12.5 References

CEN (Comitee Europeen de Normalisation). *EN 15129: Anti-seismic devices*, Brussels, 2009.

CEN (Comitee Europeen de Normalisation). EN1993-1-1, *Eurocode 3: Design of steel structures - Part 1-1: General rules and rules for buildings*. Brussels, 2005(1).

CEN (Comitee Europeen de Normalisation). EN1998-1-1, *Eurocode 8: Design of structures for earthquake resistance – Part 1-1: General rules, seismic actions and rules for buildings*. Brussels, 2005(2).

CSI (Computer & Structures, INC). *SAP2000 – Reference Manual*. California, Berkeley, 2016.

INNOSEIS XX/2017. *Information Brochure - TRSH device*. 2017.

LESSLOSS 2007/03. *Innovative Anti-Seismic Systems Users Manual*. Available online at <http://elsa.jrc.ec.europa.eu/events.php?id=4#reports>.

12.6 Annex A: “FEMA 695” q-factor estimation

The “FEMA 695 method” (FEMA, 2009) consist of a series of provisions that allow to estimate the behaviour factor q of a structure by means of a non-linear static analysis (Pushover). The calculation method is represented in Figure 12.5.

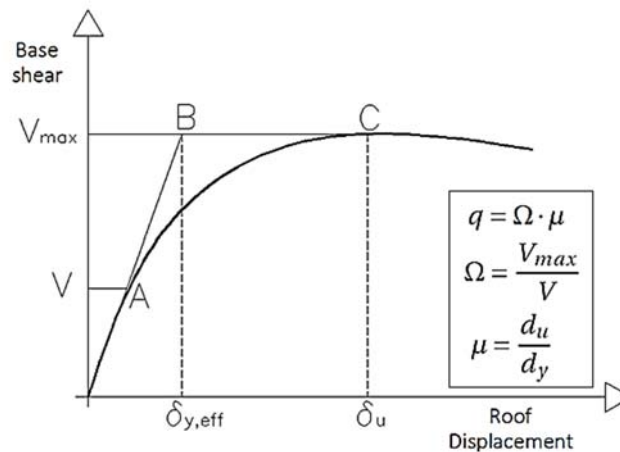


Figure 12.5: Behaviour factor q calculation method according to FEMA 695

With regard to the considered case-study building, the structural model used for elastic analysis is extended to include the response of structural elements beyond the elastic state and estimate expected plastic mechanisms and the distribution of damage. Link elements with a bilinear behavior of in the horizontal shear direction are used to model the TRSH devices. Fiber hinges with coupled axial and bending plastic behaviors are introduced at the base of columns while other structural members (beams) are modelled as linear. Mechanical properties of TRSH elements are calculated according to the analytical models described in the Information Brochure (INNOSEIS, 2017). Since quasi-static analyses are carried out, the hysteresis of TRSH elements is neglected in behavior-diagram (Figure 12.6). On the contrary, the failure of the element due to the exceedance of the ultimate displacement is accounted for.

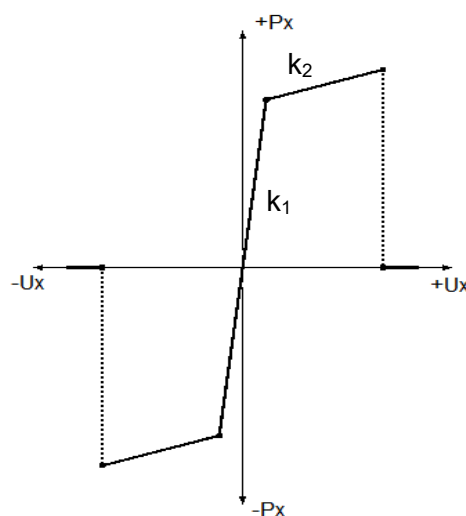


Figure 12.6: Qualitative force-displacement diagram used for TRSH elements in Pushover analyses

A Static Pushover analysis (SPO) along both horizontal directions has been performed considering the modal distribution of lateral loads. Since the structural layout (both dissipative and non-dissipative elements) is symmetric, the two capacity curves are perfectly overlapped (Figure 12.7) resulting in identical behaviour factors q along the two horizontal directions (Table 12.14).

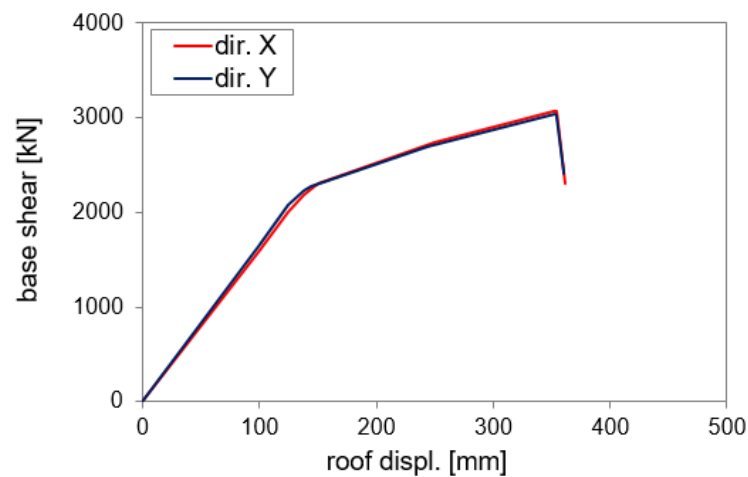


Figure 12.7: Capacity curves relevant to X and Y horizontal directions

Table 12.14: Behaviour factors q along both horizontal directions

Direction	V_{max} [kN]	V [kN]	Ω [-]	d_u [mm]	$d_{y,eff}$ [mm]	μ [-]	q [-]
X	3072.2	2073.5	1.48	354	175	2.02	2.99
Y	3072.2	2073.5	1.48	354	175	2.02	2.99

13 MSSH

13.1 General

In the present study, a specific design procedure for the implementation of Moon Shaped Steel Hysteretic (MSSH) devices in “V-bracing” systems of multi-story steel structures is proposed and applied to a high-rise (8 storeys) case-study building located in a moderate ($\text{PGA}=0.20\text{g}$) seismic area. In particular, since MSSH elements are categorized as anti-seismic devices, the EN 1993-1 (CEN, 2005-1) and EN 1998-1 (CEN, 2005-2) performance requirements are slightly modified in order to accomplish also EN 15129 (CEN, 2009) provisions. Moreover, the identified solution, thanks to an optimized layout of the MSSH devices, is shown to ensure a complete protection of the case-study structure during the seismic excitation.

13.2 Design rules

The philosophy behind the proposed design procedure aims at pursuing two main goals: (1) during the seismic excitation, the main structure (beams and columns) remain in the elastic range; (2) yielding and dissipation mechanisms occur only in MSSH elements (that are easily replaceable).

13.2.1 General

The design methodology, described in the following, is based on the provisions of EN 1993-1 (CEN, 2005-1), EN 1998-1 (CEN, 2005-2), and EN 15129 (CEN, 2009). In particular, some clauses of EN 1998-1-1 were appropriately rearranged to cover also the provisions given in EN 15129.

The proposed procedure consists of two steps: (1) a preliminary structural layout is defined by means of a simple analytical calculation (equivalent lateral loads method); (2) a linear multimodal response spectrum analysis is carried out in order to assess the suitability of the proposed structural layout against the EN 1998-1 performance requirements (the final solution is usually identified iteratively). Two different approaches can be adopted for the second step:

3. multimodal response spectrum analysis with consideration of the elastic stiffness k_1 of the MSSH devices and an appropriate q-factor;
4. Multimodal response spectrum analysis with consideration of the equivalent stiffness k_{eff} of the MSSH devices with appropriate q-factor.

In the following the structural design taken into account first approach is shown.

It is worth noting that for a more accurate design, the EN 15129 strongly recommends to perform nonlinear time-history analyses when the equivalent damping ratio related to hysteretic energy dissipation is higher than 15%.

13.2.2 Preliminary design

Assuming that the gravitational loads at Ultimate Limit States (ULS) combination ($1.3G_1 + 1.5G_2 + 1.5Q$) are entrusted to the main frame (beams and columns), at each story level of the building, the MSSH bracing system is preliminary designed in order to withstand alone the overall lateral seismic load. In this regard, according to EN 1998-1 (§ 4.3.3.2.2 - 4.3.3.2.3, CEN, 2005-2), a rough approximation of the lateral seismic load (inertia force) acting at the i -th floor level F_i can be obtained from a simple analytical calculation (equivalent lateral loads method):

$$F_i = F_b \cdot \frac{z_i \cdot m_i}{\sum z_j \cdot m_j} \quad \text{Eq. (13.1)}$$

where:

$F_b = S_a(T_1) \cdot m \cdot \lambda$	seismic base-shear;
$S_a(T_1) = (\frac{1}{q}) \cdot S_{ae}(T_1)$	inelastic spectrum;
$S_{ae}(T_1)$	reference elastic spectrum;
$q = 3.0$	assumed behavior factor;
$T_1 = C_t \cdot H^{3/4}$	fundamental period of the building.

Once known the inertia forces F_i , the shear load acting at the base of column elements at each story level $F_{b,i}$ can be calculated (sum of inertia forces at upper storey levels) and the MSSH devices shall be designed in order to accomplish the following verification:

$$N_{Rd,i} \geq N_{Ed,i} = \gamma_x \cdot \gamma_b \cdot \frac{F_{b,i}}{n_i \cdot \cos \alpha} \quad \text{Eq. (13.2)}$$

where $N_{Rd,i}$ is the design axial strength of a single MSSH device (for relevant calculation method see the Information Brochure-INNOSEIS, 2017) ; $N_{Ed,i}$ is the seismic force acting on the same; $\gamma_x = 1.2$ and $\gamma_b = 1.1$ are respectively the reliability and the partial factor according to EN 15129 (CEN, 2009); n_i is the number of MSSH elements installed at the i -esim storey level (both MSSH in tension and compression are accounted for); α is the inclination angle of MSSH elements.

In case of frame with V bracings, it is worth noting that both the tension and compression diagonals shall be taken into account and element cross-sections should be chosen in order fulfill the following checks:

$$N_{Ed,b,i} = \frac{F_{b,i} \cdot \cos \alpha}{2} \leq 0.5 \cdot N_{Rd,b,i} \quad \text{Eq. (13.3)}$$

$$\lambda_{b,i} = \sqrt{A_{b,i} \cdot f_y / N_{cr,b,i}} \leq 2.0 \quad \text{Eq. (13.4)}$$

where $N_{Ed,b,i}$ is the axial action effect; $N_{Rd,b,i}$, $N_{cr,b,i}$ are respectively the design axial strength and the critical buckling load of brace the elements; $\lambda_{b,i}$ is the a-dimensional slenderness of the same (2.0 is the limit for "V bracing systems" according to EN 1993-1 (CEN, 2005-1)).

13.2.3 Design for linear elastic analysis

13.2.3.1 Multi-modal response spectrum analysis

In the current state of the art, a building with MSSH bracing system may be simulated with linear-elastic elements with appropriate lateral stiffness (for the calculation of elastic stiffness of MSSH devices see the relevant Information Brochure-INNOSEIS, 2017). Both dissipative and non-dissipative structural elements shall be verified with reference to the seismic load combination ($G_1 + G_2 + \psi Q + E$). In this regard, the conventional method for the calculation of internal forces due to the seismic action (E) is Multi-Modal Response Spectrum Analysis, where the number of modes of vibration considered in each direction is such that the sum of the effective mass is at least equal to 85% of the total mass and there are no modes with mass participating $> 5\%$. The design spectrum shall be defined with a maximum behavior factor $q = 3.5$ which was obtained from a preliminary Pushover analysis (see the Information Brochure-INNOSEIS, 2017).

13.2.3.2 Limitation of interstory drift

Limitation of interstory drift ensures the protection of non-structural elements under seismic loading and provides an estimation of the damage for different performance levels. It leads the selection and the distribution of stiffness within the structure and eventually the size and type of the MSSH system.

Assuming that the building has ductile non-structural elements the following verification relevant of the maximum interstorey d_r shall be fulfilled:

$$d_r \cdot v \leq 0.0075 \cdot h \quad \text{Eq. (13.5)}$$

where $v=0.5$ is a reduction factor on the design displacements due to the importance class of the building (ordinary buildings) and h is the story height.

In linear analysis the displacements induced by the design seismic action d_s shall

be calculated on the basis of the elastic deformations d_e of the structural system through the expression:

$$d_s = q \cdot d_e \quad \text{Eq. (13.6)}$$

In case the capacity ratios of the dissipative elements (Ω) are low, the calculation of the design interstory drift based on d_s is conservative and a therefore reduction factor (q_Ω) equal to the capacity ratio of the devices may be employed as follows:

$$d_s = q \cdot q_\Omega \cdot d_e \quad \text{Eq. (13.7)}$$

The design interstory drift d_r is defined as the difference of the average lateral displacements at the top and bottom of the story under consideration. Depending on the type of the non – structural elements (brittle materials, ductile or not connected) and the importance class of the building, the design interstory drift d_r is compared to the corresponding values of the Code. The optimal design is achieved when the maximum interstory drifts of the structure are close to the limit values. Since the horizontal displacements are multiplied by the behaviour factor the limitation of interstory drift does not depend on it.

13.2.3.3 Second order effects

The possible influence of 2nd order effects shall be controlled by the limitation of the interstory drift sensitivity coefficient θ below the limit values of the Code. Coefficient θ is calculated as:

$$\theta = \frac{P_{tot} \cdot d_r}{V_{tot} \cdot h_{story}} \quad \text{Eq. (13.8)}$$

where P_{tot} is the total gravity load at and above the considered story, V_{tot} is the seismic story shear, d_r is the interstorey drift, and h_{story} is the interstorey height.

Alternatively, the interstory drift sensitivity coefficient θ may be calculated more accurately by a linear buckling analysis through the factor α_{cr} , the factor by which the design loading would have to be increased to cause elastic instability in a global mode. The analysis is carried out under conditions of the constant gravity loads of the seismic combination ($1,0 \cdot G + 0,3 \cdot \varphi \cdot Q$) and produces the buckling modes. The modes that move the building at x and y directions are chosen and the correspondent α_{cr} values are calculated as follows:

$$\alpha_{cr} = \frac{1}{\theta} = \frac{F_{cr}}{F_{Ed}} \quad \text{Eq. (13.9)}$$

where F_{cr} is the elastic critical buckling load for global instability mode based on initial elastic stiffnesses and F_{Ed} is the design loading for the seismic combination. To take into consideration the inelastic displacements of the building, α_{cr} shall be divided by the q factor. The values of θ in this case are:

$$\theta = \frac{q}{\alpha_{cr}} \quad \text{Eq. (13.10)}$$

The relevant EC3-1 (CEN, 2005-1) provisions require for buildings that the interstory drift sensitivity coefficient is limited to $\theta \leq 0.1$, if second order effects are ignored. If $0.1 < \theta < 0.2$, second-order effects may approximately be taken into account by multiplying the relevant seismic action effects by a factor equal to $1/(1 - \theta)$. If $0.2 < \theta < 0.3$ a more accurate second order analysis applies. In any case it shall be $\theta < 0.3$.

13.2.3.4 Dissipative elements (MSSH devices)

At each generic i -th story level it shall be verified that: the seismic action $N_{Ed,i}$, taking into account $\gamma_x = 1.2$ as reliability factor and $\gamma_b = 1.1$ as partial safety factor for MSSH devices, does not exceed their design resistance $N_{Rd,i}$ (see EN 15129, section 4.1.2):

$$N_{Rd,i} \geq \gamma_b \cdot \gamma_x \cdot N_{Ed,i} \quad \text{Eq. (13.11)}$$

Moreover, to achieve a uniform dissipative behavior at each storey level, it should be checked that the maximum over-strength ratio Ω of MSSH elements over the entire structure do not differ from the minimum value Ω more than 25%:

$$\frac{\max \Omega_i}{\min \Omega_i} \leq 1.25 \quad \text{Eq. (13.12)}$$

where $\Omega_i = N_{Rd,i}/N_{Ed,i}$.

In all above checks, in safety favour, upper and lower bound design properties of MSSH devices (provided by the manufacturer) should be considered.

2.3.5 Non-dissipative elements

In order to ensure that the yielding occurs only in the MSSH elements, non-dissipative structural members (beams, columns and braces) shall be capacity designed for increased values of internal forces compared to the ones derived from the analyses with the most unfavourable seismic combination:

$$\begin{cases} N_{Rd} \geq N_{Ed,G} + 1,1 \cdot \gamma_{ov} \cdot \Omega \cdot N_{Ed,E} \\ M_{Rd} \geq M_{Ed,G} + 1,1 \cdot \gamma_{ov} \cdot \Omega \cdot M_{Ed,E} \\ V_{Rd} \geq V_{Ed,G} + 1,1 \cdot \gamma_{ov} \cdot \Omega \cdot V_{Ed,E} \end{cases} \quad \text{Eq. (13.13)}$$

where:

- N_{Rd} (M_{Rd} , V_{Rd}) is the axial (bending or shear accordingly) design resistance of the structural element;
- $N_{Ed,G}$ ($M_{Ed,G}$, $V_{Ed,G}$) is the axial (bending or shear accordingly) force acting on the structural element due to the non-seismic actions;
- $N_{Ed,E}$ ($M_{Ed,E}$, $V_{Ed,E}$) is the axial (bending or shear accordingly) force acting on the structural element due to the design seismic action;
- γ_{ov} is the overstrength factor ($\gamma_{ov} = 1,25$ for steel S355);
- $\Omega = \min(N_{Rd,i}/N_{Ed,E,i})$ over all the bracing diagonals.

13.3 High-rise case-study building

Equations, element properties, design recommendations, critical checks and proposed behaviour factor (q-factor), included in the Information Brochure (INNOSEIS, 2017), are verified hereafter through numerical analyses on a 3D high-rise case-studies building equipped with the MSSH devices. Both dissipative and non-dissipative elements of the resisting frame are preliminary designed with a simplified analytical procedure (equivalent lateral loads method, see Section 13.2.2). Eventually a multi-modal response spectrum analysis is carried out and relevant results are verified by means of structural checks prescribed in EC8 (see Section 13.2.3) in order to assess the suitability of the proposed structural design (the final solution is usually defined iteratively). All numerical analyses are carried out by means of the commercial software SAP2000 v.19 (CSI, 2016).

13.3.1 Description of the building frame

13.3.1.1 Geometry

Both front-view and planar geometries of the considered case-study frame are represented in Figure 13.1.

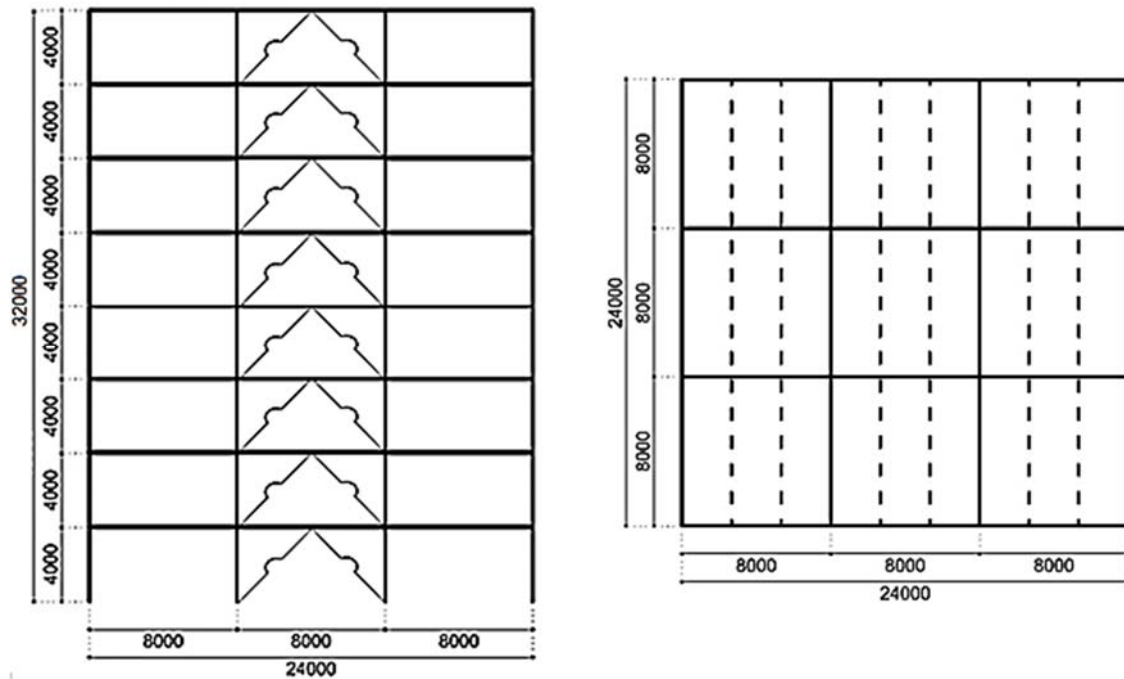


Figure 13.1: Front (left) and planar (right) geometry views of the case-study frame

13.3.1.2 Load analysis

The following Dead Loads (G) have been assumed in structural calculations:

- steel self-weight: 78.5 kN/m^3 ;
- composite slab: $g_{2,c} = 2.75 \text{ kN/m}^2$ (concrete self-weight 25.0 kN/m^3 , steel sheeting height 73 mm , thickness 1 mm , slab thickness 150 mm , equivalent uniform slab thickness 110 mm);
- services, ceilings, raised floors: $g_{2,if} = 0.70 \text{ kN/m}^2$ for intermediate floors, $g_{2,tf} = 1.00 \text{ kN/m}^2$ for top floor;
- perimeter walls (1.00 kN/m^2): $g_{2,per} = 4.00 \text{ kN/m}$.

Live Loads (q) have been estimated as:

- offices (class B): $q = 3.00 \text{ kN/m}^2$
- movable partitions ($\leq 2.00 \text{ kN/m}^2$): $q_{add} = 0.80 \text{ kN/m}^2$
- total live load: $q_{add} = 3.80 \text{ kN/m}^2$
- coeff. for the seismic combinations: $\psi_2 = 0.60$
- roof accessible and snow load neglected.

Seismic Loads (E) have been defined through the EC8 reference elastic spectrum assuming:

- importance factor: $\gamma_I = 1.0$;
- peak ground acceleration: $a_{gR} = 0.20g$;
- ground Type B, Type 1 spectrum: $S = 1.2$, $T_B = 0.15s$, $T_C = 0.50s$, $T_D = 2.00s$;
- vertical ground acceleration not accounted for.

13.3.2 Preliminary design

The non-dissipative elements of the resisting frame (beams and columns) are preliminary designed in order to withstand ($N_{Rd} \geq N_{Ed}$, $V_{Rd} \geq V_{Ed}$, and $M_{Rd} \geq M_{Ed}$) alone the gravitational loads at Ultimate Limit States (ULS) combination ($1.3G_1 + 1.5G_2 + 1.5Q$). All columns are hinged at their base and beams as well to columns. The resulting beams and columns cross-sections are reported in Table 13.1.

Table 13.1: Beam and column cross-section at each storey level

storey level	column	beam	steel
1	SHS 340x340x20	IPE 400	S 355
2	SHS 340x340x20	IPE 400	S 355
3	SHS 300x300x16	IPE 400	S 355
4	SHS 300x300x16	IPE 400	S 355
5	SHS 220x220x16	IPE 400	S 355
6	SHS 220x220x16	IPE 400	S 355
7	SHS 180x180x16	IPE 400	S 355
8	SHS 180x180x16	IPE 400	S 355

The MSSH dissipative bracing system is then preliminary designed according to the procedure described in Section 13.2.2. Assuming a behaviour factor $q = 3.5$ (see Information Brochure-INNOSEIS, 2017), the base-shear $F_b(T_1)$ is calculated as:

$$T_1 = C_t \cdot H^{\frac{3}{4}} = 1.01s \quad \text{Eq. (13.14)}$$

$$S_a(T_1) = S_{ae}(T_1)/q = 0.09g \quad \text{Eq. (13.15)}$$

$$F_b(T_1) = m_{tot} \cdot \lambda \cdot S_a(T_1) = 2380.3kN \quad \text{Eq. (13.16)}$$

Resulting inertia F_i ($F_i = F_b \cdot (z_i \cdot m_i) / (\sum z_j \cdot m_j)$) and shear $F_{b,i}$ forces on column elements at each storey level are reported in Table 13.2.

Table 13.2: Mass and inertia force distribution at each storey level

storey level	m_i [kg]	F_i [kN]	$F_{b,i}$ [kN]	$\gamma_x \cdot \gamma_b \cdot F_{b,i}$ [kN]
1	354000	66.1	2380.3	3142.0
2	354000	132.2	2314.2	3054.8
3	354000	198.4	2182.0	2880.2
4	354000	264.5	1983.6	2618.4
5	354000	330.6	1719.1	2269.3
6	354000	396.7	1388.5	1832.9
7	354000	462.8	991.8	1309.2
8	354000	529.0	529.0	698.2

MSSH devices installed at all storey level have the geometric and mechanical properties reported in Table 13.3.

Table 13.3: Geometric and mechanical properties of MSSH devices

b [mm]	h [mm]	t [mm]	k_{el} [kN/m]	$N_{Rd,T} = N_{Rd,C}$ [kN]
110	390	60	7569	103.5

The number n_i of MSSH elements to be installed at each storey level can be determined as:

$$n_i = \frac{N_{Ed,i}}{N_{Rd}} = \frac{\gamma_x \cdot \gamma_b \cdot \frac{F_{b,i}}{\cos \alpha}}{N_{Rd}} \quad \text{Eq. (13.17)}$$

where N_{Rd} is the design axial strength of a single MSSH device (for relevant calculation method see the Information Brochure-INNOSEIS, 2017) ; $N_{Ed,i}$ is the seismic force acting on the same; $\gamma_x = 1.2$ and $\gamma_b = 1.1$ are respectively the reliability and the partial factor according to EN 15129 (CEN, 2009); n_i is the number of MSSH elements installed at the i-esim storey level (both MSSH in tension and compression are accounted for); α is the inclination angle of MSSH elements.

Resulting design parameters of MSSH devices at each story level are reported in Table 13.4 (notes: (1) two bracing systems are provided along each horizontal direction; (2) MSSH elements under both tension and compression are supposed reacting to seismic inertia forces).

Table 13.4: Layout of MSSH devices along both horizontal directions

storey level	n_i [-]	$n \cdot N_{Rd}$ [kN]	$n \cdot k_{el}$ [kN/m]
1	2x2x11	2x2x1138.5	2x2x83259
2	2x2x11	2x2x1138.5	2x2x83259
3	2x2x10	2x2x1035	2x2x75690
4	2x2x9	2x2x931.5	2x2x68121
5	2x2x8	2x2x828	2x2x60552
6	2x2x7	2x2x724.5	2x2x52983
7	2x2x5	2x2x517.5	2x2x37845
8	2x2x3	2x2x310.5	2x2x22707

Moreover, the cross-section of brace-elements are chosen in order to fulfil the requirements related to both axial resistance and non-dimensional slenderness (see Section 13.2.2). Relevant design parameters are reported in Table 13.5 (notes: (1) two bracing systems are provided along each horizontal direction; (2) bracing elements under both tension and compression are supposed reacting to seismic inertia forces).

Table 13.5: Bracing elements cross-sections at each storey level

storey level	cross section	$N_{Rd,i}$ [kN]	l_0 [m]	$N_{cr,i}$ [kN]	$\lambda_{b,i}$ [-]
1	2x(2UPN300)	2x(2x3795)	5.26	2x(2x943.5)	2.0
2	2x(2UPN300)	2x(2x3795)	5.26	2x(2x943.5)	2.0
3	2x(2UPN300)	2x(2x3795)	5.26	2x(2x943.5)	2.0
4	2x(2UPN300)	2x(2x3795)	5.26	2x(2x943.5)	2.0
5	2x(2UPN300)	2x(2x3795)	5.26	2x(2x943.5)	2.0
6	2x(2UPN300)	2x(2x3795)	5.26	2x(2x943.5)	2.0
7	2x(2UPN300)	2x(2x3795)	5.26	2x(2x943.5)	2.0
8	2x(2UPN300)	2x(2x3795)	5.26	2x(2x943.5)	2.0

13.3.3 Linear elastic analysis

A linear elastic analysis is carried out in accordance with the EN 1998-1-1 provisions (CEN, 2005-2) described in Section 13.2.3. In particular, both dissipative and non-dissipative structural elements are verified with reference to the seismic load combination ($G_1 + G_2 + \psi Q + E$). Since the solution initially

defined through the preliminary design does not satisfy some EC8 verifications, the final structural layout is identified by changing iteratively only the configuration of MSSH devices until the configuration reported in Table 13.6 and represented in Figure 13.2 is reached.

Table 13.6: Final layout of MSSH devices along both horizontal directions

storey level	n_i [-]	$n \cdot N_{Rd}$ [kN]	$n \cdot k_{el}$ [kN/m]
1	2x2x10	2x2x1035	2x2x75690
2	2x2x10	2x2x1035	2x2x75690
3	2x2x8	2x2x828	2x2x60552
4	2x2x8	2x2x828	2x2x60552
5	2x2x6	2x2x621	2x2x45414
6	2x2x6	2x2x621	2x2x45414
7	2x2x4	2x2x414	2x2x30276
8	2x2x4	2x2x414	2x2x30276

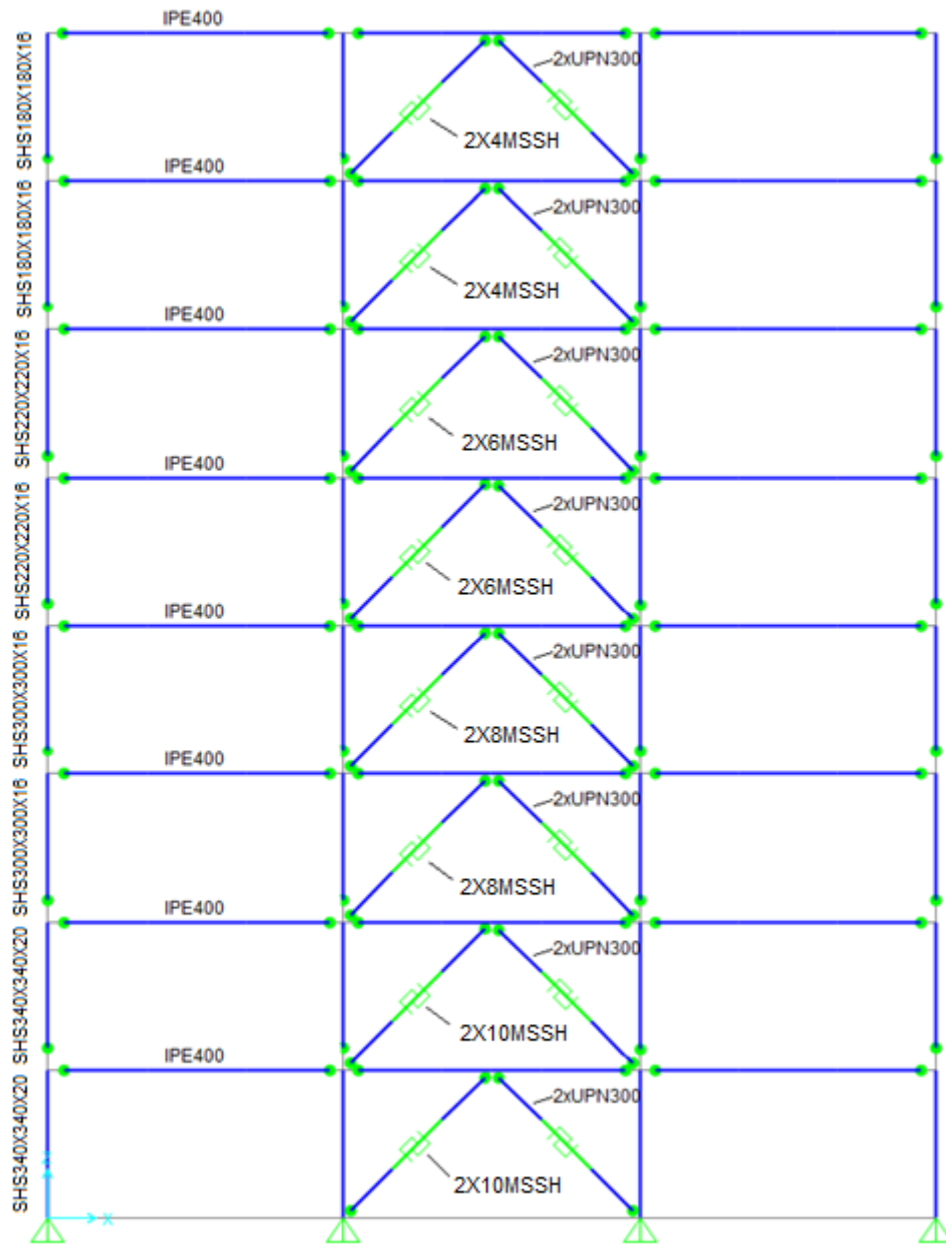
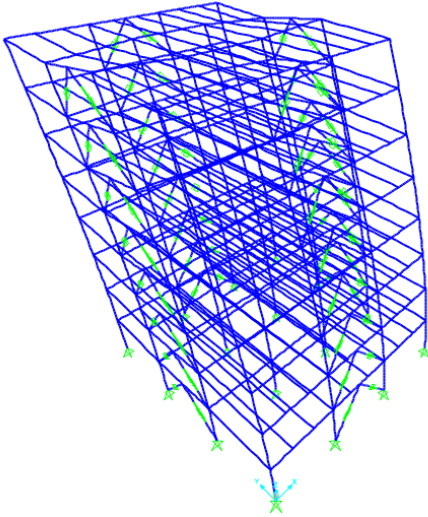


Figure 13.2: Final structural layout

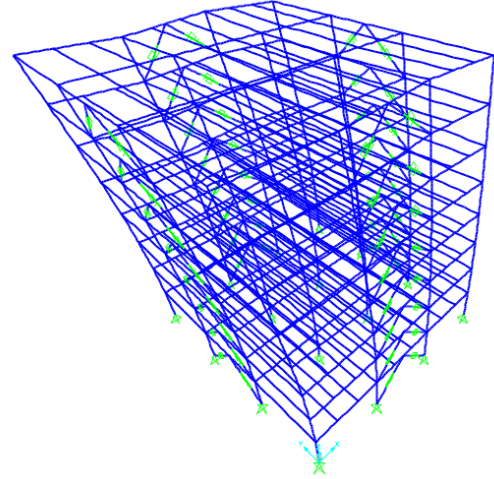
13.3.3.1 Multi-modal response spectrum analysis

A multi-modal response spectrum analysis has been performed taking into account inertia seismic loads relevant to the first mode shapes (Figure 13.3) that jointly activate at least the 90% of the total mass of the building along both horizontal directions.

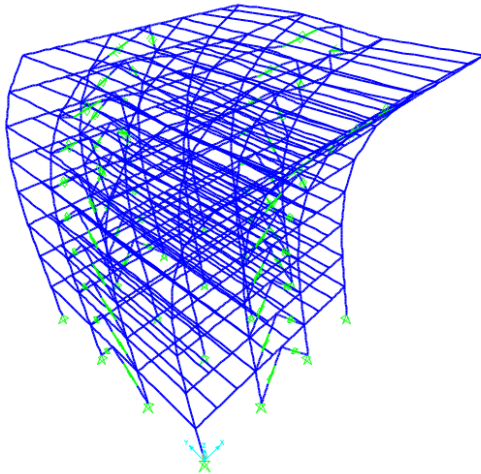
Mode 1



Mode 2



Mode 3



Mode 4

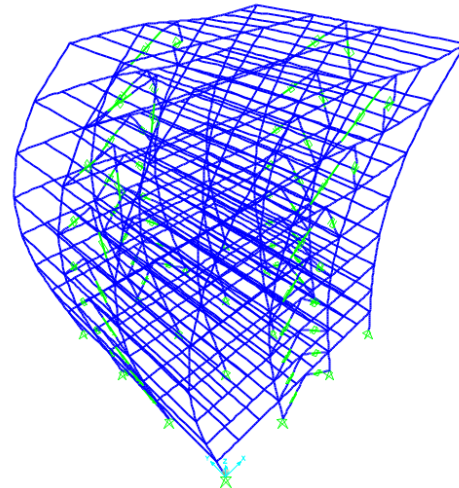


Figure 13.3: Mode shapes considered in response-spectrum analysis

Relevant modal parameters are summarized in Table 13.7. It is worth noting that the CQC rule has been used to combine modal results while the SRSS rule for the directional combination (seismic spectrum loads are simultaneously applied along both horizontal directions).

Table 13.7: Periods and participating mass ratios of considered mode shapes

Mode n°	Period [s]	Part. mass X [%]	Part. mass Y [%]	Sum X [%]	Sum Y [%]
1	2.05	0	78	0	78
2	2.05	78	0	78	78
3	0.75	0	14	78	92
4	0.75	14	0	92	92

13.3.3.2 Limitation of interstory drift

Assuming that the building is equipped with ductile non-structural elements, the following limitation of the maximum interstory drift d_r has been verified (see Section 13.2.3):

$$d_r \cdot v \leq 0.0075 \cdot h = 30\text{mm} \quad \text{Eq. (13.18)}$$

As witnessed by results reported in Table 13.8, this requirement is fulfilled at each storey level.

Table 13.8: Results of interstory drift verifications at each storey level

Storey level	$d_{e,top}$ [mm]	$d_{e,bottom}$ [mm]	$d_r = q \cdot d_{e,top} - d_{e,bottom} $ [mm]	$d_r \cdot v$ [mm]
1	8.7	0	30.4	15.2
2	17.9	8.7	32.1	16.1
3	28.2	17.9	36.2	18.1
4	38.6	28.2	36.2	18.1
5	50	38.6	40.1	20.1
6	61	50	38.4	19.2
7	72.7	61	40.8	20.4
8	81.9	72.7	32.3	16.2

13.3.3.3 Verification of second order effects

The possible influence of 2nd order effects has been controlled by the limitation of the interstory drift sensitivity coefficient θ below the limit values of the Code (see Section 13.2.3):

$$\theta = \frac{P_{tot} \cdot d_r}{V_{tot} \cdot h_{story}} \quad \text{Eq. (13.19)}$$

Since in three cases $0.1 < \theta < 0.2$ (Table 13.9), the second-order effects are taken into account by multiplying the seismic action by the factor $1/(1 - \theta)$.

Table 13.9: Results of 2nd order effects verification at each storey level

Storey level	P_{tot} [kN]	d_r [mm]	V_{tot} [kN]	h_{story} [mm]	θ [-]	$1/(1 - \theta)$ [-]
1	27878	32.2	1175.4	4000	0.19	1.24
2	24346	32.5	1094.8	4000	0.18	1.22
3	20815	33.9	976.4	4000	0.18	1.22
4	17289	33.5	868.5	4000	0.17	1.20
5	13764	34.8	776.8	4000	0.15	1.18
6	10264	33.1	682.3	4000	0.12	1.14
7	6764	34.2	574.3	4000	0.10	1.11
8	3269	24.9	355.0	4000	0.06	1.06

13.3.3.4 Verification of dissipative elements

It has been verified that, along both horizontal directions, the maximum seismic action ($\gamma_x \cdot \gamma_b \cdot N_{Ed,i}$) on the MSSH device has not exceeded the axial strength $N_{Rd,i}$ of the element (see Section 13.2.3):

$$N_{Rd,i} \geq \gamma_b \cdot \gamma_x \cdot N_{Ed,i} \quad \text{Eq. (13.20)}$$

This requirement is fulfilled at each storey level as witnessed by results reported in Table 13.10. Moreover, to achieve a uniform dissipative behavior among all storey levels, the following requirement related to the distribution of the over-strength ratios Ω of the MSSH elements over the entire structure has been verified (see Section 13.2.3):

$$\frac{\max \Omega_i}{\min \Omega_i} \leq 1.25 \quad \text{Eq. (13.21)}$$

where $\Omega_i = N_{Rd,i}/N_{Ed,i}$.

Table 13.10: Resistance verification on MSSH elements at each storey level

Storey level	$ N_{Ed,C} = N_{Ed,T} $ [kN]	$N_{Rd,C} = N_{Rd,C}$ [kN]	N_{Ed}/N_{Rd} [-]	Ω [-]
1	595	1035	0.57	1.74
2	591	1035	0.57	1.75
3	479	828	0.58	1.73
4	465	828	0.56	1.78
5	387	621	0.62	1.60
6	370	621	0.60	1.68
7	288	414	0.70	1.44
8	240	414	0.58	1.73
$max\Omega_i/min\Omega_i = 1.78/1.44 = 1.24$				

It is worth noting that the over strength factor used for structural checks of non-dissipative element is $\Omega = 1.44$ (the minimum among obtained values).

13.3.3.5 Verification of non-dissipative elements

In order to ensure that the yielding occurs only in MSSH devices, non-dissipative structural members (beams, columns, and braces) have been verified according to capacity design requirements (see Section 13.2.3). Due to the structural scheme adopted for the resisting frame, column and brace elements are subjected only to axial loads and the relevant verification is (see Section 13.2.3):

$$N_{Rd} \geq N_{Ed,G} + 1,1 \cdot \gamma_{ov} \cdot \Omega \cdot N_{Ed,E} \quad \text{Eq. (13.22)}$$

Relevant results are reported in Table 13.11.

Table 13.11: Verification of non-dissipative element under max axial load (columns and braces)

element type	N_{Rd} [kN]	$N_{Ed,G} + 1,1 \cdot \gamma_{ov} \cdot \Omega \cdot N_{Ed,E}$ [kN]
column – SHS340x340x20	7903	5882
column – SHS300x300x16	5618	3997
column – SHS220x220x16	4044	2379
column – SHS180x180x16	3448	1068
brace – 2UPN300	3795	1035

Beams elements are instead subjected to both shear and bending actions and the relevant verification is (see Section 13.2.3):

$$\begin{cases} V_{Rd} \geq V_{Ed,G} + 1,1 \cdot \gamma_{ov} \cdot \Omega \cdot V_{Ed,E} \\ M_{Rd} \geq M_{Ed,G} + 1,1 \cdot \gamma_{ov} \cdot \Omega \cdot M_{Ed,E} \end{cases} \quad \text{Eq. (13.23)}$$

Relevant results are reported in Table 13.12.

Table 13.12: Verification of beam elements under max shear loads and bending moments

element type	V_{Rd} [kN]	M_{Rd} [kNm]	$V_{Ed,G} + 1,1 \cdot \gamma_{ov} \cdot \Omega \cdot V_{Ed,E}$ [kN]	$M_{Rd} \geq M_{Ed,G} + 1,1 \cdot \gamma_{ov} \cdot \Omega \cdot M_{Ed,E}$ [kNm]
beam IPE400	905.5	949,2	816.0	621.0

It should be noted that in order to fulfil the resistance verification to bending moments ($M_{Rd} = 621.0 \text{ kNm}$) the concrete slab (thickness 150mm) above beam elements has been assumed as a collaborative part of the composite cross-section.

13.4 Conclusions

In the present study, a specific design procedure for the implementation of MSSH devices in “V-bracing” systems of steel structures is proposed and applied to a 3D case-study high-rise (8 storeys) building located in a moderate (PGA=0.20g) seismic area. The preliminary design of the resisting frame is defined by means of a simple analytical procedure (equivalent lateral loads method) and then the proposed structural layout is assessed in a multi-modal response spectrum analysis. The final solution, usually obtained iteratively adjusting the preliminary design, is shown to widely fulfil all the requirements relevant to both dissipative and non-dissipative structural elements provided by EC8-1 (CEN, 2005-2).

Since based on simple calculations, the proposed method can be easily adopted by practitioners; however, for a more accurate design, the EN 15129 strongly recommends to perform nonlinear time-history analyses when the equivalent damping ratio related to hysteretic energy dissipation is higher than 15%.

13.5 References

- CEN (Comitee Europeen de Normalisation). *EN 15129: Anti-seismic devices*, Brussels, 2009.
- CEN (Comitee Europeen de Normalisation). EN1993-1-1, *Eurocode 3: Design of steel structures - Part 1-1: General rules and rules for buildings*. Brussels, 2005(1).
- CEN (Comitee Europeen de Normalisation). EN1998-1-1, *Eurocode 8: Design of structures for earthquake resistance – Part 1-1: General rules, seismic actions and rules for buildings*. Brussels, 2005(2).
- CSI (Computer & Structures, INC). *SAP2000 – Reference Manual*. California, Berkeley, 2016.
- INNOSEIS XX/2017. *Information Brochure - MSSH device*. 2017.

LESSLOSS 2007/03. *Innovative Anti-Seismic Systems Users Manual*. Available online at <http://elsa.jrc.ec.europa.eu/events.php?id=4#reports>.

13.6 Annex A: “FEMA 695” q-factor estimation

The “FEMA 695 method” (FEMA, 2009) consist of a series of provisions that allow to estimate the behaviour factor q of a structure by means of a non-linear static analysis (Pushover). The calculation method is represented in Figure 13.4.

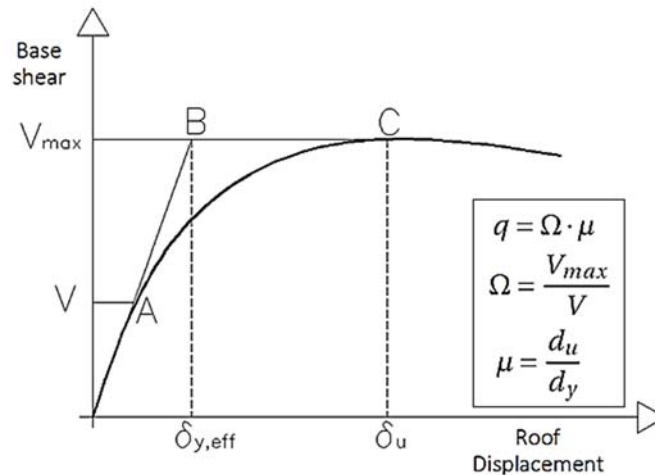


Figure 13.4: Behaviour factor q calculation method according to FEMA 695

With regard to the considered case-study building, the structural model used for elastic analysis is extended to include the response of structural elements beyond the elastic state and estimate expected plastic mechanisms and the distribution of damage. Link elements with a multilinear behavior in the horizontal shear direction are used to model the MSSH devices while other structural members (beams, column and braces) are modelled as linear. Mechanical properties of MSSH elements are calculated according to the analytical models described in the Information Brochure (INNOSEIS, 2017). Since quasi-static analyses are carried out, the hysteresis of MSSH elements is neglected in behavior-diagram (Figure 13.5). On the contrary, the failure of the element due to the exceedance of the ultimate displacement is accounted for. Moreover, according to EN1998-1-1 (CEN, 2005-2), both uniform and modal distributions of lateral loads are accounted for.

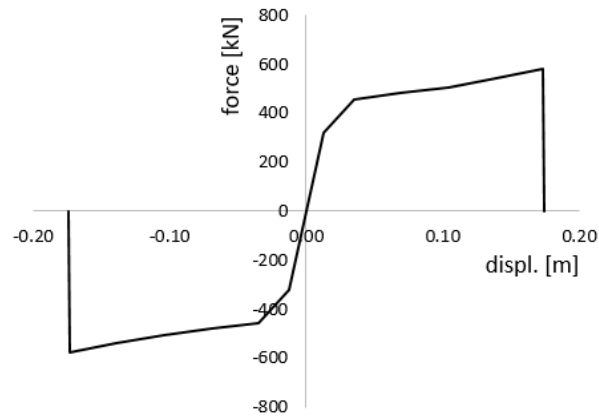


Figure 13.5: Qualitative force-displacement diagram used for MSSH elements

Since the structure is symmetric in the two horizontal directions, a static pushover analysis has been performed only along X direction considering both the modal and uniform distributions. Relevant capacity curves are represented in Figure 13.6.

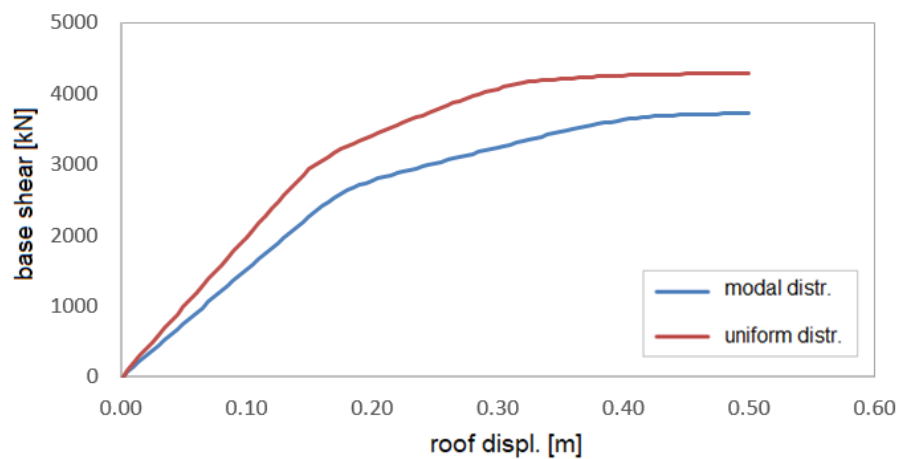


Figure 13.6: Capacity curves relevant to X and Y horizontal directions

Obtained behaviour factors are reported in Table 13.13. The recommended value to be used in multimodal response spectrum analyses is the lower among obtained ones and, on the safe side, $q = 3.0$ could be a reasonable choice.

Table 13.13: Behaviour factors q resulting from pushover analyses

Distribution	μ [-]	Ω [-]	q [-]
modal	1,69	1,87	3,17
uniform	1,54	1,97	3,03